

**Cumulus Convection and Larger-Scale Circulations
Part I**

A Parametric Model of Cumulus Convection

By

Raül Erlando López

Principal Investigator
William M. Gray

Department of Atmospheric Science
Colorado State University
Fort Collins, Colorado

**Colorado
State
University**

**Department of
Atmospheric Science**

A PARAMETRIC MODEL OF CUMULUS CONVECTION

by

Raúl Erlando López

Preparation of this report

has been supported by

NSF Grant GA 19937 (Main Support)

NSF Grant GI 31460 (G) (Partial Support)

Principal Investigator: William M. Gray

Department of Atmospheric Science

Colorado State University

Fort Collins, Colorado

June 1972

Atmospheric Science Paper No. 188

ABSTRACT

A PARAMETRIC MODEL OF CUMULUS CONVECTION

The interaction of cumulus convection with larger-scale systems is perhaps the most fundamental problem confronting meteorology today. The main obstacle to the clarification of this problem, however, is the lack of understanding of the dynamics of individual cumulus clouds and of the processes by which they impart heat and mass to their surroundings. As a tool in the investigation of these subjects, a numerical time-dependent model has been developed that can simulate the entire life-cycle of different types of cumuli under different environmental conditions.

The model is basically one-dimensional and parametric. In this type of formulation the complex turbulent and microphysical phenomena are expressed in terms of cloud-scale variables, while the more straightforward dynamical and thermodynamical processes are treated in detail in a prognostic fashion. Although the model is fundamentally one-dimensional, the clouds are assumed to consist of two regions: a protected core and an exposed surrounding shell. The entire depth of the cloud is numerically simulated for each of these mutually interacting regions.

The mixing between cloud and environment is parameterized in the model in terms of the turbulence intensity of the interior and exterior of the cloud. In this way, the commonly used but physically invalid assumption of similarity is avoided. Additional equations have been introduced in the model to predict the turbulence level of the cloud at all times.

The internal circulation of the clouds and the attending redistribution of mass between levels is parameterized in the model in terms of the one-dimensional velocity field of the core. Laboratory and

theoretical information about spherical vortices is used in the parameterization.

Results of several cloud simulations under different environmental and initial conditions are presented. These illustrate the capability of the model in simulating the entire life-cycle of cumulus clouds subject to different forcing conditions.

Raúl Erlando López
Atmospheric Science Department
Colorado State University
Fort Collins, Colorado 80521
June, 1972

TABLE OF CONTENTS

	Page
ABSTRACT	ii
I. INTRODUCTION	1
Previous Parametric Models	1
Two Dimensional Models	2
II. BASIC ASSUMPTIONS (THE LAGRANGIAN FRAME- WORK)	4
Geometrical Make Up	4
Generation of New Parcels	4
Computational Procedures	6
Limitations of the Model	7
Warner's Critique of Steady-State One-Dimen- sional Models	7
III. PHYSICAL FRAMEWORK OF THE MODEL (MATH- EMATICAL FORMULATION)	9
List of Symbols	9
Geometric Variables	9
Time Variables	9
Thermodynamic Variables	9
Mass Variables	10
Dynamic Variables	11
Microphysical Variables	11
Turbulence and Turbulent Mixing Variables	12
Physical Constants	13
Miscellaneous	13

TABLE OF CONTENTS (cont'd)

	Page
Thermodynamic Equations	13
Equations of Motion	23
Basic Equations	23
Change in Notation	25
The Vertical Pressure Gradient	25
Effect of the Weight of the Retained	
Liquid Water	26
Frictional Effects	27
Mass Balance and Cloud Geometry	30
Internal Rotation	30
Generation of the Outer Shell of the Cloud	33
Cloud Microphysics	34
Generation	35
Autoconversion	36
Collection	36
Fallout Scheme (Partitioning of Falling	
Water into Eight Velocity Groups)	38
Evaporation	41
Radar Reflectivity	42
The Mixing Process	42
Turbulence Intensity Equations	44
The Kinetic Energy Equation for Turbu-	
lent Motion	45
The Generation of Turbulence	46
The Dissipation of Turbulence	47
Equation of Buoyancy Fluctuations	48
Initial Conditions (Boundary Layer Forcing)	50
Computational Scheme	53
IV. RESULTS	55
Description of Three Basic Types of Cumuli	55

TABLE OF CONTENTS (cont'd)

	Page
Environmental Parameters	55
Initial Updraft Parameters	57
Physical Constants	59
Upper Boundary of the Cloud	59
Lower Boundary of the Cloud	61
Accumulated Rainfall	63
 Time-Sections of Various Cloud Variables	 66
Virtual Temperature Difference	66
Vertical Velocity	68
Hydrometeor Water Content	70
Cloud Liquid Water Content	72
 Geometrical Shape of the Clouds	 74
 Comparison of Some Properties of the Shell and Core	 79
Vertical Velocity	79
Liquid Water Content	79
 Sensitivity of the Model to the Different Control- ling Parameters and Initial Conditions	 83
Effect of Varying the Initial Updraft Radius	83
Effect of Varying the Duration of the Initial Forcing	84
Effect of Varying the Initial Convergence of Mass Under Cloud Base	85
Effect of Varying the Drag Coefficient	88
Effect of Varying the Autoconversion Thresh- old	88
Effect of Varying the Entrainment Coefficient	91
Effect of Different Levels of Environmental Turbulence	91
Effect of Varying the Computational Time Step	92
 V. CONCLUSION AND OUTLOOK	 94
 BIBLIOGRAPHY	 96
 ACKNOWLEDGEMENTS	 100

I. INTRODUCTION

A numerical model of cumulus clouds is described in this dissertation. This model was developed as a tool in the investigation of the effects of cumulus clouds on larger-scale circulations. The model is one-dimensional and parametric. In this type of formulation the complex turbulent and microphysical processes are expressed in terms of cloud-scale parameters, while the more straightforward dynamical and thermodynamical processes are treated in detail in a prognostic scheme. The parameterizations are observationally guided, and information from measurements in the atmosphere and laboratory is used.

Previous Parametric Models. The design of the present model was undertaken in view of the fact that the parametric models in existence are too simplified for the purpose of investigating the interactions between cloud and synoptic scales. So, for example, the models developed by Simpson and collaborators (1965, 1969, 1971) Weinstein and Davies (1968) only consider the advancing edge of clouds and furthermore do not simulate the behavior of the cloud during its entire life cycle of growth and decay. Recently Weinstein has improved his model considerably (Weinstein 1970), but still the entire life cycle of the cloud is not considered, nor is the variation of the radius with time and height treated satisfactorily. Nevertheless, the present

formulation has drawn substantially from these earlier experiences with simplified conditions.

Two-Dimensional Models. There is another group of cloud models in existence, which are two-dimensional, and treat the mixing process from a mixing-length viewpoint (Ogura, 1962, 1963; Murray, 1967, 1968; Orvill, 1965, 1968, 1970; Takeda, 1969). These, too, were found inadequate for our purposes in view of the large amounts of computer time and storage required, and in view of the several uncertainties and problems in their formulation. Some of the major limitations of these two-dimensional models are as follows:

1. The difficulty of expressing turbulent entrainment and detrainment in terms of the mixing-length theory. Very little is known as to the values of the diffusion coefficients to be used and their fluctuations in time and space. In addition, artificial implicit diffusion effects are produced by the various finite-difference schemes applied.
2. Sound and short gravity waves come into the picture with the necessity of filtering. The anelastic equations have then to be used for deep convection to assure a reasonable time increment in the finite difference integration schemes (Ogura and Phillips, 1962). This introduces the unsolved problem of the implicitness between vapor and dynamic pressures that makes the formal integration of the complete equations an impossibility at the present time.
3. The necessity of working within confined vertical boundaries. The particular set of boundary conditions used can have a severe influence on the development of the clouds and their effect on the environment.

It was felt that at this stage it would be better to use a simpler one-dimensional model, free from many unsolved complications, to obtain the general features of the development of different types of clouds.

In the first chapters of this paper the mathematical and physical framework of the present model is developed. Results are then presented for different types of clouds, and their main features described. Lastly, the effect of different values of the parameters and conditions on the results of the model are discussed.

II. BASIC ASSUMPTIONS (THE LAGRANGIAN FRAMEWORK)

Geometrical Make Up. The clouds simulated in this study are assumed to be composed of two regions: a protected vertical core and an exposed surrounding shell. These regions are not isolated but interact with one another by a parameterized mutual exchange of mass. Only the shell, however, mixes directly with the environmental air. Each of the two regions consists of a vertical stack of adjacent parcels or layers (Fig. 1). Each layer or parcel rises under its own local buoyancy but interacts with the others by exchanging hydrometeor particles and mass. These layers by themselves are assumed to be vertically and horizontally uniform. Thus, in each of the separate regions of the cloud, the dynamic and thermodynamic variables can change only in the vertical, as they take different values from layer to layer. However, although the model in this form is basically one-dimensional, some resolution in the horizontal is obtained by considering the cloud to consist of two regions. In addition, information about the shape of the cloud can be obtained by careful consideration of the mass balance of each of the layers.

Generation of New Parcels. At each time-step of the computations a new core parcel is generated at cloud base according to a prespecified updraft pulse. The new parcel rises under the forcing of this subcloud-layer updraft and its own buoyancy, following the parcels that have gone before it. After some time (controlled by the subcloud

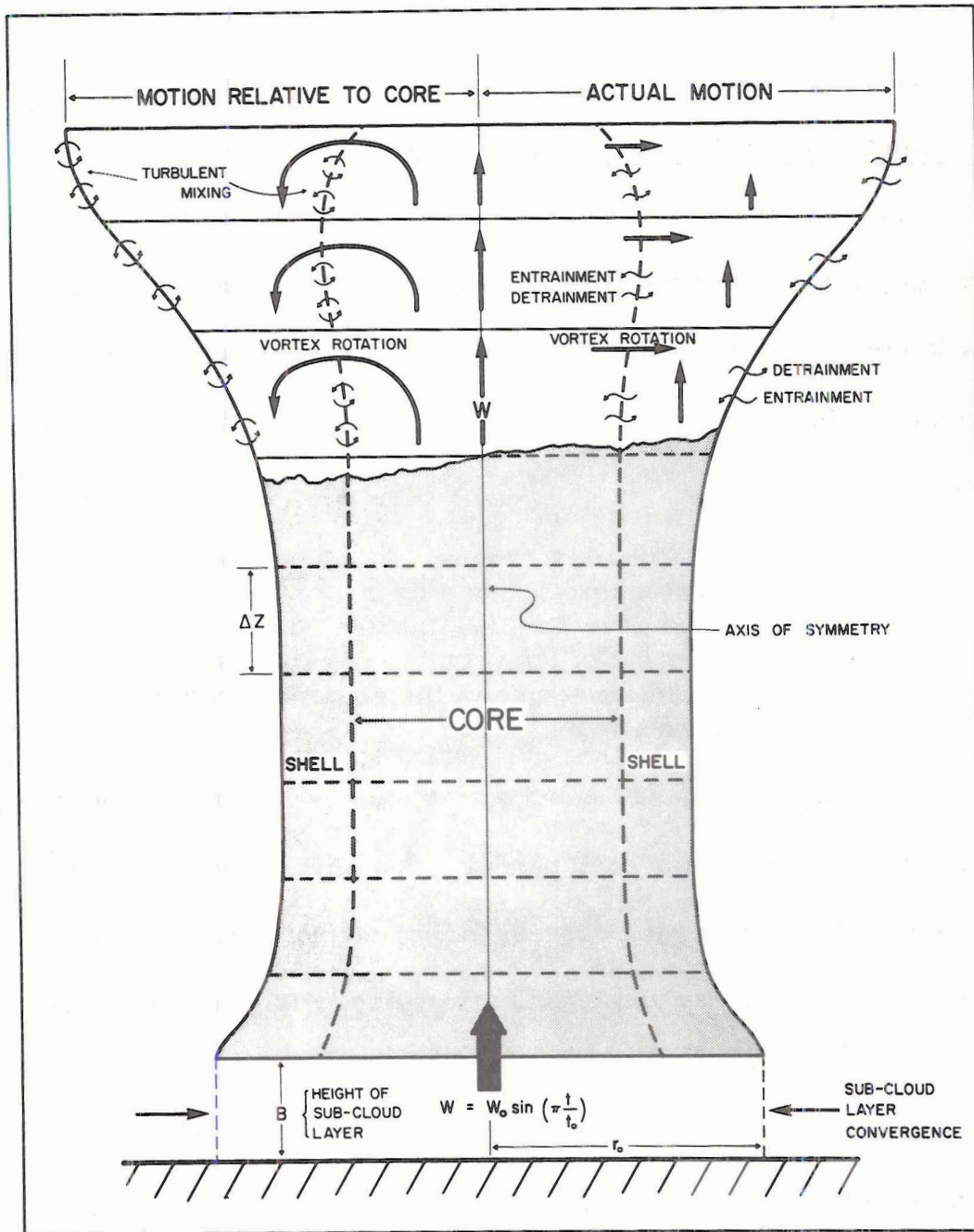


Fig. 1. Schematic representation of model cloud geometry. The right hand side of the picture illustrates actual vertical motions and mass exchanges typically reproduced in the core and shell of the cloud. The left hand side depicts this same motion relative to the core.

layer forcing function and the drag of the falling rain) the generating updraft ceases and no more core parcels are produced.

Computational Procedure. Each layer or parcel is followed in time, as an entity, in a Lagrangian way. That means that the dynamic, thermodynamic and microphysical equations are expressed in terms of substantial derivatives. The Lagrangian approach has certain advantages in the description of cumulus convection. The two principal ones are:

1. The entrainment process can be handled as a flux of mass across a boundary rather than in terms of mixing length arguments.
2. One gets rid of the problem of expressing the advective terms of the equations in finite difference form.

At each time-step, new positions and new values for all of the variables are calculated for each parcel. The ambient sounding is then interpolated to provide the corresponding environmental values of temperature, humidity and turbulence intensity for each of the new heights. This information is used in computing the mixing between cloud and environment, and the buoyancy of the parcels during the next time-step. The equations are again solved simultaneously for each layer and the process repeated.

In the next chapter the equations that are applied to each layer are described in detail. The general plan of the derivations is to treat the motion, continuity and thermodynamic equations in considerable detail, while the microphysical process, internal turbulence, rotation,

and the mixing with the environment are expressed as semi-empirical relationships in terms of large-scale cloud variables.

Limitations of the Model. At this point, some of the limitations of this model should be brought out.

1. The basic one-dimensionality of the model precludes the treating of sloping updrafts in strong vertical wind shear conditions. In order to attack this problem, the horizontal equations of motion should be included, and provisions made for the pressure gradients generated across the cloud due to the horizontal drag suffered by the ascending slanted currents.
2. No dynamic pressure effects are allowed in the vertical. This again is a result of the basic one-dimensionality of the model. As in all one-dimensional treatments of convection, the vertical pressure gradient inside the cloud will have to be assumed equal to the hydrostatic pressure gradient of the environment.
3. No attempt is made in this scheme to model the effect of the falling rain on the environment. In reality the falling rain usually produces considerable sinking motion in the air around and beneath the cloud as a result of the evaporational cooling and drag produced by the hyrometeor water particles.

Warner's Critique of Steady-State One-Dimensional Models. Warner (1970) has criticized the existing one-dimensional steady-state models in the light of direct observations of cloud-top height and liquid-water content for shallow non-raining Australian cumuli. These cloud models were found to be unable to simultaneously predict values for the liquid-water content and cloud-top height in agreement with his observations. Warner asserts that the reason for this failure lies in the invalid physical bases of the models. Thus, he argues that

contrary to the assumptions of one-dimensional steady-state models

1. a cumulus cloud is not a steady-state process,
2. the mixing at one level is not independent of conditions in higher levels,
3. entrainment of environmental air into cumuli occurs not only at the sides but also at the top of the cloud,
4. and that the assumption of similarity implicitly used in the formulation of the entrainment process is not applicable to cumulus clouds.

The above criticisms are not applicable to the model described in this paper. The present model is time-dependent and treats the entire depth of the cloud. Furthermore, the model allows interaction between different levels by virtue of internal vortex circulations in the cloud. In this way, a cloud layer can experience an extra exchange of mass from the surrounding layers in addition to the incorporation of environmental mass through the process of lateral entrainment. The mixing with the environment is also allowed to take place through the top of the uppermost cloud layer, not only through the sides. In addition, the flux of entrained air is assumed to be proportional to the turbulence intensity of the cloud layer. This formulation has been developed by Telford (1966) and Morton (1968) for the case of non-similar plumes. Thus, the assumption of similarity implicitly introduced in previous one-dimensional parametric models, is not used in the present case.

III. PHYSICAL FRAMEWORK OF THE MODEL (MATHEMATICAL FORMULATIONS)

List of Symbols

Geometric Variables

B	height of the cloud base
r	radius of a cloud parcel
V	volume
v	specific volume
z	height
δz	height of a cloud parcel

Time Variables

t	time
dt	time interval
T_0	duration of the forced updraft through cloud base

Thermodynamic Variables

c_{pa}	specific heat at constant pressure for dry air
c_{pv}	specific heat at constant pressure for water vapor
c_{pw}	specific heat at constant pressure for liquid water
H	total enthalpy
h	total specific enthalpy
h_a	specific enthalpy of dry air
h_v	specific enthalpy of water vapor
h_w	specific enthalpy of liquid water

L_v	latent heat of condensation
P	pressure
P_v	water vapor pressure
Q	heat
q	specific heat
T	temperature
T_{ve}	virtual temperature of the environment
T_{vp}	virtual temperature of a parcel
X_v	mixing ratio of water vapor
X_w	mixing ratio of liquid water

Mass Variables

m	mass
m_a	mass of dry air
m_v	mass of water vapor
m_w	mass of liquid water
dm	change in mass
dm_{ent}	change in mass due to entrainment
dm_{det}	change in mass due to detrainment
dm_{rot}	change in mass due to mixing due to internal cloud rotation
$d_i m$	internal change in mass due to condensation
$d_e m$	external change in mass due to mixing
ρ	density of moist air
ρ_e	density of environment

ρ_L density of liquid water

ρ_p density of a cloud parcel

Dynamic Variables

C_D drag coefficient

F total frictional retardation force

F_{form} frictional retardation force due to external turbulent dissipation (form drag)

F_{turb} frictional retardation force due to internal turbulent dissipation

u velocity component in the x-direction

v velocity component in the y-direction

w velocity component in the z-direction

u' eddy component of the x-direction velocity

v' eddy component of the y-direction velocity

w' eddy component of the z-direction velocity

w_0 maximum value of the forced updraft through cloud base

α rotation correction factor in the momentum equation

δw difference in vertical velocity across a cloud layer

Microphysical Variables

a threshold value of the cloud-water density at which the autoconversion process starts. Autoconversion is the process by which small cloud droplets grow by direct diffusion of water vapor into droplets of hydrometeor size ($\sim 100 \mu$)

b constant of proportionality between λ and the mass-median diameter of a partition of the total hydrometeor water mass

D	diameter of a hydrometeor
E	efficiency of collection
f	a fraction of the total hydrometeor water mass
K_1	constant for the autoconversion equation
K_2	constant for the collection equation
N	number of hydrometeor particles per unit volume in the diameter range dD
N_0	intercept of the Marshall-Palmer distribution for vanishing diameter
Q	total liquid water density
Q_{Cl}	cloud water density
Q_{Hy}	hydrometeor water density
V_T	terminal velocity of hydrometeors
$\overline{V_{T_i}}$	terminal velocity of a particle with the mass-median diameter of the i th partition of the total hydrometeor water mass
λ	parameter in the Marshall-Palmer distribution inversely related to the total mass of hydrometeors per unit volume

Turbulence and Turbulent Mixing Variables

i	turbulence intensity of a parcel
e	turbulence intensity of the environment
ϵ	entrainment constant
L	scale length of the turbulent fluctuations
\overline{v}_{ent}	mean velocity of entrainment
\overline{v}_{det}	mean velocity of detrainment
ν	kinematic coefficient of viscosity

- $\theta = T_{vp} - T_{ve}$ buoyancy of a cloud parcel
- θ' buoyancy fluctuations of a cloud parcel
- $\tau = \sqrt{\theta'^2}$ intensity of the buoyancy fluctuations

Physical Constants

- g acceleration of gravity
- R_a gas constant for dry air
- ϵ 0.622

Miscellaneous

- ' (prime) cloud parcel
- " (double prime) entrained parcel
- ___ (bar) average quantity over the cloud parcel

Thermodynamic Equations

A cloud is an open system that exchanges heat and mass with the environment. A particularly important aspect of this exchange is the dilution of the cloud's properties produced by the entrainment of dryer and cooler ambient air. As an entrained element comes inside a cloud parcel, heat, liquid water and water vapor are given to it from the cloud air until both systems attain the same temperature and composition. The final common properties will be intermediate between those of the environment and the original cloud. The rate of change of the cloud's temperature and composition as a result of this mixing can be determined by specifying the entrainment rate, the constraint of

final equilibrium, and by applying the first law of thermodynamics to both systems. Since the theory of open systems has not been discussed thoroughly in the meteorological literature, the thermodynamic equations for an entraining parcel will be derived in detail.

Consider first a closed system; it can exchange heat with the environment through radiation and conduction, but mass cannot be transported across its boundaries. For such a system, the first law of thermodynamics can be written as:

$$dq = dh - vdp \quad , \quad (1)$$

where $dq = \frac{dQ}{m}$ is the specific heat exchanged with the surrounding (dQ is the total heat exchanged with the surrounding),
 $h = \frac{H}{m}$ is the specific enthalpy,
 $v = \frac{V}{m}$ is the specific volume of the parcel, and
 dp is the change in pressure experienced by the parcel.

Equation (1) in this form is independent of mass and as such cannot be applied to an open system, whose mass changes through mixing with the environment. If equation (1) is multiplied by the mass of the parcel (m) we obtain

$$dQ + hdm = dH - Vdp \quad , \quad (2)$$

where dQ is the total heat exchanged with the surroundings,
 dH the change in total enthalpy and
 V the total volume of the system.

Equation (2) can now be applied to an entraining parcel. In this case dQ represents the heat exchanged with the environment through radiation, conduction and mass transport. Notice that the total amount of heat gained by the parcel is composed of the heat dQ absorbed by the original mass m , plus the heat contained in the incorporated mass (hdm) after attaining the original temperature of the parcel. Equation (2) represents the first law of thermodynamics applied to an open system (Van Mieghem and Dufour, 1948).

The cloud parcel and the entrained element are both open systems. Denoting with a prime the variables corresponding to the cloud and with a double prime those of the entrained element, we have the following system of equations:

$$dQ' + h'dm' = dH' - V'dp' \quad , \quad (3a)$$

$$dQ'' + h''dm'' = dH'' - V''dp'' \quad . \quad (3b)$$

The mass of each system is composed of dry air, water vapor, and liquid water. So,

$$m' = m'_a + m'_v + m'_w \quad (4a)$$

$$m'' = m''_a + m''_v + m''_w \quad , \quad (4b)$$

where m'_a , m'_v , m'_w are the masses of dry air, water vapor and liquid water respectively. The total enthalpy of each system is the sum of the enthalpies of its constituents:

$$H' = m_a' h_a' + m_v' h_v' + m_w' h_w' \quad (5a)$$

$$H'' = m_a'' h_a'' + m_v'' h_v'' + m_w'' h_w'' \quad (5b)$$

where h_a , h_v , h_w are the specific enthalpies of dry air, water vapor and liquid water. The specific enthalpies are a function of temperature (T) only, so that in terms of specific heats at constant pressure

$$\frac{\partial H'}{\partial T'} = m_a' c_{pa} + m_v' c_{pv} + m_w' c_{pw} \quad (6a)$$

$$\frac{\partial H''}{\partial T''} = m_a'' c_{pa} + m_v'' c_{pv} + m_w'' c_{pw} \quad (6b)$$

where c_{pa} , c_{pv} , c_{pw} are the specific heats at constant pressure for air, water vapor and liquid water, respectively. The changes in the mass of the constituents of each system can be produced by mixing $d_e m$ (external changes) or by changes of phase $d_i m$ (internal changes).

The total change in the enthalpy can then be expressed as:

$$dH' = \frac{\partial H'}{\partial T'} dT' + \frac{\partial H'}{\partial m_a'} d_e m_a' + \frac{\partial H'}{\partial m_v'} d_e m_v' + \frac{\partial H'}{\partial m_w'} d_e m_w' + \frac{\partial H'}{\partial m_v'} d_i m_v' + \frac{\partial H'}{\partial m_w'} d_i m_w' \quad (7a)$$

$$dH'' = \frac{\partial H''}{\partial T''} dT'' + \frac{\partial H''}{\partial m_a''} d_e m_a'' + \frac{\partial H''}{\partial m_v''} d_e m_v'' + \frac{\partial H''}{\partial m_w''} d_e m_w'' + \frac{\partial H''}{\partial m_v''} d_i m_v'' + \frac{\partial H''}{\partial m_w''} d_i m_w'' \quad (7b)$$

or, in view of the definitions (5) and (6),

$$dH' = (m_a' c_{pa} + m_v' c_{pv} + m_w' c_{pw}) dT' + h_a' d_e m_a' + h_v' d_e m_v' + h_w' d_e m_w' + h_v' d_i m_v' + h_w' d_i m_w' \quad (8a)$$

$$dH'' = (m_a''c_{pa} + m_v''c_{pv} + m_w''c_{pw})dT'' + h_a''d_e m_a'' + h_v''d_e m_v'' \\ + h_w''d_e m_w'' + h_v''d_i m_v'' + h_w''d_i m_w'' \quad . \quad (8b)$$

The mixing process between the cloud and entrained parcel can be visualized as taking place in the following manner: When the entrained mass is engulfed by the cloud parcel, an exchange of heat, water vapor and liquid water takes place so that at the end the two parcels attain the same thermodynamic state and are undistinguishable from one another. The entrained parcel can be thought of as either retaining its identity while coming to an equilibrium with the cloud parcel, or as breaking up into small elements that are scattered throughout the cloud parcel, and that individually reach a thermodynamic equilibrium with their surroundings. In mathematical form

$$dQ' + h'dm' = -(dQ'' + h''dm'') \quad (9a)$$

$$d_e m_a' = d_e m_a'' = 0 \quad (9b)$$

$$d_e m_v' = -d_e m_v'' \quad (9c)$$

$$d_e m_w' = -d_e m_w'' \quad . \quad (9d)$$

Furthermore, the continuity of water substance demands that due to phase changes

$$d_i m_v' = -d_i m_w' \quad (10a)$$

$$d_i m_v'' = -d_i m_w'' \quad . \quad (10b)$$

Equations (3a) and (3b) are now added together, and the definition of the mixing process (equations 9a to d), the constraints of mass continuity (equations 10a and b), and the expression for the total change in enthalpy (equations 8a and b) are substituted therein. After some algebraic manipulations one obtains

$$\begin{aligned} & (m_a' c_{pa} + m_v' c_{pv} + m_w' c_{pw}) dT' + (m_a'' c_{pa} + m_v'' c_{pv}) dT'' - V' dp' \\ & - V'' dp'' + (h_v' - h_w') d_i m_v' + (h_v'' - h_w'') d_i m_v'' + (h_v' - h_v'') d_e m_v' \\ & + (h_w' - h_w'') d_e m_w' = 0 \end{aligned} \quad (11)$$

From the definition of latent heat we obtain

$$L_v = h_v' - h_w' = h_v'' - h_w'' \quad , \quad (12)$$

where L_v denotes the latent heat of condensation. Furthermore,

$$h_v' - h_v'' = c_{pv}(T' - T'') \quad (13)$$

$$h_w' - h_w'' = c_{pw}(T' - T'') \quad . \quad (14)$$

With these definitions equation (11) becomes

$$\begin{aligned} & (m_a' c_{pa} + m_v' c_{pv} + m_w' c_{pw}) dT' + (m_a'' c_{pa} + m_v'' c_{pv}) dT'' = \\ & -L_v(d_i m_v' + d_i m_v'') - (c_{pv} d_e m_v' + c_{pw} d_e m_w')(T' - T'') \\ & + V' dp' + V'' dp'' \end{aligned} \quad (15)$$

At this point it is better to define the masses of water vapor and liquid water in terms of their respective mixing ratios:

$$x_v' = \frac{m_v'}{m_a'} = \epsilon \frac{P_v'}{P' - P_v'} \quad (16a)$$

$$x_v'' = \frac{m_v''}{m_a''} = \epsilon \frac{P_v''}{P'' - P_v''} \quad . \quad (16b)$$

Also

$$V' = \frac{m_v' R_v T'}{P_v'} = \frac{m_a' R_a T'}{(P' - P_v')} \quad (17a)$$

$$V'' = \frac{m_v'' R_v T''}{P_v''} = \frac{m_a'' R_a T''}{(P'' - P_v'')} \quad . \quad (17b)$$

The constraint of a common temperature and composition after mixing require that

$$T' + dT' = T'' + dT'' \quad (18)$$

$$X_v' + dX_v' = X_v'' + dX_v'' \quad . \quad (19)$$

In addition we impose the additional requirement that the final state is saturated so that the Clausius-Clapeyron equation holds

$$\frac{\epsilon L_v}{T'^2} dT' = R_a \frac{dp_v'}{p_v'} \quad . \quad (20)$$

When equations (16a), (16b), (17a), (17b), (18), and (19) are introduced in equation (15) we obtain, after some algebraic manipulation,

$$\left\{ \left[(m_a' + m_a'') c_{pa} + (m_v' + m_v'') c_{pv} + m_w' c_{pw} \right] + \left[(m_a' + m_a'') \frac{x_v' (\epsilon + x_v') L_v^2}{T'^2 R_a} \right] \right\} dT' =$$

$$(m_a' + m_a'') \frac{L_v X_v' dp'}{P' - P_v'} - L_v (x_v' - x_v'') m_a'' - (c_{pv} d_e m_v' + c_{pw} d_e m_w') (T' - T'') - \quad (21)$$

$$(m_a'' c_{pa} + m_v'' c_{pv}) (T' - T'') + R_a \left(\frac{m_a' T'}{P' - P_v'} dp' - \frac{m_a'' T''}{P'' - P_v''} dp'' \right) \quad .$$

The preceding equation can be greatly simplified by considering the fact that the enthalpy changes of the water vapor and liquid water are much smaller than the corresponding enthalpy changes of the dry air. This is so on account of the small water vapor and liquid water mixing ratios encountered in meteorological conditions, even in moist convection. The following assumptions can thus be made.

$$\begin{aligned}
 P_v &\ll P && \sim 1:100 \\
 x_v'' c_{pv} &\ll c_{pa} && \sim 1:1000 \\
 x_v' &\ll \epsilon && \sim 1:600 \\
 m_v'' c_{pv} &\ll m_a'' c_{pa} && \sim 1:200 \quad (22) \\
 m_v' c_{pv} + m_w' c_{pw} &\ll m_a' c_{pa} && \sim 1:1000 \\
 c_{pv} d_e m_v' (T' - T'') &\ll c_{pa} m_a'' (T' - T'') && \sim 1:1000 \\
 c_{pw} d_e m_w' (T' - T'') &\ll c_{pa} m_a'' (T' - T'') && \sim 1:200.
 \end{aligned}$$

In addition it will be assumed that both cloud and entrained parcels are at the same pressure before mixing and that the pressure changes experienced during the mixing process are the same and hydrostatic.

Thus

$$\begin{aligned}
 p' &= p'' = p \\
 dp' &= dp'' = dp = -\rho g dz \quad . \quad (23)
 \end{aligned}$$

Under these assumptions equation (21) reduces to

$$dT' = \frac{\frac{-g}{c_p} dz \left[\overbrace{\frac{L_v x_v'}{R_a T'}}^{(a)} + 1 \right] - \left[\overbrace{(T' - T'')}^{(c)} + \overbrace{\frac{L_v}{c_p} (x_v' - x_v'')}^{(d)} \right] \frac{m_a''}{m_a' + m_a''}}{1 + \frac{x_v' \epsilon L_v^2}{c_{pa} R_a (T')^2}} \quad (24a)$$

If the process is saturated, the equation for the mixing ratio can be obtained from the definition of mixing ratio (equation 16a) and the Clausius-Clapeyron relationship (equation 20), by logarithmically differentiating both equations and substituting one into the other. Thus

$$dx_v'_{\text{sat.}} = \frac{x_v' g dz}{R_a T'} + \frac{x_v' dT' \epsilon L_v}{R_a (T')^2} \quad (25a)$$

In the case that the cloud parcel becomes subsaturated, the condensation terms in equation (24a) drop out, as well as term (d) which represents the evaporation of cloud water to bring the entrained parcel to the saturated state of the cloud. Thus, equation (24a) reduces to

$$dT' = -\frac{g}{c_p} dz - \frac{m_a''}{m_a' + m_a''} (T' - T'') - \text{Evaporational cooling} \quad (24b)$$

The evaporation of liquid water now depends on the degree of subsaturation and the amount of liquid water present. The equation for the mixing ratio of the subsaturated parcel can be expressed as

$$dx_v' = -\frac{m_a''}{m_a' + m_a''} (x_v' - x_v'') + \text{Evaporation} \quad (25b)$$

The evaporation term will be discussed in connection with the micro-physical computations.

Equation (24) describes the four principal thermodynamic processes experienced by an entraining cloud parcel. Term (b) represents the dry adiabatic cooling undergone by the cloud parcel. Term (a) and the denominator modify this cooling in lieu of the released condensation heat. Terms (c) and (d) have to do with the mixing of cooler and dryer environmental air with the parcel. Notice that the dilution effect is distributed among both the cloud and entrained masses.

Equations similar to (24) have been derived from basic principles by Dufour (1956) and by simplified or intuitive thermodynamical schemes by Stommel (1947) and Austin and Fleisher (1948). None of these formulations take into consideration that the entrained mass participates in the sharing of the total energy of the system. In the case of the detailed derivation by Dufour (1956), the problem arises because of the inaccurate representation of the mixing process between the parcel and the entrained element. The consideration of the mass of the entrained parcel in equation (24) will be unimportant when the entrainment rate is small. However, in the case of actively-growing cumuli the ratio of entrained to cloud masses may be of such a large magnitude that its neglect could affect the simulation of the dynamics considerably. The magnitude of the entrainment rates observed in the present model will be discussed in subsequent sections.

Equations of Motion

Basic Equations. The vertical equation of motion for a cloud parcel that does not interact with the environment can be written as

$$\frac{dw}{dt} = -\frac{1}{\rho_p} \frac{\partial P}{\partial z} - g + F \quad , \quad (26)$$

where w , p , ρ_p and F represent the vertical velocity, pressure, density and frictional retardation of the cloud parcel. The corresponding momentum equation for an interacting or open parcel can be obtained by multiplying equation (26) by the mass m of the parcel

$$m \frac{dw}{dt} = -\frac{m}{\rho_p} \frac{\partial P}{\partial z} - gm + mF \quad . \quad (27)$$

Consider now an element of external air that is entrained into the cloud. It also can be regarded as an open system that suffers a change in momentum. Indicating the variables that refer to the cloud with a prime and those referring to the entrained mass with a double prime, we have the following system of equations:

$$m' \frac{dw'}{dt} = -\frac{m'}{\rho_p'} \frac{\partial P'}{\partial z} - gm' + m'F' \quad (28)$$

$$m'' \frac{dw''}{dt} = -\frac{m''}{\rho_p''} \frac{\partial P''}{\partial z} - gm'' + m''F'' \quad . \quad (29)$$

Upon addition we obtain

$$m' \frac{dw'}{dt} + m'' \frac{dw''}{dt} = -\frac{m'}{\rho_p'} \frac{\partial P'}{\partial z} - \frac{m''}{\rho_p''} \frac{\partial P''}{\partial z} - g(m' + m'') + m'F' + m''F'' \quad (30)$$

After mixing, both cloud parcel and entrained element will have attained the same velocity; i. e.,

$$w' + dw' = w'' + dw''$$

Dividing by dt we obtain

$$\frac{dw''}{dt} = \frac{dw'}{dt} + \frac{(w' - w'')}{dt} \quad (31)$$

We further assume that the mixing proceeds at constant pressure (equation 23) and that the density difference between the two systems is small. If these assumptions, and the definition of the mixing process (equation 31) are introduced in equation (30), we can write

$$\frac{dw'}{dt} = -\frac{1}{\rho_p'} \frac{\partial P'}{\partial z} - g + \frac{m'F' + m''F''}{m' + m''} - \frac{(w' - w'')}{dt} \frac{m''}{m' + m''} \quad (32)$$

The last term represents the change in momentum of the cloud parcel due to the entrainment of an element of air from the environment. Note that the total mass of the system cloud-entrained air enters into the equation. This means that the entrained excess or deficit of momentum is distributed among the masses of both cloud and entrained parcels.

Change in Notation. From now on everything will refer to the cloud parcel; the primes will be dropped, and the entrained mass m'' will be denoted by dm_{ent} (the increase in mass of the cloud parcel due to entrainment). Furthermore, the assumption will be made that the environment is at rest ($w'' = 0$). Equation (32) now becomes

$$\frac{dw}{dt} = -\frac{1}{\rho} \frac{\partial P}{\partial z} - g - \frac{w}{(m + dm_{ent})} \frac{dm_{ent}}{dt} + F, \quad (33)$$

where F represents the total retardation force on the system

$$\left(F = \frac{m'F' + m''F''}{m' + m''} \right).$$

The Vertical Pressure Gradient. The usual procedure in dealing with equation (33) is to assume that the vertical pressure gradient inside the cloud is the same as the hydrostatic pressure gradient of the environment. In this way the classical Archimedean relationship is obtained

$$\frac{dw}{dt} = g \frac{(\rho_e - \rho)}{\rho} - \frac{w}{(m + dm_{ent})} \frac{dm_{ent}}{dt} + F, \quad (34)$$

where ρ_e is the density of the environment. Actually, the vertical pressure gradients inside the cloud are determined by both hydrostatic and dynamic effects. The dynamic components might be fairly large in the case of high liquid water contents. In this case the fall of water droplets through the updraft current can produce regions of convergence and divergence that affect the vertical pressure gradient

in the cloud (Lozowki and List, 1969; List and Lozowski, 1970). In a one-dimensional model these dynamic effects cannot be easily incorporated. However, comparisons of the results of this model with results from two-dimensional models that do incorporate these effects seem to indicate that the error in neglecting the nonhydrostatic terms is not critical at this stage. Since one of the purposes in developing this model is to have a fast and simple scheme to be applied to other problems, we feel confident that neglecting the dynamic effects of falling precipitation on the vertical pressure gradient is an adequate assumption for our present objectives.

Effect of the Weight of the Retained Liquid Water. In equation (34) the density ρ_p is made up of the density of the moist air plus the density of liquid water in the parcel. Following Saunders (1957) and Das (1964) the effect of liquid water on the dynamics of the cloud is explicitly expressed as

$$\frac{dw}{dt} = g \frac{(\rho_a - \rho)}{\rho} - g \frac{Q}{\rho} - \frac{w}{(m + dm_{ent})} \frac{dm_{ent}}{dt} + F, \quad (35)$$

where now ρ is the density of the moist air of the parcel and Q is the total liquid water density. The drag exerted by the liquid droplets is actually the weight of the liquid mass. Their acceleration due to gravity is imparted to the air as the droplets either drift or fall at a terminal velocity with respect to the updraft current.

Frictional Effects. The last term (F) of equation (35) represents the total frictional retardation that the parcel experiences. It is the result of internal frictional dissipation and external drag. Due to the turbulent interior of the parcels, some kinetic energy of mean motion (cloud-scale motion) is converted into turbulent (subcloud-scale) energy. The subcloud scale motions can be organized in the form of a ring vortex or can be composed of random turbulent fluctuations. In the latter case the dissipation (F_{turb}) of mean momentum will be related to the working of the Reynolds stresses on the mean motion. This term will be derived in the section dealing with the turbulent intensity of the cloud parcel. If the cloud parcel possesses an organized internal rotation, some of the kinetic energy generated by the buoyancy forces will be used to generate the internal vorticity. In the case of a Hill's vortex, for example (see Fig. 2), the kinetic energy of translation is only $7/15$ of the total kinetic energy possessed by the vortex as a whole (Lamb, 1945). If the vortex were accelerating due to buoyancy forces, the acceleration of the translatory motion would be only $\sqrt{7/15} = .6834$ times the total acceleration produced. This same factor will be applied to the buoyancy term of equation (35). The internal rotation of clouds in the atmosphere probably differs from the pattern of a Hill's vortex. Thermals in laboratory tanks, however, seem to rotate very much like Hill's vortices (Scorer, 1957; Woodward, 1959; Turner, 1959, 1963). In view of the

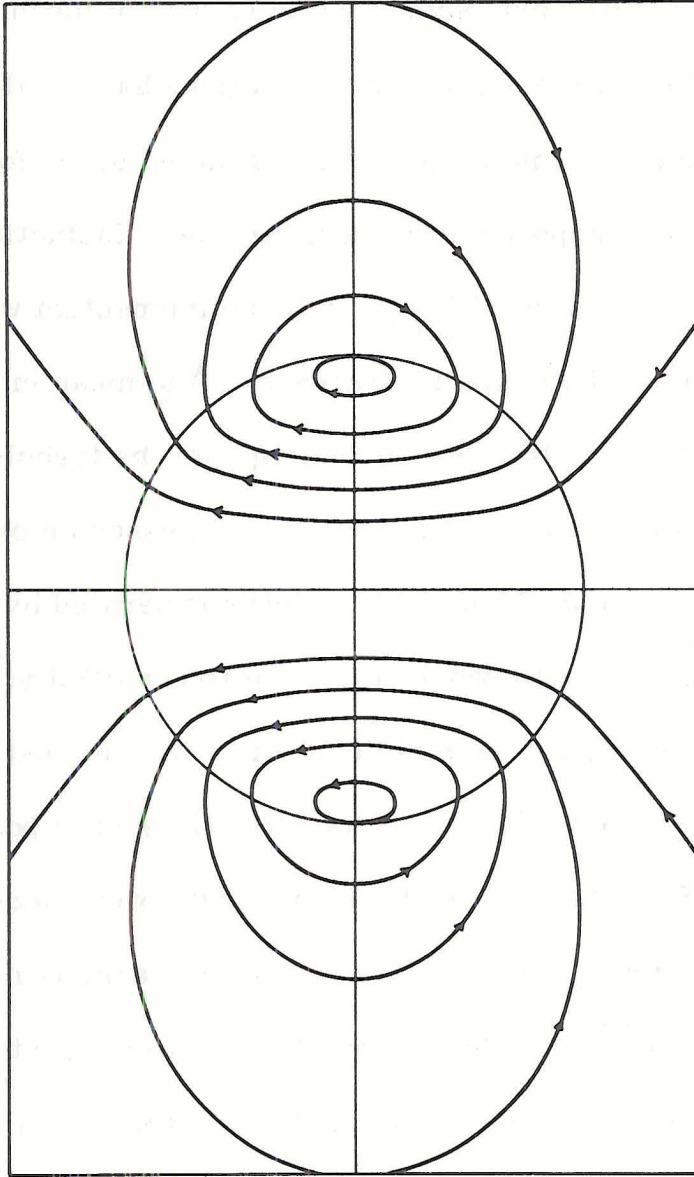


Fig. 2. Streamlines of the flow, relative to axes at rest, of the motion in and around Hill's spherical vortex. From Turner, 1963.

lack of information of the internal rotation of clouds, it was felt that the assumption of a correction factor similar to that for a spherical vortex would be appropriate in our case.

On the other hand, as the cloud moves through the environment some of its mean kinetic energy is used in setting the external air in motion around the parcel. This form drag is experienced by the top of the cloud and by those layers that move against slower-moving ones. In the latter case the faster-moving parcel displaces the air of the layer ahead and forces it to move around itself, thus losing some momentum. The classical expression for the form drag (Prandtl and Tietjens, 1957) is

$$F_{\text{form}} = - \frac{C_D \pi r^2 \frac{\rho w^2}{2}}{m + dm_{\text{ent}}} , \quad (36)$$

where C_D is the drag coefficient and πr^2 is the cross-sectional area of the parcel normal to the direction of motion.

With these formulations for the frictional retardation, equation (35) becomes

$$\frac{dw}{dt} = \alpha g \left(\frac{\rho_c - \rho}{\rho} \right) - g \frac{Q}{\rho} - \frac{w}{(m + dm_{\text{ent}})} \frac{dm_{\text{ent}}}{dt} + F_{\text{turb}} - \frac{C_D \pi r^2 \frac{\rho w^2}{2}}{m + dm_{\text{ent}}} , \quad (37)$$

where α is the Hill's vortex rotation correction of 0.6834.

The buoyancy term in equation (37) can be expressed in terms of the virtual temperature difference between cloud and environment.

Assuming that the pressure of the cloud parcel is the same as the pressure of the environment at the same height we obtain

$$\frac{dw}{dt} = \alpha g \left(\frac{T_v - T_{ve}}{T_{ve}} \right) - g \frac{Q}{\rho} - \frac{w}{(m + dm_{ent})} \frac{dm_{ent}}{dt} + F_{turb} - \frac{c_D \pi r^2 \frac{\rho w^2}{2}}{m + dm_{ent}}, \quad (38)$$

where T_v and T_{ve} are the virtual temperature of the cloud parcel and environment respectively.

Mass Balance and Cloud Geometry

Since we are working on a Lagrangian scheme, the mass balance of each layer is simple to calculate. Actually, only the entrainment-detrainment process and the mixing between levels due to internal rotation have to be considered. So,

$$\frac{dm}{dt} = \frac{dm_{ent}}{dt} - \frac{dm_{det}}{dt} + \frac{dm_{rot}}{dt}, \quad (39)$$

where dm_{ent} , dm_{det} and dm_{rot} represent the change in mass due to entrainment, detrainment, and mixing due to rotation, respectively.

Internal Rotation. When a parcel of air moves through the environment in which it is embedded, the retarding effects of drag and entrainment are initially concentrated in a thin layer around the parcel. As a result, the air in the interior moves at a faster speed against the advancing edge of the parcel and past the slower-moving sides. This pattern of convergence in the front and a shearing flow on

the sides can generate a vortex motion in which air from the center moves forward, decelerates, moves radially out and finally moves downward relative to the faster moving core.

A vortex motion of this kind has been observed in laboratory experiments with dense bubbles falling in water (Scorer, 1957). The circulation pattern of the bubbles closely resembles spherical Hill vortices (Woodward, 1959). Fig. 2 portrays the streamlines of a Hill's vortex. Clouds are also observed to possess vortex circulations (Warner, 1970). Such a flow pattern probably exists in the cap and in those regions of a cloud where there is a negative vertical velocity gradient (velocity decreasing with height). This rotation has also been reproduced by two-dimensional numerical models of clouds (Ogura, 1962; Orville, 1965; Murray, 1967).

In a one-dimensional model, ring vortex circulations cannot be reproduced, but have to be parameterized in terms of the mean vertical velocity fields. In the present model this rotation has been parameterized in terms of the vertical velocity gradient across the layers. A vortex circulation is assumed to set in whenever a faster moving layer pushes against a slower moving one. The squeezed-out mass of the slower layer is then circulated backwards around the faster moving one. (At this point the rotation correction factor is also introduced in the equation of motion as explained in the previous section). If the mass-transport by rotation were not considered, a sharp increase in the radius of a squeezed layer would occur. In fact, the

From the change of mass given by (39), and assuming a cylindrical configuration, the radius of each layer can be obtained.

Cloud Microphysics

The microphysical cloud processes possess a high degree of complexity. All we can attempt to do in a general model of cumulus convection is to simulate the combined, or bulk, effect of the hydrometeors on the dynamics of the cloud without going into the details of the growth and aggregation process of water particles.

Following Kessler (1969) we have divided the total liquid water into two parts: cloud water, composed of small droplets which do not fall relative to the cloud (less than about 100μ in diameter) and hydrometeor water, composed of drops which have a terminal velocity relative to the cloud (larger than about 100μ in diameter). So,

$$Q = Q_{Cl} + Q_{Hy} \quad , \quad (42)$$

where Q is the total liquid water content (gm/m^3) and Q_{Cl} and Q_{Hy} are the cloud and hydrometeor water contents, respectively. All of the newly condensed water vapor is initially put into the cloud water category. After the amount of cloud water increases above a certain threshold value, conversion of cloud to hydrometeor water takes place. (This scheme tacitly assumes that the condensation nuclei distribution can produce a broad spectrum of cloud droplets, and that given some time, some of the droplets will grow by diffusion to hydrometeor size.) Once hydrometeor water is present, the collection

process takes place and the hydrometeor water increases at the expense of the cloud water. Some of the hydrometeors will fall out of the parcels, while some will fall in from the layers above. In general we will have

$$\frac{dQ_{Cl}}{dt} = \text{Generation} - \text{Conversion} - \text{Collection} \quad (43)$$

$$\frac{dQ_{Hy}}{dt} = \text{Conversion} + \text{Collection} - \text{Fall out} + \text{Fall in} \quad (44)$$

In the case that the layer becomes unsaturated, equations (43) and (44) become

$$\frac{dQ_{Cl}}{dt} = - \text{Conversion} - \text{Collection} - \text{Evaporation (Cl)} \quad (43a)$$

$$\frac{dQ_{Hy}}{dt} = \text{Conversion} + \text{Collection} - \text{Fall out} + \text{Fall in} - \text{Evaporation (Hy)}. \quad (44a)$$

Generation. The generation rate of liquid water through condensation is given by

$$\text{Generation} = - \frac{dx_{v \text{ sat}}^i}{dt} - \frac{m_a''}{m_a' + m_a''} (x_v^i - x_v'') \quad (45)$$

The first right-hand term is given by equation (25) and represents the change of rate of the saturation vapor pressure of the cloud parcel.

Notice carefully that it is not equivalent to the net generation rate of liquid water through condensation, as some of the condensed water is used for the resaturation of drier entrained air from outside the cloud. This effect is represented by the second term of equation (45).

Autoconversion. The autoconversion of cloud into hydrometeor water is initiated when $Q_{Cl} > a \sim 0.5 \text{ gm/m}^3$. According to Kessler (op. cit.) the rate of autoconversion can be expressed as

$$\left(\frac{dQ_{Hy}}{dt}\right)_{\text{conv.}} = -\left(\frac{dQ_{Cl}}{dt}\right)_{\text{conv.}} = K_1(Q_{Cl} - a), \quad Q_{Cl} > a \quad (46a)$$

$$= 0, \quad Q_{Cl} \leq a \quad (46b)$$

The autoconversion constant (K_1) has been evaluated by Kessler as 0.001 sec^{-1} .

Collection. To obtain the expression for the rate of collection of cloud water Kessler assumes that the hydrometeor sizes are distributed according to the Marshall-Palmer law (1948):

$$N = N_0 e^{-\lambda D} dD \quad (47)$$

Here D is the diameter of a hydrometeor and N is the number of particles in the diameter range dD per unit volume. N_0 is the intercept of the curve for vanishing diameter. Physically it is a measure of the total number of particles per unit volume. The order of magnitude of N_0 for natural rains is 10^7 m^{-4} . The parameter λ is inversely related to the total mass of hydrometeor water per unit volume. Numerically it has units of m^{-1} .

Now, the volume swept per unit time by a hydrometeor of diameter D with a terminal velocity V_T is

$$-\pi \frac{D^2}{4} V_T .$$

If E is the efficiency with which the cloud particles are caught, the growth in mass of the collecting hydrometeor is given by

$$-\pi \frac{D^2}{4} E V_T Q_{Cl} ,$$

where the terminal velocity is related to the radius (Spilhaus, 1948) by the empirical formula

$$V_T = -130 D^{1/2} , \quad (48)$$

where V_T is in m/sec when D is expressed in meters. The increase in total hydrometeor mass per unit volume due to collection, can then be evaluated by integrating the rate of growth of each particle due to collection over all diameters,

$$\left(\frac{dQ_{Hy}}{dt} \right)_{coll} = - \int_0^{\infty} \pi \frac{D^2}{4} E (-130 D^{1/2}) Q_{Cl} (N_0 e^{-\lambda D} dD) , \quad (49)$$

expressed in units of $gm m^{-3} sec^{-1}$. Assuming that the collection efficiency is the same for particles of all diameters Kessler (1969) obtains

$$\left(\frac{dQ_{Hy}}{dt} \right)_{coll} = - \left(\frac{dQ_{Cl}}{dt} \right)_{coll} = 6.96 \times 10^{-4} E N_0^{0.125} Q_{Cl} Q_{Hy}^{0.875} . \quad (50)$$

Fallout Scheme (Partitioning of Falling Water into Eight Velocity Groups). To compute the amount of water falling out of a layer, we partition the total mass of hydrometeor water in each parcel into eight groups according to particle diameter. The diameter range of each partition is chosen so that each group contains the same mass. All the particles in the same partition are assumed to fall with the terminal velocity of a particle with the diameter that divides the partition into two equal mass segments (mass-median). This procedure has proven to be superior to the scheme used by Kessler and by Simpson and Wiggert (1969, 1971), in which all the particles are assumed to fall with the terminal velocity of the droplet corresponding to the median diameter of the entire hydrometeor distribution. By having eight different terminal velocities for the water in a layer, the hydrometeors spread themselves downwards in a more realistic way. The high liquid water concentrations experienced in other experiments using a monodispersive droplet population is thereby avoided (Das, 1964; Srivastava, 1964, 1967; Srivastava and Atlas, 1969).

The rate of fallout of hydrometeor water per unit volume from a given layer can then be expressed as

$$\begin{aligned} \left(\frac{dQ_{Hy}}{dt}\right)_{\text{fall-out}} &= \sum_{i=1}^8 \left(\frac{1}{8} Q_{Hy}\right) \bar{V}_{T_i} \pi r^2 / \pi r^2 \Delta z \\ &= \frac{1}{8} \frac{Q_{Hy}}{\Delta z} \sum_{i=1}^8 \bar{V}_{T_i} \quad , \end{aligned} \quad (51)$$

where \bar{V}_{T_i} is the terminal velocity of a particle with the mass-median diameter of the i^{th} partition, and r and Δz are the radius

and height of the layer. The fallout rate cannot be larger than Q_{Hy}/dt . The terminal velocities can be obtained by using equation (48) once the mass-median diameters of the eight partitions are obtained. To calculate these we used a combined numerical-graphical approach as follows: The mass of liquid water per unit volume contained in the diameter range zero to D in the Marshall-Palmer distribution is given by

$$\int_0^D (\rho_L \frac{\pi}{6} D^3) N_0 e^{-\lambda D} dD \quad , \quad (52)$$

where ρ_L is the density of liquid water. This mass corresponds to a fraction f of the total mass of liquid water per unit volume Q_{Hy} . So, (52) can be written as

$$f Q_{Hy} = \rho_L \frac{\pi}{6} N_0 \int_0^D D^3 e^{-\lambda D} dD \quad . \quad (53)$$

We are interested in values of $f = 1/8, 2/8, \dots, 7/8$. The integral in (53) can be evaluated analytically to yield

$$\frac{f Q_{Hy}}{\rho_L \frac{\pi}{6} N_0} = -\frac{1}{\lambda^4} (\lambda^3 D^3 e^{-\lambda D} + 3\lambda^2 D^2 e^{-\lambda D} + 3! \lambda D e^{-\lambda D} + 3! e^{-\lambda D} - 3!) \quad . \quad (54)$$

The relationship between Q_{Hy} and the parameter λ can be obtained by integrating (52) between zero and infinity. Thus,

$$Q_{Hy} = \int_0^{\infty} (\rho_L \frac{\pi}{6} D^3) N_0 e^{-\lambda D} dD = \frac{\pi}{6} \rho_L N_0 \frac{3!}{\lambda^4} \quad . \quad (55)$$

So, from (54)

$$f = -\frac{1}{3!} (\lambda^3 D^3 e^{-\lambda D} + 3\lambda^2 D^2 e^{-\lambda D} + 3! \lambda D e^{-\lambda D} + 3! e^{-\lambda D} - 3!) \quad (56)$$

Or,

$$1-f = e^{-\lambda D} \left(1 + \lambda D + \frac{(\lambda D)^2}{2!} + \frac{(\lambda D)^3}{3!} \right)$$

Expanding the exponential and multiplying we obtain the series

$$1-f = 1 - \frac{(\lambda D)^4}{4 \cdot 3!} + \frac{(\lambda D)^5}{5 \cdot 3!} - \frac{(\lambda D)^6}{6 \cdot 3! \cdot 2!} + \dots \quad (57)$$

Now, from equation (55) we see that λ is determined by the total mass of hydrometeor water present in a layer and that it fixes or defines a specific Marshall-Palmer distribution. So, any other statistic that could define the Marshall-Palmer distribution corresponding to a given water density can be used to determine λ and vice versa. Now, the diameter that partitions the distribution into two groups with masses equal to fQ_{Hy} and $Q_{Hy}(1-f)$ is such a statistic. So we can set

$$\lambda = \frac{b}{D(f)} \quad (58)$$

where b is a fixed parameter depending on D , which is in turn a function of f . Equation (57) now becomes

$$f = \frac{1}{6} \left(\frac{b^4}{4} - \frac{b^5}{5 \cdot 1} + \frac{b^6}{6 \cdot 2!} - \frac{b^7}{7 \cdot 3!} + \frac{b^8}{8 \cdot 4!} - \dots \right) = \sum_{m=0}^{\infty} \frac{b^{4+m}}{(4+m)6m!} \quad (59)$$

Equation (59) defines the ogive of the Marshall-Palmer distribution. It can be evaluated numerically for different values of \underline{b} and plotted. The values of \underline{b} corresponding to the central points of the eight equal mass groups ($f = 1/8, 2/8, 3/8, \dots, 7/8$) can then be obtained graphically. By using (58) and (48) the terminal velocities needed in equation (51) can be evaluated.

The falling droplets in each of the eight size-groups of each layer are then distributed downwards according to their terminal velocities. Their displacement distances ($\overline{V}_{T_i} dt$) are compared with the height and thickness of the layers below, and the water is applied to the layer in which it falls. By working from the top parcel downwards each layer will accumulate the water terminating at its height that has fallen from all the layers above. This water is added to the remaining hydrometeor water of the layer, and the sum is assumed to be rearranged into a new Marshall-Palmer distribution.

The water that falls through cloud base is called precipitation. As the sub-cloud layer is not considered in this model, the evaporation of the rain as it falls into dry air is not specified.

Evaporation. In the case that subsaturation is produced in a cloud parcel, some of the cloud and hydrometeor water is evaporated. Following Kessler (1969) the evaporation is given by

$$\left(\frac{dQ_{Cl}}{dt}\right)_{\text{evap}} = 1.93 \times 10^6 N_0^{.35} (x_v' - x_{v\text{sat}}') Q_{Cl}^{.65} \quad (60)$$

$$\left(\frac{dQ_{Hy}}{dt}\right)_{\text{evap}} = 1.93 \times 10^6 N_0^{.35} (x'_v - x'_{v\text{sat}}) Q_{Hy}^{.65} \quad (61)$$

here $(x'_v - x'_{v\text{sat}})$ is the saturation deficit existing in the parcel.

Radar Reflectivity. The radar reflectivity is estimated from the new values of Q_{Cl} and Q_{Hy} . By definition, the radar reflectivity factor is the summation of the sixth powers of the drop diameters:

$$Z = \int_0^{\infty} N_0 e^{-\lambda D} D^6 dD = N_0 \frac{7!}{\lambda^7} = 720 \frac{N_0}{\lambda^7} \quad (62)$$

But λ can be obtained in terms of the total hydrometeor mass density from (55). So, (62) becomes

$$Z = 3.2 \times 10^9 N_0^{-.75} Q_{Hy}^{1.75} \text{ (mm}^6/\text{m}^3) \quad (63)$$

The Mixing Process

Most of the available information about the nature of entrainment has been obtained from laboratory experiments in which a parcel of denser fluid is dropped in a tank of still water (Scorer and Ronne, 1956; Scorer, 1957; and Turner, 1962a). These studies reveal that the entrainment mechanism is of a turbulent nature. Because of the turbulent fluctuations inside the denser parcel, cavities and protuberances develop on the surface, trapping environmental fluid and drawing it inside. In these experiments no mass is detrained from the parcel to the exterior. However, if the turbulence level of the tank is artificially increased (Turner, 1962a) detrainment occurs, the

eddies in the environmental fluid removing mass away from the parcel. Thus, entrainment seems to be dependent on the turbulence level of the parcel, while detrainment seems to be dependent on the turbulence level of the surrounding fluid.

According to this evidence, Telford (1966) and Morton (1968) have suggested that the mean velocity of entrainment into a parcel (\bar{V}_{ent}) is proportional to the turbulence intensity of the cloud parcel (i), while the mean velocity of detrainment out of the parcel (\bar{V}_{det}) is proportional to the turbulence intensity of the environment (e). Thus,

$$\bar{V}_{ent} = \mathcal{E} i \quad (64a)$$

$$\bar{V}_{det} = \mathcal{E} e \quad , \quad (64b)$$

where \mathcal{E} is the entrainment constant and i and e are the turbulence intensities of the cloud parcel and the environment, respectively. The turbulence intensity is defined as

$$i^2 = \overline{u_p^2} + \overline{v_p^2} + \overline{w_p^2} \quad (65a)$$

$$e^2 = \overline{u_e^2} + \overline{v_e^2} + \overline{w_e^2} \quad , \quad (65b)$$

here u' , v' and w' are the eddies of the x , y , and z velocity components respectively. The subscript p and e refer to parcel and environment. The entrainment ($\frac{dm}{dt}^{ent}$) and detrainment ($\frac{dm}{dt}^{det}$) rates are then the fluxes of mass into and out of the parcel. So,

$$\frac{dm}{dt}^{ent} = \rho_e \bar{V}_{ent} 2\pi r \Delta z \quad (66a)$$

$$\frac{dm_{det}}{dt} = \rho_p \bar{v}_{det} 2\pi r \Delta z \quad . \quad (66b)$$

In order to evaluate these fluxes the turbulence intensities of the cloud and the environment have to be known at all times. The next section discusses the procedure used in the model to evaluate these quantities.

Turbulence Intensity Equations

In order to obtain information on the distribution of turbulence in a cloud, the kinetic energy equations for the fluctuating or turbulent motion can be considered. Since these are obtained by taking velocity moments of the momentum equations, correlations of the form $\overline{u'w'}$, $\overline{w'T'}$ and $\overline{w'^2}$ are introduced. These can only be evaluated by introducing equations involving higher order correlations, and so on. It is, however, more convenient to truncate the procedure by making assumptions about the form of the turbulence. In this case the different correlations are expressed, in approximate form, in terms of large scale parameters of the cloud flow. The justification for this procedure lies in the fact that the changes in the thermodynamic and dynamic variables produced by the process of turbulent entrainment are generally an order of magnitude smaller than the corresponding changes produced by cloud-scale processes. Thus, the terms involving turbulent entrainment in the thermodynamic, momentum and continuity equations can be determined to a lesser degree of accuracy

without introducing serious errors in the computed mean properties of the cloud.

The Kinetic Energy Equation for Turbulent Motion. In general, the kinetic energy equation for the fluctuating motion of the cloud parcel (i) can be written as

$$m' \frac{d(1/2 i^2)}{dt} = m' \frac{d(1/2 i^2)}{dt} G - m' \frac{d(1/2 i^2)}{dt} D \quad , \quad (67a)$$

where G and D indicate generation and viscous dissipation, respectively. Similarly, for the entrained parcel,

$$m'' \frac{d(1/2 e^2)}{dt} = m'' \frac{d(1/2 e^2)}{dt} G - m'' \frac{d(1/2 e^2)}{dt} D \quad . \quad (67b)$$

Upon addition, and noting that because of the constrain of final equilibrium

$$i^2 + d(i^2) = e^2 + d(e^2) \quad ,$$

we have

$$\begin{aligned} (m' + m'') \frac{d(1/2 i^2)}{dt} &= m' \frac{d(1/2 i^2)}{dt} G + m'' \frac{d(1/2 e^2)}{dt} G - m' \frac{d(1/2 i^2)}{dt} D \\ &\quad - m'' \frac{d(1/2 e^2)}{dt} D - \frac{m''}{dt} \frac{1}{2} (i^2 - e^2) \quad . \end{aligned} \quad (68)$$

In view of the fact that the horizontal shear of the vertical winds are more concentrated in the cloud than in the environment, the generation of turbulence intensity in the entrained element $\left(m'' \frac{d(1/2 e^2)}{dt} G \right)$

will be small compared to the generation of turbulence intensity in the cloud parcel $(m' \frac{d(1/2 i^2)}{dt} G)$. With this assumption, dropping the primes and setting $m'' = dm'$, we have

$$\begin{aligned} \frac{d(1/2 i^2)}{dt} = & \frac{m}{m+dm} \frac{d(1/2 i^2)}{dt} G - \frac{l}{m+dm} \frac{dm}{dt} (1/2 i^2 - 1/2 e^2) \\ & - \frac{m}{m+dm} \frac{d(1/2 i^2)}{dt} D - \frac{dm}{m+dm} \frac{d(1/2 e^2)}{dt} D \end{aligned} \quad (69)$$

The Generation of Turbulence. Morton (1968) has performed an order-of-magnitude analysis of the complete kinetic energy equations for the turbulence of plumes. Most of the following discussion is based on his study. The generation of turbulence intensity is believed to be principally produced from the horizontal shear of the mean vertical wind between cloud and exterior, and by the turbulent fluctuations of the temperature field. The principal terms contributing to the generation of turbulence intensity are those representing the rate of working of the Reynolds stresses against the radial gradient of mean flow $(\overline{u'w'} \frac{\partial \bar{w}}{\partial r})$, and the rate of working of the fluctuating buoyancy $\overline{w'\theta'}$ on the velocity fluctuations. Thus

$$\frac{d(1/2 i^2)}{dt} G = \overline{u'w'} \frac{\partial \bar{w}}{\partial r} + \frac{g}{T_{ve}} \overline{w'\theta'} \quad , \quad (70)$$

where u is along r , T_{ve} is the virtual temperature of the environment and $\theta' = (T_{vp} - T_{ve})'$ is the fluctuation in buoyancy. The following assumptions about the form of the turbulence in the cloud are made:

$$\overline{u'w'} \sim \overline{w'^2} \sim \frac{1}{3} i^2 \quad (71a)$$

$$\frac{\partial \overline{w}}{\partial r} \sim \frac{w}{r} \quad (71b)$$

$$\overline{w'\theta'} \sim \left(\frac{1}{3}\right)^{1/2} i \tau \quad , \quad (71c)$$

where $\tau = \sqrt{\theta'^2}$ is the intensity of the buoyancy fluctuation. With these simplifications

$$\frac{d(1/2 i^2)}{dt} G = \frac{1}{3} i^2 \frac{w}{r} + \left(\frac{1}{3}\right)^{1/2} \frac{g}{T_{ve}} i \tau \quad . \quad (72)$$

The negative of the first term enters into the equation of motion as the retardation of the mean flow due to internal dissipation into turbulence.

The Dissipation of Turbulence. The viscous dissipation can be expressed as

$$\frac{d(1/2 i^2)}{dt} D = \frac{3}{2} \frac{A'}{L} (\overline{w'^2})^{3/2} \quad . \quad (73)$$

In this expression according to Townsend (1956), A' is a constant of the order of unity and L is the scale of turbulence. Assume further that

$$A' \sim 1 \quad (73a)$$

$$r \sim 5L \quad (73b)$$

$$\overline{w'^2} \sim \frac{1}{3} i^2 \quad . \quad (73c)$$

So, equation (73) becomes

$$\frac{d(1/2 i^2)}{dt} D = \frac{5}{2} \left(\frac{1}{3}\right)^{1/2} \frac{i^3}{r} \quad (74a)$$

Under the same assumptions, the viscous dissipation for the entrained air can be approximated as

$$\frac{d(1/2 e^2)}{dt} D = \frac{5}{2} \left(\frac{1}{3}\right)^{1/2} \frac{e^3}{r} \quad (74b)$$

Finally, by introducing the expressions for generation (equation 72) and dissipation (equation 74) into equation (69), the equation for the change in turbulence intensity of the parcel can be written as

$$\begin{aligned} \frac{di}{dt} = & \left[\frac{1}{3} i \frac{w}{r} + \left(\frac{1}{3}\right)^{1/2} \frac{g}{T_{ve}} \tau \right] \frac{m}{m+dm} - \frac{5}{2} \left(\frac{1}{3}\right)^{1/2} \frac{1}{r} \left[i^2 m + \frac{e^3}{i} dm \right] \frac{1}{m+dm} \\ & - \frac{1}{2} \frac{dm}{dt} \left(i - \frac{e^2}{i} \right) \frac{1}{m+dm} \quad (75) \end{aligned}$$

Equation of Buoyancy Fluctuations. To complete the system, an equation predicting the buoyancy fluctuation is needed. In this case, the environment air is assumed to be devoid of buoyancy fluctuations. In analogy to equation (69) we can write

$$\frac{d(1/2 \tau^2)}{dt} = \frac{m}{m+dm} \frac{d(1/2 \tau^2)}{dt} G - \frac{m}{m+dm} \frac{d(1/2 \tau^2)}{dt} D - \frac{1}{m+dm} \frac{dm}{dt} (1/2 \tau^2) \quad (76)$$

where $\tau = \sqrt{\theta'^2}$ takes the place of i . The generation term is given by

$$\frac{d(1/2 \tau^2)}{dt} G = \overline{u' \theta' \frac{\partial \theta}{\partial r}} \quad (77)$$

Assuming

$$\overline{u'\theta'} \sim \left(\frac{1}{3}\right)^{1/2} i\tau \quad (78a)$$

$$\frac{\partial \overline{\theta}}{\partial r} \sim \frac{\theta}{r} \quad , \quad (78b)$$

we write

$$\frac{d(1/2 \tau^2)}{dt} G = \left(\frac{1}{3}\right)^{1/2} i\tau \frac{\theta}{r} \quad . \quad (79)$$

The dissipation of buoyancy fluctuations by conduction can be expressed, according to Townsend (1959), as

$$\frac{d(1/2 \tau^2)}{dt} D = \frac{B'}{L} (\overline{w'^2})^{1/2} \overline{\theta'^2} \quad , \quad (80)$$

where B' is a constant of approximately 0.3, and L is the scale of the buoyancy fluctuations. Assume that

$$B' \sim 0.3 \quad (81a)$$

$$r \sim 5L \quad (81b)$$

$$\overline{w'^2} \sim \frac{1}{3} i^2 \quad . \quad (81c)$$

So

$$\frac{d(1/2 \tau^2)}{dt} D = 1.5 \left(\frac{1}{3}\right)^{1/2} \frac{i\tau^2}{r} \quad . \quad (82)$$

Equation (76) becomes finally

$$\frac{d\tau}{dt} = \frac{m}{m+dm} \left(\frac{1}{3}\right)^{1/2} i \frac{\theta}{r} - \frac{m}{m+dm} 1.5 \left(\frac{1}{3}\right)^{1/2} \frac{i\tau}{r} - \frac{1}{m+dm} \frac{dm}{dt} \frac{1}{2} \tau \quad . \quad (83)$$

Equations (75) and (83) are used in the model to obtain the turbulence intensity of the cloud parcel at every time step. The entrainment rate can then be evaluated using (66a). The turbulence intensity of the environment, necessary to compute the detrainment rate, is obtained from the horizontal wind profile of the particular sounding used in the computations. This will be discussed in the following sections.

Initial Conditions (Boundary Layer Forcing)

When soundings over tropical oceans are analyzed, the thermal stability of the sub-cloud layer stands out sharply. It is, in fact, surprising that clouds exist at all. Even under moist, disturbed conditions, a surface parcel will not rise freely until it is two or three hundred meters above the lifting condensation level. Evidently a strong dynamic forcing in the sub-cloud layer is necessary to develop any deep cumulus convection. This forcing must also be capable of generating a steady flux of moisture through the cloud base for several minutes in order to produce and maintain the growth of strong cumuli.

Cloud surveys over the tropical oceans (Malkus and Riehl, 1964) reveal that areas of deep convection are almost invariably associated with areas of synoptic convergence. The vertical velocity induced at the top of the boundary layer by the low level convergence can provide the source of moisture needed for the production and maintenance

of deep clouds. Since less than 1% of the area of a disturbance is actually covered by active clouds, the local convergence beneath the clouds can be hundreds of times larger than the synoptic values.

The precise mechanism by which the synoptic boundary layer convergence is concentrated into smaller areas of intense inflow under the clouds is not well understood. Probably the actual mechanism of the cloud generation in disturbed conditions is a combination of both thermal instability and low-level dynamic forcing. Accelerating moist but unsaturated bubbles embedded in slowly rising boundary-layer air can modulate the low-level convergence into scattered areas of intense inflow.

For lack of any detailed information on the initiation of cumulus clouds, we have assumed the existence of a local concentrated convergence in the layer directly beneath the cloud base. This local convergence is assumed to have magnitudes 10^2 to 10^3 times larger than the synoptic values. The resulting forced updraft into the base of the cloud is assumed to vary in time as the positive branch of a sinusoidal curve, or

$$W = W_0 \sin\left(n \frac{t}{T_0}\right) \quad , \quad (84)$$

where w_0 is the maximum value, and T_0 the duration of the forced updraft. The value of w_0 can be obtained from the assumed local sub-cloud convergence ($\nabla \cdot w_0$) and the height of the cloud base (B) as

$$W_0 = -\nabla \cdot w_0 \times B \quad . \quad (85)$$

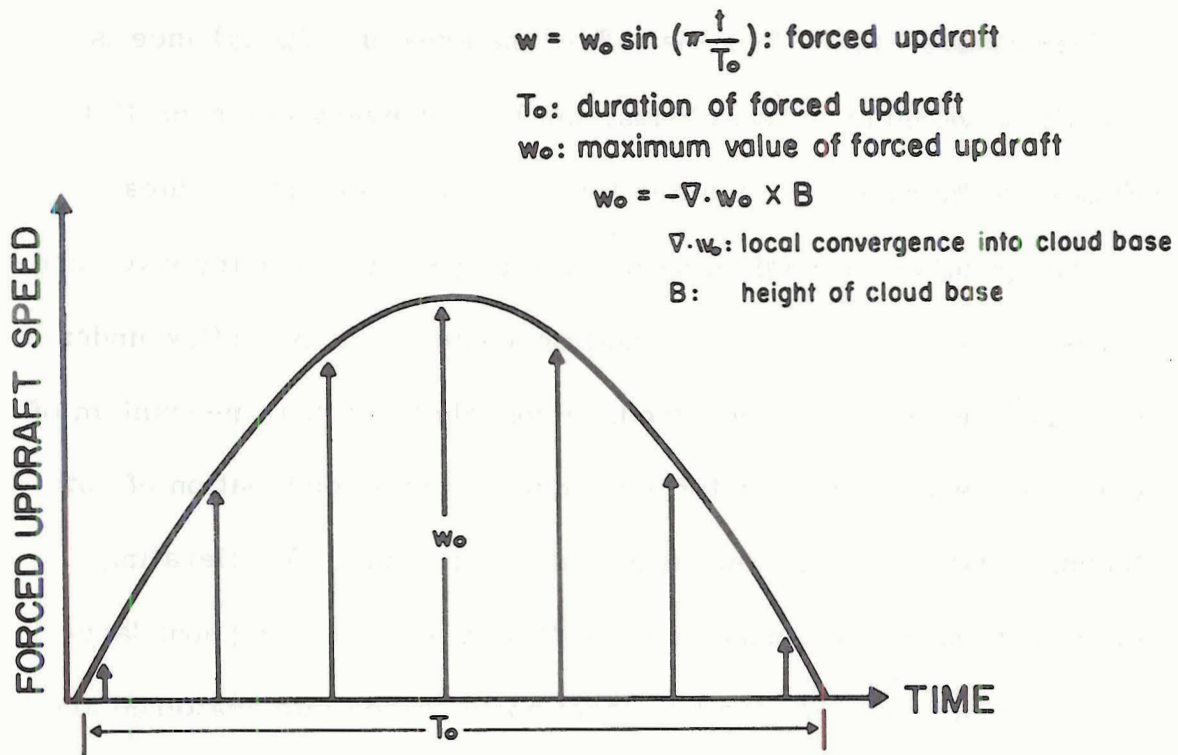


Fig. 3. Schematic representation of the forced updraft function applied at cloud base during the initial growth period of the different clouds.

Fig. 3 portrays these relationships. The mean updraft through cloud base during the time interval T_0 is equivalent to $2w_0/\pi$. The total mass used by the cloud during the initial forcing period is $2\rho_0 w_0 R_0^2 T_0$, where ρ_0 is the density of the sub-cloud layer and R_0 is the initial updraft radius. By specifying different values of the sub-cloud convergence, the height of the cloud base and the radius, duration and peak value of the initial updraft through cloud base, different cumulus cloud types can be defined. The air entering at cloud base is assumed to have the mixing ratio of the surface air and a temperature such that saturation is achieved.

Computational Scheme. At each time step of the computations, equations (24), (25), (38), (39), (43), (44), (75) and (83) are integrated in time for each of the layers of the core and shell of the cloud. A forward finite-difference scheme is used. In this way new positions and new values for all the variables are calculated for each layer. The ambient sounding is then interpolated to provide the corresponding environmental values of temperature, humidity and turbulence intensity for each of the new heights. This information is used in computing the mixing between cloud and environment, and the buoyancy of the parcels during the next time-step. The equations are again solved simultaneously for each layer and the process repeated.

Whenever a core layer starts to overtake another, a rotation routine is applied (equation 40) and a new shell layer is generated around the compressed core parcel from the mass that diverges out from it. In case that a shell layer already exists around the compressed core parcel, the diverging core mass is incorporated to the preexisting shell.

Equations (24), (25), (38), (39), (43), (44), (75) and (83) are integrated in time for each of the layers of the shell independently of the core. At the end of every time step, however, the layers of the shell are interpolated with height to coincide with the positions of the layers of the core. This procedure simplifies greatly the computational scheme of the model.

A more detailed description of the computational procedure and of the computer program is being prepared and will be made available to interested individuals.

IV. RESULTS

The nature of a simulated cloud depends on the values assigned to the different controlling parameters. The basic ones are:

1. the environmental sounding
2. the level of external turbulence
3. the height of the cloud base
4. the magnitude, duration and size of the initial updraft at cloud base
5. the entrainment and microphysical constants
6. and the drag coefficient

A great number of cloud types could be defined by specifying different combinations of the values of these parameters. In this section a few of the possible cloud simulations will be presented in detail for the purpose of illustrating the capability of the model. In addition, the sensitivity of the model to the different controlling parameters will be investigated by briefly describing a number of cloud simulations in which only one parameter is allowed to change at a time.

Description of Three Basic Types of Cumuli

Three typical maritime tropical cumuli will now be discussed in detail. They represent a cumulonimbus (Cb), a towering cumulus (TWG) and a small cumulus (Cu).

Environmental Parameters. The environment sounding used for the simulation of these three typical clouds is representative of conditions in tropical disturbances. It was obtained by averaging 00Z radiosonde data for disturbances in the Caribbean region during August and September, 1968. Fig. 4 shows the sounding plotted on a

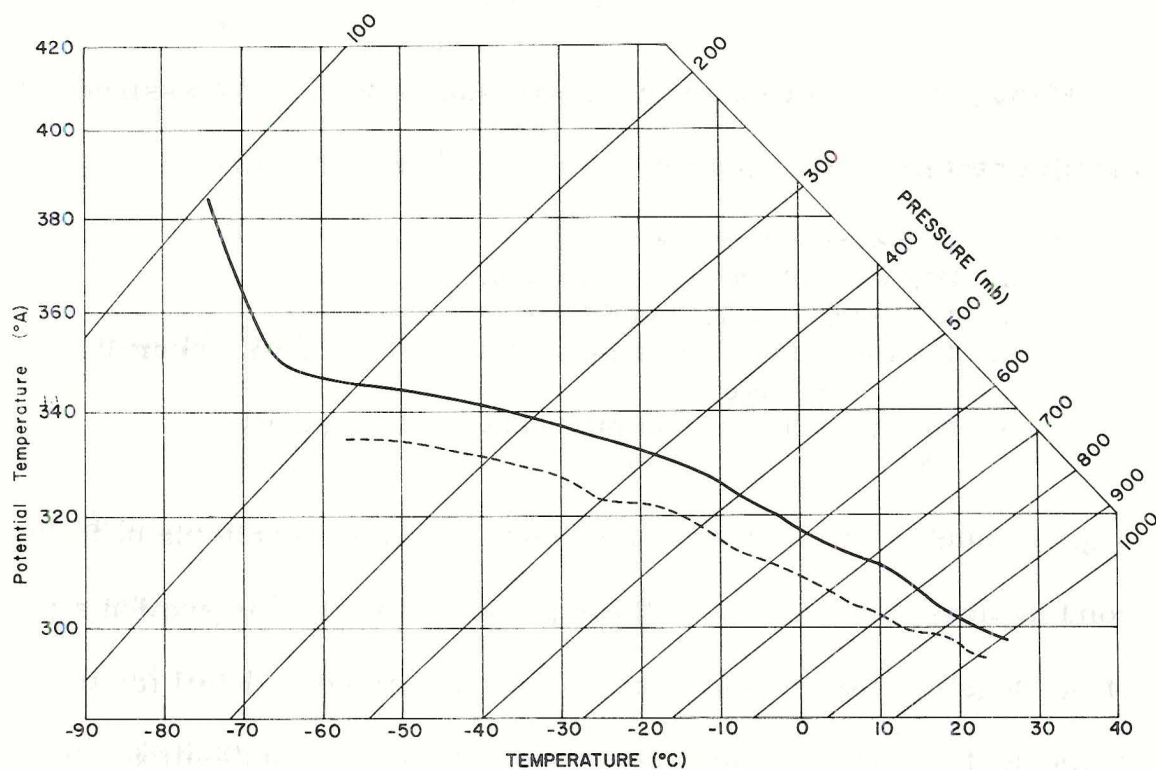


Fig. 4. Mean disturbance sounding, 00Z August and September 1968.

tephigram. The turbulence level of the environment was computed from the corresponding wind profile. It was assumed that

$$\overline{u'^2} \sim \overline{u'w'} = -\nu \frac{\partial \bar{u}}{\partial z} \quad (86a)$$

$$\overline{v'^2} \sim \overline{v'w'} = -\nu \frac{\partial \bar{v}}{\partial z} \quad , \quad (86b)$$

where ν is the kinematic coefficient of viscosity and \bar{u} and \bar{v} are the x and y velocity components for the mean sounding. The turbulence intensity of the environment can then be evaluated as

$$e^2 \sim \overline{u'^2} + \overline{v'^2} = -\nu \left(\frac{\partial \bar{u}}{\partial z} + \frac{\partial \bar{v}}{\partial z} \right) \quad . \quad (87)$$

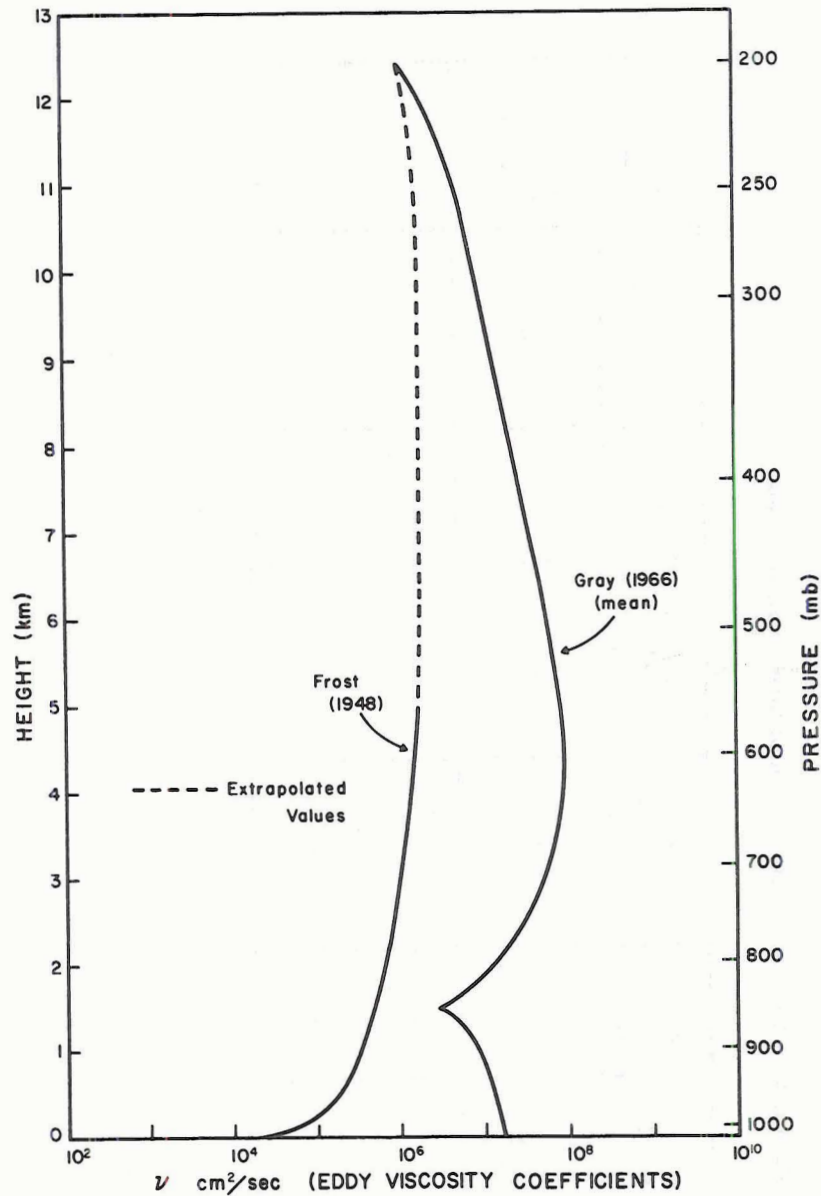


Fig. 5. Kinematic coefficient of viscosity used in computing the turbulence level of the environment.

The values used for ν were obtained from Frost (1948). Fig. 5 shows the profiles used in the computations. The height of the base of the clouds was kept constant at 520 meters (950 mb).

Initial Updraft Parameters. The values that characterize the initial sub-cloud layer forcing for the three typical clouds are listed in Table 1. In the case of the Cb a low-level forcing updraft with a

Table 1. Parameters used in the simulation of three typical clouds.

	Entrainment Constant E	Drag Coefficient C_D	Autoconversion Threshold a (gm/m ³)	Cloud Base Height B (meters)	Local Convergence under Cloud $\nabla \cdot w_0$ (sec ⁻¹)	Computational Time Step dt (sec)	Initial Radius R_0 (meters)	Duration of Forced Updraft through Cloud Base T_0 (minutes)	Maximum Value of Forced Updraft w_0 (m/sec)
Cb	.3	.3	.5	520	10^{-2}	7.5	2,000	20	5.2
TWG	.3	.3	.5	520	5×10^{-3}	7.5	1,000	15	2.6
Cu	.3	.3	.5	520	5×10^{-3}	7.5	500	15	2.6

radius of 2000 meters was applied at cloud base for a period of 20 minutes. The local low-level convergence used was 10^{-2} sec^{-1} , which with a cloud base height of 520 meters gives a peak updraft value of 5.2 m/sec. The mean updraft during the forcing period is 3.3 m/sec. In the cases of the TWG and small Cu the duration of the initial updraft was 15 minutes for both clouds. A local convergence of $5 \times 10^{-3} \text{ sec}^{-1}$ gave peak and mean updraft values of 2.6 and 1.7 m/sec in both cases. The radius of the initial updraft for the TWG Cu, however, was 1000 meters while for the small Cu it was only 500 meters.

Physical Constants. The entrainment and autoconversion constants as well as the drag coefficient were kept the same for all three clouds. Their values are listed in Table 1. The reasons for choosing these particular values will be discussed in a latter section.

Upper Boundary of the Cloud. Fig. 6 portrays the heights of the lower and upper boundaries of each of these three clouds plotted against time. In addition, the level of vanishing cloud liquid-water content (dashed line) and the region producing a 30 radar echo (shaded) are also indicated. The Cb cloud rises to a height of 14 km (150 mb) while the TWG Cu and Cu attain maximum heights of 6.5 km (650 mb) and 3 km (700 mb) respectively. The rate of ascent of the top of the cloud varies also with the size of the cloud, averaging 8 m/sec for the Cb, 4 m/sec for the TWG Cu, and 2 m/sec for the small Cu. Once the clouds reach their maximum height their tops sink back somewhat

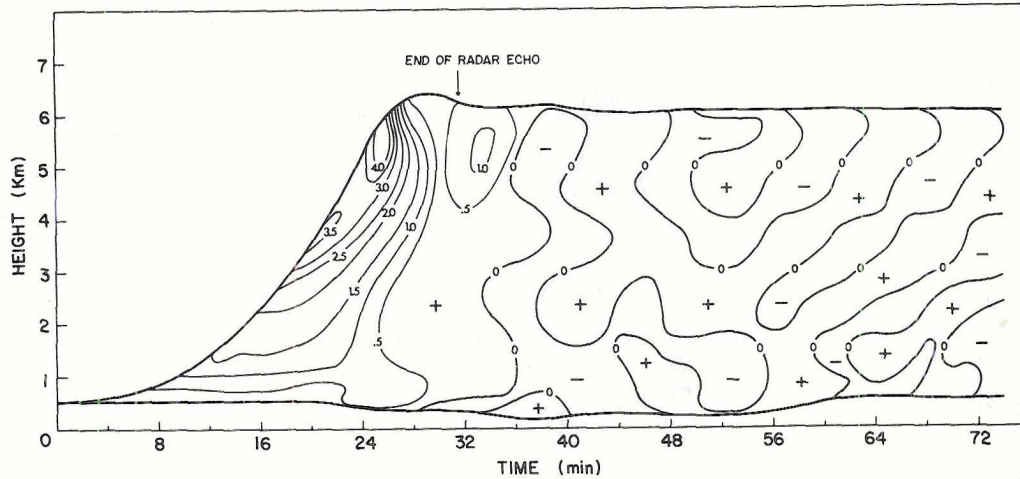
those layers further up which contain some suspended liquid water. These clear layers keep interacting with the rest of the cloud by virtue of the internal circulations in the cloud, and with the environment through the processes of entrainment and detrainment. As hydrometeor water continues to fall through the rest of the (visible) cloud, more layers will be depleted of their suspended water and the base of the (visible) cloud will occur at increasingly higher levels. Eventually all that remains of the visual cloud is a thin layer containing a very small amount of liquid water.

Sinking also helps to "dry" the cloud of its suspended liquid water. Thus, as downdrafts develop inside of the convective element, the resulting compressional warming leads to an increased evaporation which reduces the liquid water content of the sinking layers. Because subsidence in the cloud is associated with high concentrations of hydrometeors, the collection process further adds to the depletion trend.

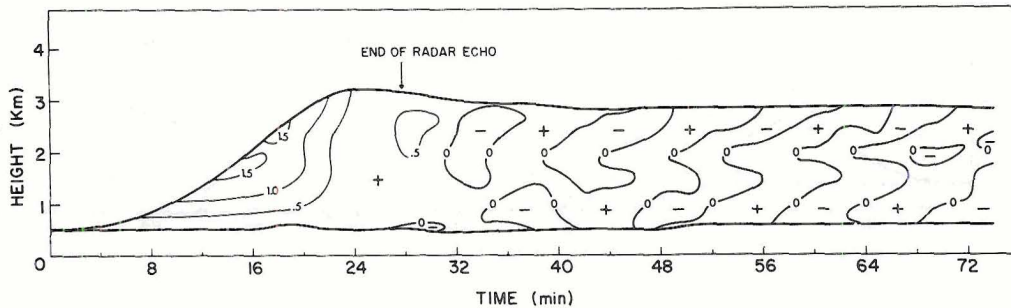
These clear layers between the visual base and the lowest boundary of the cloud are composed of turbulent cloud air slowly pulsating up and down. The temperature of this clear cloud air changes from slightly warmer to slightly cooler than the environment as the parcels oscillate in the vertical. The humidity in these layers is slightly higher than outside, although not in any appreciable amount. (Details about the thermal and dynamic structure of the clouds will be discussed in connection with Figs. 8 and 11). It is difficult to determine from this one-dimensional model when to stop calling these layers

"cloud" and start naming them "environment". In the real atmosphere, vertical and horizontal wind shears between the cloud region and the environment might lead to mixing and deformation on a scale larger than that of the turbulent entrainment and detrainment processes. As a result of this mixing, the clear turbulent cloud region might be disintegrated and incorporated into the environment at a much faster rate than can be accomplished by detrainment alone. In the case of the three model clouds presented here, these layers of clear but turbulent cloud air maintain their identity even at the end of a computation period of about three hours of cloud life. However, because of the low kinetic energy level of these layers, and the fact that their thermodynamic properties are so similar to those of the environment, the effects of the clouds on the environment at these late stages are very small.

Accumulated Rainfall. Fig. 7 illustrates the rainfall produced by each of the three typical clouds as a function of time. The cumulonimbus produces a total of 240 acre-ft during its lifetime, while the towering and small cumuli produce 4 and .3 acre-ft, respectively. Assume that the clouds were stationary and that the rain was falling underneath the clouds on a circular area having the radius of the initial cloud base. The rainfall for the Cb ($R_0 = 2$ km) would then be 2.4 cm; and it would be 0.2 and .05 cm for the TWG ($R_0 = 1$ km) and small



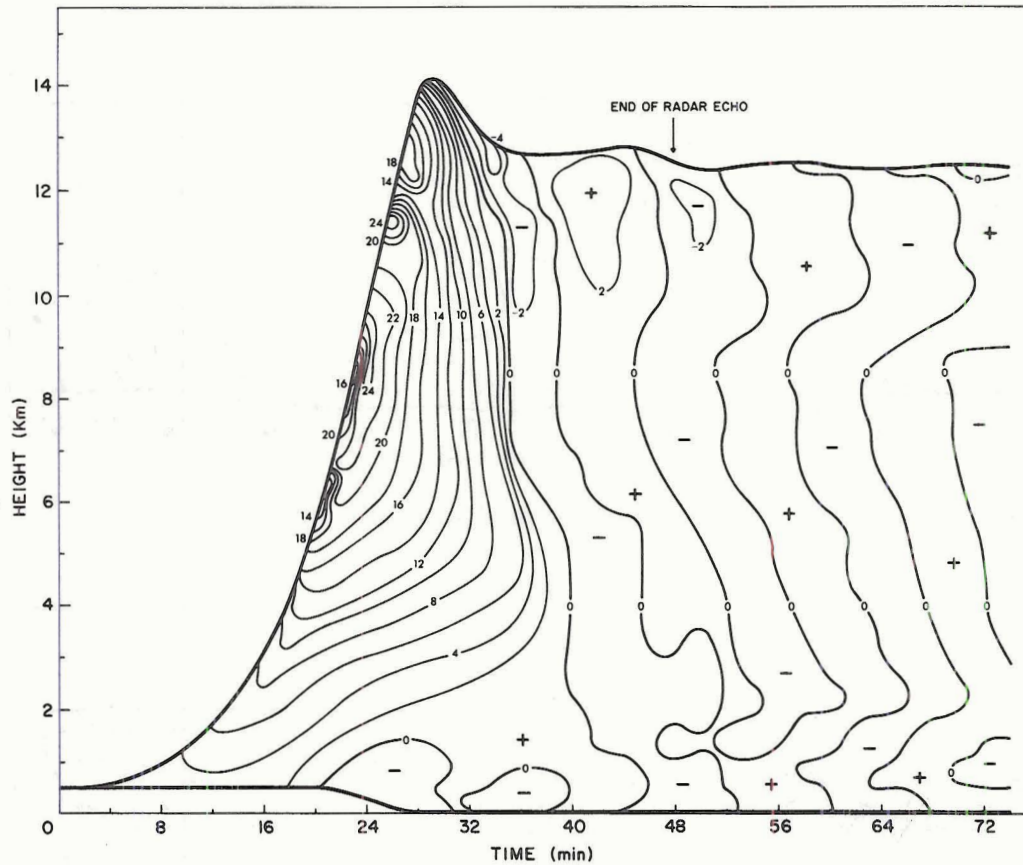
b. Towering Cumulus



c. Small Cumulus

the virtual temperature difference between cloud and environment is very small and negative. Throughout the cloud residue, the small virtual temperature difference alternates in time between positive and negative values with a period of about 10 minutes. This is mostly the result of up and down oscillations of the inert residual mass (see Fig. 9).

The time-height cross section for the towering and the small cumulus follow similar patterns except that the maximum virtual temperature difference is 4 and 1.5°C, respectively. Also, the zone of negative virtual temperature difference observed at the top of the Cb

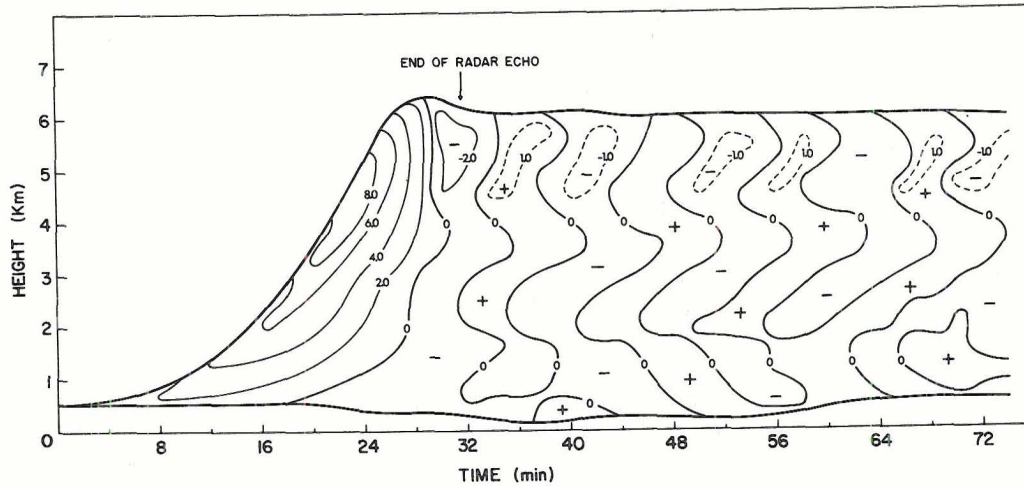


a. Cumulonimbus

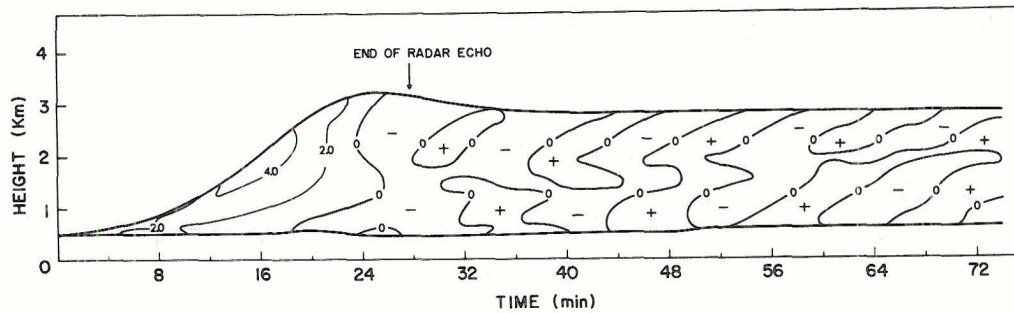
Figs. 9a-c. Time-height sections of the vertical velocity (m/sec) at the core of three typical clouds.

at the time of overshooting, is not present in the TWG and small Cu. However, although a very slight positive buoyancy is present in these smaller clouds at the time of overshooting, the tops sink afterwards due to the weight of the considerable liquid water still present in the cloud.

Vertical Velocity. Fig. 9 shows the time-height sections of vertical velocity for each of the clouds. In general, the velocity patterns follow very closely the virtual temperature difference distributions shown in Fig. 8. The maximum velocity attained by the cumulonimbus is 24 m/sec while the towering and small cumulus reach peak values

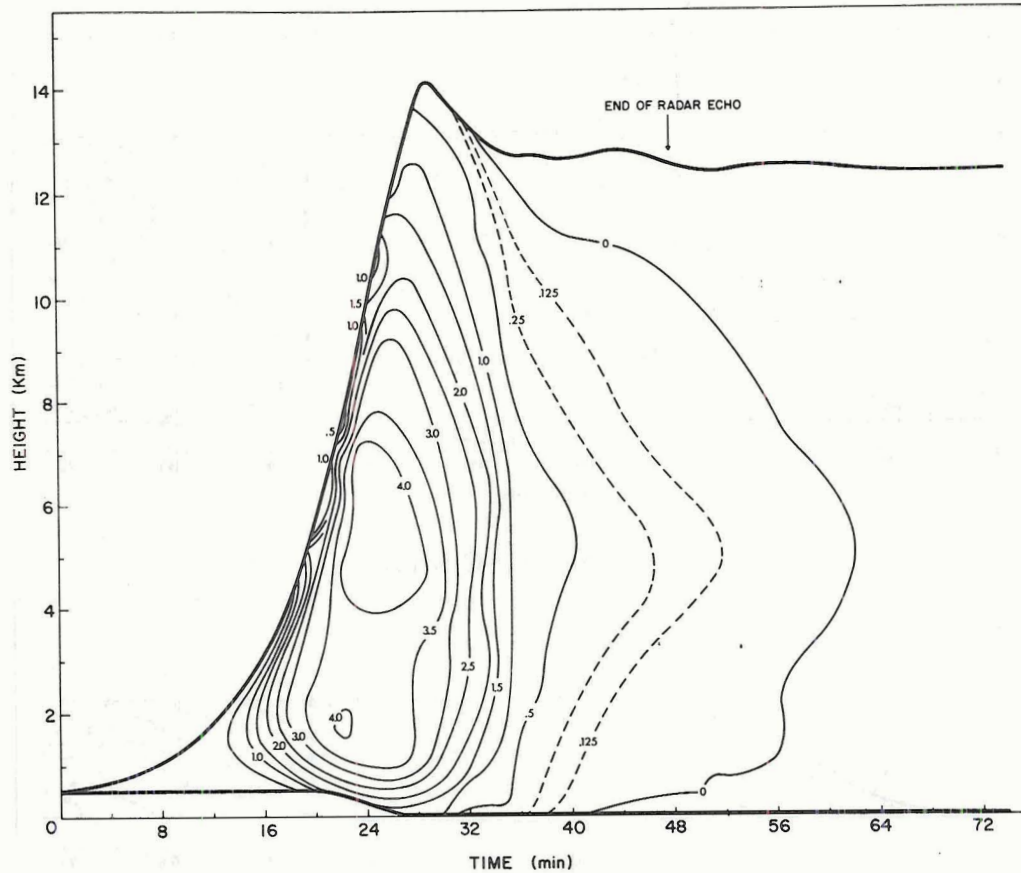


b. Towering Cumulus



c. Small Cumulus

of 8 and 4 m/sec, respectively. It is interesting to note that a weak downdraft develops in the lowest levels of the cumulonimbus after 20 minutes of cloud life. At this time the hydrometeor liquid water content has reached a maximum concentration at those levels (see Fig. 10) and the drag of the raindrops overcomes the Archimedian buoyancy still present at that height. The downdraft attains a maximum speed of 1.5 m/sec, bringing the cloud air to the ground. As time progresses the downdraft extends higher up, so that after 40 minutes of cloud life the entire depth of the cloud is slowly descending. After forty minutes the bulk of the rain has fallen through, and the upper regions

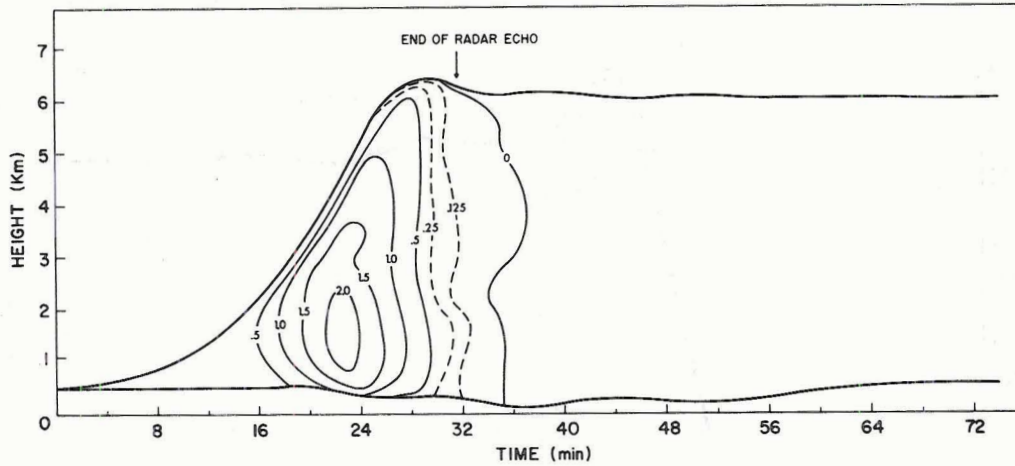


a. Cumulonimbus

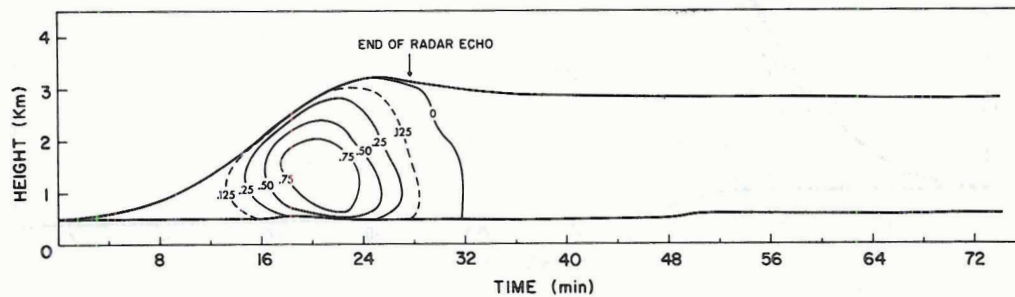
Figs. 10a-c. Time-height sections of hydrometeor water content (g m^{-3}) at the core of three typical clouds.

of the cloud mass rise slowly, only to cool and start descending again. From there on, the residual clear cloud air performs weak up and down oscillations with a period of about 10 minutes. The other two clouds follow similar patterns of development and decay, except that the magnitudes of the velocity and life intervals are smaller.

Hydrometeor Water Content. The time-height sections of hydrometeor water content (g m^{-3}) at the core of the three cloud types are displayed in Fig. 10. The peak concentrations attained by the cumulonimbus, towering and small cumulus are 4, 2, and $.75 \text{ g m}^{-3}$,

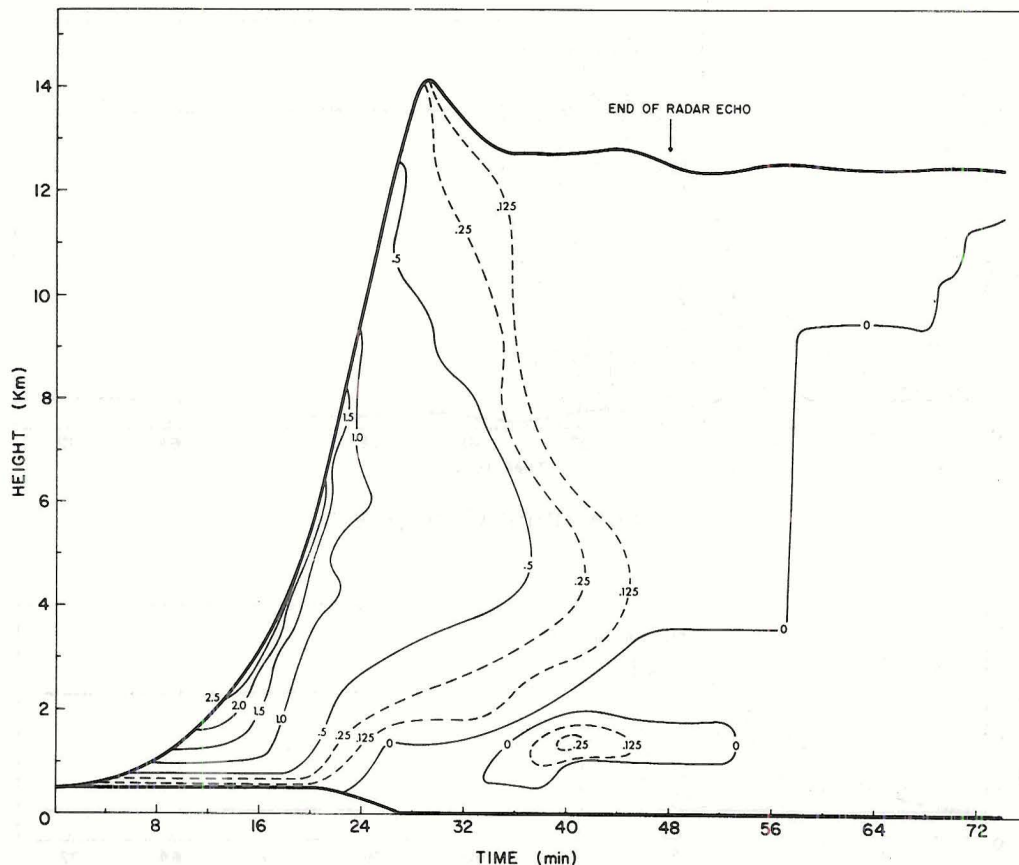


b. Towering Cumulus



c. Small Cumulus

respectively. These values are comparable to typical concentrations of total liquid water measured in hurricane clouds by Ackerman (1963). Peak values as high as 6 gm/m^3 of hydrometeor water have been reported for tropical clouds over the Caribbean by Mee and Takeuchi (1968) and over south Florida by Simpson and Woodley (1968). In the case of the Cb, a zone of hydrometeor water accumulation develops at five kilometers of height. Zones of accumulation are found in the towering and small cumuli at a height of about one km. Shortly after the peak values of water are reached, downdrafts develop in the lower parts of the clouds, extending in time throughout the entire depth

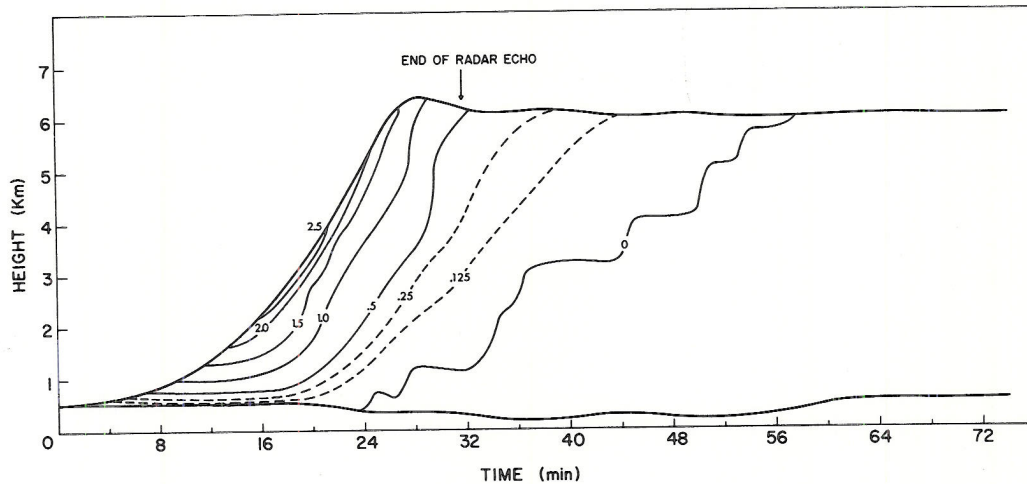


a. Cumulonimbus

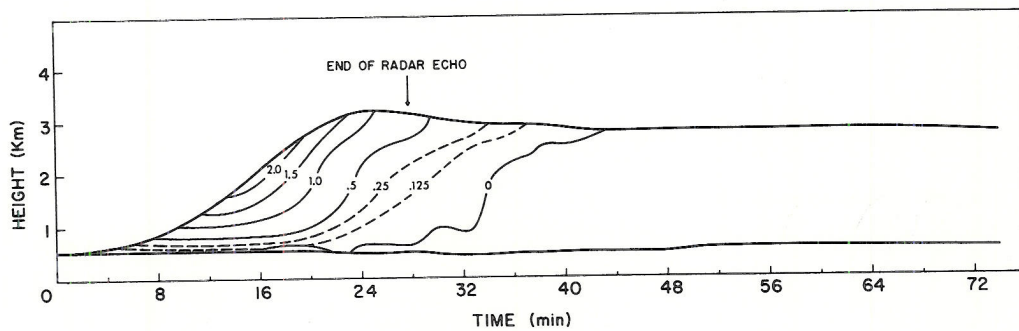
Figs. 11a-c. Time-height sections of cloud water content (small droplets) (gm/m^3) at the core of three typical clouds.

of the column. The accumulation zones of hydrometeor water are present for about ten minutes only. As time progresses, the water content becomes much more uniform with height and of a gradually diminishing magnitude. No significant rain water is present in the Cb after about 48 minutes, nor after 32 and 30 minutes in the case of the TWG and small Cu, respectively.

Cloud Liquid Water Content. Fig. 11 portrays the time-height sections of cloud liquid water content (concentration of droplets with diameter less than about 100μ) at the core of the three typical clouds.



b. Towering Cumulus



c. Small Cumulus

The maximum values reached by the three clouds are very close together and range from 2 to 2.5 gm/m^3 . Values above 1 gm/m^3 are concentrated in the first 20 minutes of cloud life only. During this time the cloud updraft is very strong and the condensation rate (and attending production of small droplets) is consequently fast. After that, as the updraft weakens and the hydrometeor water increases, the concentration of small cloud droplets diminishes considerably as a result of the reduced condensation rate and the increased collection activity of the numerous hydrometeor particles. As rain water falls through the lower layers of the cloud, the cloud liquid water is

depleted by collection until these layers become devoid of any small suspended liquid water droplets. The lower limit of the visual cloud will be seen rising as explained previously. In the case of the Cb, once the bulk of the rain droplets have fallen through, a weak updraft develops in the lower layers of the cloud at around 40 minutes. As a result of the weak ascent, a shallow layer of condensation occurs that is reflected as a small "cloud" underneath the main visible cloud mass. This "scud" cloud material is often observed around and underneath large cumuli.

Geometrical Shape of the Clouds

Figs. 12 to 14 represent the variation with time of the geometrical shape of the three typical clouds. Vertical profiles of the external radius of the clouds are presented at intervals of 4 minutes. The solid-line contours outline the portion of the cloud which would be visible to the eye (i. e., cloud liquid water content non-zero), while the dashed lines delineate that part of the cloud mass without suspended liquid water and therefore invisible or clear.

In particular, Fig. 12 illustrates the changes in shape that the Cb cloud experiences throughout its lifetime. In the very early stages of growth, the cloud appears as a flattened, shallow dome. After about 12 minutes of life, considerable vertical development occurs and the cloud acquires a columnar profile as the upper layers accelerate. The top of the cloud, however, moves at a lower speed than the layers

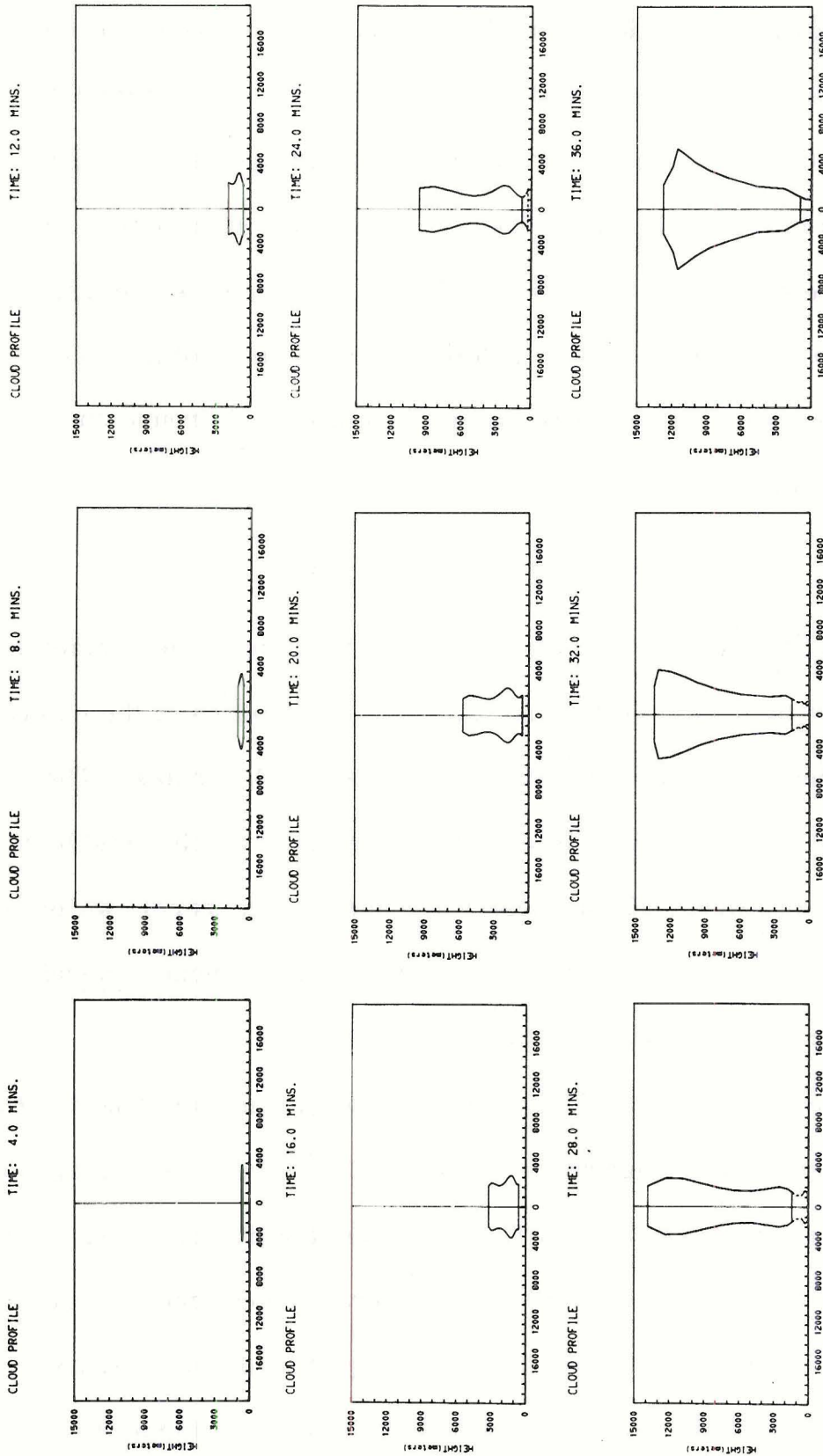


Fig. 12. Vertical profiles of the external radius (m) of the cumulonimbus cloud at intervals of four minutes. Solid lines delineate the visible portion of the cloud (cloud liquid water content non-zero) while the dashed lines trace the contours of the invisible or clear parts (no suspended liquid water).

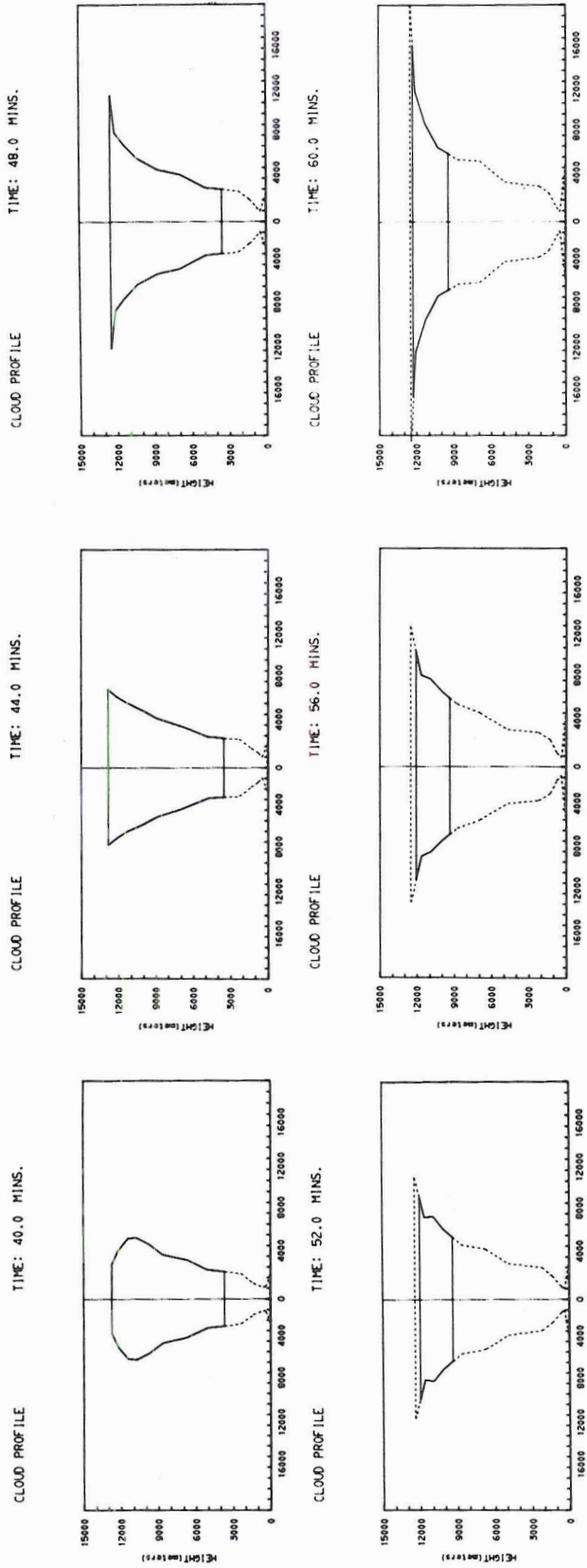


Fig. 12. (Continued)

immediately behind. This slowing down results from the form drag and the stronger diluting effect of entrainment experienced by the cap of the cloud. The velocity gradient across the upper layers results in squeezing and radial spreading of the mass of the cloud at the top. Because of the vortex rotation parameterized in the model (Fig. 2), the squeezed-out mass is allowed to rotate and move down along the sides of the cloud into the layers below. In this manner a gentle bulging of the cloud is observed, instead of the unrealistically large radial expansion that would be produced if the vortex motion were not taken into account.

The top of the cloud soon overshoots its equilibrium level and starts sinking against the still rising layers below. Thus, gradual expansion of the upper layers occurs, which leads to the development of an anvil. Meanwhile, the vertical extent of the visual cloud has diminished, as the visual cloud-base appears at higher and higher levels. By 60 minutes only a shallow layer of cloud remains visible, extending horizontally to about 20 km from the axis of the cloud.

The towering and small cumuli (Figs. 13 and 14) go through a similar pattern of profile changes, except that no anvil is developed. Only a slight bulging is experienced at the top and the visual cloud dissipates as a small flattened dome.

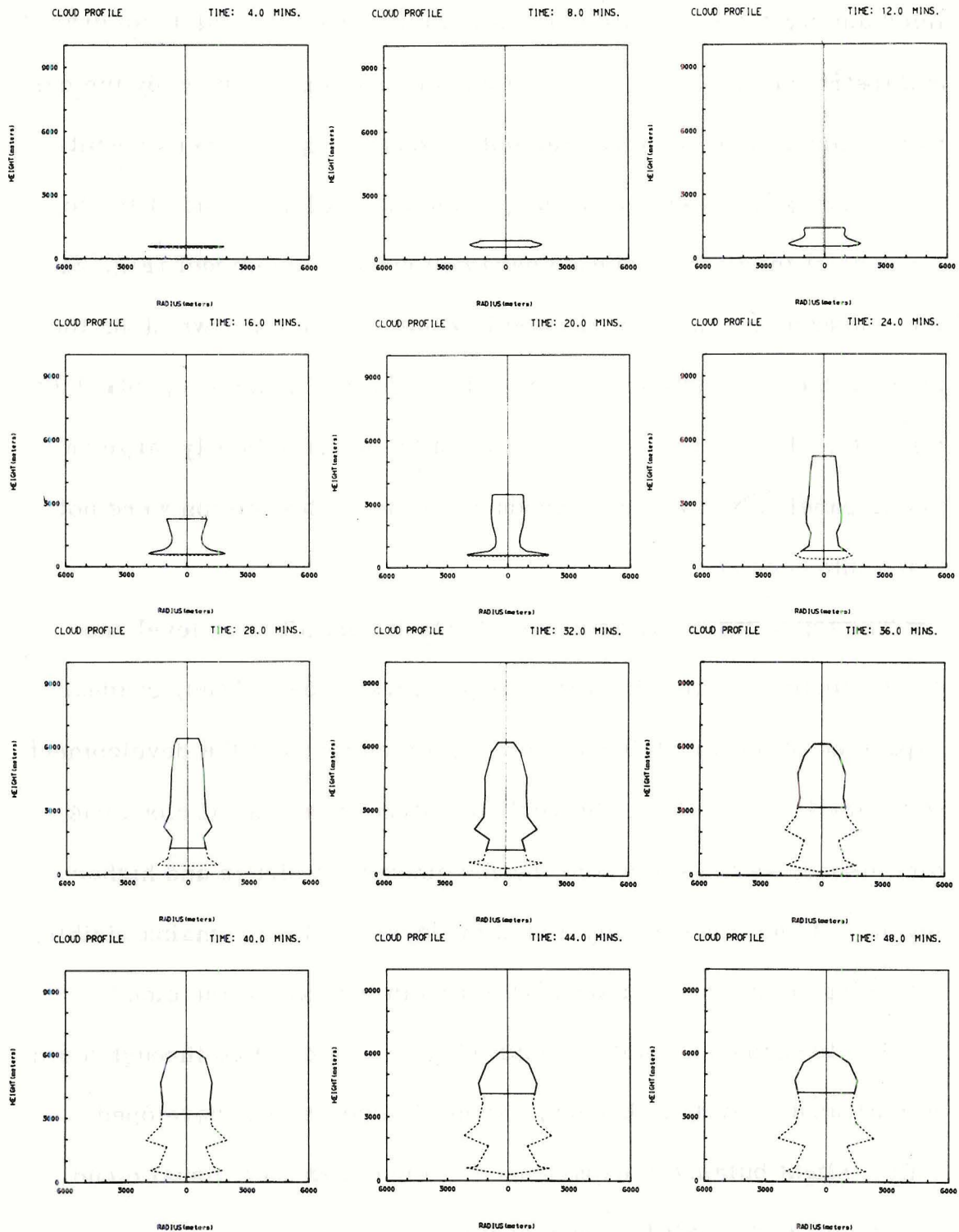


Fig. 13. Vertical profiles of the external radius (m) of the towering cumulus cloud at intervals of four minutes. Solid lines delineate the visible portion of the cloud (cloud liquid water content non-zero) while the dashed lines trace the contours of the invisible or clear parts (no suspended liquid water).

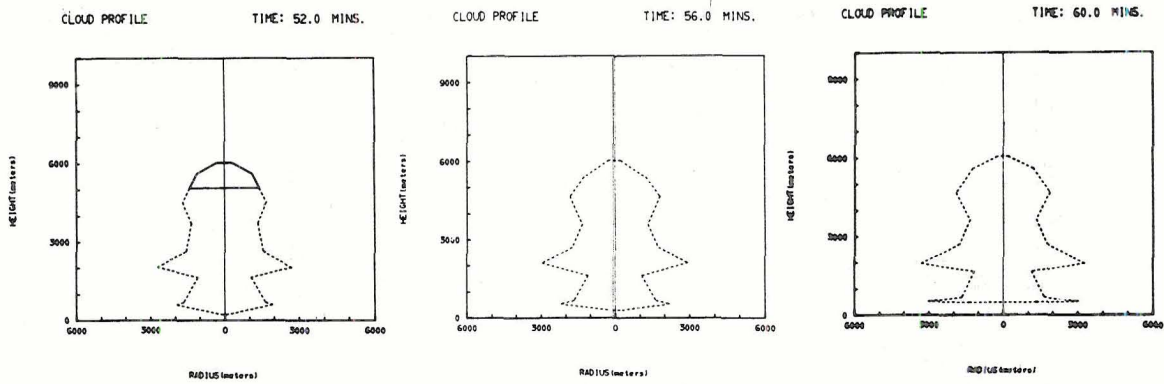


Fig. 13. (Continued)

Comparison of Some Properties of the Shell and Core

Vertical Velocity. Fig. 15 portrays vertical profiles of the vertical velocity of the core and outer shell of the cumulonimbus cloud at intervals of four minutes. The solid lines correspond to the outer shell and the dashed lines to the core of the cloud. It is interesting to note that the updraft velocity is considerably higher in the protected core than in the exposed shell. At some times this difference amounts to more than 10 m/sec. Thus, the protection from the diluting effect of entrainment afforded to the core by the shell is of considerable importance to the dynamics of the cloud.

The profiles also indicate the damping influence exerted by the form drag and increased entrainment that is experienced in the upper layers. In some instances, the deceleration from these effects is shown to be almost 10 m/sec in two km of height.

Liquid Water Content. Fig. 16 shows vertical profiles of the total liquid water content of the core and outer shell of the cumulonimbus

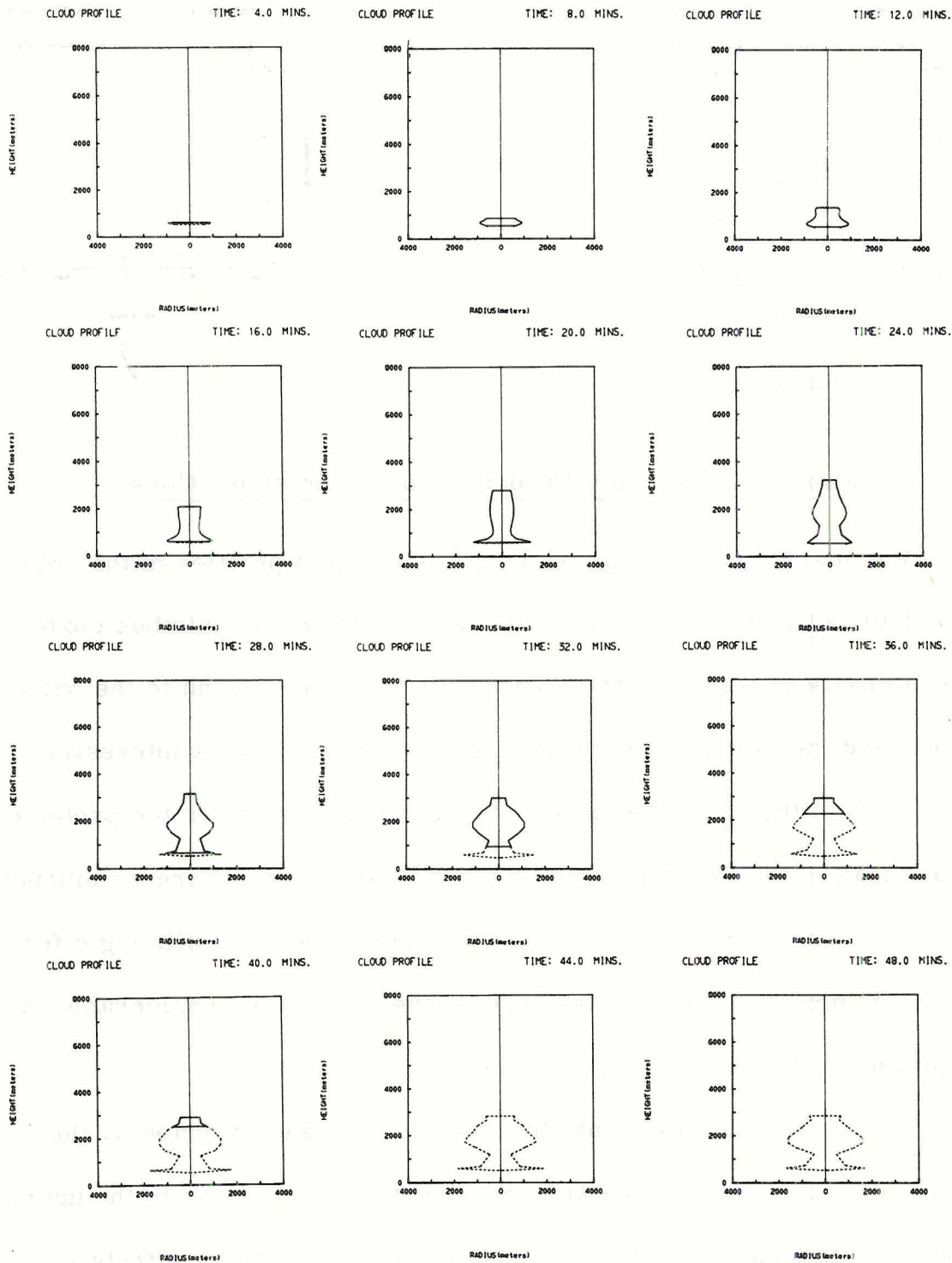


Fig. 14. Vertical profiles of the external radius (m) of the small cumulus cloud at intervals of four minutes. Solid lines delineate the visible portion of the cloud (cloud liquid water content non-zero) while the dashed lines trace the contours of the invisible or clear parts (no suspended liquid water).

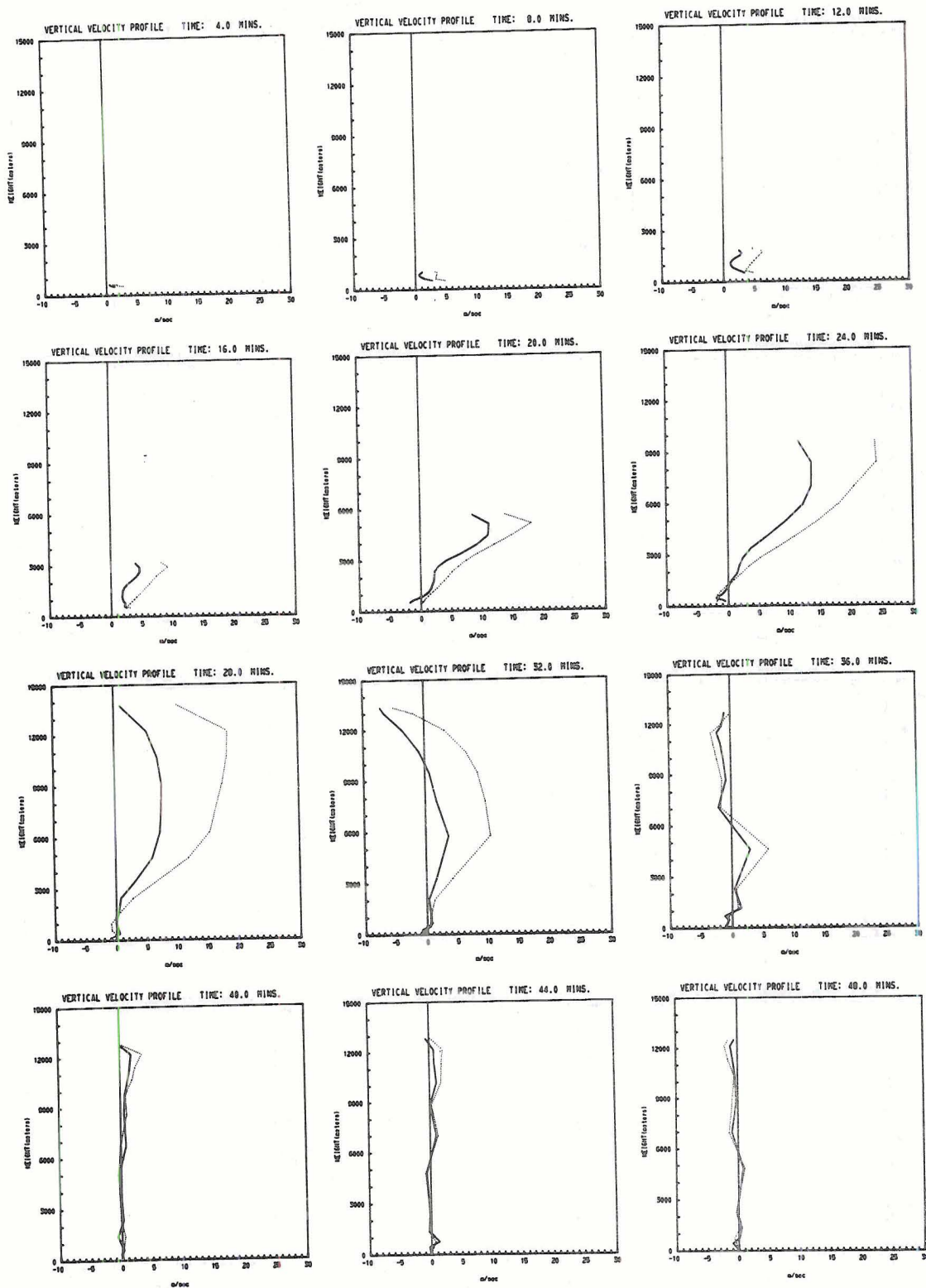


Fig. 15. Vertical profiles of the vertical velocity of the core (dashed lines) and outer shell (solid lines) of the cumulonimbus cloud at intervals of four minutes. The ordinate is calibrated in units of 1000 meters, while the abscissa is calibrated in units of one m/sec.

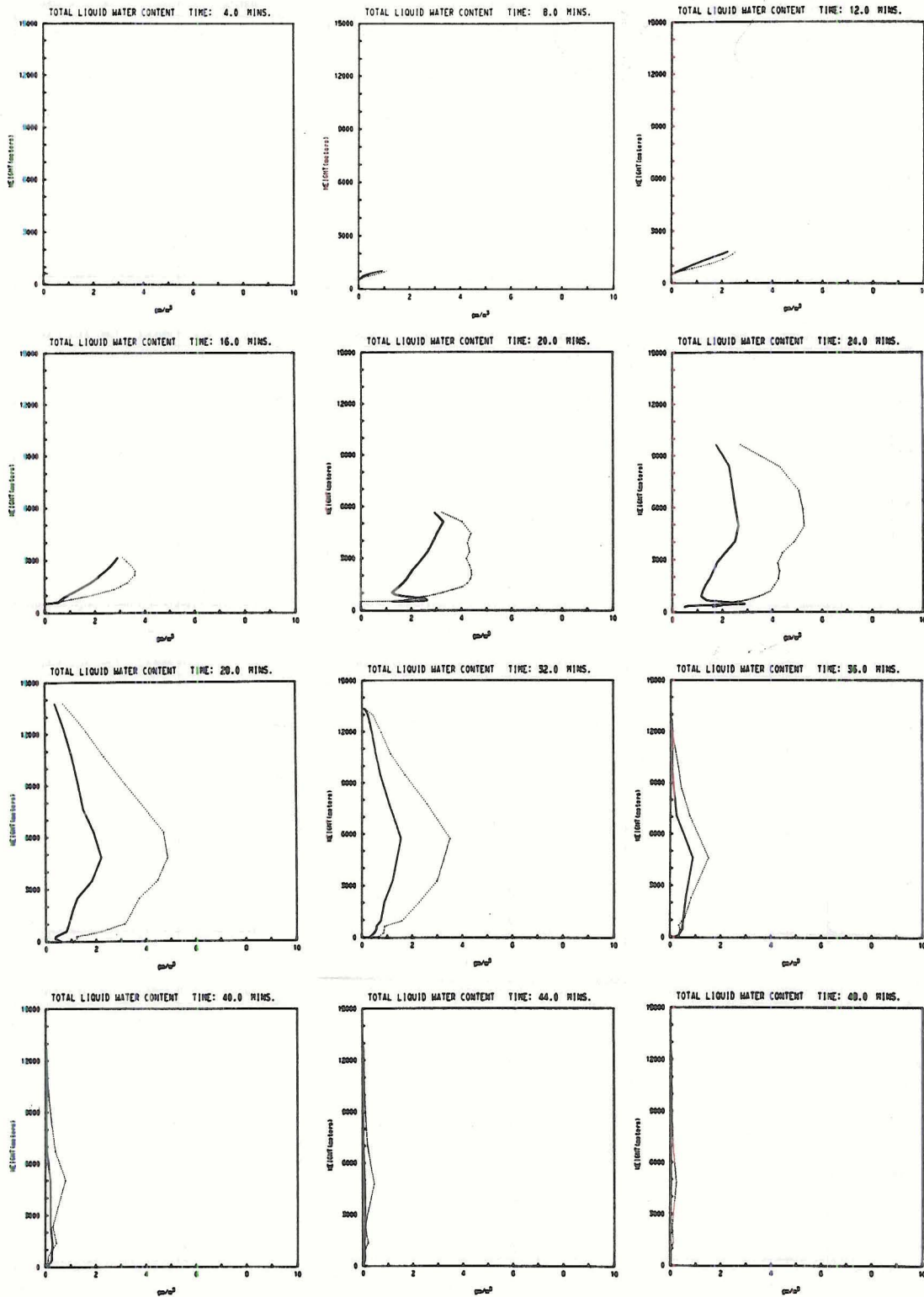


Fig. 16. Vertical profiles of the total liquid water content of the core (dashed lines) and outer shell (solid lines) of the cumulonimbus cloud at intervals of four minutes. The ordinate is calibrated in units of 1000 meters, while the abscissa is calibrated in units of one gm/m^3 .

cloud at intervals of four minutes. The solid lines correspond to the shell and the dashed lines to the core of the cloud. Again the difference between protected and exposed regions is very marked. In most cases the total liquid water of the core is twice the value for the shell. The profiles also indicate that the maximum liquid water is present at the middle of the cloud and that from here the values taper to zero toward both the top and the bottom of the cloud.

Sensitivity of the Model to the Different Controlling Parameters and Initial Conditions

Effect of Varying the Initial Updraft Radius. In order to investigate the importance of the radius of the initial updraft, three clouds were simulated with different initial radii, but having otherwise identical parameters. Fig. 17 presents the growth curves (cloud-top height versus time) of the different clouds. The cloud having an initial radius of 2000 meters rose to a height of 10.5 km, while the clouds with a radii of 1000 and 500 meters attained maximum heights of 6.5 and 3.0 km respectively. Thus, it can be seen that the radius of the initial updraft is a very strong factor in determining the overall dynamics of a cloud. This influence is probably linked to the effect of entrainment on the thermodynamics of the cloud, which is dependent on the surface-to-volume ratio of the cloud parcels. Thus, parcels having smaller radii will be diluted more by the entrainment of dryer, cooler air than the parcels of larger dimensions.

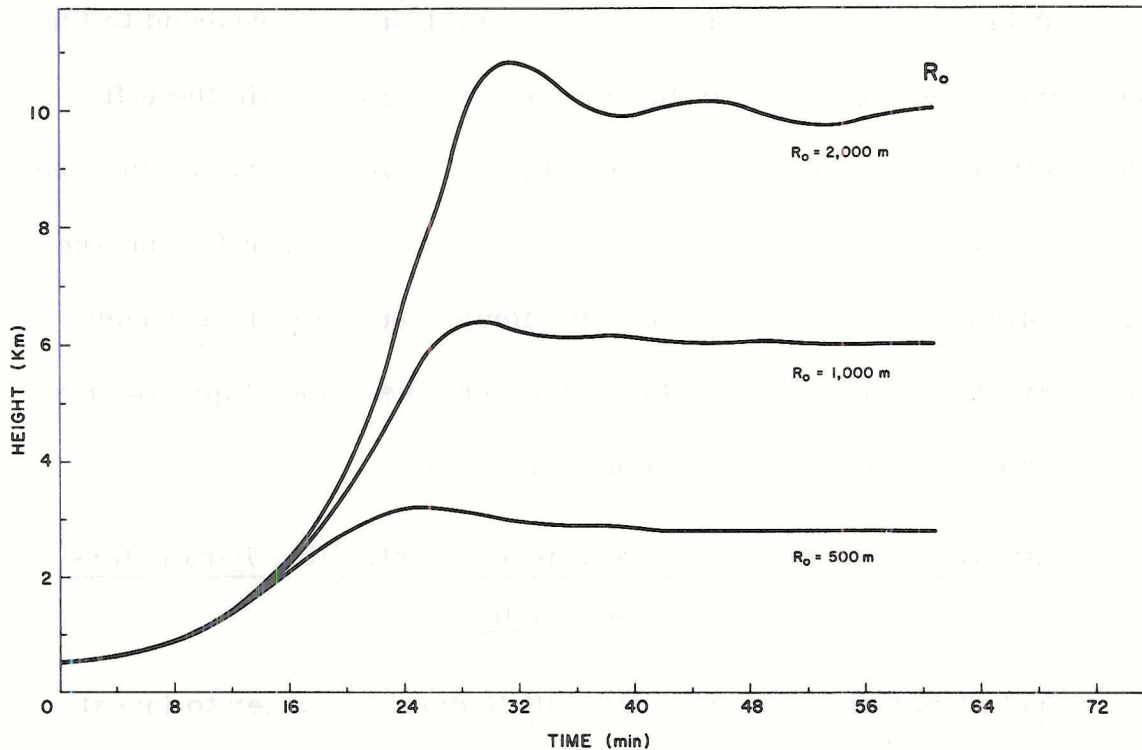


Fig. 17. Comparison of the growth curves of clouds with different initial radii (R_o) but having otherwise identical parameters. ($T_o = 15$ mins, $Div = -5 \times 10^{-3} \text{ sec}^{-1}$, $C_D = .3$, $K_1 = .5$, $\epsilon = .3$, $dt = 7.5$ secs).

Effect of Varying the Duration of the Initial Forcing. The importance of the duration of the initial updraft was similarly investigated by simulating three clouds with different updraft durations, but holding the other parameters (including the radius and peak value of the initial updraft) constant. Fig. 18 portrays the growth curves of the three different clouds. The cloud with an initial updraft lasting 10 minutes attained a maximum height of 5.5 km. When the duration of the initial forcing is increased to 15 minutes the cloud grows one km taller. However, increasing the forcing to 20 minutes has a much smaller effect. Thus, although the duration of the sub-cloud layer

forcing does control the overall dynamics of a cloud, a point is reached when increasing the duration of the forcing does not greatly change the rate of ascent and the maximum height attained by the convective element. This point is probably controlled by other initial conditions such as the size and magnitude of the forcing updraft.

Effect of Varying the Initial Convergence of Mass Under Cloud-Base. The sub-cloud layer convergence determines the magnitude of the initial updraft. Together with the radius and duration of the initial forcing, it determines the amount of sub-cloud air available for storm growth. Its effect on the overall dynamics of a cloud can be ascertained by computing the growth curves of various clouds with different sub-cloud layer convergence but having all other parameters constant. Fig. 19 shows the growth curves for three such clouds. A cloud having a sub-cloud convergence of 10^{-3} sec^{-1} (peak initial updraft of 0.5 m/sec) reaches only a height of about 1.5 km. On the other hand increasing the convergence of 10^{-3} sec^{-1} (initial updraft maximum of 2.5 m/sec) carries the cloud to a maximum height of 6.5 km in. A value of 10^{-2} sec^{-1} (5 m/sec) increases further the maximum height of the cloud to 8.5 km. Thus, we can say that the value of the low-level convergence, together with the radius of the initial updraft are the two most important initial conditions in determining the overall dynamics of a cloud. These two conditions, and the duration of the initial forcing, will determine the amount of latent energy supplied to the cloud from the boundary layer.

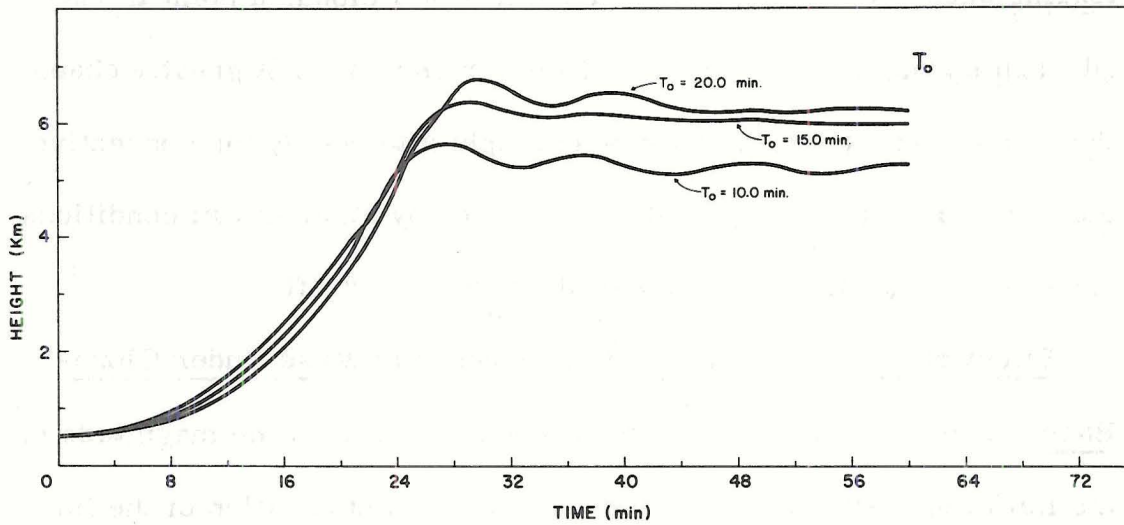


Fig. 18. Comparison of the growth curves of clouds with different durations of the initial forcing (T_0) but having otherwise identical parameters. ($R_0 = 1,000$ m, $\text{Div} = -5 \times 10^{-3} \text{sec}^{-1}$, $C_D = .3$, $K_1 = .5$, $\epsilon = .3$, $dt = 7.5$ secs).

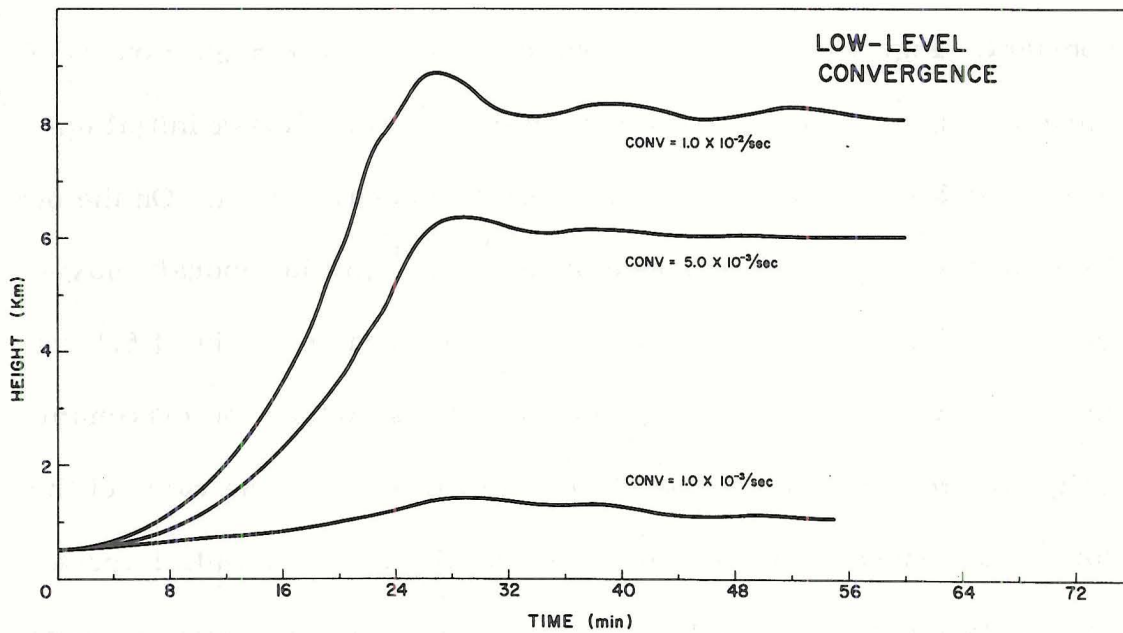


Fig. 19. Comparison of the growth curves of clouds with different initial forcings (convergence) under cloud base but having otherwise identical parameters. ($R_0 = 1,000$ m, $T_0 = 15$ mins, $C_D = .3$, $K_1 = .5$, $\epsilon = .3$, $dt = 7.5$ secs).

The mechanism that determines the type of forced updraft that the boundary layer will produce in a particular case, is not well understood. It is possible that the clouds themselves take part in controlling the production of boundary-layer forced updrafts. In the case of very large clouds, in particular, it is difficult to conceive how the large, strong, and long-lasting currents of sub-cloud air needed for development could be furnished spontaneously by the convective instability of the boundary layer. Instead, the clouds themselves could organize and control the sub-cloud layer so that it can produce the large mass-flux needed for the development of increasingly larger clouds.

There are several mechanisms which can be responsible for the production of strong forced updrafts from the sub-cloud layer. The principal ones are:

1. The concentration of large-scale horizontal wind shears in the boundary layer into small regions of intense positive vorticity. The strong frictionally induced vertical velocity could provide the forcing needed for the development of large clouds.
2. The production of a local mass sink in the boundary layer by a rapidly ascending buoyant parcel. The rapid mass convergence that would result from the temporary mass sink could provide the steady flux of boundary layer needed for cloud growth.
3. The development of downdrafts by the falling rain.
4. The development of horizontal pressure gradients in the boundary layer as a result of a tall cloud rising up in strong vertical wind shears.

Effect of Varying the Drag Coefficient. The drag coefficient is an indication of the retardation suffered by the cloud as it grows and forces the air to flow around it. The sensitivity of the model to this effect can be ascertained by simulating clouds with different coefficients but with all other parameters constant. Fig. 20 presents the growth curves of three such different clouds. Assuming no drag coefficient results in a cloud that reaches the 8 km level in 26 minutes. Increasing the drag coefficient to .3 and .6 the clouds attain the lower heights of 6.5 and 4.5 km and also take longer to reach maximum development, 30 and 32 minutes respectively. The drag coefficient is thus a very important factor in controlling the overall dynamics of cumulus clouds simulated with the present model. The typical value used in the model is 0.3. This value was chosen a priori by considering the typical Reynolds number of the atmosphere and by reference to classical laboratory experiments of form-drag retardation on cylinders (Prandtl and Tietjens, 1934).

Effect of Varying the Autoconversion Threshold. The autoconversion threshold is an indication of the colloidal stability of the clouds. If the threshold is very high, rain particles ($>100\mu$) will be slow in forming by the autoconversion process (diffusional growth). On the other hand, if the threshold is small rain particles will form very rapidly. The effect of this parameter on the dynamics of a cloud can be brought out by considering the growth characteristics of clouds having different autoconversion threshold but otherwise similar

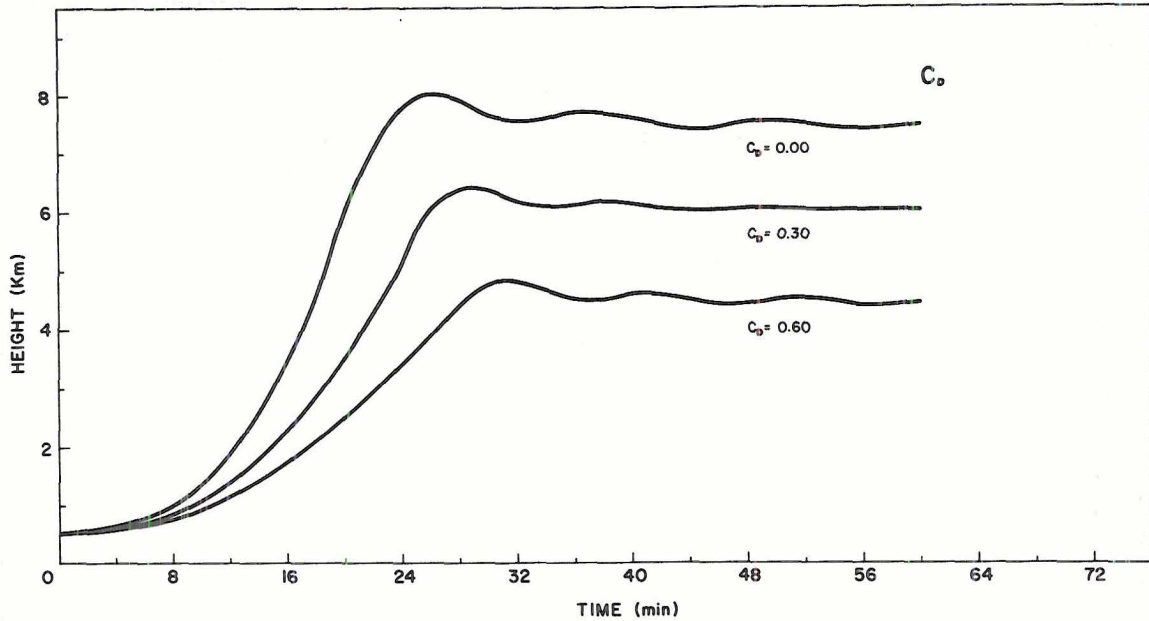


Fig. 20. Comparison of the growth curves of clouds with different drag coefficients (C_D) but having otherwise identical parameters. ($R_0 = 1,000$ m, $T_0 = 15$ mins, $\text{Div} = -5 \times 10^{-3} \text{sec}^{-1}$, $K_1 = .5$, $\epsilon = .3$, $dt = 7.5$ secs).

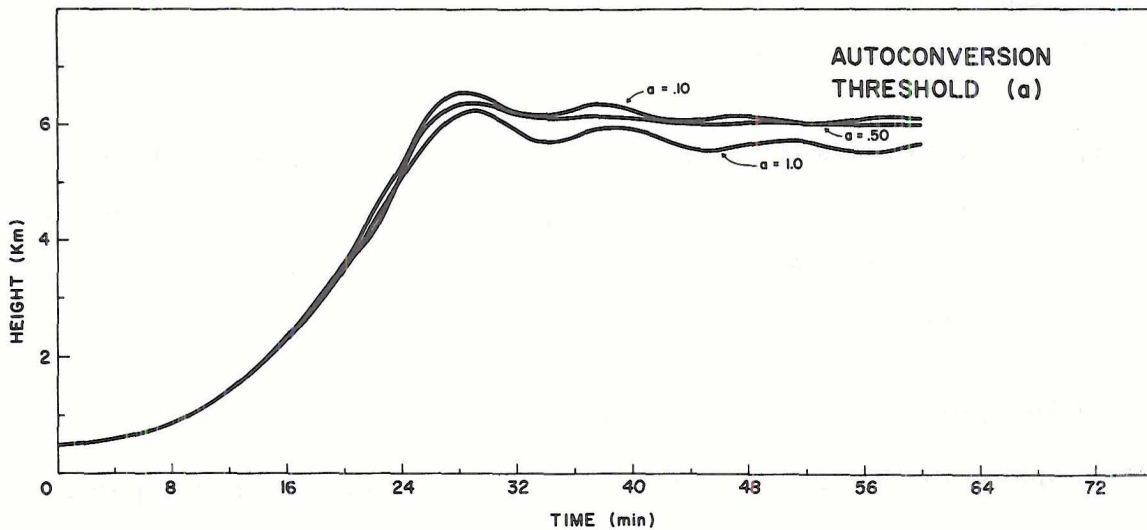


Fig. 21. Comparison of the growth curves of clouds with different autoconversion threshold (α) but having otherwise identical parameters. ($R_0 = 1,000$ m, $T_0 = 15$ mins, $\text{Div} = -5 \times 10^{-3} \text{sec}^{-1}$, $C_D = .3$, $\epsilon = .3$, $dt = 7.5$ secs). The units of α are gm/m^3 .

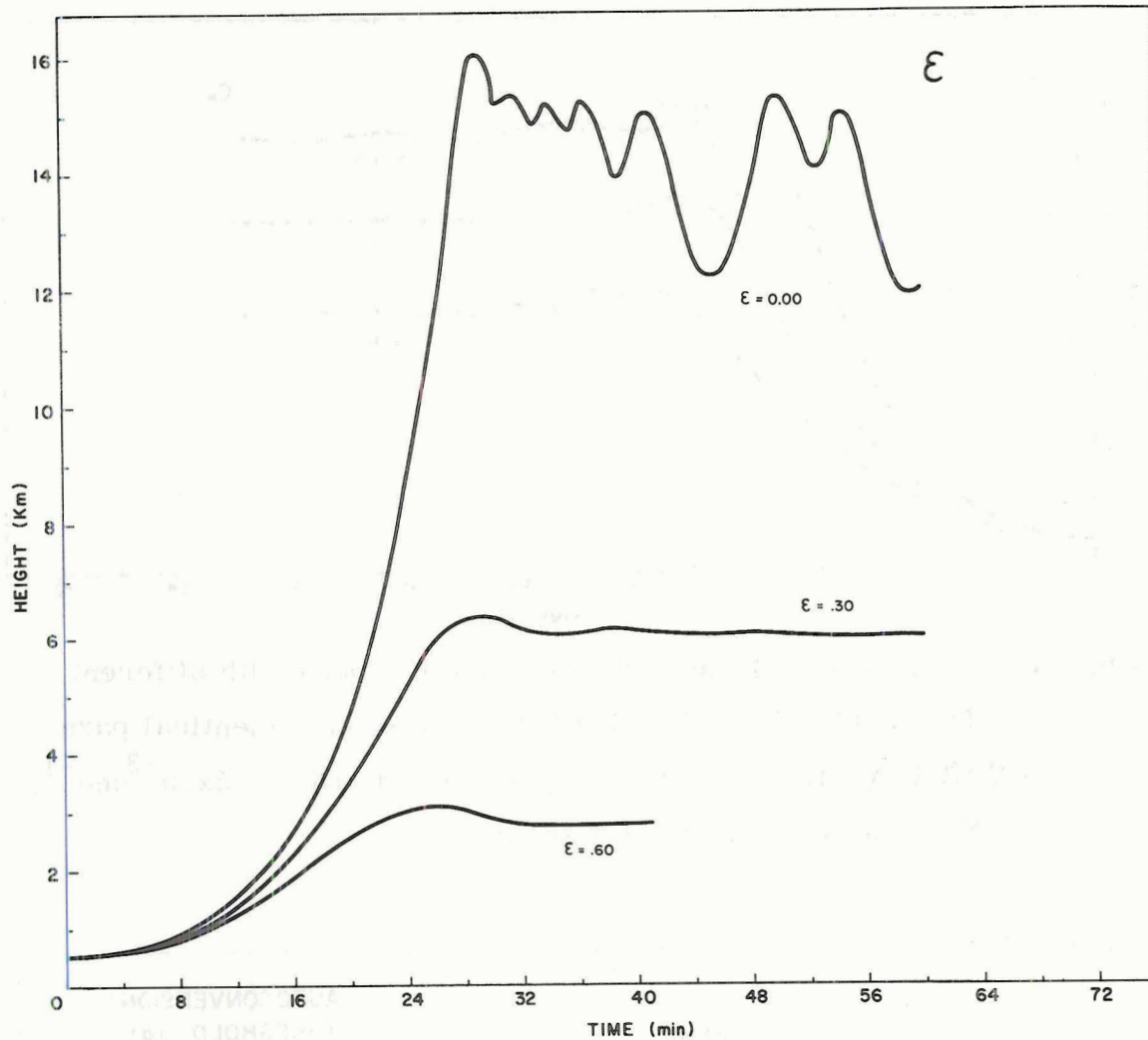


Fig. 22. Comparison of the growth curves of clouds with different entrainment coefficients (ϵ) but having otherwise identical parameters. ($R_0 = 1,000$ m, $T_0 = 15$ mins, $\text{Div} = -5 \times 10^{-3} \text{ sec}^{-1}$, $C_D = .3$, $K_1 = .5$, $dt = 7.5$ secs).

parameters. This is shown in Fig. 21. Although values of the autoconversion threshold ranging from 0.1 to 1.0 were used no significant difference in the growth curves of the different clouds is observed. The microphysical processes as simulated by the present model appear to be rather insensitive to the autoconversion threshold. This is probably due to the high moisture content of the tropical sounding used.

Because of this, large cloud-water levels are invariably attained in the early stages of cloud growth. Thus, even if the autoconversion threshold is high, hydrometeor particles will be formed almost as rapidly as with low threshold values. Once these rain particles are present, the collection process dominates the picture and the importance of the autoconversion threshold is overshadowed.

Effect of Varying the Entrainment Coefficient. The sensitivity of the model to the value of the entrainment coefficient is indicated in Fig. 22, where growth curves for three clouds differing only in their entrainment coefficient are presented. The differences in the growth characteristics are very large. The cloud with no entrainment reaches a maximum height of 16 km and performs violent oscillations around its equilibrium level. A much lower height of 6.5 km is reached by the cloud having an entrainment coefficient of 0.3. The oscillations around its equilibrium level also become more dampened and slower. Increasing the entrainment coefficient to 0.6 further reduces the maximum height of the cloud to only 3 km. The value used in this model for the entrainment constant is 0.3. This value was also chosen a priori by reference to laboratory experiments.

Effect of Different Levels of Environmental Turbulence. In order to study the effect of the turbulence intensity of the environment on the development of a cloud, two different simulations were performed with identical conditions except for the kinematic viscosity coefficient used in equations (86). In one case, the values of Frost (1948) were

used, while in the other, the larger values of Gray (1966) representing hurricane conditions were utilized (Fig. 5). The different growth curves are presented in Fig. 23. The effect of the increased turbulence of the environment is to stunt the growth of the cloud and to dissipate much faster the mass of the cloud, especially at the top. As a result, the vertical extent of the cloud is severely reduced after reaching the (already smaller) maximum height. The effect of an increased environmental turbulence acts both in a direct and indirect way. In the direct way, the mass of the cloud is eroded away rapidly. Indirectly, this reduced mass is reflected in a smaller radius, a large surface-to-volume ratio of the parcels, and consequently a much greater dilution and reduction of the intensity of the cloud.

Effect of Varying the Computational Time Step. Growth curves for clouds simulated with different computational time-steps, but with all other conditions kept the same, are portrayed in Fig. 24. The effect of varying the integration interval from 3.75 to 15.00 seconds is very small. After several trials it was decided that a value of 7.5 seconds was the optimum one providing a very good compromise between computer economy and accuracy of results.

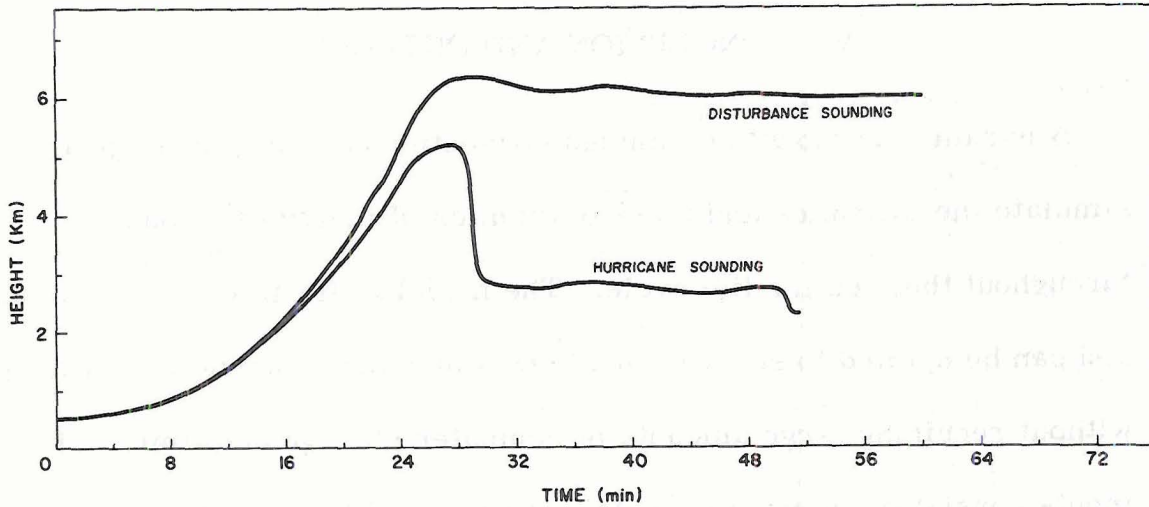


Fig. 23. Comparison of the growth curves of clouds with different environmental turbulence level but having otherwise identical parameters. ($R_0 = 1,000$ m, $T_0 = 15$ mins, $\text{Div} = -5 \times 10^{-3} \text{ sec}^{-1}$, $C_D = .3$, $K_1 = .5$, $\epsilon = .3$, $dt = 7.5$ secs).

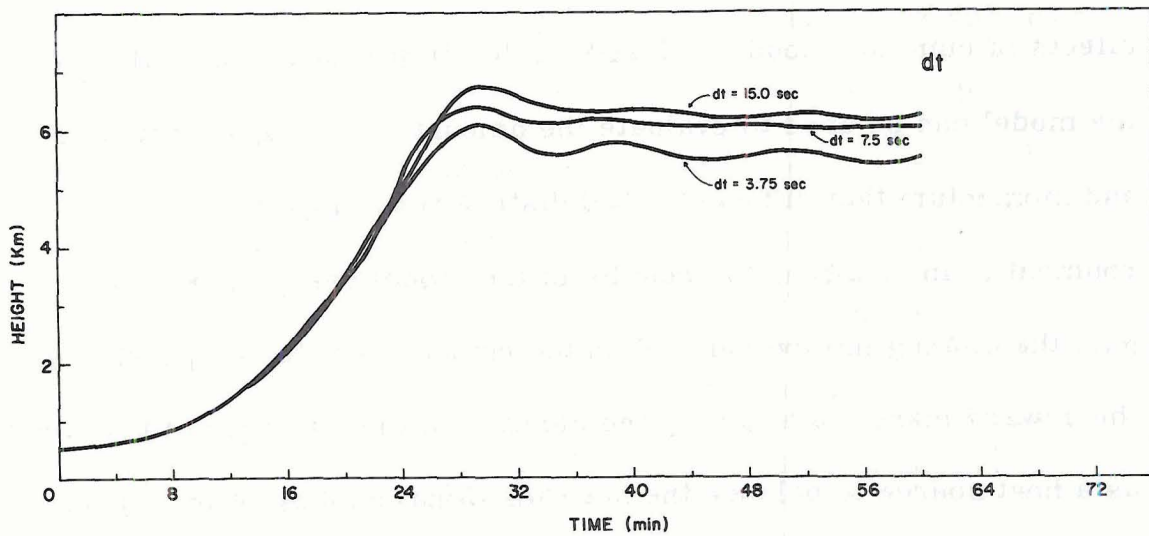


Fig. 24. Comparison of the growth curves of clouds with different computational time steps (dt) but having otherwise identical parameters. ($R_0 = 1,000$ m, $T_0 = 15$ mins, $\text{Div} = -5 \times 10^{-3} \text{ sec}^{-1}$, $C_D = .3$, $K_1 = .5$, $\epsilon = .3$).

BIBLIOGRAPHY

- Ackerman, B., 1963: Some observations of water content in hurricanes. J. Atmos. Sci., 20, 288-298.
- Austin, J. M., and A. Fleisher, 1948: A thermodynamic analysis of cumulus convection. J. Meteor., 5, 240-243.
- Byers, H. R., and Braham, R. R., Jr., 1949: The Thunderstorm. U. S. Weather Bureau, Washington.
- Das, P., 1964: Role of condensed water in the life cycle of a convective cloud. J. Atmos. Sci., 21, 404-418.
- Dufour, L., 1956: Thermodynamical study of the entrainment of air into a cumulus. Tellus, 8, 202-205.
- Frost, R., 1948: Atmospheric turbulence. Quart. J. Roy. Meteor. Soc., 74, 316-338.
- Gray, W. M., 1966: On the scales of motion and internal stress characteristics of the hurricane. J. Atmos. Sci., 23, 278-288.
- Kessler, E., 1969: On the Distribution and Continuity of Water Substance in Atmospheric Circulations. Meteorological Monograph, American Meteorological Society, Boston, Vol. 10, No. 32, 84 pp.
- Lamb, H., 1945: Hydrodynamics. Dover Publications, Inc., New York, 738 pp.
- List, R., and E. P. Lozowski, 1970: Pressure perturbations and buoyancy in convective clouds. J. Atmos. Sci., 27, 168-170.
- Lozowski, E. P., and R. List, 1969: Updraft divergence associated with hydrometeor drag: A numerical computation. Proc. 6th Conf. on Severe Storms, 55-58.
- Malkus, J. S., and H. Riehl, 1964: Cloud structure and distribution over the tropical Pacific Ocean. Tellus, 16, 275-287.
- Marshall, J. S., and W. Palmer, 1948: Shorter contributions--the distribution of raindrops with size. J. Meteor., 5, 165-166.
- Mee, T. R., and D. M. Takeuchi, 1968: Natural Glaciation and Particle Size Distribution in Marine Tropical Cumuli, Final Report.

BIBLIOGRAPHY (cont'd)

- MR168 FR-823, Meteorology Research Inc., Altadena, California, August, 71 pp.
- Morton, B. R., 1968: Non-similar Turbulent Plumes. Dept. of Mathematics GFDL Paper #7, Geophysical Fluid Dynamic Lab., Monash University, Clayton, Victoria 3168, Australia, 50 pp.
- Murray, F. W., 1967: Numerical Simulation of Cumulus Convection. Memorandum RM-5316-NRL, The Rand Corp., April, 34 pp.
- _____, 1968: Numerical Models of a Tropical Cumulus Cloud with Bilateral and Axial Symmetry. Memorandum RM-5870-ESSA, The Rand Corp., November, 48 pp.
- Ogura, Y., 1962: Convection of isolated masses of a buoyant fluid: A numerical calculation. J. Atmos. Sci., 19, 492-502.
- _____, 1963: The evolution of a moist convection element in a shallow, conditionally unstable atmosphere: A numerical calculation. J. Atmos. Sci., 20, 407-424.
- _____, and N. Phillips, 1962: Scale analysis of deep and shallow convection in the atmosphere. J. Atmos. Sci., 19, 173-179.
- Orville, H. D., 1965: A numerical study of the initiation of cumulus clouds over mountainous terrain. J. Atmos. Sci., 22, 684-699.
- _____, 1968: Ambient wind effects on the initiation and development of cumulus clouds over mountains. J. Atmos. Sci., 25, 385-403.
- _____, and L. J. Sloan, 1970: A numerical simulation of the life history of a rainstorm. J. Atmos. Sci., 27, 1148-1159.
- Prandtl, L., and O. G. Tietjens, 1957: Fundamentals of Hydro- and Aeromechanics. Dover Publications, Inc., New York, 270 pp.
- Saunders, P. M., 1957: The thermodynamics of saturated air: A contribution to the classical theory. Quart. J. Roy. Meteor. Soc., 83, 342-350.
- Scorer, R. S., 1957: Experiments on convection of isolated masses of buoyant fluid. J. Fluid Mech., 2, 583-594.

BIBLIOGRAPHY (cont'd)

- _____, and C. Ronne, 1956: Experiments with convection bubbles. Weather, 11, 151-154.
- Simpson, J., R. Simpson, D. Andrews and M. A. Easton, 1956: Experimental cumulus dynamics. Rev. Geophys., 3, 387-431.
- Simpson, J., and V. Wiggert, 1969: Models of precipitating cumulus towers. Mon. Wea. Rev., 97, 471-489.
- _____, 1971: 1968 Florida cumulus seeding experiments: Numerical model results. Mon. Wea. Rev., 99, 87-118.
- Simpson, J., and W. L. Woodley, 1969: Intensive Study of Three Seeded Clouds on May 16, 1968. ESSA Technical Memorandum ERLTM-APCL8.
- Spilhaus, A. F., 1948: Raindrop size, shape, and falling speed. J. Meteor., 5, 108-110.
- Srivastava, R. C., 1964: A Model of Convection with Entrainment and Precipitation. Scientific Report MW-38, Stormy Weather Group, McGill University.
- _____, 1967: A study of the effect of precipitation on cumulus dynamics. J. Atmos. Sci., 24, 36-45.
- _____, and D. Atlas, 1969: Growth, motion and concentration of precipitation particles in convective storms. J. Atmos. Sci., 26, 535-544.
- Stommel, H., 1947: Entrainment of air into a cumulus cloud. J. Meteor., 4, 91-94.
- Takeda, Takao, 1969: Numerical Simulation of Large Convective Clouds. Scientific Report MW-64, Stormy Weather Group, McGill University, 65 pp.
- Telford, J. W., 1966: The convective mechanism in clear air. J. Atmos. Sci., 23, 652-666.
- Townsend, A. A., 1956: The Structure of Turbulent Shear Flow. Cambridge University Press, Cambridge, England

BIBLIOGRAPHY (cont'd)

- _____, 1959: Temperature fluctuations over a heated horizontal surface. J. Fluid Mech., 5, 209-219.
- Turner, J. S., 1959: A comparison between buoyant vortex rings and vortex pairs. J. Fluid Mech., 7, 419-432.
- _____, 1962a: The motion of buoyant elements in turbulent surroundings. J. Fluid Mech., 16, 1-16.
- _____, 1962b: The "starting plume" in neutral surroundings. J. Fluid Mech., 13, 356-368.
- _____, 1963: The flow into an expanding spherical vortex. J. Fluid Mech., 18, 195-208.
- Warner, J., 1970: The microstructure of cumulus cloud: Part III. The nature of the updraft. J. Atmos. Sci., 27, 682-688.
- _____, 1970: On steady-state one-dimensional models of cumulus convection. J. Atmos. Sci., 27, 1035-1040.
- Weinstein, A. I., 1970: A numerical model of cumulus dynamics and microphysics. J. Atmos. Sci., 27, 246-255.
- _____, and L. G. Davis, 1968: A Parameterized Numerical Model of Cumulus Convection. Dept. of Meteorology, The Pennsylvania State University, Rpt. No. 11 to the NSF, GS-777, 44 pp.
- Woodley, W. L., 1969: Precipitation Results from a Pyrotechnic Cumulus Seeding Experiment. ESSA Tech. Memorandum ERLTM-AOML 2, August, 50 pp.
- Woodward, Betsy, 1959: The motion in and around isolated thermals. Quart. J. Roy. Meteor. Soc., 85, 144-151.
- Von Miegheem, J., and L. Dufour, 1948: Thermodynamique de L'Atmosphère. Institut Royal Météorologique de Belgique, Mémoires, Vol. xxx, 247 pp.

ACKNOWLEDGMENTS

The author wishes to express his sincere gratitude to Professor William M. Gray under whose guidance this investigation was performed. His kind criticism and encouragement are very much appreciated. Special thanks are due to Mr. Edward Buzzel, Mrs. Barbara Brumit and Mr. Larry Kovacic who helped with the programming, manuscript typing and drafting.

**Cumulus Convection and Larger-Scale Circulations
Part II**

Cumulus and Mesoscale Interactions

By

Raül Erlando López

Principal Investigator
William M. Gray

Department of Atmospheric Science
Colorado State University
Fort Collins, Colorado

**Colorado
State
University**

**Department of
Atmospheric Science**

Paper No. 189

CUMULUS CONVECTION AND LARGER-SCALE CIRCULATIONS

Part II

Cumulus and Meso-Scale Interactions

by

Raúl Erlando López

Preparation of this report

has been supported by

NSF Grant GA 19937

Principal Investigator: William M. Gray

Department of Atmospheric Science

Colorado State University

Fort Collins, Colorado

June 1972

Atmospheric Science Paper No. 189

ABSTRACT

This report (Part II) discusses the magnitude and implication of the vertical circulation patterns of the tropical cloud cluster as derived from cumulus scale and meso scale considerations. It is to be compared with the vertical circulation patterns derived from broad-scale considerations as discussed by Gray (1972) in Part III of this series.

A numerical model of individual convective clouds has been used to investigate the effects of a typical population of cumulus clouds on the large-scale features of a tropical disturbance. The typical cloud population has been determined from radar and synoptic data. Results show that the detrainment of cloud mass from the population produces a net cooling of the air around the clouds. This occurs because the cooling produced by the evaporation of the detrained cloud liquid-water overcompensates the detrainment of sensible heat excess. The typical cumulus population also induces a descending motion in the environment in which the clouds are embedded in order to compensate for the net upward mass-transport of the clouds. The induced subsidence results in the warming and drying of the environment of the clouds.

Using the typical cloud population, a heat and moisture budget for a steady-state tropical disturbance has been computed. Under the assumption of steady-state, the heat liberated in the condensation of rainfall is exported to the exterior in the form of potential energy at the level of the disturbance's outflow after provision is made for the radiational losses. Inside the disturbance the warming resulting from the induced sinking motion is compensated by the net cooling resulting from detrainment plus the cooling resulting from infrared radiational losses. Similarly, the dryness resulting from the induced subsidence is compensated by the detrainment of water vapor and liquid water from the clouds.

A mass budget of the disturbance further reveals that the required vertical mass circulation has a magnitude which is about five times larger than the synoptic mass circulation. The large-scale vertical mass circulation is in fact the residual between the upward mass transport by the clouds and the downward mass transport induced in the environment in which the clouds are embedded. The importance of the results of this investigation on the problem of hurricane development are discussed, and a scheme for the intensification of disturbances into hurricanes is presented.

The vertical circulation requirements of the cloud cluster as determined by this cumulus and meso scale approach compare very closely with the independent larger-scale approach of Gray, 1972 (Part III).

TABLE OF CONTENTS

	Page
ABSTRACT	ii
LIST OF SYMBOLS	v
I. THE INTERACTION OF CUMULUS CLOUDS WITH TROPICAL CLOUD CLUSTERS	1
Introduction	1
II. THE EFFECTS OF DETRAINMENT FROM CUMULUS CLOUD ON THE ENVIRONMENT	5
General Concepts	5
Evaluation of the Net Heating	9
Results of Detrainment from Cumulus Clouds	13
Temperature Changes	13
Moisture Changes	15
Other Evidences of the Direct Cooling Action of Cumulus Clouds	17
The "Cooling Tower" Hypothesis	18
III. THE CONVERGENCE-DIVERGENCE PATTERN INDUCED BY THE CLOUDS	20
General Concepts	20
Evaluation of the Divergence Profile	22
Results of Divergence Computations	22
The Effect of the Divergence Field Produced by the Clouds	25
IV. A MODEL CLOUD POPULATION	27

TABLE OF CONTENTS (cont'd)

	Page
Radar Information	27
A Cloud Population from Radar and Numerical Model Data	29
The Effect of a Typical Cloud Population on the Disturbance's Atmosphere	39
V. THE INTERACTION OF A MODEL CLOUD - POPULATION WITH THE SYNOPTIC FEATURES OF A TYPICAL TROP- ICAL DISTURBANCE	43
Introduction	43
Interaction of a Steady-State Disturbance with the Environment	44
The Interaction of the Model Cloud Population With the Disturbance's Atmosphere	46
Results of the Heat and Moisture Budget	49
Vertical Mass Circulation in a Steady-State Disturbance	53
Developing Disturbances	55
VI. SUMMARY	58
ACKNOWLEDGEMENTS	60
BIBLIOGRAPHY	61

LIST OF SYMBOLS

Geometric Variables

- B - height of the cloud base
- R - radius of a large vertical cylinder enclosing a region of cumulus activity
- r_0 - radius of the forced updraft through cloud base during the growth stage of the cloud
- z - height
- Δz - height of a horizontal section of a cylinder enclosing a region of cumulus activity

Time Variables

- t - time
- dt - small time interval
- Δt - large time interval
- T_0 - duration of the forced updraft through cloud base
- τ_i - lifetime of a cloud of type i

Thermodynamic Variables

- c_p - specific heat at constant pressure for dry air
- L - latent heat of condensation
- Q - heat
- T - temperature
- x_v and x - mixing ratio of water vapor
- ΔQ - total heating of a layer of a disturbance during a long period of time Δt
- ΔT - total change in the temperature of a layer of a disturbance during a long period of time Δt

LIST OF SYMBOLS (cont'd)

ΔX - total change in the mixing ratio of a layer of disturbance during a long period of time Δt

Mass Variables

m - mass of a layer of a disturbance

m_a - mass of dry air

m_v - mass of water vapor

m_w - mass of liquid water

dm - change in mass

dm_a - change in the mass of dry air

dm_v - change in the mass of water vapor

dm_w - change in the mass of liquid water

Δm - total change in the mass of a layer of a disturbance over a long period of time

Δm_a - total change in the mass of a disturbance over a long period of time

Δm_v - total change in the mass of water vapor of a layer of a disturbance over a long period of time

Δm_w - total change in the mass of liquid water of a layer of a disturbance over a long period of time

dm_{det} - change in mass due to detrainment

dm_{ad} - amount of mass advected into the disturbance from the outside

δm_i - amount of mass used up by a cloud of type i during its growth period

Δm_i - amount of sub cloud-layer mass channeled into clouds of type i

LIST OF SYMBOLS (cont'd)

α_i - fraction of the total sub-cloud layer mass convergence going into clouds of type i

ρ_o - density of the sub-cloud layer

Dynamic Variables

W_o - vertical velocity of the forced updraft through cloud base during the cloud's growth period

w_s - vertical velocity of the cloud-free environment

$\nabla \cdot w$ - mean divergence of a layer of a disturbance

$\nabla \cdot w_o$ - total convergence into the clouds from the sub-cloud layer (synoptic plus sub-synoptic)

Miscellaneous

Q_{cl} - cloud water density

N_i - the total number of clouds of type i that is exerted during a time interval Δt

'prime - cloud parcel

"double
prime - entrained parcel

— bar - average quantity

i (subscript) - cloud of type i

I. THE INTERACTION OF CUMULUS CLOUDS WITH TROPICAL CLOUD CLUSTERS

Introduction

The interaction between an ensemble of cumulus clouds and the large-scale features of a tropical disturbance can be visualized as taking place in two reciprocal modes. In one mode, the large-scale synoptic properties of a disturbance will determine the types of cumulus clouds that will be produced, and the relative numbers in which they will be present. In the other mode, once the cloud population is established, the large-scale characteristics of the disturbance will be altered by the collective influence of the individual clouds. The first mode of interaction, or the problem of what determines the type of cloud population present in a disturbance, will not be considered explicitly in this investigation. However, the second mode of interaction, or the influence of the large scale on an ensemble of cumulus clouds will be implicitly considered by making use of a cloud population which is typical of tropical disturbances. This cloud distribution was obtained from actual radar observations and thus incorporates the influence of the large-scale flow on the cloud ensemble.

The way in which a group of cumulus clouds modify and control the large-scale features of a disturbance, will be studied in this investigation by making use of the numerical model of individual cumulus clouds developed in Part I (López, 1972). The main objective is to ascertain

the mechanism by which cumulus clouds impart heat to their environment for the maintenance of the energy budget of the disturbance.

The majority of the previous investigations of the interaction of cumulus clouds with large-scale circulations have been made in connection with the problem of hurricane development from weaker closed vortices. It is generally agreed that cumulus convection produces the energy necessary for hurricane development. However, the mechanism by which cumulus clouds impart their energy to their environment is imperfectly understood. Most of the present hurricane models parameterize the effects of cumulus clouds in terms of the frictionally-induced vertical velocity at the top of the boundary layer (Ooyama, 1963; Charney and Elliasen, 1964; Ogura, 1964; Kuo, 1965; Rosenthal, 1970). The resultant vertical flux of boundary-layer air is assumed to rise in undiluted cumulonimbus towers. As condensation takes place, the temperature of these ascending currents will be warmer than the environment. This excess enthalpy is then assumed to be imparted to the surrounding clear air by an unspecified diffusion mechanism.

The excess sensible heat that a cloud parcel has at a given time, however, is not available to the environment in its entirety. Most of it is converted into potential energy as the warmer parcel continues to rise. Only a fraction of this heat is given directly to the

environment when part of the cloud mass is detrained to the exterior. This exportation of sensible heat from the cloud, however, is counteracted by the simultaneous cooling produced by the evaporation of the detrained cloud water. The net result of the direct diffusion of cloud mass may even result in the cooling of the cloud's environment. Results of the cloud model, developed in Part I, are used in this section to compute the warming due to detrainment for different cloud populations and environmental conditions.

Another way in which cumulus clouds interact with their environment is by generating local mass sources and sinks by virtue of their large upward mass-transport. As a result, a cloud-produced convergence-divergence field is imposed on the environment. A compensatory downward transport of mass will then be induced in the cloud-free regions. With the usually stable stratification of the tropics, considerable compressional warming can result from the descending branch of the convective circulation. The model of Part I is also used to calculate the convergence-divergence field imposed on the environment as a result of the upward mass transport performed by a typical population of cumulus clouds.

The role of detrainment and subsidence on the energetics of a disturbance will be investigated in this section by performing a heat and moisture budget computation on the effects of a typical cloud population on the large-scale vertical pattern of temperature and humidity

of a mean tropical disturbance. The typical cloud population will be obtained by applying the results of the numerical cloud model on radar and synoptic data representative of tropical disturbances.

II. THE EFFECTS OF DETRAINMENT FROM CUMULUS CLOUD ON THE ENVIRONMENT

General Concepts

As a cloud grows and decays, some of its mass is given off to the environment by the process of detrainment. In this way excess sensible heat, liquid water, and water vapor are exported to the surrounding air. The magnitude of these transports depends on the detrainment rate and the thermodynamic properties of the cloud. Thus, the rate at which a layer of an individual cloud gives off excess sensible heat can be expressed as

$$\frac{dQ}{dt} = c_p (T' - T'') \frac{dm_d}{dt} . \quad (1)$$

Here the primes refer to the cloud, the double primes to the environment, $\frac{dm_d}{dt}$ is the detrainment rate for the cloud layer and Q represents sensible heat. Similarly, the rates at which cloud air, excess water vapor, and liquid water are given to the environment by a cloud segment can be written as

$$\frac{dm_a}{dt} = \frac{dm_d}{dt} , \quad (2)$$

$$\frac{dm_v}{dt} = (x'_v - x''_v) \frac{dm_d}{dt} , \quad (3)$$

$$\frac{dm_w}{dt} = \frac{Q_{cl}}{\rho} \frac{dm_d}{dt} . \quad (4)$$

In these expressions x refers to the mixing-ratio of water vapor, Q_{cl} to the cloud liquid water content, and m_v and m_w to the mass of water vapor and liquid water, respectively.

Consider now a group of active cumulus clouds. Assume that this field of clouds is surrounded by a large vertical cylinder of radius R which extends from the surface to the level of the tropopause. This cylinder is divided into horizontal layers of height Δz and mass m (Fig. 1). The rate at which a layer of this enclosing cylinder receives excess sensible heat from the clouds can be obtained by adding the heating rates produced by each of the cloud segments contained in the layer. Thus, equation (1) becomes

$$\frac{dQ}{dt} = \sum_{\substack{\text{all cloud} \\ \text{segments} \\ \text{in the layer}}} c_p (T' - T'') \frac{dm_d}{dt} . \quad (5)$$

The total heating of the cylinder during a long period of time, Δt , can be obtained by integrating equation (5) with respect to time. Thus

$$\Delta Q = N_1 \int_0^{\tau_1} c_p (T' - T'') \frac{dm_d}{dt} dt + N_2 \int_0^{\tau_2} c_p (T' - T'') \frac{dm_d}{dt} dt + \dots , \quad (6)$$

where N_i is the total number of clouds type i that existed during the time interval Δt and τ_i is the lifetime of cloud type i . N_i is

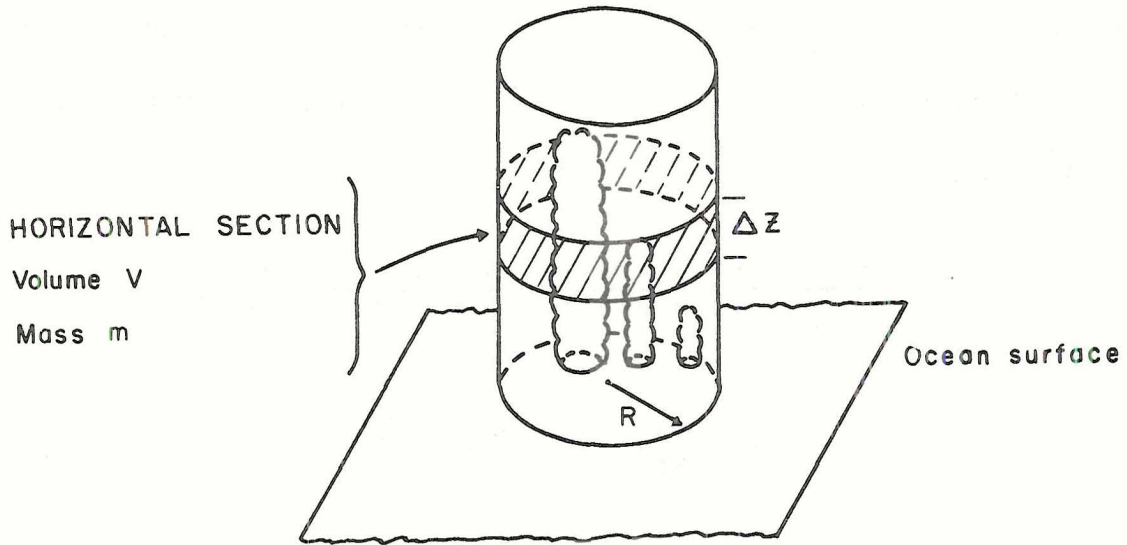


Fig. 1. Geometrical set up for the computations of the effect of cumulus clouds on the surrounding environment.

dependent on the total low-level mass available to form clouds of type i , and on the amount of sub-cloud layer mass that a cloud of type i uses during its growth period. The mass channeled into clouds of type i from the sub-cloud layer during the time interval Δt is given by

$$\Delta m_i = -\alpha_i \nabla \cdot \mathbf{w}_0 \rho_0 B \pi R^2 \Delta t \quad , \quad (7)$$

where $\nabla \cdot \mathbf{w}_0$ is the total convergence (synoptic plus subsynoptic) of sub-cloud layer mass into the clouds of the disturbance, ρ_0 is the density of the sub-cloud layer, B is the height of cloud base, R is the radius of the cylinder enclosing the disturbance and α_i is the fraction of the total mass-convergence going into clouds of type i . The sub-cloud layer mass used up by a cloud of type i during the forced stage is given by

$$\delta m_i = \int_0^{t_0} \rho_0 \pi r_0^2 w_0 dt \quad , \quad (8)$$

where r_0 , w_0 and t_0 are the radius, velocity and duration of the forced updraft through cloud base. Thus, the number of clouds of type i (N_i) can now be obtained as

$$N_i = \frac{\text{Total mass available from sub-cloud layer}}{\text{Mass used by cloud } i \text{ during its forced stage}}, \text{ or}$$

$$N_i = \frac{\Delta m_i}{\delta m_i} = -\alpha_i \frac{\nabla \cdot w_0 \rho_0 B \pi R^2 \Delta t}{\int_0^{t_0} \rho_0 \pi r_0^2 w_0 dt} \quad (9)$$

Equations similar to (6) can be readily derived for the increase in air mass, excess water vapor and liquid water produced by the process of detrainment for a layer of the cylinder surrounding the clouds. These equations have the following form:

$$\Delta m_a = N_1 \int_0^{\tau_1} \frac{dm_d}{dt} dt + N_2 \int_0^{\tau_2} \frac{dm_d}{dt} dt + \dots \quad (10)$$

$$\Delta m_v = N_1 \int_0^{\tau_1} (x' - x'') \frac{dm_d}{dt} dt + N_2 \int_0^{\tau_2} (x' - x'') \frac{dm_d}{dt} dt + \dots \quad (11)$$

$$\Delta m_w = N_1 \int_0^{\tau_1} \frac{Q_{cl}}{\rho} \frac{dm_d}{dt} dt + N_2 \int_0^{\tau_2} \frac{Q_{cl}}{\rho} \frac{dm_d}{dt} dt + \dots \quad (12)$$

The net change in temperature of a section of the enclosing cylinder is produced by the combined effect of the direct diffusion of sensible-heat and the evaporation of the liquid-water which is diffused from the clouds at the same time. Thus, the rate of temperature change of the layer can be expressed as

$$\frac{\Delta T}{\Delta t} = \frac{l}{(m + \Delta m_a) c_p} \frac{\Delta Q}{\Delta t} - \frac{L}{(m + \Delta m_a) c_p} \frac{\Delta m_w}{\Delta t} . \quad (13)$$

Similarly, the rate of moisture alteration is

$$\frac{\Delta x}{\Delta t} = \frac{l}{(m + \Delta m_a)} \frac{\Delta m_v}{\Delta t} + \frac{l}{(m + \Delta m_a)} \frac{\Delta m_w}{\Delta t} . \quad (14)$$

In these formulas m is the mass of the layer of the enclosing cylinder and is defined as

$$m = \rho \pi R^2 \Delta z . \quad (15)$$

Evaluation of the Net Heating

Equations (13) and (14) were evaluated for fixed layers of 500 meters by using the thermodynamic properties and detrainment rates that were computed for the three typical clouds of Part I. The temperature and humidity of the environment were assumed to remain constant throughout the lifetime of the individual clouds. The integrals of equations (6), (11) and (12) were then evaluated for each of the cloud types by adding up in time the contributions of the particular cloud to the heating of the specified layer. The integration was carried out throughout the entire life cycle of the cloud in time steps of 7.5 seconds. The denominator of equation (9) was calculated in a similar way by adding up the flux of mass through the cloud base during the growing stages of the cloud in time steps of 7.5 seconds.

Although the radius of the enclosing cylinder and the averaging time interval Δt enter into the numerator of equation (9), these quantities do not have to be specified in the final evaluation of the heating and moisture-alteration rates (see equations (13), (14) and (15)). In order to determine absolute values for these rates, however, the total (synoptic plus sub-synoptic) convergence of subcloud-layer mass into the clouds ($\nabla \cdot \mathbf{w}_c$) and the distribution of cloud types (α_i) have to be specified as external conditions to the model.

For the time being, the heating rates will be computed for only one cloud type at a time, so that $\alpha_i = 1$. Later on, the different types of clouds will be apportioned according to a model cloud-population, and a computation will be made of their integrated effect on the environment. Typical values of low-level synoptic convergence, ranging from 1 to $5 \times 10^{-6} \text{ sec}^{-1}$, have been estimated for tropical disturbances and cloud clusters (Lopez 1968, Williams 1970). The actual convergence of mass into regions of active convection, however, is probably several times larger than these values. The downdrafts generated by cloud growth and evaporation of rain will obscure the true value of the low-level mass convergence which is available for cloud formation (Riehl and Malkus 1958 and Gray 1972). If the rain-producing efficiency of the cloud population of a disturbance is known, an estimate of the total low-level convergence into the cloud (from synoptic and sub-synoptic sources) could be obtained from the

associated rainfall data. In the case of the cumulonimbus simulated in Part I, for example, the total rain produced was 240 acre-ft (3.0×10^{11} gm of water) while the total mass of sub-cloud layer air flowing into the cloud throughout its growing stage was $\delta m = 5.6 \times 10^{13}$ gm (equation 8). On the other hand, Williams (1970) calculated a mean rainfall of 2.5 cm per day for tropical cloud clusters over a 4° latitude square area. This corresponds to a total mass of water of $2.5 \times A$ gm per day, where A is the area of the disturbance. That means that a total of $N = 2.5 A / 3.0 \times 10^{11}$ cumulonimbi of the type simulated in Part I would be needed to provide the observed daily rainfall, if only that type of cloud is assumed to be present in the disturbance. The total mass of sub-cloud layer air needed for the growth of those clouds in one day would be then $N \times \delta m$. This amount of low-level mass has to be supplied to these particular clouds in one day in order to account for the typically observed rainfall rates. Thus, from equation (7)

$$\Delta m = -\nabla \cdot \mathbf{w}_0 \rho_0 B A \Delta t = N \times \delta m \quad ,$$

where Δt is an interval of one day. The equivalent low-level convergence into the sub-cloud layer of the disturbance can now be evaluated as

$$-\nabla \cdot \mathbf{w}_0 = 0.94 \times 10^{-4} \text{ sec}^{-1} \quad .$$

The towering and small cumulus simulated in Part I would similarly

require convergences of $5.8 \times 10^{-4} \text{ sec}^{-1}$ and $1.6 \times 10^{-3} \text{ sec}^{-1}$ if the cloud population of the disturbance was composed of only clouds of their type.

These convergences are much larger than the synoptically evaluated ones. The actual magnitude of the convergence of mass into the growing clouds, however, hinges on the rain-producing efficiency of the convective system (i. e., how much sub-cloud moisture is needed to produce a gm of rain water) and the mean rainfall rate over the area of the disturbance. The more efficient precipitator a cloud is, the less convergence of water vapor is needed to produce the same amount of rain. In the case of our simulated cumulonimbus, the efficiency is 40%, which would put this cloud in the category of "efficient", and thus put the computed convergence values on the conservative side. Similarly, a rainfall rate of 2.5 cm per day for a tropical disturbance is not large. Thus, a mass convergence into the sub-cloud layer of 10^{-4} sec^{-1} does not seem unrealistic. For purposes of illustration, this last figure will be used in the computation of the heating and moisture-alteration rates. Recently, Betts (1972) has computed mass convergences into the cloud base of Venezuelan cumulonimbi as high as $5 \times 10^{-4} \text{ sec}^{-1}$.

If the observationally evaluated convergences of 10^{-6} to 10^{-5} sec^{-1} are real, a large part of the mass required for the growth of clouds, as computed above, must come from the subsidence induced in the clear regions around the clouds by the penetration of the convective elements themselves. This extra vertical exchange can be very

significant in the momentum and heat budget of tropical disturbances. Some of these concepts will be explored later.

Results of Detrainment from Cumulus Clouds

Temperature Changes. Fig. 2 portrays the rate of change of the temperature of a disturbance as a result of detrainment of mass from different cloud-populations. For purposes of illustration no other heating and cooling mechanisms, such as subsidence or radiation, have been included. It is assumed that each of the populations is made up of clouds of only one type, present at all stages of their life cycle. A low-level convergence of 10^{-4} sec^{-1} has been assumed for all the cases. The solid lines in Fig. 2 indicate the net cooling or warming of the environment due to detrainment; dotted lines correspond to the direct diffusion of excess enthalpy; dashed lines represent the cooling due to the evaporation of detrained liquid water.

The net temperature change of the troposphere, as a result of detrainment alone, is -0.24°C per day for the population of cumulonimbi (Cb), while in the case of towering (TWG) and small cumuli (Cu), the net tropospheric temperature change is -0.16 and -0.06°C per day, respectively. In the last two cases the cooling is concentrated in the lower layers of the troposphere with mean local cooling rates of 0.26 and 0.15°C per day. In all three cases the cooling due to the evaporation of detrained liquid water is the dominant effect. Thus, in the case of the population of Cb's the warming due to direct

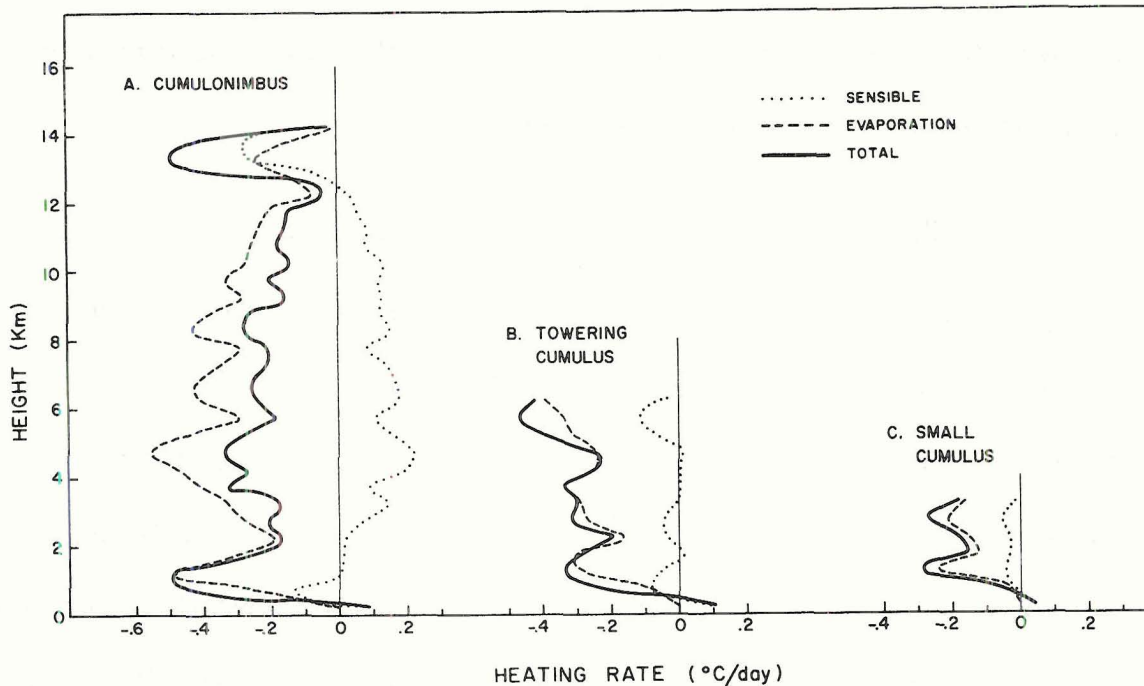


Fig. 2. Vertical profiles of the temperature-alteration rate of a tropical disturbance produced only by detrainment of mass from different types of cloud populations. No other heating and cooling mechanisms, such as subsidence or radiation, have been included. A low-level convergence of 10^{-4} sec^{-1} has been assumed in each of the cases. Solid lines indicate the net cooling or warming resulting from detrainment; dotted lines correspond to the direct diffusion of excess enthalpy; dashed lines represent the cooling due to the evaporation of detrained liquid water. A. Cloud population entirely consisting of cumulonimbi. B. The same for towering cumuli. C. The same for small raining cumuli.

diffusion of excess enthalpy amounts to only 0.07°C per day, but the evaporational cooling is 0.31°C per day. The direct sensible warming produced by a population of TWG Cu's is barely positive in the middle of the cloud layer, while in the case of the small Cu's the effect is entirely negative. This indicates that in the smaller clouds the mean excess enthalpy is very small or negative.

The vertical profile of temperature-changes due to direct diffusion of heat from Cb's shows a direct cooling of the environment at very high and very low altitudes. The lower cooling-maximum arises from the fact that in the early stages of growth the saturated air feeding into the clouds through cloud-base is colder than the environment. This is a direct consequence of the initial conditions assumed in Part I, whereby the mixing ratio of the air feeding into the clouds is that of the surface, but the temperature is that which produces saturation at cloud base. The upper cooling at high levels is mainly a product of the overshooting of the top of the clouds. The high detrainment resulting from the large surface area of the clouds at those two altitudes serves to emphasize the effect of the cooler temperatures inside the cloud.

Moisture Changes. Fig. 3 portrays the corresponding moisture-alteration rates produced only from detrainment effects by the populations of Fig. 2. For purposes of illustration no other moisture-changing mechanisms, such as subsidence, have been incorporated. The solid lines indicate the net rate of change of the humidity of the environment; this net change is produced by the detrainment of excess water vapor (dotted lines); and by the evaporation of detrained liquid water (dashed lines).

The total tropospheric moisture increase from pure detrainment effects produced by the population of Cb's is 0.48 gm/kgm per day.

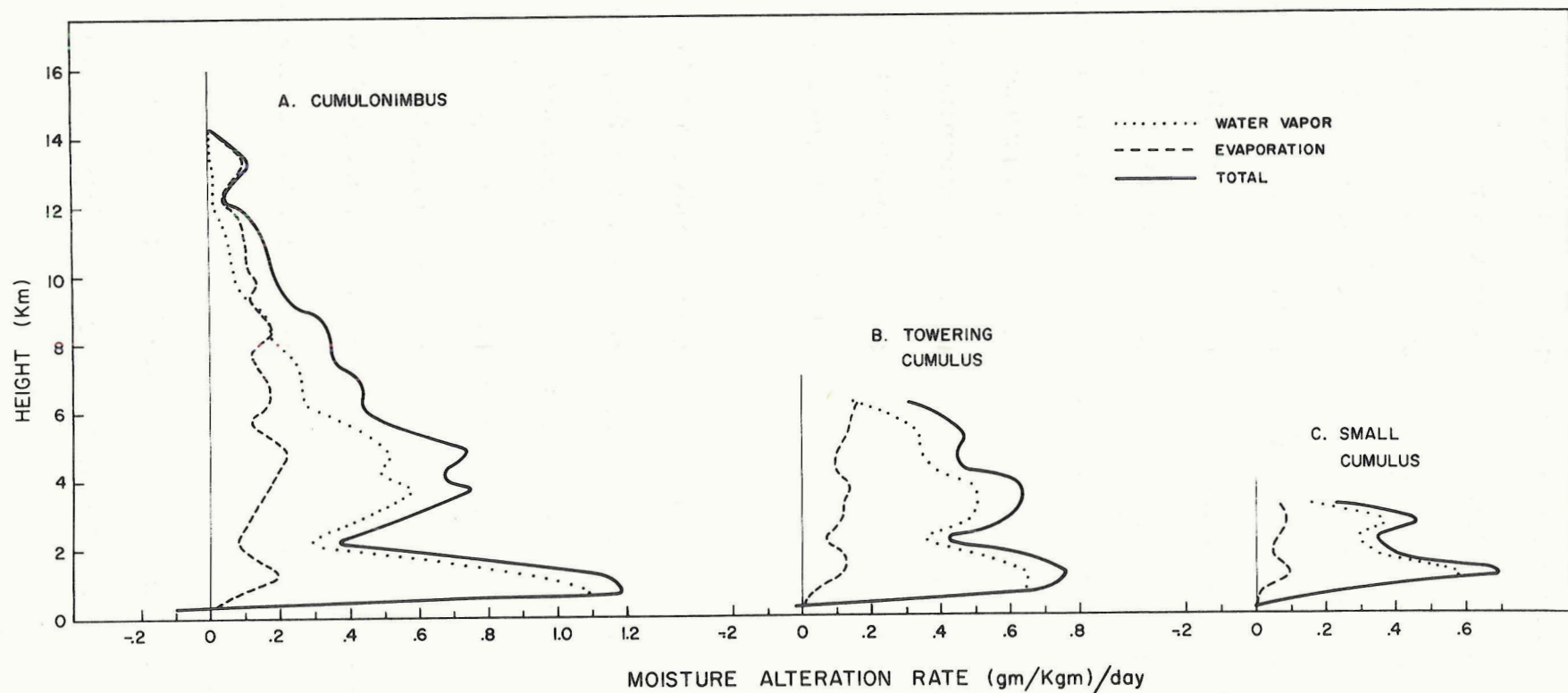


Fig. 3. Vertical profiles of the moisture-alteration rate of a tropical disturbance produced by detrainment of mass from different types of cloud populations. No other moisture-changing mechanisms, such as subsidence, have been included. A low-level convergence of 10^{-4}sec^{-1} has been assumed in each of the cases. Solid lines indicate the net rate of change of the humidity resulting from detrainment; dotted lines correspond to the direct diffusion of excess water vapor; dashed lines represent the increase in mixing ratio due to the evaporation of detrained liquid water. A. Cloud population entirely consisting of cumulonimbi. B. The same for towering cumuli. C. The same for small raining cumuli.

In the case of TWG and small Cu the equivalent tropospheric change is 0.31 and 0.13 gm/kgm per day respectively. The largest moisture increases occur in the lower two kilometers of the atmosphere in all three cases; local changes of about 1 gm/kgm per day are produced in that region. In all cases the diffusion of water vapor is the dominant effect. Thus, in the case of the population of Cb's the increase in the moisture of the environment due to the diffusion of excess water vapor amounts to 0.36 gm/kgm per day, while the water vapor produced from the evaporation of detrained cloud liquid water is only 0.12 gm/kgm per day.

The vertical profiles show a maximum increase in the moisture of the environment at a height of about one kilometer. These maxima are related to the large water vapor excess of the saturated air in the low levels of the cloud during its initial stages of growth. As the cloud parcels rise, however, entrainment reduces the water vapor excess so that the amount given to the environment by detrainment becomes smaller with height. The fact that at higher altitudes the environment is close to saturation, further reduces the rate of moisture excess exportation which depends on the difference of water vapor content between cloud and environment (see equation (3)).

Other Evidences of the Direct Cooling Action of Cumulus Clouds

Direct sensible-temperature decreases, around and after cumulus convection has taken place, have been reported by Kinnenmonth (1970)

from data of the VEMHEX project of 1969. Further evidence of the direct cooling action of cumulus clouds is the lower troposphere cool temperatures found in tropical disturbances and waves of the easterlies (Riehl, 1945). It is interesting to note that in the study of one thousand Pacific trade wind cloud clusters, Williams (1970) found no appreciable tropospheric warming or surface pressure falls even though the rainfall was appreciable. The average cloud cluster precipitation was computed to be 2.5 cm per day for a 4° latitude square area. The 1500 calories/per cm^2 per day liberated through the condensation of this rainfall resulted in no tropospheric warming even though the ventilation of the storms was small. Recent computations by Gray (1972a) also indicate that it is impossible to explain the tropospheric sensible temperature balance around the globe, which is required by the rainfall observations, without invoking a direct cloud sensible-cooling which averages about two thirds of the net tropospheric radiational cooling.

The "Cooling Tower" Hypothesis

The results of the computations performed in this section indicate that by itself, detrainment of air from active cumuli produces a net cooling of the air in which the clouds are embedded. The evaporation of detrained liquid water overcompensates for any direct diffusion of sensible heat from the clouds. Even in the case of vigorous cumulonimbi with temperature excesses of 5 and 6°C , enough liquid water

is present to produce a net cooling effect on the environment. It is interesting to note, in this regard, that regions of high enthalpy excess are coupled to regions of high cloud liquid water content (see Figs. 6 and 10). If the results of the computations presented here are verified, the classical view (Riehl and Malkus, 1958) of cumulus clouds providing heat to the environment through direct diffusion must be revised. It appears that as a result of detrainment alone (direct diffusion of cloud mass), cumulus clouds act as "cooling towers" instead of performing the often hypothesized warming role (Ooyama, 1963; Charney and Ellissen, 1964; Ogura, 1964; Kuo, 1965; Rosenthal, 1970).

III. THE CONVERGENCE - DIVERGENCE PATTERN INDUCED BY THE CLOUDS

General Concepts

The vertical transport of mass by individual clouds produces local mass sources and sinks that are reflected on the environment as regions of divergence and convergence. At any particular level the magnitude of this divergence field will depend on the change of mass of the individual clouds present at that location. In turn, the rate at which the mass of a layer of an individual cloud changes is determined by the internal vertical advection of mass, and by the mass gained and lost through entrainment and detrainment. Thus,

$$\frac{dm}{dt} = \left(\frac{dm}{dt}\right)_{\text{ADVECTION}} + \left(\frac{dm}{dt}\right)_{\text{ENTRAINMENT}} - \left(\frac{dm}{dt}\right)_{\text{DETRAINMENT}} \quad (16)$$

The rate of entrainment and detrainment are given by equations (66a) and (66b) of Part I while the advection term can be conveniently estimated from the rate of change of the geometry of the cloud segment. So,

$$\left(\frac{dm}{dt}\right)_{\text{ADVECTION}} = \frac{d}{dt} (\rho \pi r^2 \Delta z) = 2\pi r \Delta z \frac{d(\rho z)}{dt} + \pi r^2 \frac{d(\rho \Delta z)}{dt} \quad (17)$$

where r , ρ and Δz are the radius, density and height of a cloud layer.

Consider now a group of clouds surrounded by the same control volume used in the last section. The combined change in mass experienced by all the cloud segments contained in a layer of the enclosing cylinder can be expressed as

$$\frac{dm}{dt} = \sum_{\substack{\text{all cloud} \\ \text{segments} \\ \text{in the layer}}} \frac{\delta m}{\delta t} \quad (18)$$

By integrating equation (18) over a long period of time, Δt , the total mass change experienced by the clouds can be expressed as

$$\Delta m = N_1 \int_0^{\tau_1} \frac{dm}{dt} dt + N_2 \int_0^{\tau_2} \frac{dm}{dt} dt + N_3 \int_0^{\tau_3} \frac{dm}{dt} dt + \dots \quad (19)$$

where the different symbols have the same meaning as in the last section.

The average divergence in the layer of the cylinder during a large period of time, Δt , can now be expressed as

$$\nabla \cdot w = -\frac{1}{m} \frac{\Delta m}{\Delta t} \quad (20)$$

where m is given by equation (15). If the values of Δm , m and N_i from equations (19), (5) and (9) are introduced in equation (20), the expression for the mean divergence of the layer becomes

$$\nabla \cdot w = -\frac{\nabla \cdot w_0 B}{\rho \Delta z \int_0^{\tau_1} r_0^2 w_0 dt} \left[\alpha_1 \int_0^{\tau_1} \frac{dm}{dt} dt + \alpha_2 \int_0^{\tau_2} \frac{dm}{dt} dt + \alpha_3 \int_0^{\tau_3} \frac{dm}{dt} dt + \dots \right] \quad (21)$$

Evaluation of the Divergence Profile

Equation (21) was evaluated for fixed layers of 500 meters by using the geometry and the entrainment and detrainment rates computed for the three typical clouds of Part I. The integrals of equation (21) were evaluated for each of the cloud types by adding up all the changes in mass of the particular cloud in specified layer. The integrations were carried out through the entire life cycle of the cloud in time steps of 7.5 seconds. As in the last section, populations of only one cloud type were considered and a low-level convergence into the clouds of 10^{-4} sec^{-1} was assumed. All other parameters entering into equation (21) have the same values as those in equations (6), (11) and (12).

Results of Divergence Computations

Fig. 4 portrays the vertical profiles of divergence computed from equation (21) for different cloud populations. In the case of the cumulonimbus population, the convergence and divergence produced directly by the clouds is concentrated at very low and very high altitudes, while in the intervening regions very little effect is noticed. The convergence at very low levels is the reflection of the mass-sink that results from the continuous ascent of low-level air into the base of the growing clouds. As these growing clouds penetrate through the environment, the surrounding air is pushed aside and local mass-sources are produced along the path of the ascending current.

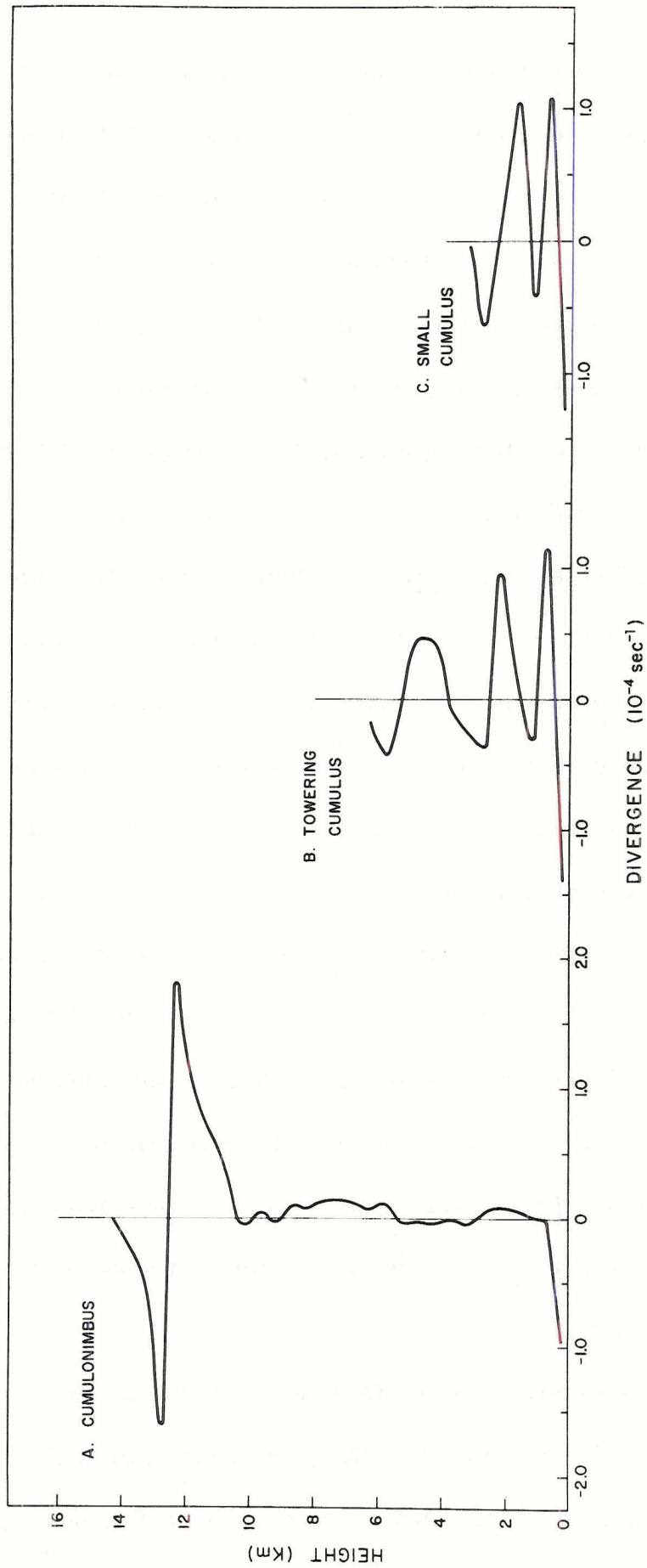


Fig. 4. Vertical profiles of divergence imposed on a tropical disturbance by the upward mass transport performed by different types of cloud populations. The effect of the downward compensatory sinking motion induced in the clear areas around the clouds is not included. A. Cloud population entirely consisting of cumulonimbi. B. The same for towering cumuli. C. The same for small raining cumuli.

However, as the source of low-level air is gradually cut off and while the top of the cloud is still buoyant, local mass-sinks are induced in the environment as a result of the shrinking radius of the stretched cloud stems. These two effects tend to cancel one another among clouds of different growth stages, so that in the mean, no marked convergence or divergence is observed throughout most of the cloud layer. The cloud air penetrating high altitudes, however, accumulates continually at the equilibrium level of the clouds. Consequently, a region of high horizontal divergence is induced in the environment at around 12 kilometers. An anvil also develops at this location. The large convergence at around 13-14 kilometers results from the fast subsidence of negatively buoyant cloud air that has overshot the equilibrium position and captured surrounding air particles. A large amount of entrained environmental air is brought down from higher levels together with the descending cloud mass. This sinking motion tends to further emphasize the large divergence of mass at around 12 kilometers. This large divergence region has also been observed by Williams, 1970, and by Reed and Recker, 1971. It will be interesting to explore the implications of this effect on the vertical transport of horizontal momentum as well as on the dynamics of severe storms under vertical wind shear.

The divergence profiles for the towering and small cumuli have the same top and bottom features as the profile for cumulonimbus clouds. The middle regions, however, are somewhat different. Here

the mass-sources resulting from the penetration of the growing clouds are not completely compensated by the shrinking of the radius. The divergence and convergence maxima present in the middle regions of both profiles were a result of local subsidence inside the clouds against parcels that were still rising. This multiple "anvilng" can be seen in the radius profiles of Figs. 12 and 13. The effect of these smaller clouds on the divergence profile has been greatly exaggerated by requiring that they produce by themselves a rainfall rate typical of a tropical disturbance. In reality, however, a considerable amount of the rain is produced by the larger Cb clouds. Thus, in the case of a combined typical population of Cb, TWG and small Cu, the effect of the smaller clouds will not be as marked as indicated in Fig. 4. The problem of a combined population of clouds will be considered in Section IV.

The Effect of the Divergence Field Produced by the Clouds

The divergence field that results from the growth of the clouds will induce a downward flow of mass around the clouds to compensate for their upward mass transport. In this descending branch of the convective circulation, potential energy is converted into sensible heat, and the temperature of the environment is raised. The resultant warming, however, will be compensated by the cooling produced from the evaporation of detrained cloud-water and by the cooling resulting from long-wave radiational loses. In addition, some of the

high-level mass-divergence will result in compensatory sinking motions away from the clouds, in the clear areas outside of the disturbance. Depending on the magnitude of this sinking current, a net warming of the clear areas around the disturbance could result after compensating for the radiational losses of the cloud-free air.

The divergence profiles presented in this section are not to be compared to the synoptic profiles that have been obtained for tropical disturbances by Williams (1970), and by Reed and Recker (1970). The present profiles are a result of the upward mass transport of the clouds alone, and do not include the effect of the downward sinking motion that will be induced in the clear areas around the clouds. It is the difference between the upward and downward mass transports that produces the large-scale divergence profiles that are reflected in the synoptic data. The problem of the compensatory sinking motions in the clear areas around the clouds, and the net divergence profile produced, will be considered in Section V and in Part III of this series.

IV. A MODEL CLOUD POPULATION

Radar Information

A realistic assessment of the role of convection in the heat and moisture budgets of tropical storms should take into consideration the type of cumulus population present in the disturbance. The combined effect of all the convective elements depends on the proportion in which the different cloud types are present. So for example, if most of the low-level moisture convergence is channelled into small cumuli, only a fraction of the storm's latent heat input can be realized as sensible heat. Not only is the magnitude of the latent-heat release dependent on the cloud population, but also its distribution with height. Although it is realized that cumulus convection is of utmost importance to the energetics of disturbances, very little effort has been devoted to investigating the types of clouds present in tropical cloud clusters. Holle (1968) has performed some studies on tropical oceanic cloud populations. His results, however, do not intend to answer the question of what are the different types and relative frequencies of cumulus clouds present in a disturbance at a given time.

During the 1968 Barbados Meteorological Experiment the author flew with the Navy's Weather Reconnaissance Squadron Four into about a dozen tropical disturbances in the West Indies region. The scope of the airborne, 10 cm APS-20 radar, was photographed on every other scan. From these sequential pictures the life-times of the new

individual echoes that appear on the scope every five minutes have been estimated. Clusters of individual echoes have not been considered. Very large echoes are probably composed of several individual cells and their life-times would not be representative of individual convective elements. It is felt that by considering only individual isolated echoes, a frequency distribution of echo-duration can be obtained that is representative of the entire population of convective elements, whether they appear singly or in clusters. From more than 600 individual echoes the histogram of Fig. 5 has been constructed. This echo life-time distribution is typical of all the disturbances encountered. Several different stratifications of the data were tried (amount of cloud cover, surface pressure, latitude, range, time of the day, etc.) with no significant departure from the form of the overall average distribution.

The average echo life-time for all the data is 14.5 minutes. This is smaller than the average for hurricanes obtained by Senn, Hiser and Low (1959), 32 min; and by Senn and Stevens (1965), 35 minutes. However, they have not considered echoes of short duration (10 minutes or less). On the other hand, McIntyre (1956) has found 17 minutes to be the average for hurricane situations by tracing echoes which lasted from 4-1/2 to 46 minutes. Nevertheless, these previous studies and the present one agree on the fact that both in hurricanes and tropical disturbances, there are many more short-lived echoes

than there are long-lived ones. A similar conclusion can also be derived from echo life-time distributions obtained for middle latitudes for both winter and summer storms (Blackmer, 1955; Battan, 1953).

It is reasonable to assume that in general, the long-lived echoes are wider and taller than the short-lived ones (Battan, 1953; Senn and Stevens, 1965). In the case of the present data it has not been possible to determine quantitatively the horizontal and vertical sizes corresponding to the different life-time categories. The available evidence, however, suggests that, qualitatively, the longer-lived echoes are indeed wider and taller than the short-lived ones. This would tend to indicate that the cloud populations of tropical disturbances are composed of a majority of small cumuli, some towering cumuli, and a few cumulonimbus towers. Thus, a large portion of the latent heat contained in the low-level moisture input is not realized as sensible heat since condensation in clouds of small vertical extent is severely limited. This fact must be taken into consideration if the effect of cumulus convection on tropical disturbance energetics is to be properly evaluated.

A Cloud Population from Radar and Numerical Model Data

It is interesting to note that, although in very small numbers, there are some clouds in Fig. 5 that produce echoes of very long duration (50-90 mins). One or two of such long-lived echoes were detected in each of the disturbances considered in this study. In order

to produce these persistent echoes, a local source of low-level mass of long duration is necessary. With the present model it has been possible to produce radar echoes lasting 40 to 50 minutes by forcing an 8 km wide updraft through cloud base, for 40 minutes, with a peak speed of 5 m/sec. It is hard to visualize such a persistent low-level forcing without postulating the existence of a strong mesoscale organization of the sub-cloud layer. When considering echoes of long duration, we are probably dealing with cloud systems that have organized the planetary boundary layer so that it can provide a constant source of low-level mass for the close reformation of individual convective cells of a shorter life-span. The simulation of such a mesoscale cloud system is beyond the scope of the present cloud model. Thus, it will be assumed that the effect on the environment of a cloud having a 60 minute radar echo is equivalent to the effect produced by two clouds having a 30 minute echo; similarly, a 90 minute echo cloud will be represented by three 30 minute-echo clouds and so on.

Using the results of the cloud model developed in Part I, some information can be obtained about the distribution of cloud sizes corresponding to the echo life-time distribution of Fig. 5. Thus, Fig. 6 has been prepared from the results of the numerical model by plotting the radar-echo duration versus the maximum height attained by clouds of different initial conditions. For this diagram it has been assumed that the minimum reflectivity (Z) detected by the radar corresponds to 30 decibels ($10 \text{ Log}_{10} Z$). It can be seen that maximum cloud height

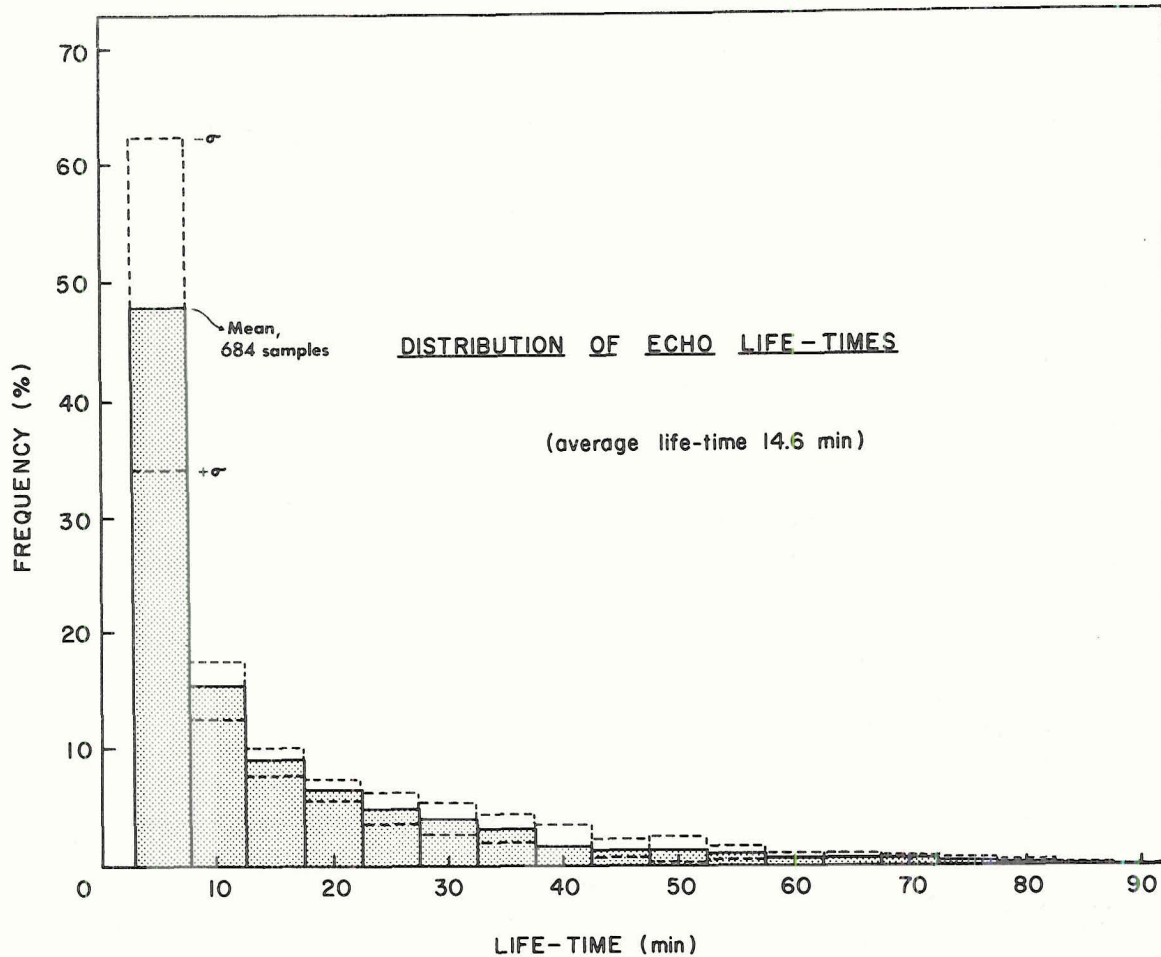


Fig. 5. Frequency distribution of echo life-times.

and echo duration are closely correlated so that clouds exhibiting long-lived echoes penetrate high into the troposphere. The maximum height obtained by a cloud, however, is not a good representation of its overall size: clouds with small initial radii can rise to high altitudes providing that the initial forcing is intense and of a long duration (see Figs. 17, 18 and 19 in Part I). On the other hand, the total mass of sub-cloud layer air flowing into a cloud during its growing stage is a better indication of the overall size of a convective element. Fig. 7 shows the duration of the radar-echo as a function of the total

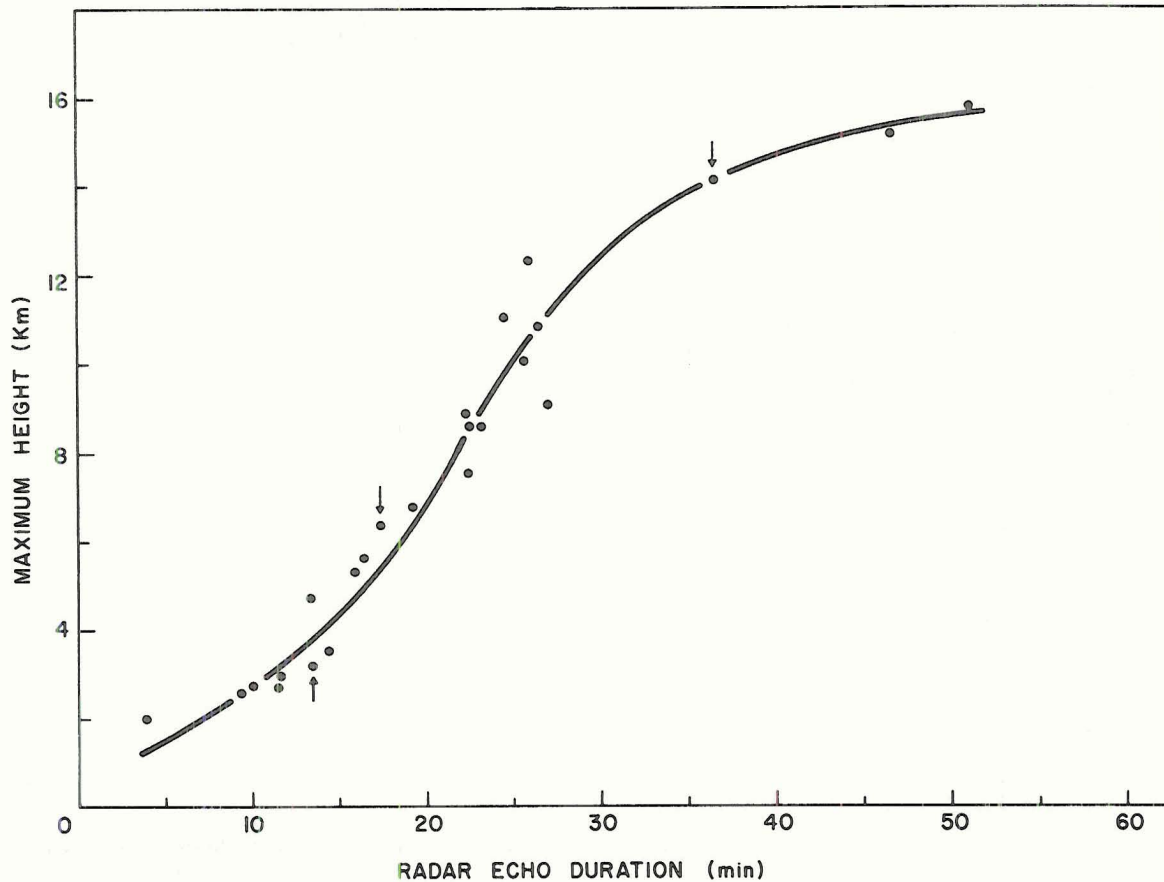


Fig. 6. The relationship between radar-echo duration and the maximum height attained by clouds simulated with the numerical model of Part I by assuming different initial conditions. It is assumed that the minimum reflectivity (Z) detected by the radar corresponds to 30 decibels ($10 \log_{10} Z$). Arrows identify the three typical clouds described in detail in Part I.

sub-cloud layer mass-input for clouds of different initial configuration; for facility of presentation, the abscissa has been plotted on a logarithmic scale. Values of 400 to 2,200 meters have been used for the initial radius, 5 to 20 minutes for the growth period, and 2.5 to 5.5 m/sec for the maximum updraft velocity through cloud base. Clouds having radar echoes lasting more than 40 minutes have been composed of two or three clouds with shorter lived echoes. It seems that good correlation exists between echo duration and the amount of mass

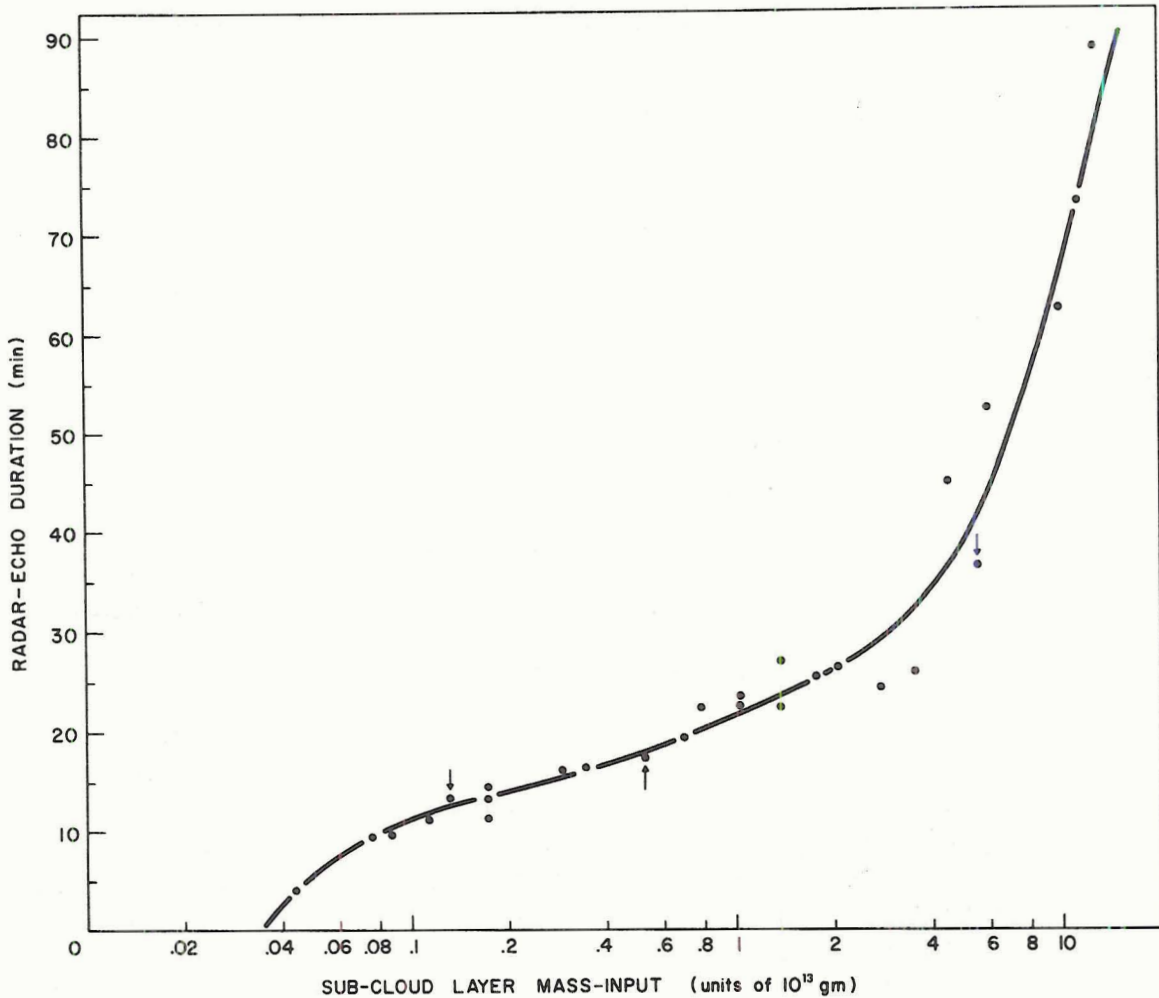


Fig. 7. The relationship between radar-echo duration and the total sub-cloud layer mass-input for clouds simulated with the numerical model of Part I by assuming different initial configurations. The same criteria for the existence of a radar-echo used in Fig. 6 is also used in this figure. Arrows identify the typical clouds described in detail in Part I.

necessary for cloud growth. It is interesting to note that there is a very rapid decrease in echo duration with decreasing mass input for the smaller clouds (those utilizing 0.1×10^{13} gm or less for growth). Clouds with mass inputs less than about 3×10^{11} gm do not produce "detectable" radar echoes. On the other hand, clouds having very long radar echoes require large amounts of sub-cloud layer mass to grow.

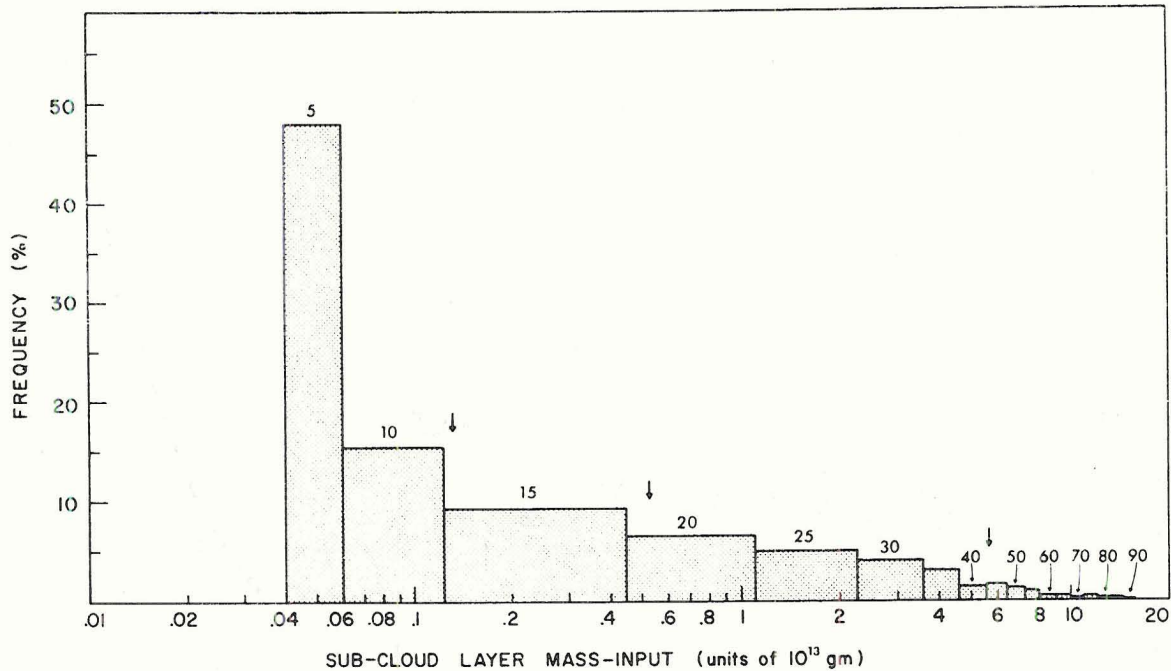


Fig. 8. Typical cloud population for trade-wind tropical disturbances shown as a frequency distribution of classes of clouds using different amounts of sub-cloud layer mass during their growth stages. The observational evidence contained in Fig. 5 and the results of the numerical model of Part I presented in Fig. 7 have been used. The mass-input classes correspond to the echo-lifetime classes of Fig. 5. The corresponding echo-lifetimes are indicated in parenthesis. Arrows identify the three typical clouds described in detail in Part I.

Using the curve of Fig. 7 and the radar information in Fig. 5, a typical cloud population for trade-wind tropical disturbances has been developed. This is shown in Fig. 8 as the frequency distribution of classes of clouds having different amounts of sub-cloud layer mass-inputs during their growth stages. The class-intervals of the distribution of echo duration (Fig. 5) have been translated in terms of sub-cloud layer mass-input classes using the relationship between lifetime and mass-input given by Fig. 7. From this diagram it can be seen that the majority of the clouds in a tropical disturbance are small,

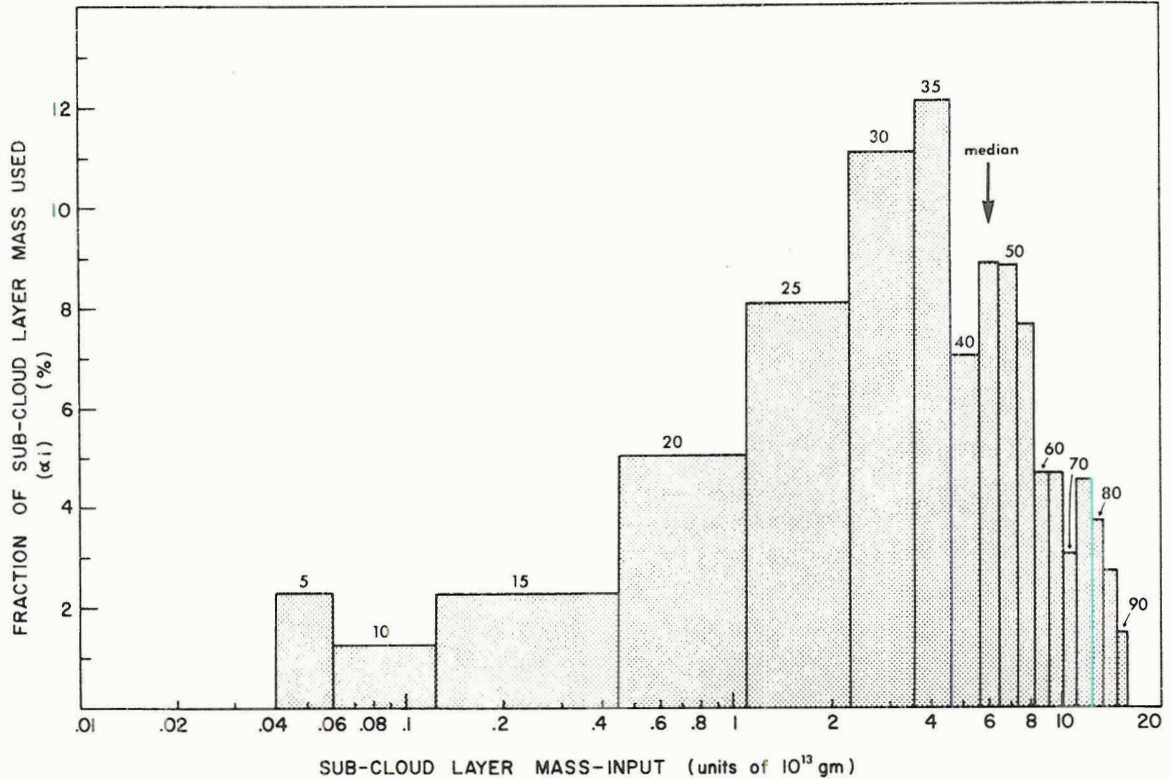


Fig. 9. Mass used by different classes of clouds as a fraction of the total sub-cloud layer mass available for cloud formation. The observational evidence contained in Fig. 5 and the results of the numerical model of Part I presented in Fig. 7 have been used. The cloud classes are expressed in terms of the sub-cloud layer mass used in their growth stages. The classes correspond to the echo lifetime classes of Fig. 5. The corresponding echo lifetimes are indicated in parenthesis. The large arrow indicates the median of the distribution.

processing individually only a very small amount of sub-cloud layer air. The very few large clouds, on the other hand, process a large amount of sub-cloud layer mass during their growth stages. The relative importance of the collective effect of the clouds in each category can be obtained by computing from Fig. 8 the mass used by each class as a fraction of the total sub-cloud layer mass utilized by all of the clouds in the population. The results of this computation are portrayed



The graph illustrates a symmetric distribution centered at 10. The frequency increases linearly from 0 at x=0 to a maximum of 10 at x=10, and then decreases linearly back to 0 at x=15. This represents a triangular distribution with a peak at the center.

The following text is extremely faint and largely illegible. It appears to be a continuation of a report or document, possibly discussing statistical analysis or data interpretation related to the graph above. The text is too light to transcribe accurately.

in Fig. 9. The large arrow indicates the median of the frequency distribution, i. e., fifty percent of the clouds in the population use more and fifty percent of the clouds in the population use less sub-cloud layer mass than the median cloud-type. It is interesting to note also that the largest fifty percent of all the clouds process approximately the same amount of low-level mass as the smallest fifty percent. So, although less important individually, the small clouds, due to their large numbers, have as much participation in the vertical mass and energy transports as the larger but less frequent cloud cells.

The ordinate of Fig. 9 is the α_i of equations (11), (12) and (21); i. e., the fraction of the total low-level mass convergence going into the different classes of clouds. Using these values of α_i , the combined effect of the typical cloud population can be evaluated from the above mentioned equations. A representative cloud from each of the classes of Fig. 9 has been used. The characteristics and defining parameters of each of these clouds are listed in Table 2. For each type of cloud the corresponding radar-echo lifetime class is listed together with the actual echo duration; radius, duration and peak speed of the generating impulse; maximum height attained; accumulated rain; percent of total sub-cloud layer mass used by the cloud class; and sub-cloud layer mass used by the typical cloud. Notice that clouds having echoes lasting 45 minutes or more have been assumed to consist of two or three cells of shorter echo duration.

Table 2.

Characteristics of the Typical Clouds of a Tropical Disturbance

i Class Number	Radar-echo Duration Class (min)	Actual Radar-echo Duration (min)	r_0 (meters)	T_0 (min)	W_0 (m/sec)	Max. Ht. (meters)	Accum. Rain (acre-feet)	α_j (percent)	δm_j (units of 10^{13} gm)
1	5	4.0	500	5	2.5	2,032	.05	2.30	.044
2	10	9.5	466	10	2.5	2,645	.13	1.28	.076
3	15	16.0	924	10	2.5	5,352	1.44	2.30	.297
4	20	20.0	1,000	20	2.5	6,759	5.35	5.05	.696
5	25	25.5	1,833	15	2.5	10,111	30.66	8.16	1.754
6	30	26.0	2,247	20	2.5	12,347	80.72	11.08	3.514
7	35	36.5	2,000	20	5.5	14,115	240.14	12.17	5.568
8	40	36.5	2,000	20	5.5	14,115	240.14	7.06	5.568
9(6+4)	45	46.0	2,247 1,000	20 20	2.5 2.5	12,347 6,759	86.07	8.91	4.210
10(7+3)	50	52.5	2,000 924	20 10	5.5 2.5	14,115 5,352	241.58	8.88	5.865
11(7+3)	55	52.5	2,000 924	20 10	5.5 2.5	14,115 5,352	241.58	7.67	5.865
12(7+6)	60	62.5	2,000 2,247	20 20	5.5 2.5	14,115 12,347	320.86	4.70	9.082
13(7+6)	65	62.5	2,000 2,247	20 20	5.5 2.5	14,115 12,347	320.86	4.70	9.082
14(7+7)	70	73.0	2,000 2,000	20 20	5.5 5.5	14,115 14,115	480.28	3.11	11.136
15(7+7)	75	73.0	2,000 2,000	20 20	5.5 5.5	14,115 14,115	480.28	4.59	11.136

Table 2. (Continued)

Characteristics of the Typical Clouds of a Tropical Disturbance

i Class Number	Radar-echo Duration Class (min)	Actual Radar-echo Duration (min)	r_0 (meters)	T_0 (min)	W_0 (m/sec)	Max. Ht. (meters)	Accum. Rain (acre-feet)	α_i (percent)	δm_i (units of 10^{13} gm)
16(7+6+4)	80	82.5	2,000	20	5.5	14,115	326.21	3.74	9.778
			2,247	20	2.5	12,347			
			1,000	20	2.5	6,759			
17(7+6+4)	85	82.5	2,000	20	5.5	14,115	326.21	2.73	9.778
			2,247	20	2.5	12,347			
			1,000	20	2.5	6,759			
18(7+6+4)	90	88.5	2,000	20	5.5	14,115	401.58	1.48	12.596
			2,247	20	2.5	12,347			
			2,247	20	2.5	12,347			

It must be emphasized at this point that the purpose in developing this typical cloud population is to obtain an order of magnitude estimate of the effects of an ensemble of different types of cumuli on the atmosphere of a disturbance. The limitations imposed by the quality of the radar data, the accuracy of the numerical model and the assumptions about the structure of large embedded cloud systems do not warrant the use of this derived cumulus population for detailed energy balances of tropical storms. With these restrictions in mind the "typical" cloud population will now be used to compute the alteration rate of temperature, moisture and mass produced on the synoptic scale of a tropical disturbance as the result of sustained cumulus convection.

The Effect of a Typical Cloud Population on the Disturbance's Atmosphere

Figs. 10, 11, and 12 present the vertical profiles of temperature, moisture and mass alteration rates imposed on the environment by the cloud population of Fig. 8. As before, these curves represent the effect of the clouds alone and do not include the effects of the compensatory sinking induced in the regions around the clouds. A low-level total convergence into the clouds of 10^{-4} sec^{-1} has been assumed. As noted in Section II, this high convergence is necessary to explain a production of 2.5 cm of rain per day over the disturbance region. The shape of these profiles are not much different from those corresponding

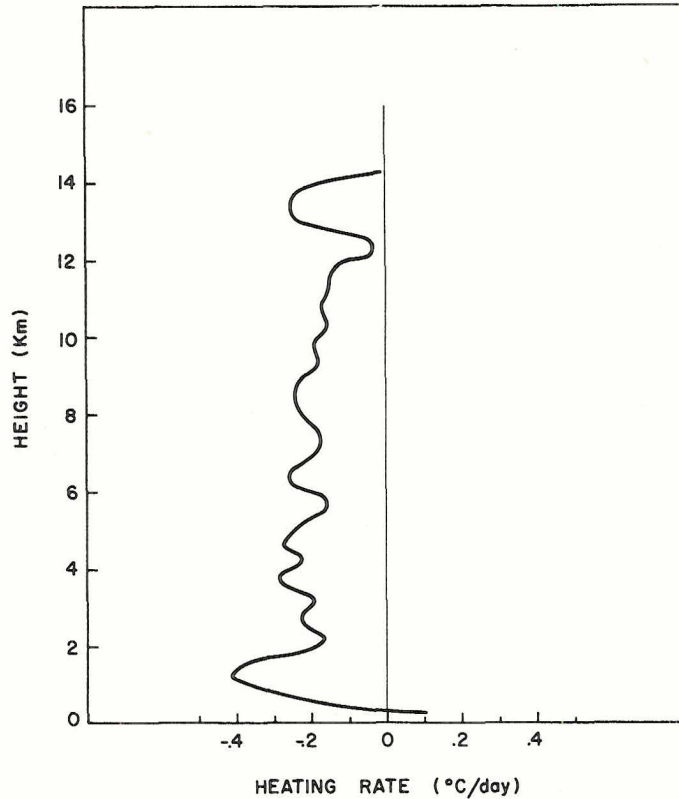


Fig. 10. Vertical profile of the temperature-alteration rate of a tropical disturbance produced by detrainment of mass from the cloud population of Fig. 8. No other heating and cooling mechanisms, such as subsidence or radiation, have been included. A low-level convergence of 10^{-4} sec^{-1} has been assumed. The curve represents the net cooling or warming rate resulting from both detrainment of excess sensible heat and evaporation of detrained cloud liquid water.

to a population consisting entirely of cumulonimbus clouds (Figs. 2a, 3a and 4a). It appears that the effect of including smaller clouds in the population is to reduce the magnitude of the rates of heat, moisture and mass alteration produced by the Cb's, and to make the distribution of the rates with height more uniform, especially in the lower layers.

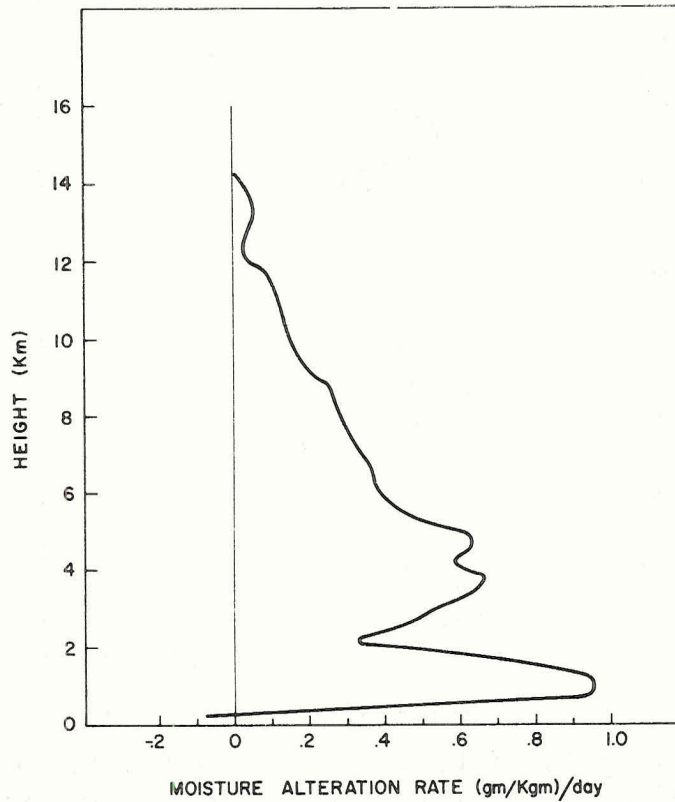


Fig. 11. Vertical profile of the moisture-alteration rate of a tropical disturbance produced by detrainment of mass from the cloud population of Fig. 8. No other moisture-changing mechanisms, such as subsidence, have been included. A low-level convergence of 10^{-4}sec^{-1} has been assumed. The curve represents the net change in humidity resulting from both detrainment of excess water vapor and evaporation of detrained cloud liquid water.

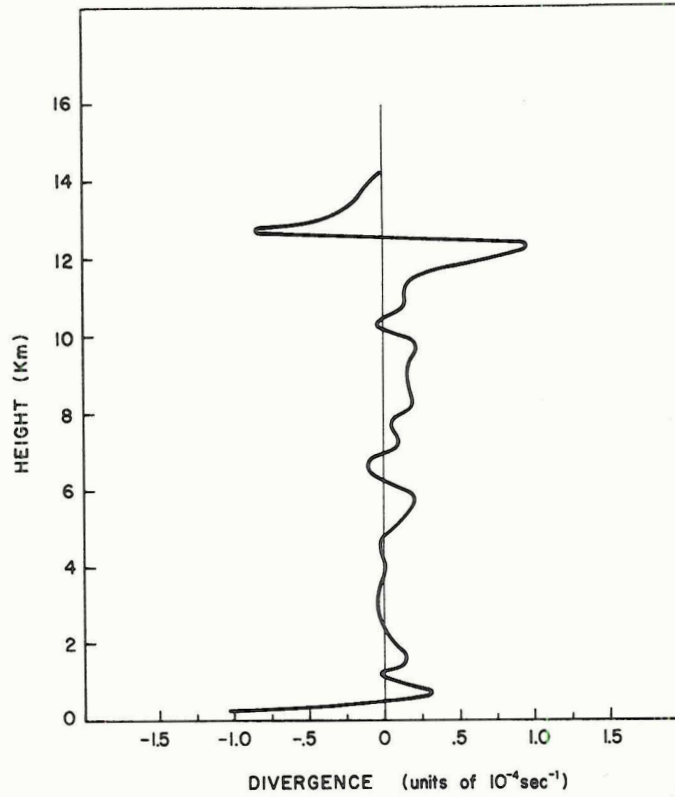


Fig. 12. Vertical profile of divergence imposed on a tropical disturbance by the upward mass transport performed by the cloud population of Fig. 8. The effect of the downward compensatory sinking motion induced in the clear areas around the clouds is not included. A low-level convergence of 10^{-4}sec^{-1} has been assumed.

V. THE INTERACTION OF A MODEL CLOUD - POPULATION WITH THE SYNOPTIC FEATURES OF A TYPICAL TROPICAL DISTURBANCE

Introduction

The model cloud-population described in the last section will now be used to investigate the interaction of an ensemble of cumulus clouds with the synoptic flow features of a tropical disturbance. The interaction between cloud and synoptic scales takes place in two reciprocal directions. Firstly, the large-scale synoptic flow and the static stability of a disturbance determine the different types of cumulus clouds that will be produced and the numbers in which they will be present. Secondly, once the cloud population is established, the large-scale fields of temperature, moisture and momentum will be altered and controlled by the collective influence of the individual clouds. The first type of interaction has been tacitly incorporated in the characterization of the model cloud-population presented in Figs. 9, 10, 11 and 12. Here the types of clouds present and their relative frequencies were obtained from radar observations, while their actual numbers and characteristics were determined from the typically observed rainfall rate and the vertical distribution of temperature and moisture in a tropical disturbance. The numerical cloud model, serves as the linking agent that combines all of these pieces of information into a coherent model of the cloud population that is determined by the large-

scale flow. The second type of interaction, that by which the clouds modulate and alter the synoptic scale, will now be explored further by computing a heat and moisture budget for a typical tropical disturbance.

One of the most interesting features of tropical disturbances is the fact that despite the copious amounts of rain produced in a day, the majority of the storms travel for hundreds of miles over the oceans without apparent change in intensity. Williams (1970) has considered a sample of 1257 individual satellite-observed trade-wind clusters over the Pacific Ocean. Of these, 537 were classified as conservative, 166 developed into tropical storms or typhoons, and the rest were either in the formative or dying stages. While the conservative clusters were tracked in the satellite pictures for 12-18 degrees of longitude, no appreciable tropospheric warming or surface pressure falls were detected even though the rainfall was computed as 2.5 cm per day. Thus, the typical tropical disturbance can be considered as constituting a quasi-steady state system. In the following only the conservative steady-state cloud clusters will be considered.

Interaction of a Steady-State Disturbance with the Environment

Since the steady-state condition implies that the total moisture content of the system must stay constant, the same amount of water that precipitates out of the clouds of such a disturbance must be brought in from the outside in the form of evaporation from the ocean surface

and by low- and-middle-level synoptic water-vapor convergence. Conversely, the heat released by the condensation of this rain-water must be exported to the exterior of the disturbance if the steady-state balance is to be met. The mechanism by which this is accomplished, however, is not direct. Firstly, the latent heat of condensation is converted into potential energy insomuch as air from lower levels is lifted up and carried aloft inside the clouds. Because of this vertical mass-transport, a convergence zone is produced at the top of the disturbance that generates an outflow region at high levels. Finally, potential energy is exported to the outside as mass leaves the disturbance. Under steady-state conditions, the potential energy advected from the disturbance plus the long-wave radiational losses must be equal to the energy released through the condensation of rain-water.

The mass that leaves the disturbance at its outflow layer must be compensated by a region of convergent inflow further down. Actually, Williams (1970) has found mass convergence into the conservative clusters all the way from the surface to 400 mb. Furthermore, it is this low- and-middle-level convergence that brings into the disturbance the water-vapor necessary to establish the observed net rainfall rates. Accordingly, the water-vapor convergence into the conservative clusters was found by Williams to be equivalent to a rainfall rate of 2 cm per day. Forty-three percent of this moisture convergence occurred under 900 mb, while fifty-seven percent was found to come from convergence in the layer between 900 and 400 mb.

In general, we can view the steady-state tropical disturbance as a system that takes in the latent heat contained in the low- and middle-level water-vapor convergence, converts this latent heat into potential energy, and, after subtracting the net long-wave radiational losses, exports potential energy to the environment at the layer of divergent mass outflow. With the above mentioned heat, water- and mass-balance restrictions imposed on the disturbance as a whole, the different effects of the individual clouds on the disturbance's atmosphere should cancel one another, so that no change in the mean vertical profiles of temperature and moisture should be apparent.

The Interaction of the Model Cloud Population
With the Disturbance's Atmosphere

In computing a heat and water budget for the interior of the disturbance, the principal feature to be considered is the compensatory descending current that will be induced in the cloud-free region as a result of the divergence-convergence pattern established by the clouds (Fig. 12). The resulting dry adiabatic compression will release sensible heat to the environment. This heating will be compensated by cooling due to evaporation of cloud-liquid water (Fig. 10) and by long-wave radiational losses. The sinking motion will also result in the drying of the cloud-free regions. This will similarly be compensated by the detrainment of water-vapor and liquid-water from the different types of clouds present (Fig. 11). The advection of environ-

mental mass into the disturbance's atmosphere is another source of heat and moisture that should be included in the heat and water budgets.

In a quantitative form we can express the change in temperature of a horizontal slab of the disturbance's atmosphere as

$$dT = dT_{\text{SUBSIDENCE}} + dT_{\text{RADIATION}} + dT_{\text{ADVECTION}} + dT_{\text{DETRAINMENT}} . \quad (22)$$

The change in temperature due to subsidence can in turn be written as

$$dT_{\text{SUBSIDENCE}} = \left(\frac{dT}{dz} - \frac{g}{c_p} \right) W_s dt , \quad (23)$$

where $\frac{dT}{dz}$ is the lapse rate of the disturbance, $\frac{g}{c_p}$ is the dry adiabatic lapse rate, W_s is the vertical velocity of the cloud-free regions, and dt is a small interval of time. The vertical velocity W_s can be obtained from the vertical integration of the divergence profile presented in Fig. 12 after provision is made for the advection of mass in and out of the disturbance by the synoptic divergence profile. The radiation term has been obtained from tropical data presented by Cox (1969). His infrared cooling profile for low, middle and high cloud conditions was esteemed adequate for the representation of the long-wave radiation processes in a tropical disturbance. The corresponding short-wave warming profile was computed for similar cloudiness structures using the radiation model described in Manabe and Strickler (1964). The change in temperature due to advection of environmental air into the disturbance can be expressed as

$$dT_{\text{ADVECTION}} = (T_{\text{ENVIRONMENT}} - T_{\text{DISTURBANCE}}) \frac{dm_{\text{ad}}}{m}, \quad (24)$$

where dm_{ad} is the amount of mass advected into the disturbance during a small interval of time dt . This advected mass can be evaluated from the convergence profile obtained by Williams (1970) for conservative cloud-clusters. The changes in temperature due to detrainment from the clouds can be written as

$$dT_{\text{DETRAINMENT}} = (T_{\text{CLOUDS}} - T_{\text{DISTURBANCE}} - Q_{\text{cl}} \frac{L}{c_p}) \frac{dm_{\text{det}}}{m}, \quad (25)$$

where Q_{cl} represents the cloud liquid water content of the population. In order to evaluate this term the mean detrainment rate and the mean cloud temperature and liquid-water content of the cloud population under consideration must be known. These terms can be obtained by integrating over the lifetime of the clouds used in the typical cloud population, and combining the contributions of each type of cloud according to their relative frequencies as was done in equations (1) to (14). Fig. 10 portrays the vertical profile of the term $dT_{\text{detrainment}}$ under the assumption that no other thermodynamic effects are present. In the case when radiational cooling and sinking warming is present, however, the amount of warming or cooling experienced will be largely dependent on the difference between the clouds mean temperature and the resultant temperature of the disturbance.

The change in the mixing-ratio of water vapor of a horizontal layer or slab of the disturbance can also be expressed in the following form

$$dx = dx_{\text{SUBSIDENCE}} + dx_{\text{ADVECTION}} + dx_{\text{DETRAINMENT}} \quad (26)$$

The contribution due to subsidence is

$$dx_{\text{SUBSIDENCE}} = \frac{dx}{dz} W_s dt \quad (27)$$

where $\frac{dx}{dz}$ is the vertical gradient of mixing-ratio in the disturbance's atmosphere, and the other terms have the same meaning as in equation (23). The change in mixing-ratio due to advection becomes

$$dx_{\text{ADVECTION}} = (x_{\text{ENVIRONMENT}} - x_{\text{DISTURBANCE}}) \frac{dm_{\text{ad}}}{m} \quad (28)$$

Similarly, the water vapor contribution of the detrainment from the clouds can be written as

$$dx_{\text{DETRAINMENT}} = (x_{\text{CLOUDS}} - x_{\text{DISTURBANCE}} - Q_{\text{cl}}) \frac{dm_{\text{det}}}{m} \quad (29)$$

where the same considerations of equation (25) apply.

Results of the Heat and Moisture Budget

Equations (22) and (26) have been integrated for a period of 24 hours in time steps of 15 minutes. Every fifteen minutes the change in temperature and moisture of 500 meters-thick layers of the disturbance were found, and new temperature and mixing-ratio profiles were computed. These new values were used to evaluate the new

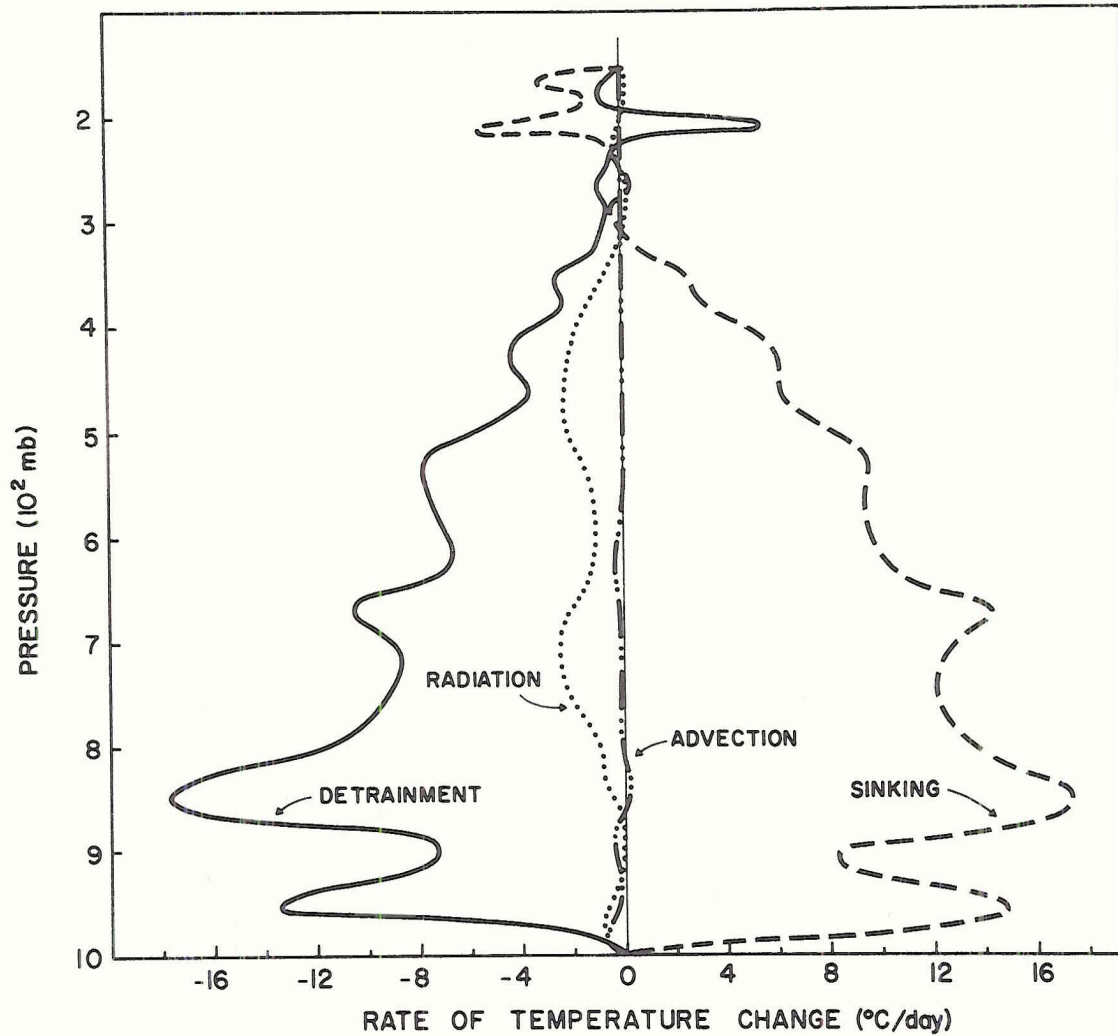


Fig. 13. Vertical profiles of the different heating terms of the heat budget of a steady-state tropical disturbance.

changes, and so on. Figs. 13 and 14 portray the accumulated effect of each of the terms of equations (22) and (26) for the time interval of one day. The final temperature profile was within 0.2°C of the initial (environmental) temperature, while the mixing-ratio profile was within 0.1 gm/kgm of the initial values.

The values with height of the different terms of the heat budget of the disturbance are shown in Fig. 13. A mean tropospheric cooling

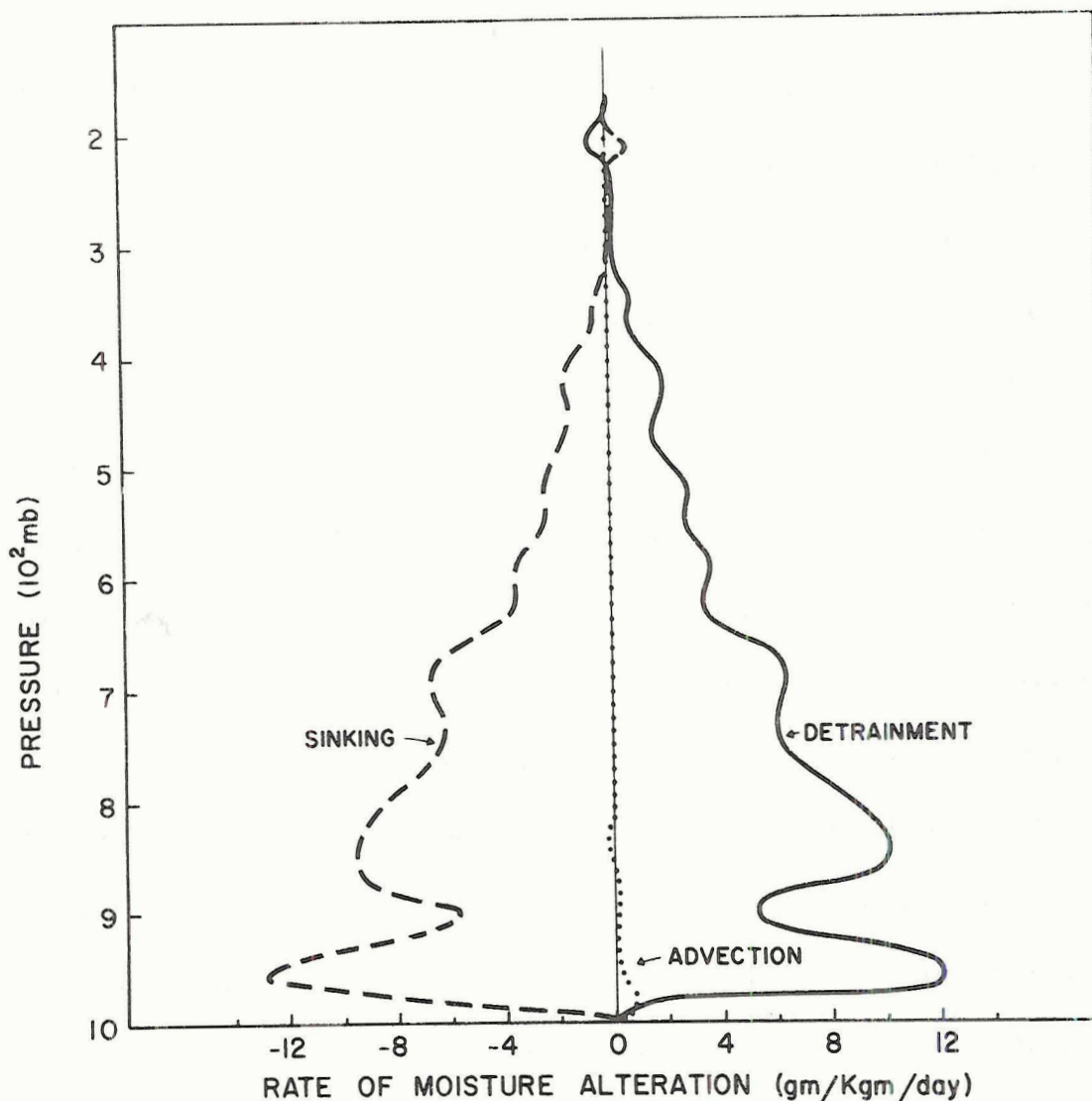


Fig. 14. Vertical profiles of the different terms of the moisture budget of a steady-state tropical disturbance.

of 1.0°C is experienced during a day due to radiational losses (dotted line). This cooling is compensated by the much larger warming produced by the induced sinking motion (dashed line). This sinking produces a mean warming of 7.5°C per day, the largest warming being experienced in the lower half of the disturbance's atmosphere (18°C). Notice that due to the induced ascent at high levels, a local cooling of about 5°C results at around 200 mb. The net effect of detrainment

is felt by the disturbance as a mean cooling of 6.1°C . It is interesting to note how the subsidence warming is modulated by the cooling due to detrainment. This close adjustment is a result of the dependence of the subsidence-warming term on the difference between the dry adiabatic lapse rate and actual lapse rate of the disturbance (see equation 23). As the detrainment cooling changes the lapse rate of the disturbance, the sinking warming changes in the opposite sense. As a result, there is a tendency in the long run for a close compensation of both effects. The effect of advection of environmental air is very small compared to any of the other terms ($\sim -0.1^{\circ}\text{C}$).

Considering the different terms of the humidity budget (Fig. 14), it can be seen that there is a very good balance between the subsidence and detrainment effects, while the advection of environmental air contributes very little to the total moisture budget. The dryness produced by the subsidence of cloud-free air is balanced very closely by the detrainment of water-vapor and cloud liquid-water at all levels. This close adjustment is a result of the dependence of the detrainment term on the difference between the mixing-ratio of the cloud and that of the disturbance (see equation 30). As a result, there is a tendency for the clouds in the long run to compensate exactly for the dryness produced by subsidence.

In the light of these results it becomes evident that in order to explain the role of cumulus clouds in the energetics of a tropical distur-

bance, both the ascending and descending branches of the cumulus convection circulation have to be considered. The effect of the ascending branch (upward mass transport inside the clouds) is to cool and increase the moisture of the disturbance by the process of detrainment, and to induce a compensatory sinking motion around the clouds. The effect of the induced descending branch of the convective circulation around the clouds is to warm the disturbance by converting potential energy into sensible heat, and to decrease the humidity of the air around the clouds by bringing down upper air of lower water vapor content.

In the quasi steady-state disturbance, the effects of the two branches of the convective circulation and of radiation balance one another so that the temperature and moisture profiles stay constant in time. From the point of view of the total disturbance, the heat, which is liberated in the condensation of the two or three centimeters of rain produced in a day, is used to compensate for the radiational losses and the exportation of potential energy to the general tropical circulation.

Vertical Mass Circulation in a Steady-State Disturbance

Fig. 15 portrays the different components of the vertical mass circulation present in a steady-state disturbance. Curve A (solid line) represents the mean upward mass transport that the model cloud population is required to perform in order to produce a rainfall rate of

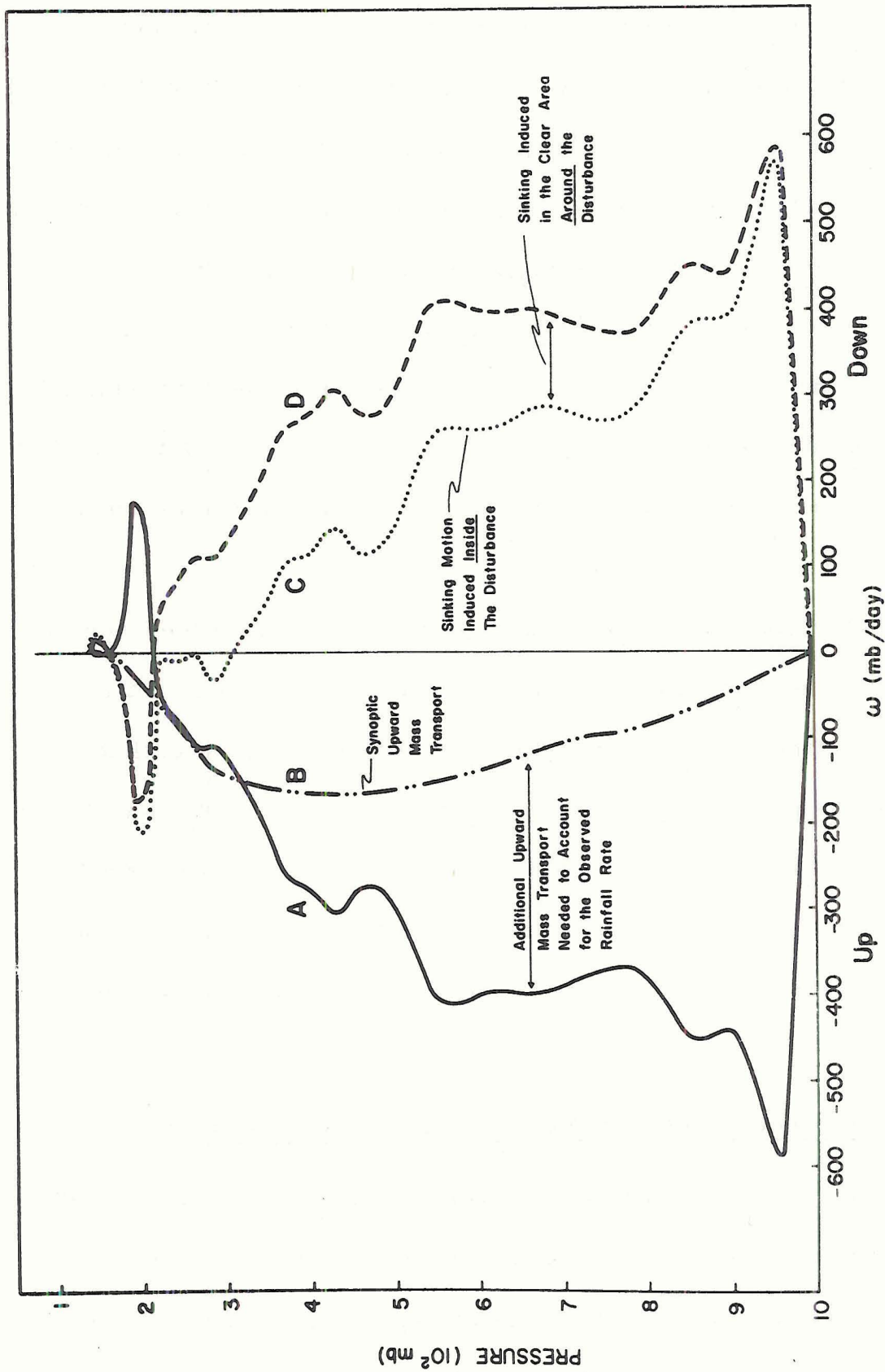


Fig. 15. The different components of the vertical mass circulation present in a steady-state disturbance.

2.5 cm per day. This means that the mass-transport by the clouds establishes the divergence profile shown in Fig. 12. Curve B (dashed-dot line) represents the upward mass transport resulting from the synoptic divergence profile of Williams (1970). The difference between the required (curve A) and the synoptic (curve B) upward mass transport must be compensated locally inside the disturbance by a downward mass transport in the clear regions between clouds. This downward mass circulation is portrayed in curve C (dotted line). It is this sinking motion that releases sensible heat to the disturbance's atmosphere as noticed previously. The compensation for the remaining upward mass circulation (the synoptic contribution) occurs outside the disturbance. Adding this downward-outside contribution to curve D, the total downward branch of the mass circulation of the disturbance is obtained (curve D). For purposes of illustration it has been assumed that the subsidence occurring outside takes place over an area equal to that of the disturbance.

Developing Disturbances

The previous computations apply to the case of a steady-state tropical disturbance, i. e., a system that exports at high altitudes (in the form of potential energy) the latent heat advected into it at low- and middle-levels. This type of disturbance represents the typical cloud cluster that travels for several days over the oceans with no appreciable change in intensity. The heat liberated in the condensa-

tion of the two or three centimeters of rain produced in a day is exported as potential energy to the general tropical circulation in which the cloud-cluster is embedded, after provision is made for the disturbance's own radiational losses.

The response of the large-scale flow to the energy exportation of a disturbance, however, can result in drastic changes in the synoptic features of the region. This is the case of hurricane development. The interaction between a disturbance and the surrounding flow can be viewed in the following way: A tropical disturbance as a whole takes in environmental mass at low- and middle-levels, and exports mass at high altitudes. To satisfy this synoptic upward mass-transport, a compensatory sinking motion is induced in the air surrounding the disturbance. In this way, the potential energy produced by the cloud cluster is converted outside of the cluster into sensible energy. The degree of the resultant warming depends, however, on the scale on which the compensatory sinking occurs. If the subsidence takes place over a broad region, a slight warming is experienced which is probably used to compensate for the radiational cooling of the area. (This idea is developed in the second paper of this report). If the compensatory subsidence occurs over a small region near the disturbance, however, enough compressional warming could take place to explain hurricane development. In fact Oliver and Anderson (1969) have found from satellite observations that the majority of hurricanes form around a circulation center that develops in the clear area ahead of

the convective region. The study of the large-scale flow features leading to a concentrated compensatory descending current is beyond the scope of this investigation. However, there are reasons to believe that the broad-scale flow at the level of the disturbance's outflow (~200 mb) might be the controlling factor. Thus, if the wind pattern at that level allows the outflow from the disturbance to be spread over a broad region, only gentle subsidence and warming will occur. However, if the upper-air wind pattern blocks somewhat the outflow, strong local subsidence and considerable warming might develop near the disturbance. The convective activity would then organize itself around the resulting warm-core low-pressure region. Further studies along these lines could provide considerable insight to the physics of hurricane development from weak tropical disturbances.

VI. SUMMARY

A numerical model of individual cumulus clouds has been used in this section to investigate the effects of cumulus convection on the large-scale features of tropical disturbances. A cloud population characteristic of tropical disturbances has been determined from radar and synoptic observations. With the help of the numerical cloud model, the effects of the typical ensemble of cumuli have been calculated. One major effect consists of the detrainment of cloud mass which will cause a direct transport of excess sensible heat, as well as cooling of the surrounding clear air as a result of the evaporation of the detrained cloud liquid-water. The net effect was found to be one of cooling as the evaporation overcompensates for the diffusion of excess sensible heat. In this regard, cumulus clouds should be considered as a basic "cooling tower" as opposed to a "hot tower" concept. The other effect produced by the typical population is the induction of a descending motion in the environment to compensate for the upward mass-transport of the clouds. The induced subsidence will result in the warming and drying of the environment.

Using all of this information, a heat and moisture budget for a steady-state tropical disturbance has been computed. Under steady-state assumptions the heat liberated from the condensation of rain-water is exported to the environment in the form of potential energy at the level of the disturbance's outflow. At the same time, the water-

vapor necessary to produce the rainfall is imported into the disturbance in the form of a low- and middle-level mass convergence. Inside of the disturbance, the warming resulting from the sinking motion is compensated by the net cooling resulting from detrainment plus the cooling resulting from infrared radiational losses. Similarly, the dryness resulting from the subsidence is compensated by the detrainment of water vapor and liquid water from the clouds.

The convergence of mass at low- and middle-levels into the disturbance as a whole, and the high altitude outflow of mass from the disturbance, will in turn induce a descending motion in the clear air surrounding the storm. The warming will be large or small depending on the scale at which the subsidence occurs. Under favorable situations the warming could be large enough to produce hydrostatically the low pressures needed for the organization of a tropical disturbance into a full-fledge hurricane. The present numerical model of cumulus clouds has proven to be useful in investigating the interaction of cumuli with the large scale features of tropical disturbances, and it is expected that future investigations using this tool will result in the clarification of the problem of formation of hurricanes from a weaker disturbance and in the maintenance of the tropical general circulation.

It was quite unexpected that the cloud cluster dynamics as determined by this cumulus and meso scale approach would correspond so well with the cloud cluster dynamics as determined by Gray (1972) in Part III of this series where the characteristics of the individual cumulus are not involved.

ACKNOWLEDGEMENTS

The author wishes to express his sincere gratitude to Professor William M. Gray under whose guidance this investigation was performed. His kind criticism and encouragement are very much appreciated. Special thanks are due to Mr. Edward Buzzel, Mrs. Barbara Brumit and Mr. Larry Kovacic who helped with the programming, manuscript typing and drafting.

vapor necessary to produce the rainfall is imported into the disturbance in the form of a low- and middle-level mass convergence. Inside of the disturbance, the warming resulting from the sinking motion is compensated by the net cooling resulting from detrainment plus the cooling resulting from infrared radiational losses. Similarly, the dryness resulting from the subsidence is compensated by the detrainment of water vapor and liquid water from the clouds.

The convergence of mass at low- and middle-levels into the disturbance as a whole, and the high altitude outflow of mass from the disturbance, will in turn induce a descending motion in the clear air surrounding the storm. The warming will be large or small depending on the scale at which the subsidence occurs. Under favorable situations the warming could be large enough to produce hydrostatically the low pressures needed for the organization of a tropical disturbance into a full-fledge hurricane. The present numerical model of cumulus clouds has proven to be useful in investigating the interaction of cumuli with the large scale features of tropical disturbances, and it is expected that future investigations using this tool will result in the clarification of the problem of formation of hurricanes from a weaker disturbance and in the maintenance of the tropical general circulation.

It was quite unexpected that the cloud cluster dynamics as determined by this cumulus and meso scale approach would correspond so well with the cloud cluster dynamics as determined by Gray (1972) in Part III of this series where the characteristics of the individual cumulus are not involved.

ACKNOWLEDGEMENTS

The author wishes to express his sincere gratitude to Professor William M. Gray under whose guidance this investigation was performed. His kind criticism and encouragement are very much appreciated. Special thanks are due to Mr. Edward Buzzel, Mrs. Barbara Brumit and Mr. Larry Kovacic who helped with the programming, manuscript typing and drafting.

BIBLIOGRAPHY

- Battan, L. J., 1953: Duration of Convective Radar Cloud Units. Bull. Meteor. Soc., 34, 227-228.
- Betts, A. U., 1972: A Composite Mesoscale Cumulonimbus Budget. Atmospheric Science Paper No. 186, Department of Atmospheric Science, Colorado State University, 48 pp.
- Blackmer, R. H., Jr., 1955: The Lifetime of Small Precipitation Echoes. Proceedings of the 5th Weather Radar Conference, 103-108.
- Charney, J. G., and A. Eliassen, 1964: On the Growth of the Hurricane Depression. J. Atmos. Sci., 21, 68-75.
- Cox, S. K., 1969: Radiation in the Free Atmosphere. Department of Meteorology, The University of Wisconsin, 68 pp.
- Gray, W. M., 1972a: The Magnitude and Character of the Radiation Induced Vertical Circulation of the Troposphere. Proceedings of the Conference on Atmospheric Radiation, August 7-9, Fort Collins, Colorado.
- _____, 1972b: Broad-scale and Meso-Scale Interaction. Atmospheric Science Paper No. 190, Department of Atmospheric Science, Colorado State University.
- Holle, R. L., 1968: Some Aspects of Tropical Oceanic Cloud Population. J. of Appl. Meteor., 7, 173-183.
- Kininmonth, W. R.: Thermal Modification of the Troposphere due to Convective Interaction. Atmospheric Science Paper No. 167, Department of Atmospheric Science, Colorado State University, 36 pp.
- Kuo, H. L., 1965: On Formation and Intensification of Tropical Cyclones Through Latent Heat Release by Cumulus Convection. J. Atmos. Sci., 22, 40-63.
- Lopez, R. E., 1968: Investigation of the Importance of Cumulus Convection and Ventilation in Early Tropical Storm Development. Atmospheric Science Paper No. 124, Department of Atmospheric Science, Colorado State University, 86 pp.

BIBLIOGRAPHY (cont'd)

- Lopez, R.E., 1972: Cumulus and Meso-Scale Interactions, Atmospheric Science Paper No. 189, Department of Atmospheric Science, Colorado State University, 100 pp.
- Manabe, S. and Strickler, R.G., 1964: Thermal Equilibrium of the Atmosphere with a Convective Adjustment. J. Atmos. Sci., 21, 361-385.
- McIntyre, H.D., 1956: Radar Study of the Motion of Small Precipitation Areas in Hurricanes "Carol" and "Edna". Technical Note No. 9, Massachusetts, Institute of Technology, 4-5.
- Ogura, Y., 1964: Frictionally Controlled, Thermally Driven Circulations in a Circular Vortex with Applications to Tropical Cyclones. J. Atmos. Sci., 21, 610-621.
- Oliver, V.J. and R.K. Anderson, 1969: Circulation in the Tropics as Revealed by Satellite Data. Bull. Am. Meteor. Soc., 50, 702-707.
- Ooyama, K., 1963: A Dynamical Model for the Study of Tropical Cyclone Development. Department of Meteorology and Oceanography, New York University, 26 pp.
- _____, 1969: Numerical Simulation of the Life Cycle of Tropical Cyclones. J. Atmos. Sci., 26, 3-40.
- Reed, R.J. and E.E. Recker, 1971: Structure and Properties of Synoptic-Scale Wave Disturbances in the Equatorial Western Pacific. J. Atmos. Sci., 28, 1117-1133.
- Riehl, H., 1945: Waves in the Easterlies and the Polar Front in the Tropics. Miscellaneous Reports No. 17, Department of Meteorology, University of Chicago, 79 pp.
- _____, and J.S. Malkus, 1958: On the Heat Balance in the Equatorial Trough Zone. Geophysica, 6, 503-538.
- Rosenthal, S.L., 1970: Circularly Symmetric Primitive Equation Model of Tropical Cyclone Development Containing Explicit Water Vapor Cycle. Mo. Wea. Rev., 98, 643-663.

BIBLIOGRAPHY (cont'd)

Senn, H. V., H. W. Hiser and E. F. Low, 1959: Studies of the Evolution and Motion of Hurricane Spiral Bands and the Radar Echoes Which Form From Them. The Marine Laboratory, University of Miami, 65 pp.

_____, and J. A. Stevens, 1965: A Summary of Empirical Studies of the Horizontal Motion of Small Radar Precipitation Echoes in Hurricane Donna and Other Tropical Storms. National Hurricane Research Laboratory, Report No. 74, 55 pp.

Williams, K. T., 1970: A Statistical Analysis of Satellite-Observed Trade Wind Cloud Clusters in the Western North Pacific. Atmospheric Science Paper No. 161, Department of Atmospheric Science, Colorado State University, 80 pp.

**Cumulus Convection and Larger-Scale Circulations
Part III**

Broadscale and Mesoscale Considerations

By

William M. Gray

Department of Atmospheric Science
Colorado State University
Fort Collins, Colorado

**Colorado
State
University**

**Department of
Atmospheric Science**

Paper No. 190

CUMULUS CONVECTION AND LARGER-SCALE CIRCULATIONS

Part III

Broadscale and Meso Scale Considerations

by

William M. Gray

Department of Atmospheric Science

Colorado State University

July 1972

Atmospheric Science Paper No. 190

ABSTRACT

This manuscript (Paper III) discusses the magnitude and implication of the vertical circulation patterns of the summertime tropical atmosphere as derived from large scale consideration. It is to be compared with the vertical circulation patterns derived from cumulus scale considerations as discussed by López (1972a, 1972b) in Papers I and II. From the large scale it is shown that very significant extra up- and-down "local" vertical motion is occurring beyond what would be prescribed by the "mean" or synoptic scale flow patterns. This typical unresolved and mass compensating extra up- and-down vertical circulation pattern can be specified from satellite observed and calculated cloud cluster scale ($\sim 4^\circ$) mass, vapor, energy and rainfall-evaporation budgets. The method of determining this extra "local" vertical circulation and its magnitude are presented and discussed. Results are very closely comparable with those obtained by López (op. cit.) from an independent small scale approach through modeling of individual cumulus elements. These two independent approaches from different scales of consideration give very similar results. This "local" vertical circulation is shown to be fundamental for the mass, vapor and energy balances of the tropical atmosphere. Other discussions of the characteristics of the cumulus convective atmosphere are made.

I. INTRODUCTION

The manner by which cumulus clouds and the broader-scale flow patterns interact with each other is not well understood at this time. It is very important that we come to grips with the physics of this interaction problem. Many meteorologists feel this to be a fundamental requirement to improved understanding and prediction of large-scale atmospheric flow patterns.

The author feels that a significant expansion of our knowledge on this problem is possible from the meteorological information already on hand if we organize our various facets of information in a judicious way. This is the purpose of the following discussion.

This research discusses the required mass, water vapor, and energy budgets of the summer, oceanic Trade Wind-Equatorial Trough belt from about 5° to 25° latitude. These budgets are obtained from resolving into a mutually consistent pattern the available broad-scale (meso, synoptic, and zonal) observational knowledge on the mass, water vapor, and energy information in this region.

It will be shown that the accomplishment of these balances requires a very substantial "local" up- and-down vertical circulation with condensation and reevaporation rates much larger than the observed rainfall-evaporation. This paper specifies the magnitude of this vertical circulation and water vapor recycling, and then discusses the resulting energy requirements. It also compares these mass-vapor-energy

budgets derived from broad-scale considerations for the cloud cluster with the same budgets obtained by López (Papers I and II) from incorporation of individual convection elements from his cumulus life cycle model. It will be shown that both approaches, one from the large scale going downward in scale (broad-scale approach), and the other using the individual convective elements and going upward in scale (cumulus scale approach) do indeed mesh with near identical mass-vapor-energy budget results. The meshing of these independent approaches from different scales of consideration lends confidence to the results to be shown.

II. DATA SOURCES

To deal with the tropical belt in a realistic way, it was indispensable that representative information be obtained on the typical tropical belt lapse rate conditions, vapor contents, divergences, shears, etc., associated with the satellite observed tropical cloud clusters, the other variable cloud areas, and with the clear regions. To accomplish this, the author performed extensive radiosonde data composite analysis of satellite observed cloud and clear areas in the Western Pacific and the West Indies. These regions have the only oceanic radiosonde networks from which associated wind-temperature-moisture information could be obtained.

Figs. 1 and 2 show the locations of the radiosonde networks which were used to composite the digitized satellite meso-scale cloud clusters, the other variable cloud regions, and the clear regions. This was accomplished for the three summer seasons of 1967-1969. Figs. 3-6 show the locations of the composited cloud clusters and clear areas within these networks. Clusters and clear areas were divided into two latitudinal groupings; those poleward and equatorwards of 18° . The methods of compositing, and a discussion of the data limitations, inaccuracies, etc. have been made in an earlier report by Williams (1970). The reader is referred to this report for more information. Fig. 7 shows typical views of these satellite observed tropical clusters and clear regions.

There were 557 clusters and 223 clear areas in the Western Pacific and 539 clusters and 212 clear areas in the West Indies networks which are included in the data composites.

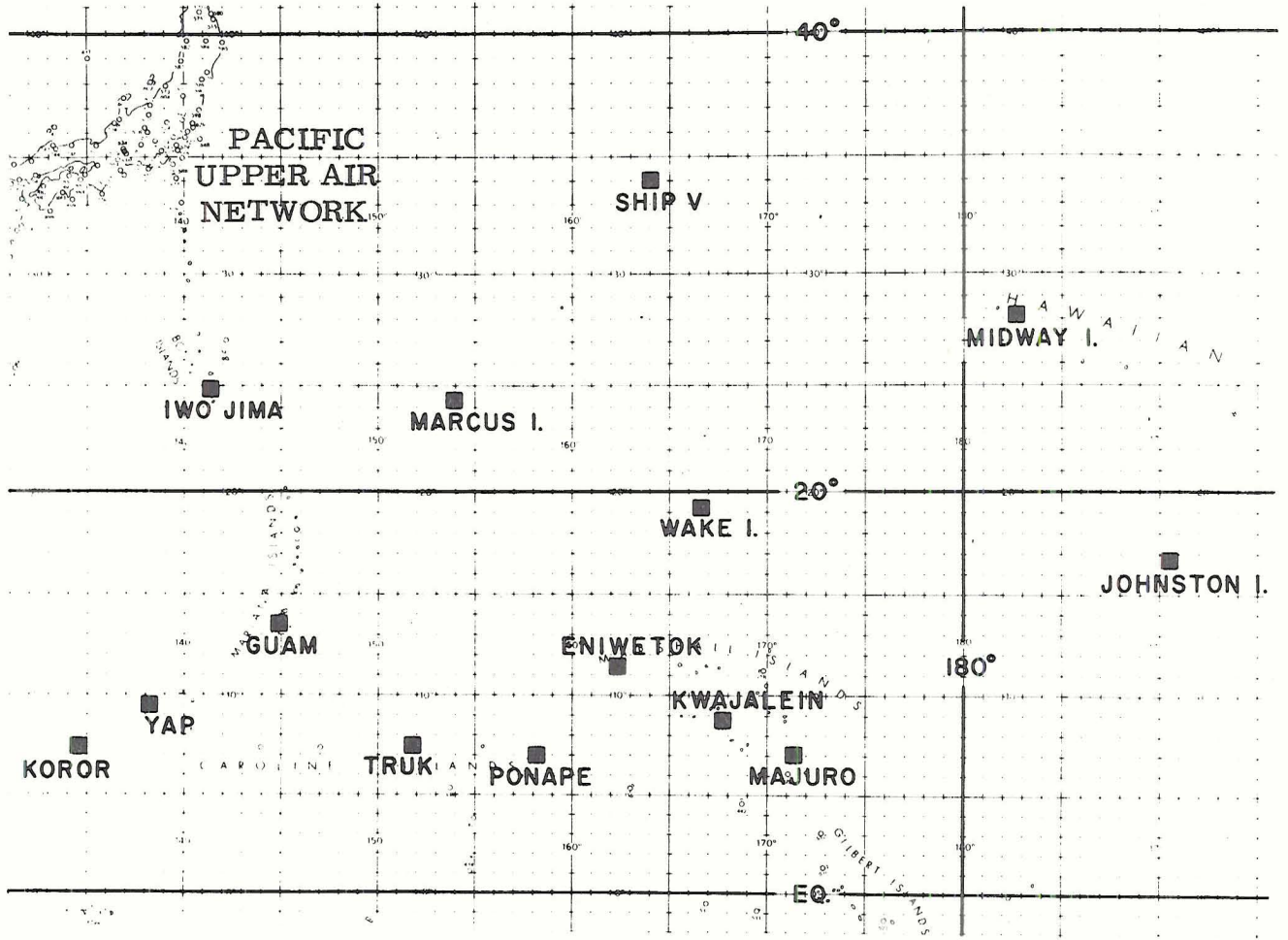


Fig. 1.

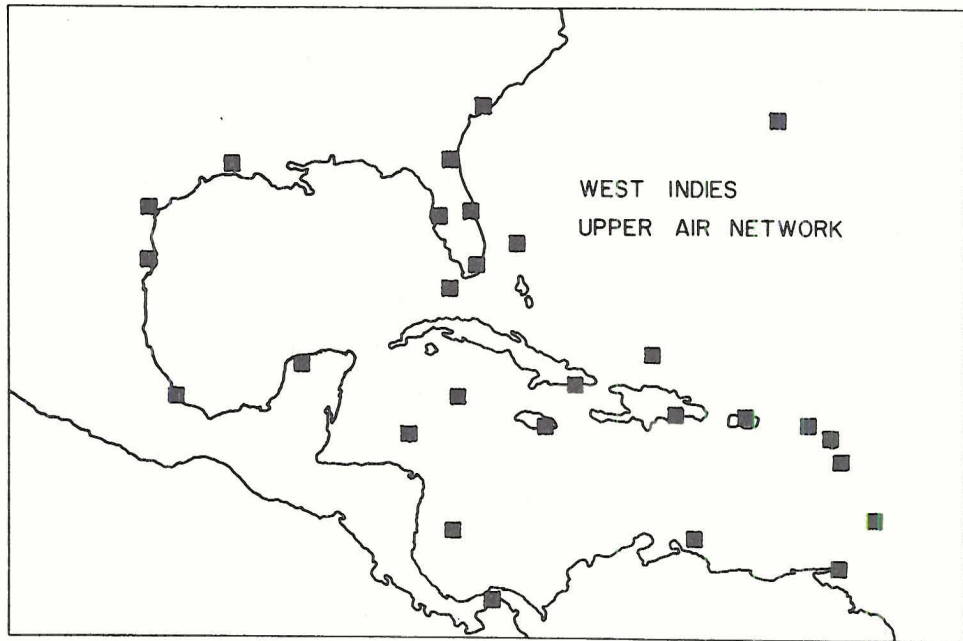


Fig. 2.

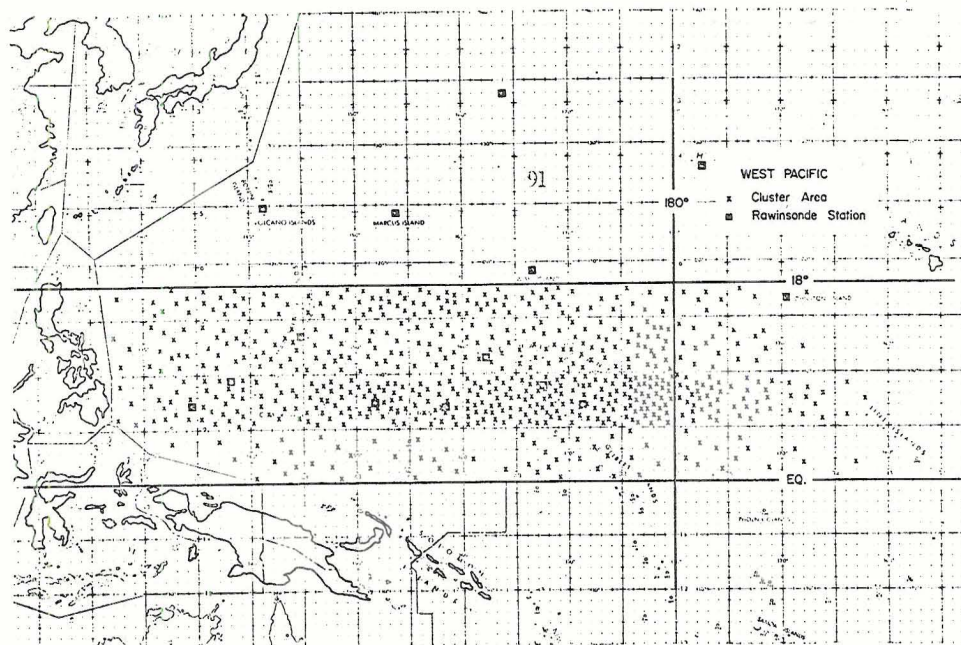


Fig. 3. Location of cluster regions in the West Pacific.

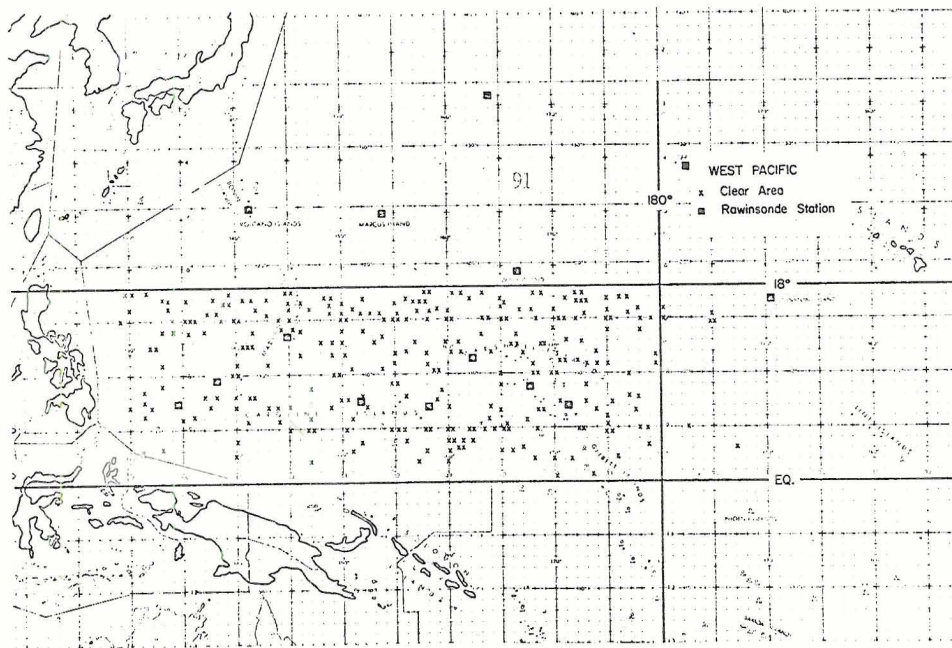


Fig. 4. Location of clear regions in the West Pacific.

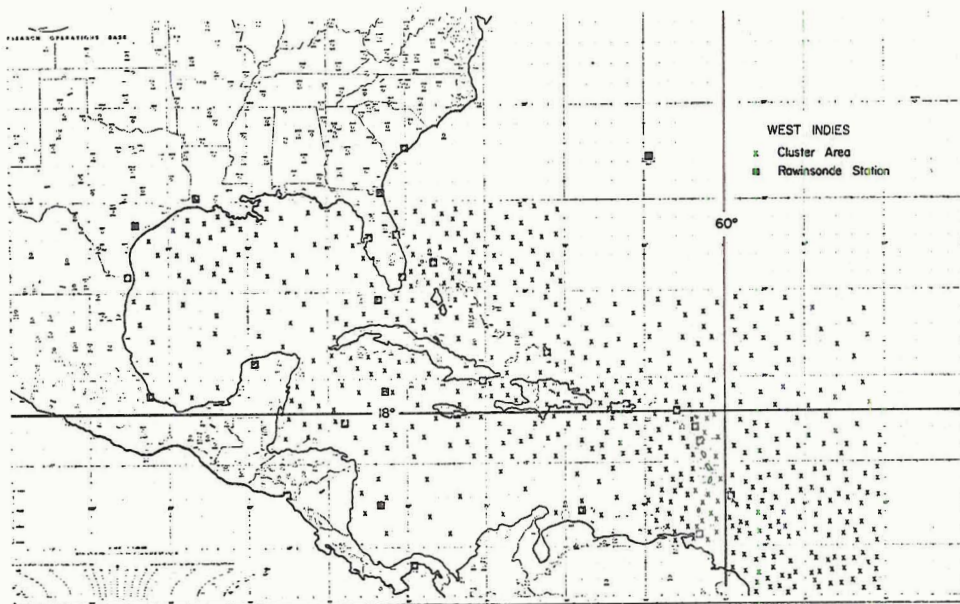


Fig. 5. Location of cluster regions in the West Indies.

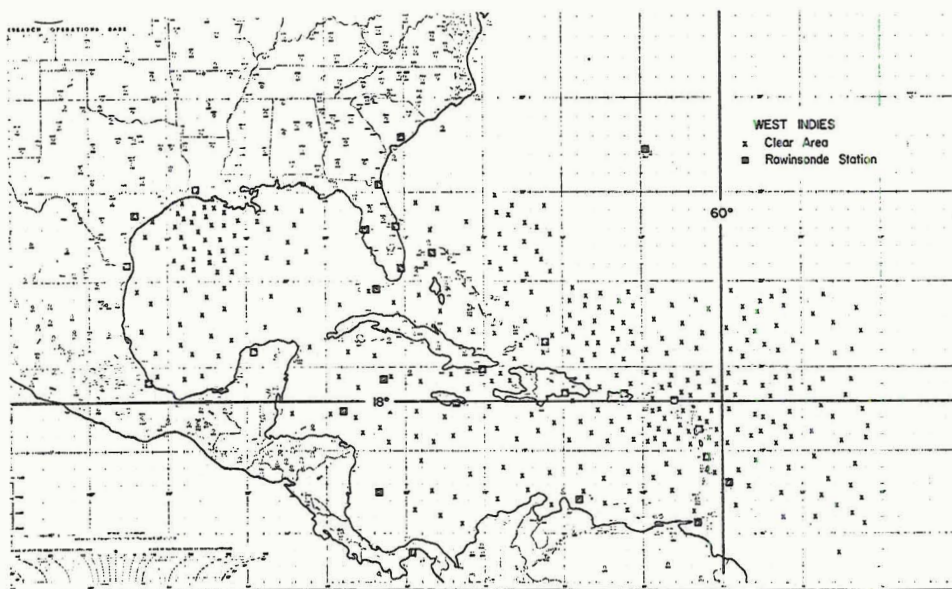
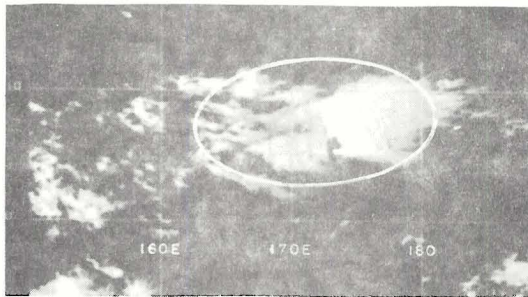
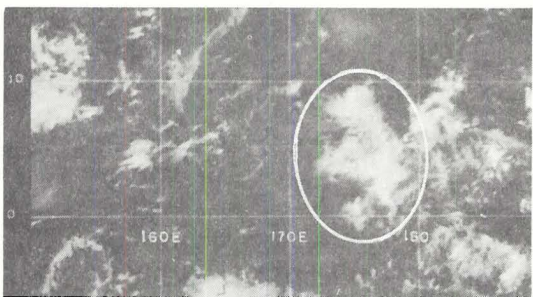
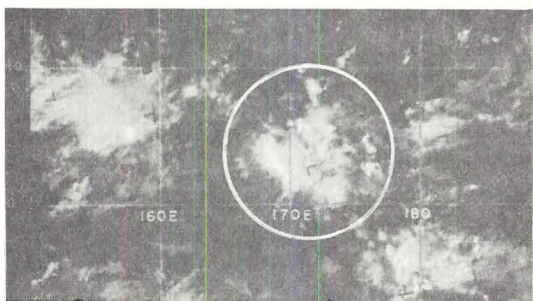
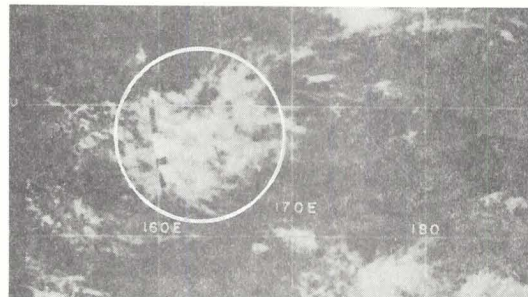
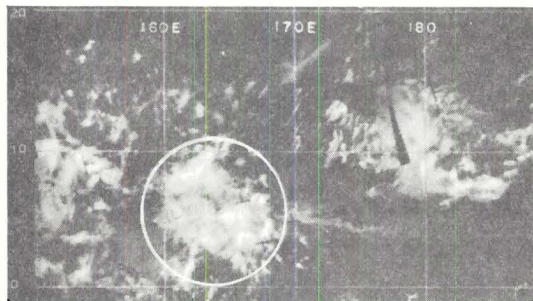


Fig. 6. Location of clear regions in the West Indies.

CLUSTER



CLEAR AREAS

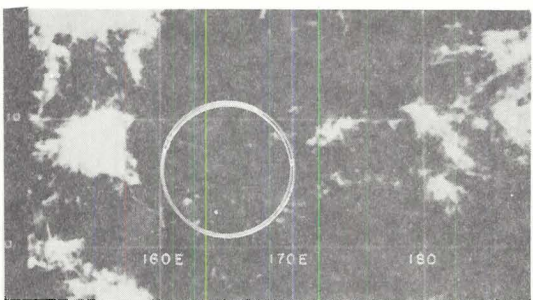


Fig. 7. Typical portrayal of cluster and clear regions.

III. GENERAL TROPICAL BELT RAINFALL, WATER VAPOR, AND ENERGY BUDGET CONSIDERATIONS

Tropospheric conditions in the whole tropical belt of summer are considered. This includes the trade wind and equatorial trough regions from approximately 5° to 25° of latitude. Oort and Rasmusson (1971) have shown (from data derived from MIT Department of Meteorology rawinsonde tapes) that this tropical area is mass, vapor, and energy budget-wise a very self contained region. Their data indicates that the net tropospheric energy divergences in the summertime latitudes from 5 - 25° latitude are very small in comparison with the net tropospheric radiational cooling. They show, that for mean tropospheric conditions over this region, the vertical motion averages but a few mb/day, meridional induced water vapor changes average only about 0.1 gm/kg and that meridional induced advective cooling-warming rates (averaged through the troposphere) are less than $0.1^{\circ}\text{C}/\text{day}$. In comparison, local vertical motion to accomplish the required rainfall and balance the net radiation cooling must be of the order of 100 mb/day, and evaporation-rainfall must average about 0.5 cm/day (or 1.3°C latent heat equivalent for the whole troposphere). Thus, in comparison with net tropospheric radiational losses, the summertime meridional fluxes in the broad tropical belt where cloud clusters exist can be largely neglected. Each latitudinal belt must very closely meet its own energy budget requirements. The longitudinal or Walker circulations allow

for some individual longitude budget imbalances, but these largely cancel in the global latitudinal average. Fig. 8 shows that the net meridional divergence of energy is very small in comparison with the net radiation loss. It will be assumed that this broadscale estimate also applies to the summertime oceanic regions by themselves.

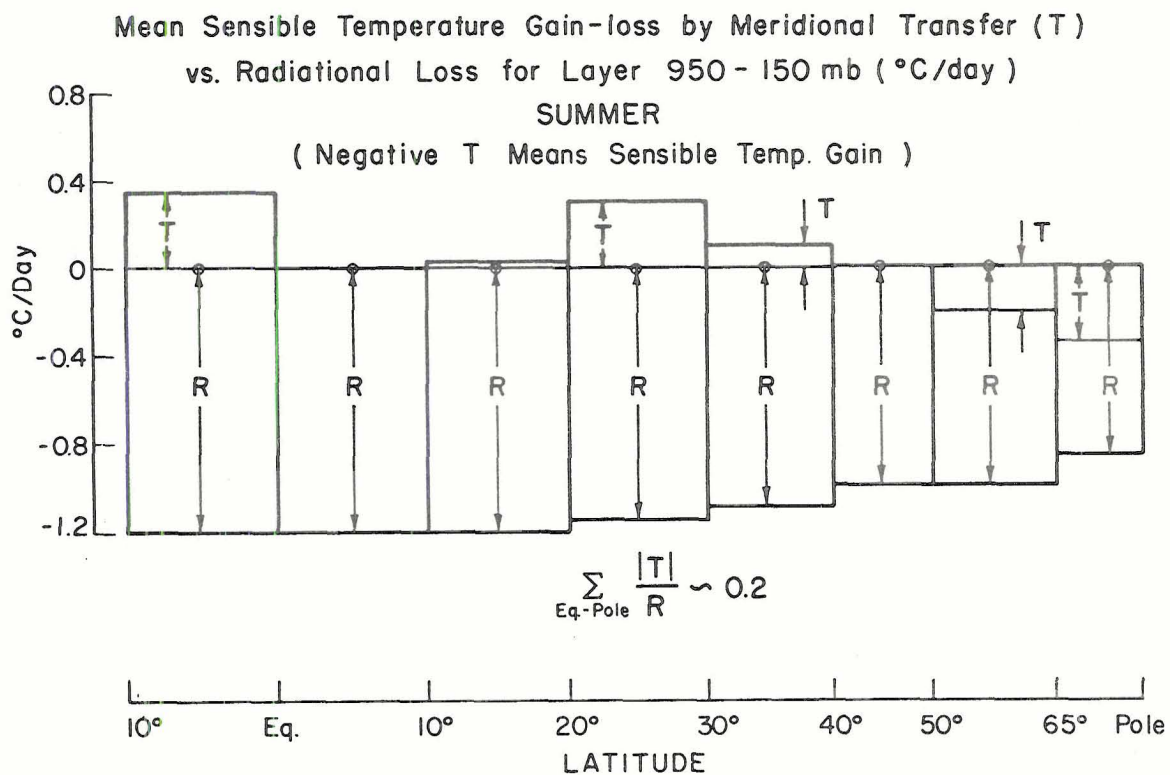


Fig. 8. Comparison of mean tropospheric temperature change due to all meridional energy convergence sources (T) by wind systems vs. net tropospheric radiation loss (R) in (°C/day) for summer. Meridional energy convergence obtained from Oort and Rasmusson (1971). Note lack of any appreciable energy convergence in Equator to 20° latitude belt.

Table 1

ESTIMATES OF EQUATOR TO 30°N NET RADIATION
COOLING IN THE LAYER FROM 1000-150 mb. (°C/DAY)

(This tropical region has little seasonal variation)

		<u>Eq-30°</u>
	London (1957)	1.12
Model	Davis (1963)	1.11
Determinations	Rogers (1967)	1.18
	Dopplick (1970)	<u>1.13</u>
	Average	1.14
	Cox and Suomi (1969)	
	Measurements	1.37
Measurements	(with Davis Short-Wave Values)	
	Vonder Haar (1971)	1.26 (Eq-20°)

Over the tropical oceans the ratio of sensible to latent heat transport is felt to be very small (Sellers, 1965). Assuming negligible sensible heat transport, the self-contained nature of the tropical belt requires that the tropospheric radiation loss of about 1.3-1.4°C/day (see Table 1 for various net radiation loss estimates) be balanced by an average summertime rainfall-evaporation rate of about 0.5 cm/day. Previous estimates (Budyko, 1956) indicate that this is about what the summertime tropical rainfall-evaporation rates are. Evaporation of 0.5 cm/day will be assumed everywhere. For simplicity the net tropospheric radiation cooling and the energy of evaporation will be taken to be constant and everywhere balanced as in Fig. 9.

PRESSURE (10 ² mb)	CLOUD CLUSTER (20%)	VARIABLE CLOUD REGION (40%)	CLEAR REGION (40%)
	0.5	0	0
1	-0.4	-0.4	-0.4
2	-0.9	-0.9	-0.9
3	-1.4	-1.4	-1.4
4	-1.5	-1.5	-1.5
5	-1.7	-1.7	-1.7
6	-1.9	-1.9	-1.9
7	-1.9	-1.9	-1.9
8	-1.6	-1.6	-1.6
9	-1.5	-1.5	-1.5
10			
	EVAP. 0.5 gm/cm ² day	EVAP. 0.5 gm/cm ² day	EVAP. 0.5 gm/cm ² day
	RAIN 2.5 gm/cm ² day	NO RAIN	NO RAIN

Fig. 9. Assumed net radiation cooling, evaporation, and rain in the three tropical regions.

Although evaporation is rather uniformly distributed, rainfall is typically concentrated in meso-scale cloud clusters, taking up but 15-20% of the area of the tropical belt. Here the total tropical belt evaporation falls out as rain in average amounts of 2-3 cm/day (Williams, 1970). Other regions possess cloudiness but with negligible amounts of precipitation. The dynamics of the rain, cloud, and clear regions must be quite different. Each region has its own distinctive mass, vapor, and energy budget which should be individually treated.

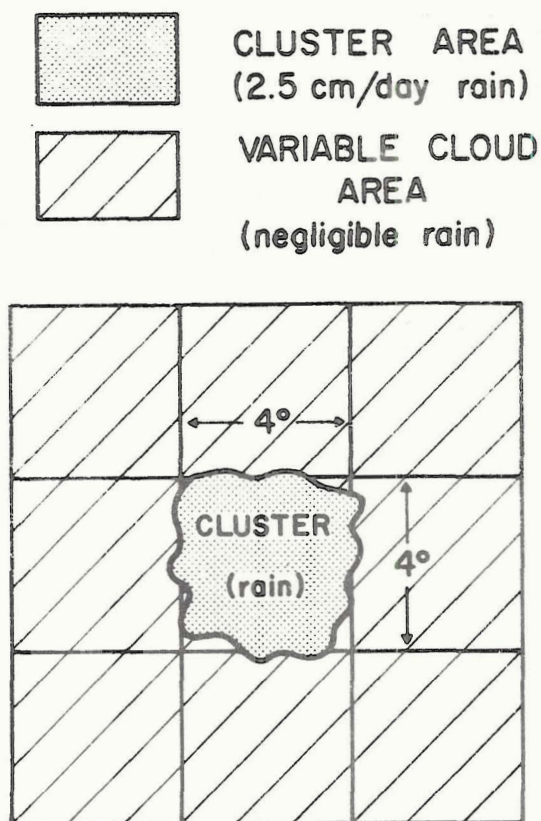


Fig. 10. Rawinsonde composite of variable cloud region was taken in the hatched region surrounding the cloud cluster (shaded area).

Simplified Division of Tropical Belt. To expedite understanding of the tropical belt it has been divided into three meteorological regions. These are:

- 1) Cloud cluster regions taking up about 20% of the area of the tropical belt and having average rainfall of 2.5 cm/day.
- 2) Variable cloud regions taking up about 40% of the area of the tropical belt which have scattered to broken cloud conditions but have no applicable rainfall. The average temperature and dew point conditions of this region were obtained from compositing the regions around the cloud cluster as seen in Fig. 10.
- 3) Clear regions taking up about 40% of the area of the tropical belt.

Fig. 11 and 12 show individual composites of the temperature and dew point for each region obtained from the rawinsonde compositing

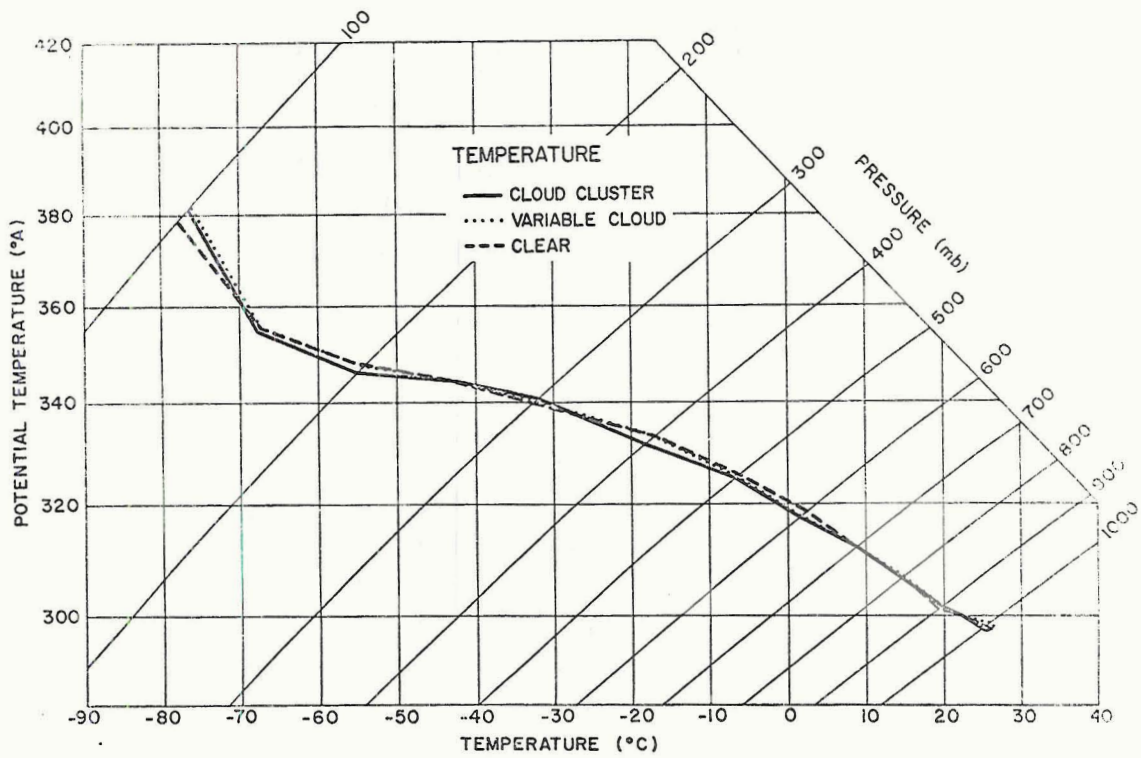


Fig. 11. Composite temperature soundings for three regions.

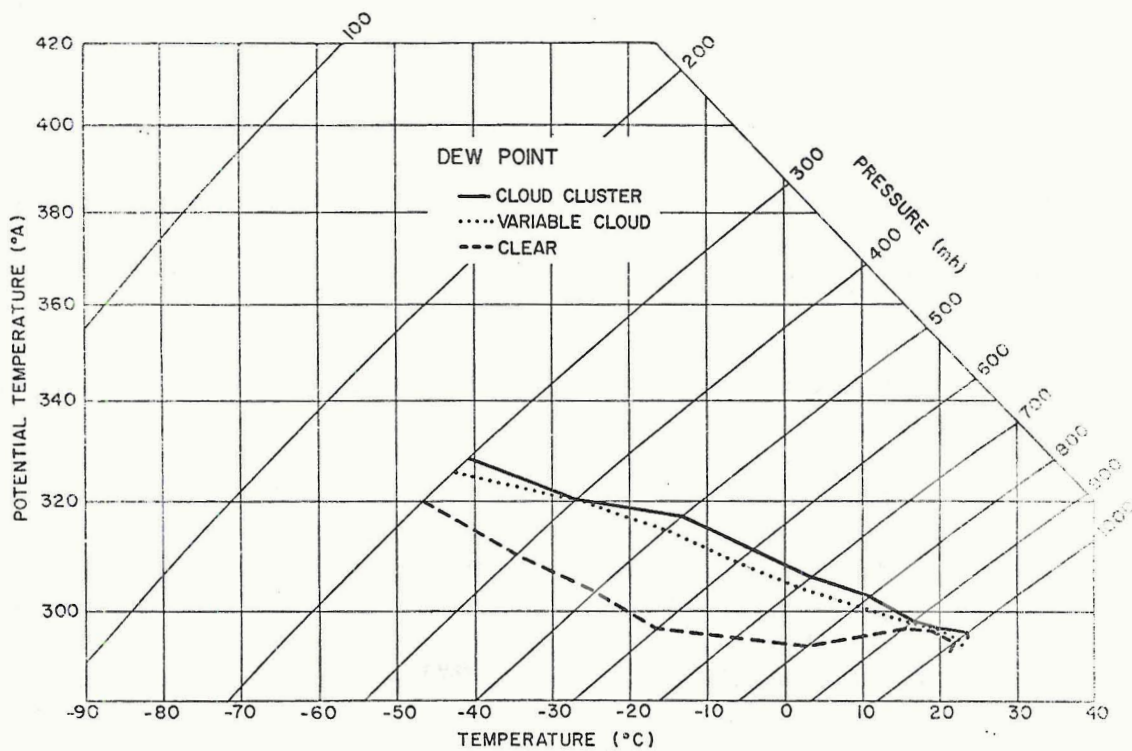


Fig. 12. Composite dew point soundings for three regions.

procedure. It is observed that no significant temperature differences exist between the three regions and that horizontal temperature advection must be near zero. The three regions are primarily contrasted by their middle and lower middle tropospheric moisture differences.

Fig. 13 portrays these three typical regions in idealized cross-section form. Observational research of Chang (1970), Frank (1970, 1971), Wallace (1970), Hayden (1970), and Martin and Suomi (1972) give general support to the above area percentage classification.

Each region will now be discussed in more detail. We will first establish the area divergence and "mean" vertical motion profiles.

Clear Area Region. This is the simplest region. The net radiation cooling as portrayed in Fig. 9 is assumed to be exactly balanced by a sinking compressional warming of about 25-30 mb/day. Composite of the winds around the clear areas independently verify this magnitude of sinking motion. The small decrease of water vapor content as a result of this sinking drying is made up at higher levels by vapor advection from the variable cloud regions.

Cloud Cluster Region. The composited cloud cluster data of the Western Pacific (Williams, 1970) and the West Indies (Gray, 1972 - report to be issued in the near future) show that the meso-scale cluster of about 4° latitude width has a deep, nearly constant convergence up to about 400 mb and a strong concentrated divergent outflow layer at 200 mb. Fig. 14 shows the way in which the data was composited. Reed and Recker (1971) and Yanai (1971) have obtained or implied a similar mass composite profile for a number of easterly waves and/or

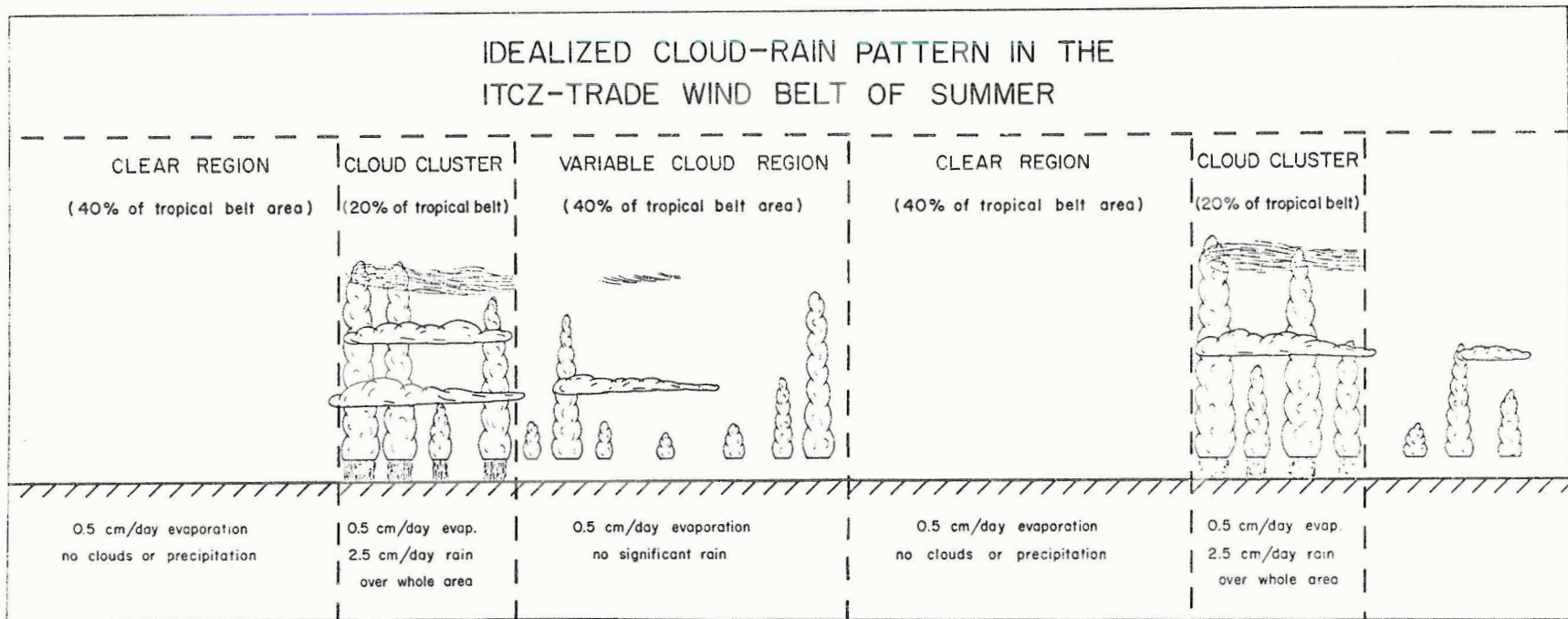


Fig. 13. Schematic picture of cloud and clear areas in the tropics.

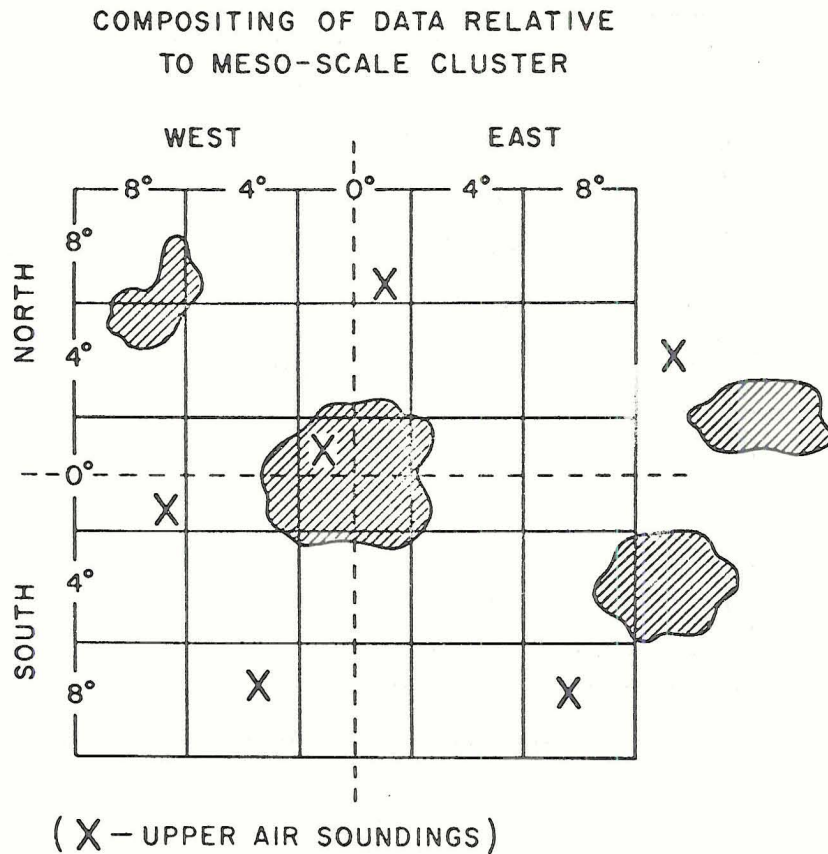


Fig. 14. Illustration of compositing scheme and rectangular grid centered on cloud cluster.

cluster systems in the central Pacific. Other information from tropical disturbances indicate a similar vertical convergence arrangement. This cluster convergence pattern up to 400 mb is responsible for an average 4° cluster water vapor inflow of about $1.5-2.0 \text{ gm/cm}^2$ per day (see Williams, p. 46). This is necessary for a mean cluster rainfall of 2.0-2.5 cm/day if 0.5 cm/day evaporation is occurring underneath the cluster. Some eddy flux of water vapor into the cluster is also occurring. These cluster rainfall estimates have been independently verified from Pacific atoll and island rainfall data composited with respect to the clusters.

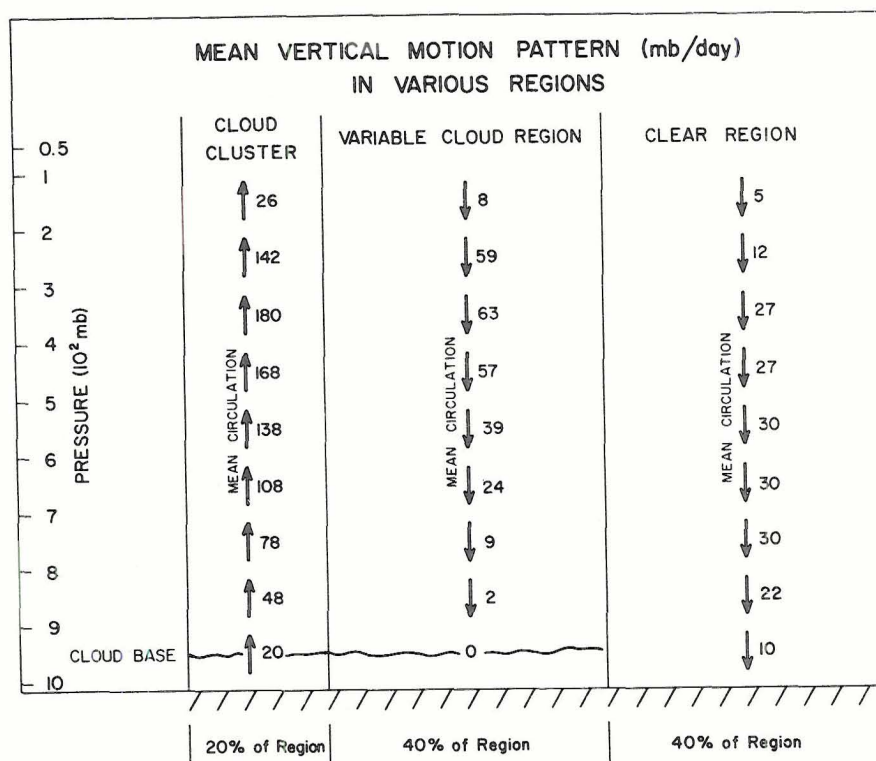


Fig. 15.

The cloud clusters and the clear areas are thus regions which import water vapor. The "mean" upward circulation at low levels as determined by the cluster convergence profile does not, however, carry sufficient water vapor upward to account for the observed upward water vapor advection at low levels. It is necessary to hypothesize a large extra "local" up-moist and down-dry circulation to accomplish all of the required upward vapor transport.

Variable Cloud Region. Given the average vertical motion pattern of the clear and cluster regions, the mean vertical motion of this region is solved for as a residual. This motion is downward everywhere except in the boundary layer. Fig. 15 portrays the mean vertical motion for the three regions in mb/day.

As the variable cloud region must export water vapor to both the cluster and the clear regions, it is also necessary (as with the cluster region) that a large "local" upward vapor transport against the downward vapor transport of the "mean" circulation takes place. The characteristics of these "local" circulations must now be discussed.

IV. DETERMINATION OF LOCAL CIRCULATION

The required local circulation in the cluster and variable cloud regions are determined from the need for upward vapor transport that cannot be accomplished by the "mean" or average upward circulation. The required upward water vapor transport (in gm/cm² per day) by the "local" circulation at any level (\hat{q}_{zi}) is obtained by adding the surface evaporation (E_{sfc}) to the integrated net inward horizontal water vapor advection q_H and subtracting from these two quantities the vapor carried upward (in gm/cm² per day) by the mean circulation (\bar{q}_z) and the vapor which has been condensed to rain (\dot{R}). The required upward vapor transport by the local circulation at any level, (\hat{q}_{zi}), is thus given by

$$\begin{array}{c}
 \left(\begin{array}{l} \text{Upward} \\ \text{Transport} \\ \text{of Vapor by} \\ \text{"local" cir-} \\ \text{culation at} \\ \text{level } i \end{array} \right) \\
 \hat{q}_{zi} \\
 \hat{q}_{zi}
 \end{array}
 \begin{array}{c}
 = \\
 = \\
 =
 \end{array}
 \begin{array}{c}
 \left(\begin{array}{l} \text{Evapora-} \\ \text{tion From} \\ \text{sfc} \end{array} \right) \\
 (E_{sfc}) \\
 \text{Evap. sfc}
 \end{array}
 \begin{array}{c}
 + \\
 + \\
 +
 \end{array}
 \begin{array}{c}
 \left(\begin{array}{l} \text{Horizontal} \\ \text{Vapor Ad-} \\ \text{vection} \\ \text{From sfc} \\ \text{to level } i \end{array} \right) \\
 (q_H) \\
 \int_{sfc}^{p_i} q_{H_i} \frac{\delta p}{g}
 \end{array}
 \begin{array}{c}
 - \\
 - \\
 -
 \end{array}
 \begin{array}{c}
 \left(\begin{array}{l} \text{Vapor} \\ \text{Carried} \\ \text{by Mean} \\ \text{Circula-} \\ \text{tion at} \\ \text{level } i \end{array} \right) \\
 \bar{q}_{zi} \\
 \bar{q}_z
 \end{array}
 \begin{array}{c}
 - \\
 - \\
 -
 \end{array}
 \begin{array}{c}
 \left(\begin{array}{l} \text{Vapor} \\ \text{Conden-} \\ \text{sation} \\ \text{to Rain} \\ \text{Below} \\ \text{level } i \end{array} \right) \\
 \dot{R} \\
 \int_{sfc}^{p_i} \left(\omega_m \frac{\partial q_s}{\partial p} + \omega_l \left(\frac{\partial q_s}{\partial p} - \frac{\partial q_e}{\partial p} \right) \right) \frac{\delta p}{g}
 \end{array}
 \begin{array}{c}
 , \quad \text{or} \\
 \\
 \\
 \end{array}
 \end{array} \quad (1)$$

- where p is pressure
- g is gravity
- i highest level of consideration
- q_s saturated specific humidity

q_e	specific humidity of the environment
ω_m	mean upward moist circulation
ω_l	is the local up-moist and compensating down-dry circulation
$\hat{\quad}$	denote local circulation
—	denote mean circulation

Figs. 16 and 17 show comparisons of the required upward water vapor transport by the mean and by the local circulations for the cloud clusters and for the variable cloud regions. In the variable cloud regions all the upward vapor transport must be accomplished by the local circulation. In the cluster the local circulation is dominant at lower levels, the mean circulation at higher levels. The circulations have equal magnitude at 800 mb.

Once the required upward vapor transport by the local circulation (\hat{q}_{zi}) has been specified at every level, the equal magnitude up-moist and down-dry local circulation (ω_{li}) necessary to accomplish this upward vapor transport is determined at each level from the equation

$$\omega_{li} = \frac{\hat{q}_{zi} (g)}{(q_s - q_e)} \quad (2)$$

where \hat{q}_{zi} is in units of gm/cm^2 day and the other symbols have been defined with equation (1).

Fig. 18 shows the magnitude of this required local mass compensating up-moist and down-dry vertical circulation in mb/day (dashed lines)

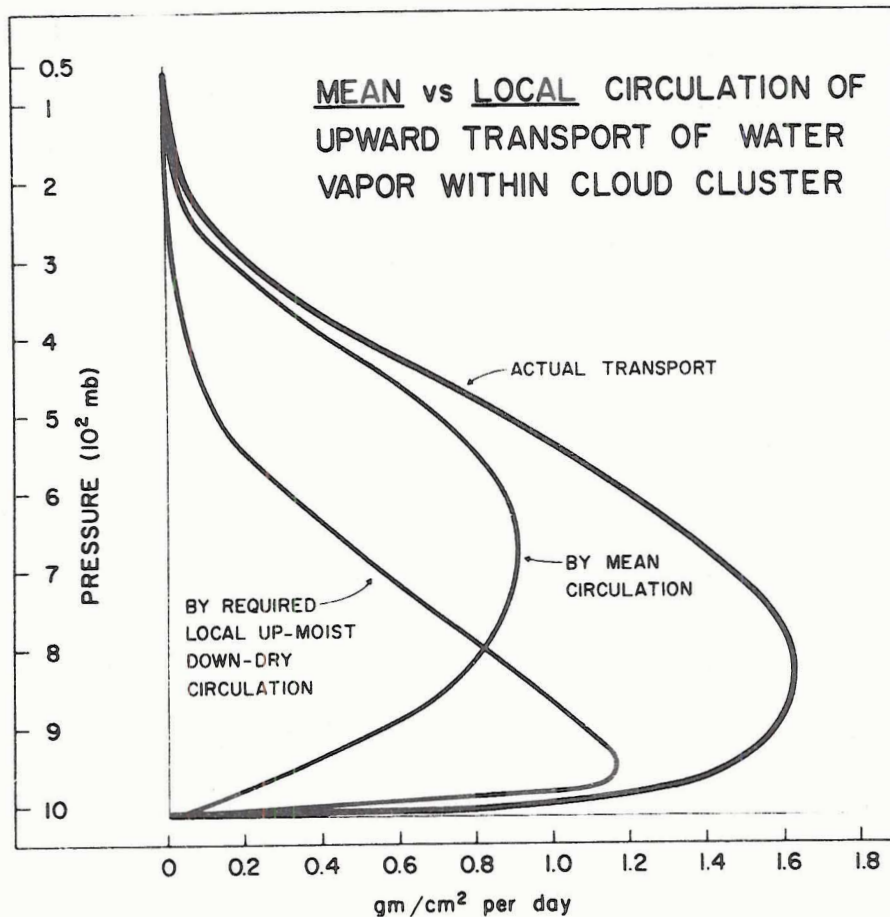


Fig. 16.

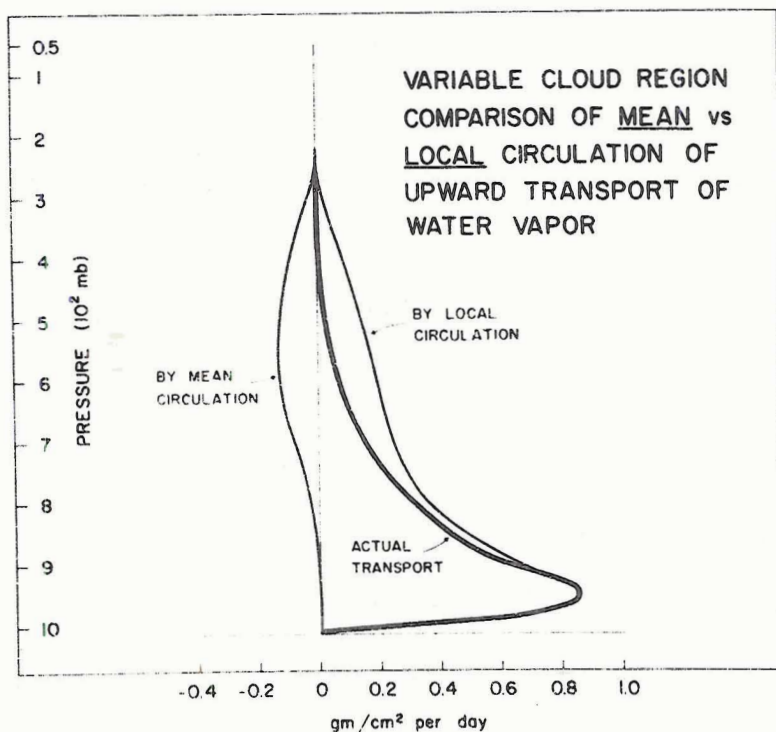


Fig. 17.

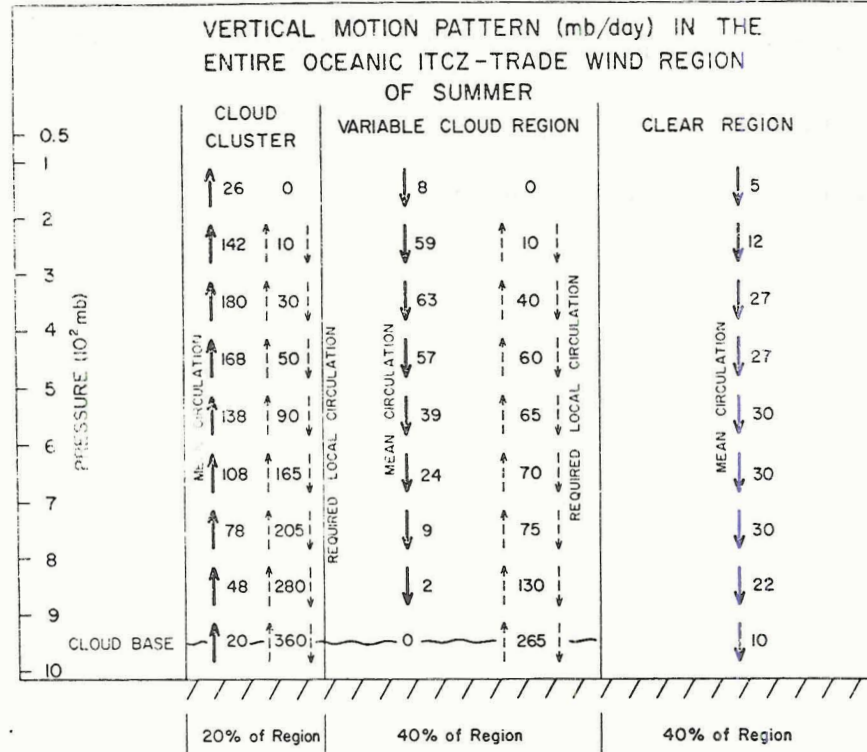


Fig. 18. Comparison of mean vs. local vertical circulation in the various tropical regions. The clear region has no local circulation.

for both the cluster and variable cloud regions and compares it with the mean circulation in these regions. At cloud base (~950 mb) this required local circulation is no less than 360 and 265 mb/day respectively. By contrast the mean circulation is only 20 and 0 mb/day respectively. Low level convergence gives little indication of the actual vertical circulation in operation.

The "local" circulation is thus seen to be a fundamental component to the upward vertical transport of water vapor in both the cluster and in the variable cloud regions. At lower levels it is responsible for most of the upward water vapor transfer. Despite its importance, this mass balancing up-moist and down-dry "local" circulation is typically

unresolved by synoptic analysis. It is time that we come to a general understanding about its very large magnitude and probable important role in the vertical circulation processes.

V. COMPUTATIONAL PROCEDURES AND REQUIRED VERTICAL CIRCULATIONS

With the definition of the three distinctive tropical regions and the general discussion of the self contained nature (lack of significant outside meridional transports) of the tropical belt, we are now in a position to estimate the complete mass, vapor, and energy budgets for each region separately. A steady-state assumption for each region has been made.

The computational steps are made in sequence and are outlined by the flow diagram shown in Fig. 19. After the whole tropical belt budgets have been made, the individual region budgets are made for

- 1) divergence for mean vertical motion, then for
- 2) water vapor, then for
- 3) local circulation, then for
- 4) resulting energy requirements.

Individual Region Divergence and Mean Vertical Motion. The method of determining this has been previously discussed. Figs. 20 and 21 show the divergence and mean vertical motion profiles.

Determination of Individual Region Water Vapor Budgets. These were made in a way similar to the mass budgets. The cluster vapor convergence vertical profile was determined from the composite radiosonde information. The clear region vapor budget was specified by the rate of drying of each region due to the mean sinking motion. The variable cloud region vapor profile was obtained as a residual of the cluster and clear regions.

FLOW DIAGRAM OF COMPUTATIONAL METHOD

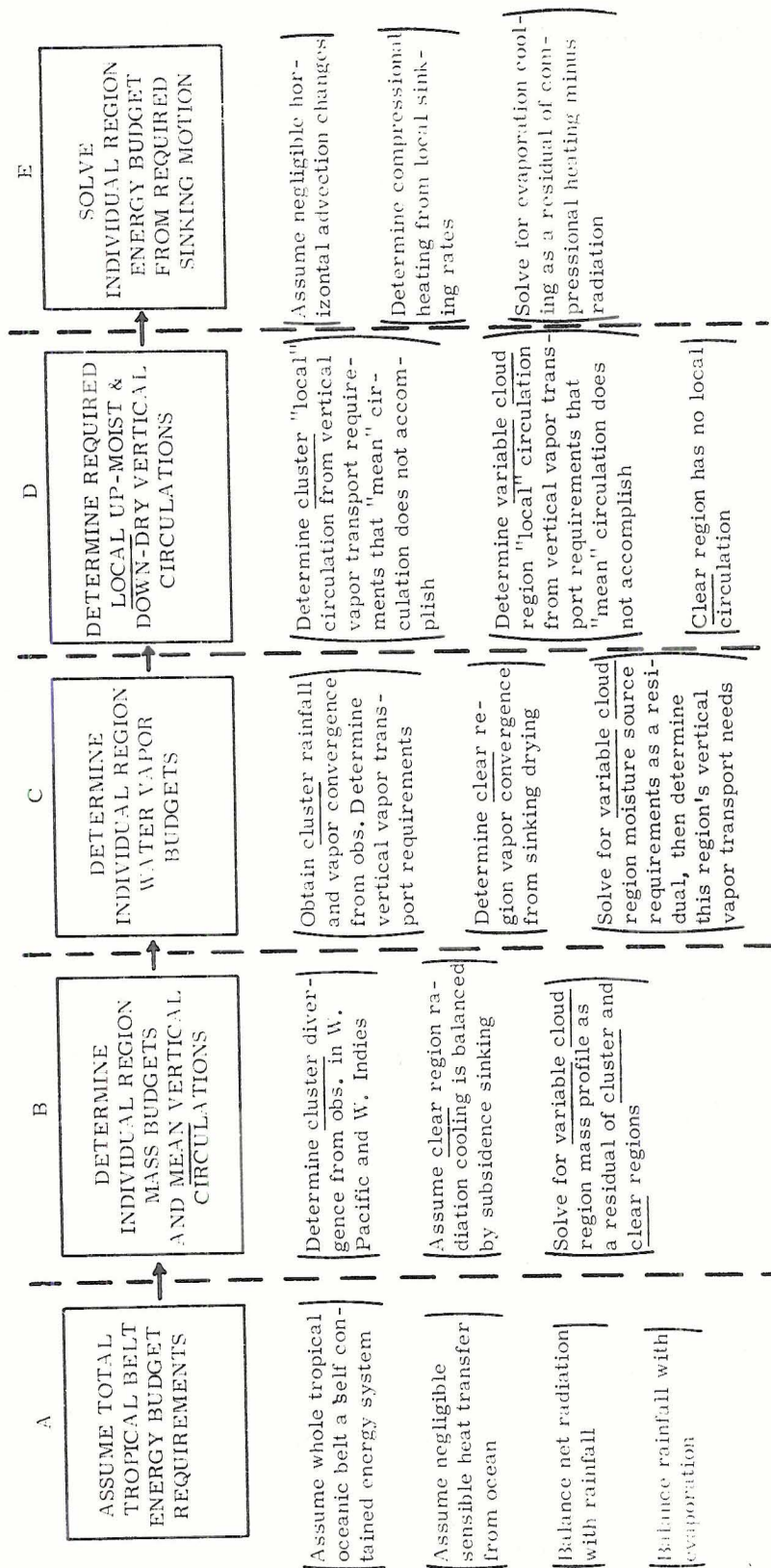


Fig. 19.

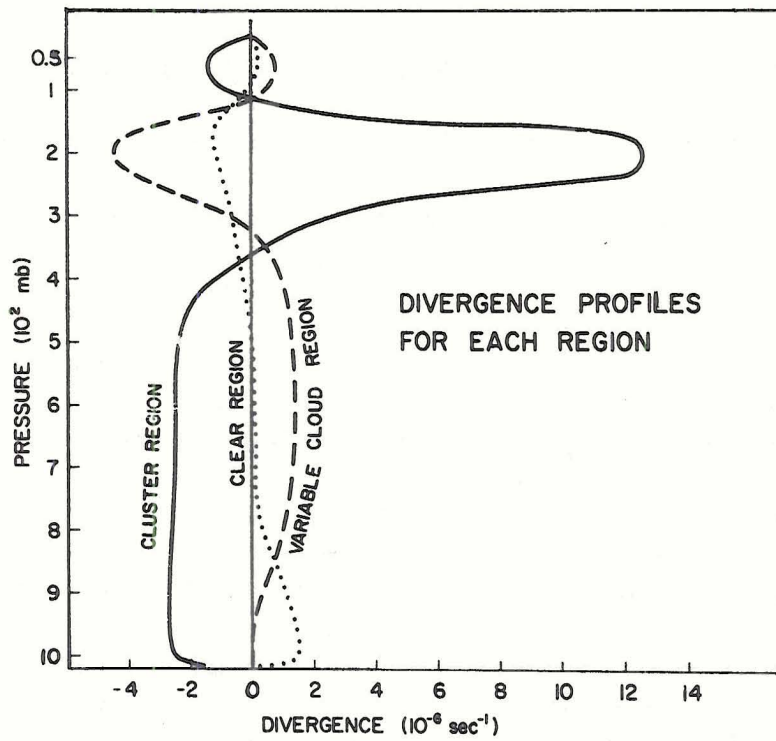


Fig. 20.

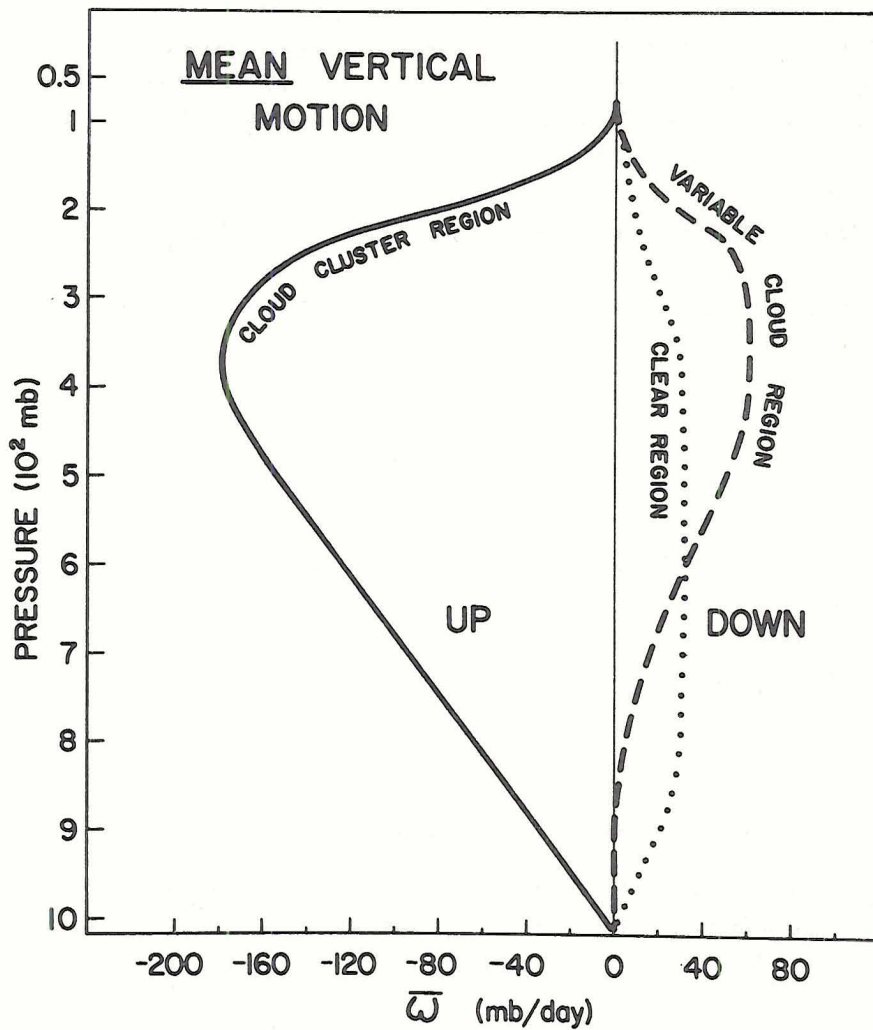


Fig. 21.

As the rainfall of the cloud cluster is approximately five times the amount of the evaporation underneath it, it is obvious that a substantial vapor import must take place. This vapor import is accomplished by two processes:

- 1) Convergence of vapor from the surface to 400 mb due to the mean convergence profile as seen in Fig. 20. This accounts for most of the vapor convergence into the cluster.
- 2) Eddy advection of vapor into the cluster beyond that specified by the divergence. This occurs primarily in the lowest 50-150 mb and is analogous to the extra vapor advection into squall lines when they overtake lower level air, as discussed by Newton, (1963). Typically, dryer downdraft air leaves the cluster on the upwind or east side while moister lower level air enters the cluster from the downwind or west side. This brings about a net moisture advection into the cluster. Zipser (1969, and personal communication) has discussed the large drying from downdrafts which occurs in clusters. Cluster surface winds are but half of the winds at the 800-900 level, as seen in Fig. 22.

An estimate of the vertical distribution of vapor advection into the cluster below any level p_i from these two processes can thus be obtained from the equation

$$\text{Vapor Advection into Cluster} = \int_{\text{sfc}}^{p_i} \underbrace{\nabla_2 \cdot q}_{\text{Vapor Transfer by Convergence}} \frac{\delta p}{g} + \int_{\text{sfc}}^{p_i} \underbrace{\Delta q_i \frac{|v_i - v_c|}{D}}_{\text{Extra Vapor into Cluster at Lower Levels by Relative Motion}} \frac{\delta p}{g} \quad (3)$$

where p_i is the pressure at any level

Δq_i vapor difference between that entering and leaving cluster at any level - typically 1-5 gm/kg at lower levels.

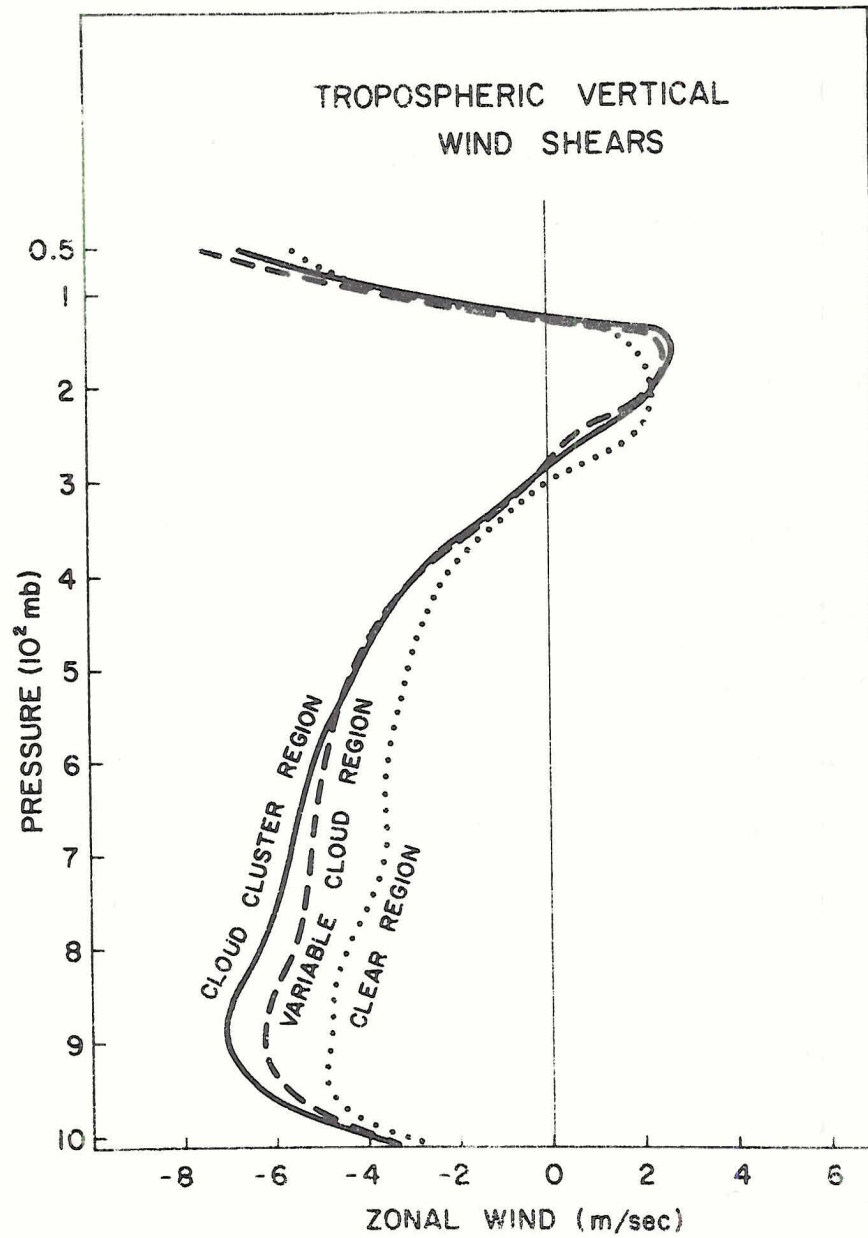


Fig. 22. Vertical profiles of average zonal wind in the three tropical regions.

- V_i is the wind at any level in the cluster
 V_c is the cluster velocity
 D is the width of the cluster - taken as 4° latitude.

The main contribution of the second term on the right of (3) comes in the boundary layer. Here the speeds are substantially less than the cluster velocity. The vapor advection determined from (3) is shown for the cluster on the left portion of Fig. 23. Note that half of the vapor advection comes in the boundary layer (surface to 950 mb).

As previously shown in Fig. 16, the mean circulation in the cluster carries a small fraction of the required upward transport of vapor necessary to produce the 2.5 cm/day mean rainfall. The rest of the upward vapor transport must be carried by the "local" circulation.

Figs. 24-25 and Table 2 discuss in more detail the water vapor characteristics of the cloud cluster. Figs. 24-25 contrast level by level the upward vapor transports and the vapor released to rain by the mean and by the local circulation. It is to be noticed that about three-quarters of the cluster condensation going to rain comes from the mean circulation, while the local circulation is primarily responsible for the recycling of vapor as most of its condensation is reevaporated in its compensating sinking motion. Table 2 explicitly lists all of the parameters going into the cluster condensation, rainfall, and local circulation determination.

It should be realized that the 2.5 cm/day rainfall is not occurring everywhere within the cluster but is probably concentrated in local rain areas (some along squall lines) taking up but 10% or less of the 4° wide

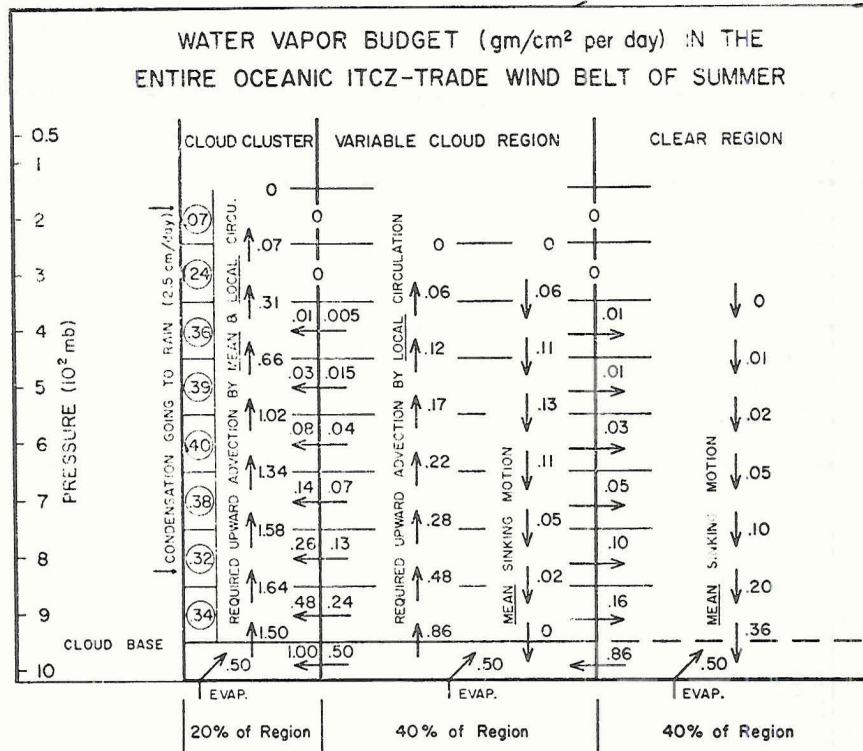


Fig. 23. Water vapor budget of the tropical belt expressed in gm/cm² per day. Doubling of vapor advection per unit area into cluster is due to variable cloud region being twice the area of cluster region.

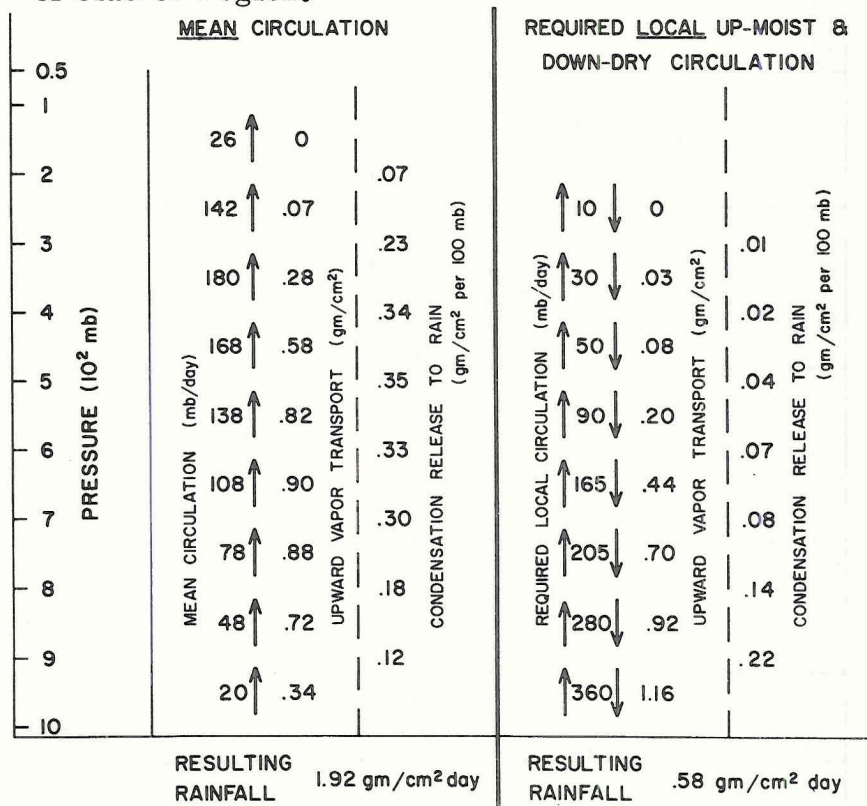


Fig. 24. Cloud cluster mean vs. local circulation values of upward vapor transport and of condensation going to rain.

Table 2

DETERMINATION OF CLUSTER <u>REQUIRED</u> LOCAL CIRCULATION										
LEVEL	Mean Circulation	Condensation to Rain	Moisture Source	Moisture Loss	Total Required Upward Vapor Advection after Subtraction of Condensation to Rain	Moisture Carried by Mean Circulation	Required Upward Vapor Advection at layer base by Local Circulation	Cluster Saturated minus Observed Specific Humidity	Required Local Up-Moist and Down-Dry Circulation	LEVEL
(mb)	(mb/day)	(gm/cm ² per 100 mb per day)	(gm/cm ² per day)	(gm/cm ² per 100 mb per day)	(gm/cm ² per day)	(gm/cm ² per day)	(gm/cm ² per day)	(gm/kg)	(mb/day)	(mb)
		Mean Local Tot								
sfc	0		EVAP. .50							
1000			sfc —							
950	20		CU 1.00		1.50	.34	1.16	3.2	360	950
900		.12 .22 .34	BASE .48	.34	1.64	.72	.92	3.3	280	850
850	48			.32	1.58	.88	.70	3.4	205	750
800		.18 .14 .32		.38	1.34	.90	.44	2.7	165	650
750	78			.40	1.02	.82	.20	2.0	90	550
700		.30 .08 .38		.39	.66	.58	.08	1.7	50	450
650	108			.36	.31	.28	.00	1.0	30	350
600		.33 .07 .40		.24	.07	.07	.002	0.2	10	250
550	138			.07	.00	.00	—	0.0	—	150
500		.35 .04 .39								
450	168									
400		.34 .02 .36								
350	180									
300		.23 .01 .24								
250	142									
200		.07 .00 .07								
150	26									
100		.00 .00 .00								
50	0									
		1.92 .58 2.50	TOTAL 2.50	2.50						
		VERTICAL TOTALS	cm/day	gm/cm ²						

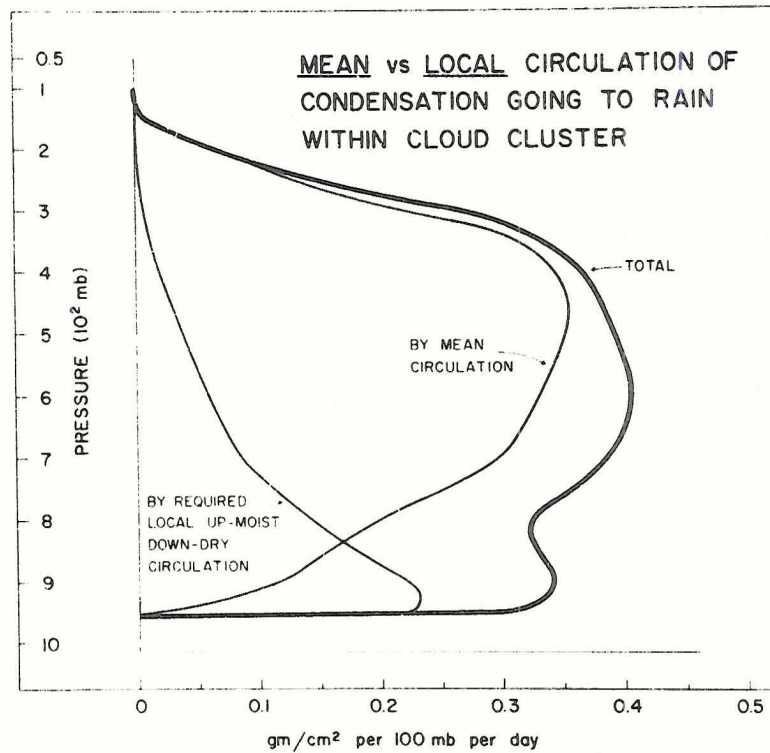


Fig. 25.

cluster. In addition it is likely that only about 10 to 20% (or 0.2 to 0.4% of the entire tropical belt) of the rain areas have active towering cumulus or cumulonimbus updrafts in operation. A similar scaling of the relative areas of the updraft, the rain regions, weather systems, etc., has been presented by Riehl and Malkus (1958). Even though the convective activity is highly concentrated within the cluster, the lack of appreciable temperature and water vapor gradients across the cluster allow for an area average treatment of the mass, vapor, and energy budgets.

The clear and variable cloud region vapor budgets are also shown in Fig. 23. The clear regions import vapor at upper levels to balance their sinking drying motion ($.36 \text{ gm/cm}^2$ per day) and export this vapor

into the boundary layer. Together with its evaporation of 0.5 gm/cm^2 , the boundary layer accumulates vapor at a rate of $.86 \text{ gm/cm}^2$. The clear areas are thus source regions of water vapor. This is due primarily to their boundary layer divergence. At upper levels they import vapor.

The variable cloud region exports the vapor which it receives from its evaporation--that is 0.5 gm/cm^2 per day. Above the boundary layer, it exports $.86 \text{ gm/cm}^2$ per day which can only occur if the vapor is carried to upper levels by a substantial local circulation. Below cloud base the variable cloud region imports $.36 \text{ gm/cm}^2$ per day.

Fig. 23 illustrates the mode by which the clear and variable cloud regions supply their evaporated vapor to the clusters.

Individual Region Local Circulations. This has been adequately discussed in Section 3. The clear areas have no local circulation. The required up-moist and down-dry circulation of the other two regions is obtained from equation (2) with the required individual level upward transports specified in Fig. 23. As previously shown in Fig. 18, this local required vertical circulation is exceedingly large in the lower troposphere.

Determination of Individual Region Energy Budgets. Once the required regional net downward motion (ω_d) from both the mean and local circulations has been determined, the compressional warming, the water vapor recycling, and the net cloud cooling can be obtained for each region from the need to maintain steady-state conditions. As previously

discussed, inter-regional temperature advection influences are negligible. Thus, at each level, the sensible temperature budget must be given as a balance between

$$\left(\begin{array}{c} \text{Sinking} \\ \text{Warming} \end{array} \right) + \left(\begin{array}{c} \text{Cloud Induced} \\ \text{Temperature Changes} \end{array} \right) + \left(\begin{array}{c} \text{Net} \\ \text{Radiation} \end{array} \right) = 0, \text{ or}$$

$$\omega_d(\Gamma_d - \Gamma_e) + \left(\begin{array}{c} \text{Cloud Sensible} \\ \text{Temperature Warming} \\ + \text{Evaporation Cooling} \end{array} \right) + R = 0, \quad (4)$$

where Γ_d and Γ_e are the dry and environment lapse rates. López (1972a) has shown in his entire life cumulus model that direct sensible temperature diffusion from cumulus to their environment is very small, and in comparison with the evaporational cooling induced by the cumulus, can be neglected. Most of the cloud-induced sensible temperature changes result from liquid water evaporation on the sides of the cumulus during their growth and throughout the cumulus' interior as they die. This is pictorially portrayed in Fig. 26.

The sensible temperature budget of the summertime tropical belt is largely determined by the balance between sinking warming and by evaporational and radiational cooling. Thus,

$$\begin{array}{l} \text{Sinking Warming} \quad \cong \quad \text{Evaporation} + \text{Radiation} \\ \omega_d(\Gamma_d - \Gamma_e) \quad \cong \quad L(\Delta q) + R, \quad (5) \end{array}$$

where Δq represents the amount of cumulus liquid water converted to vapor per unit mass and time. Throughout most of the summertime

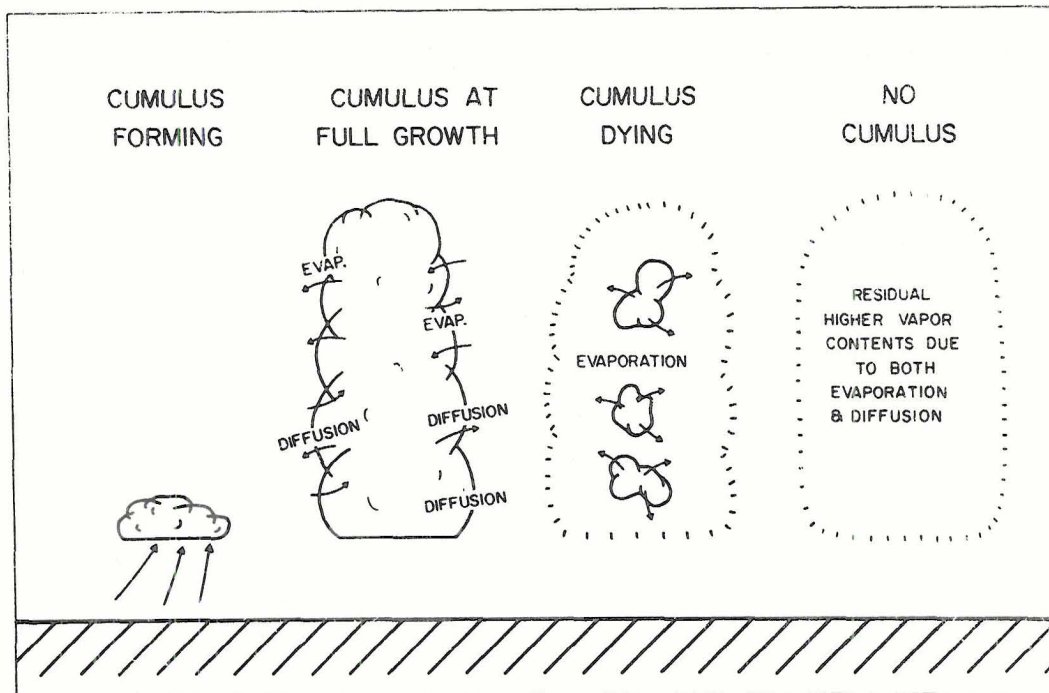


Fig. 26. Idealized picture of how the individual cumulus cools the atmosphere around it when it dies and how it raises the water vapor level.

tropical belt, the sinking warming and evaporation cooling are much larger than the radiation cooling.

Figs. 27-29 portray the vertical profile of the terms of equation (5) for each of the three tropical regions and for the entire tropical oceanic belt. In all but the clear regions, the primary balance is between the sinking warming and the evaporation cooling with the radiation cooling of much less local importance. It was not previously expected that the local cloud induced warming and cooling rates would be so large in comparison with the radiational cooling.

Fig. 30 shows the very large local recycling of water vapor for each of the tropical regions. Each region losses vapor through subsidence

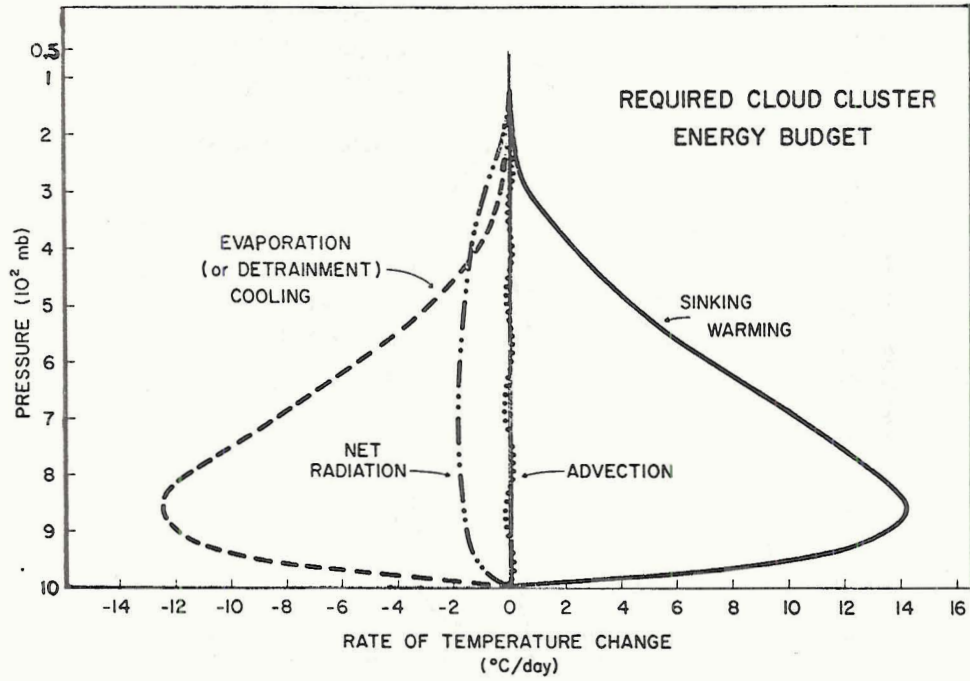


Fig. 27. Vertical distribution of required energy components in steady-state cloud cluster.

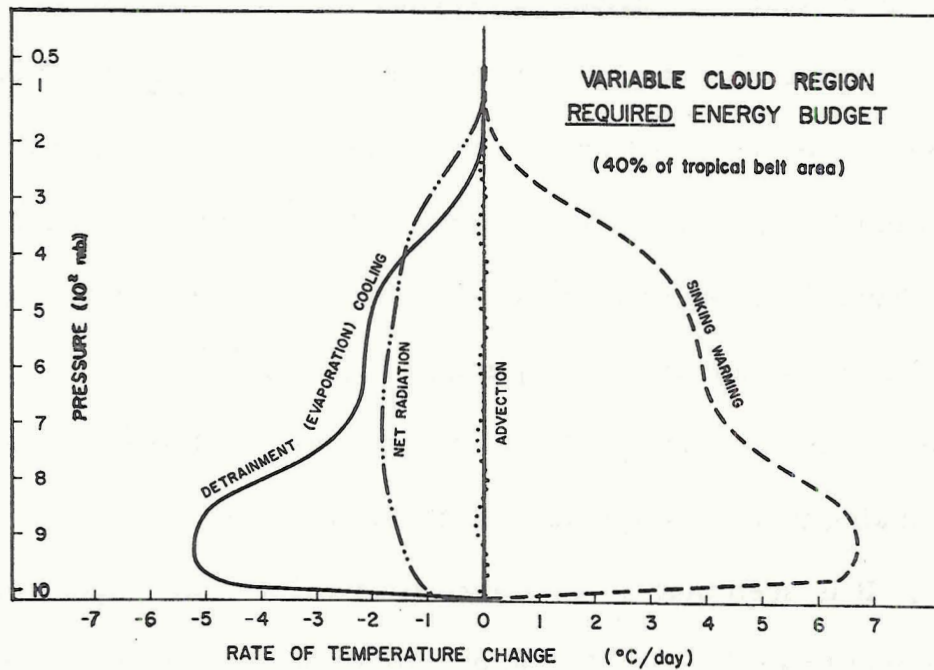


Fig. 28. Vertical distribution of required energy components in variable cloud region.

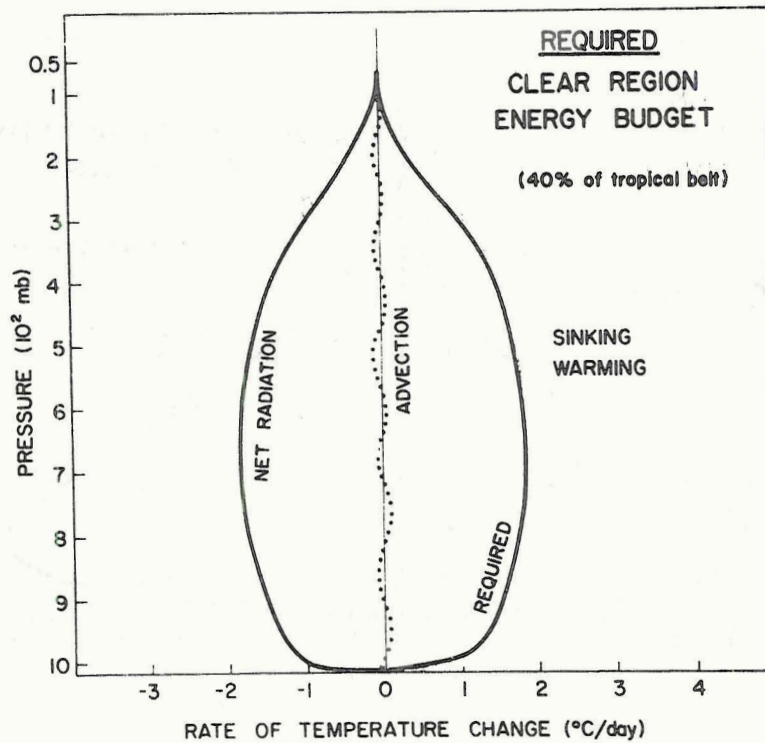


Fig. 29. Vertical distribution of required energy components in clear region.

drying. For steady conditions to prevail, the individual clouds must furnish an equal amount of vapor either by (1) direct vapor diffusion out from the clouds, or by (2) advection or mixing of liquid water (to be evaporated) out from the clouds. Both of these processes are accomplished from the sides of the clouds or throughout the region occupied by the clouds as they die, as implied in Fig. 26.

The relative magnitude of these two processes of vapor replacement to the sinking motion is specified in Figs. 31-33 for each of the tropical regions. It is seen that in the lower levels most of the vapor replacement comes from direct diffusion or advection of vapor out from the cloud. At middle and upper levels most of the vapor replacement comes

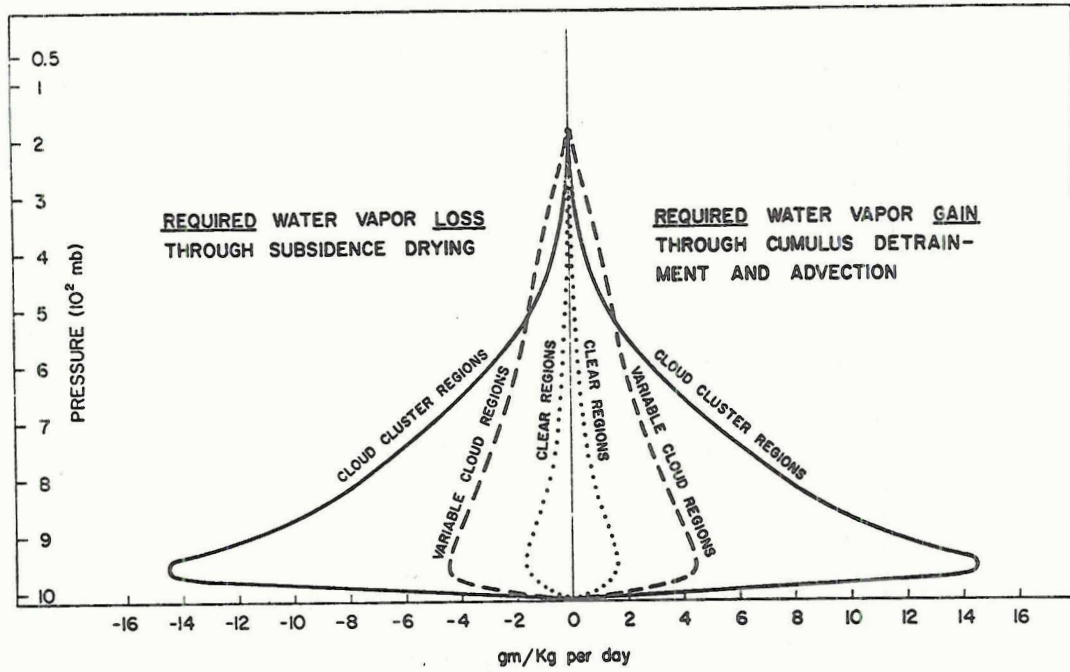


Fig. 30. Comparison of required water vapor gain and loss for each of three tropical regions.

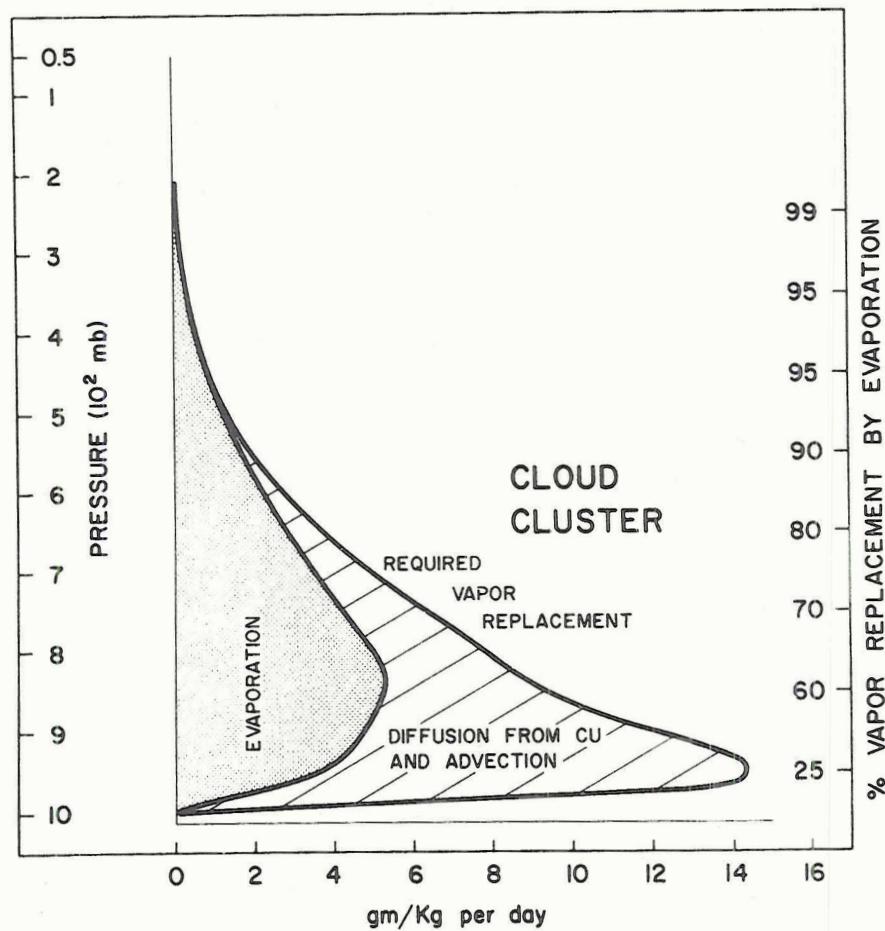


Fig. 31. Cluster required water vapor replacement to sinking motion to maintain steady state conditions and portion of vapor replacement coming from evaporation (on the right).

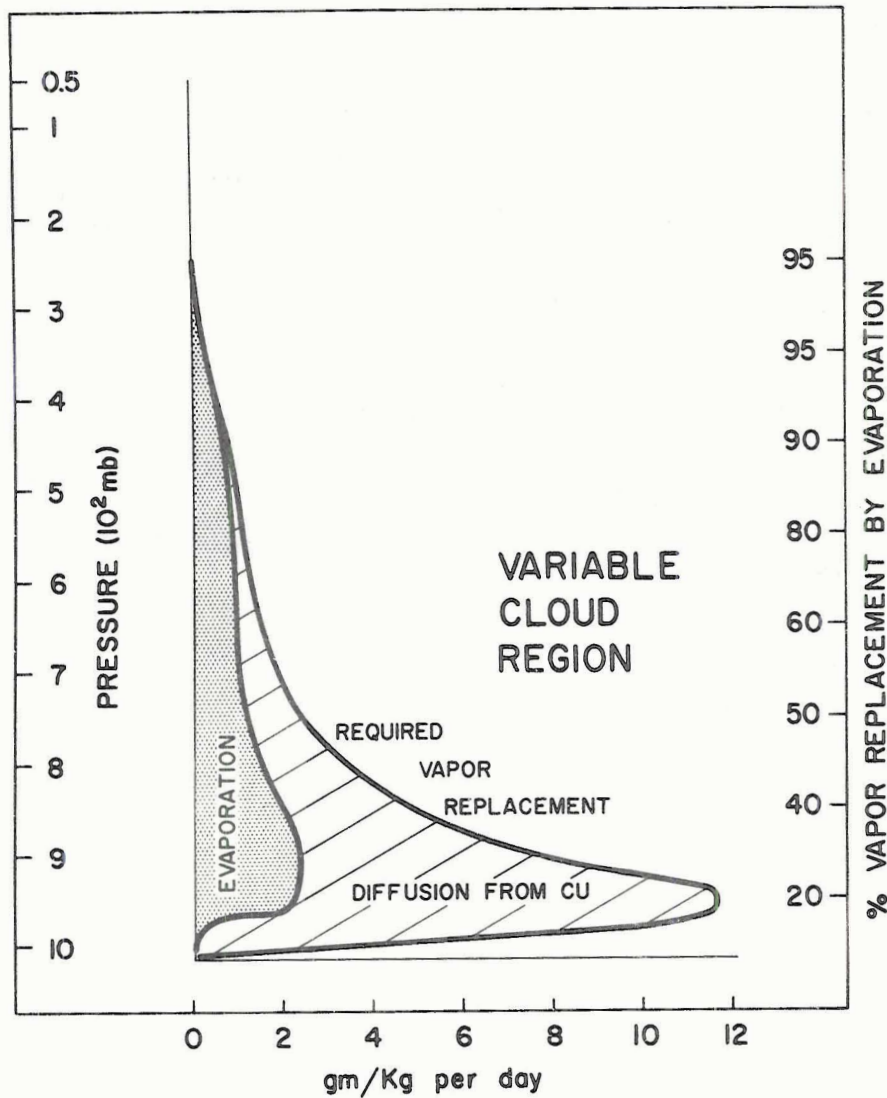


Fig. 32. Cluster required water vapor replacement to sinking motion to maintain variable cloud region conditions and the portion of vapor replacement coming from evaporation (on the right).

from evaporation. This is a result of higher liquid water detrainment from the cumulus at upper levels and the lower upper level water vapor contents. The percentage of water vapor replacement by evaporation to total required water vapor replacement is shown on the right side of these figures. It ranges from 20-25 percent at 900 mb to 80-90 percent at 500 mb.

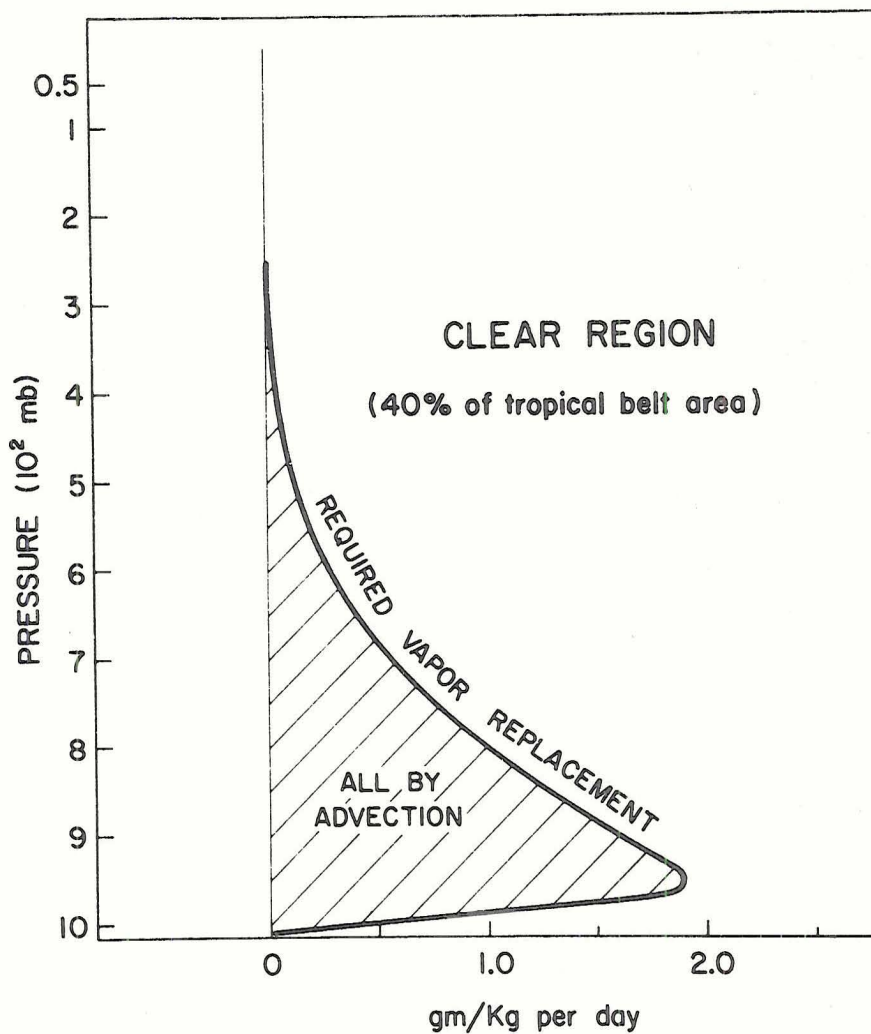


Fig. 33. Required advection of water vapor into the clear region to balance its sinking drying and maintain its steady state.

The large magnitude of this required vertical circulation and its consequent very large energy and vapor sources and sinks should be appreciated by those who wish to understand tropical circulations.

VI. ACTUAL OR PROBABLE VS. REQUIRED VERTICAL CIRCULATIONS

The previous sections have discussed the required "mean" and "local" vertical circulation necessary to satisfy simultaneously mass, vapor, and energy needs. These mean and local required circulations must continually be in operation. But this does not specify all the vertical motion going on. Besides these required circulations there is an extra or "probable" additional local circulation which does not influence the mass, vapor, or energy budgets and can only be roughly estimated. This extra mass balancing local circulation is the additional up-dry and compensating down-dry circulation which accompanies broadscale forced upward motion (often associated with layered clouds) and the up-moist and compensating down-moist downdraft circulations associated with heavy rainfall. Any additional forced up-dry circulation must be balanced by a compensating down-dry motion. Similarly, any additional moist downdraft motion must be balanced by a compensating moist upmotion. These additional mass balancing circulations, whose magnitude can only be roughly estimated, must be added to the already determined required up-moist and down-dry circulations to arrive at the actual or here defined probable real vertical circulation which is occurring. Fig. 34 portrays the author's estimate of the actual vertical circulation occurring in the cluster regions previously discussed. Seven classes of vertical circulations are shown, four

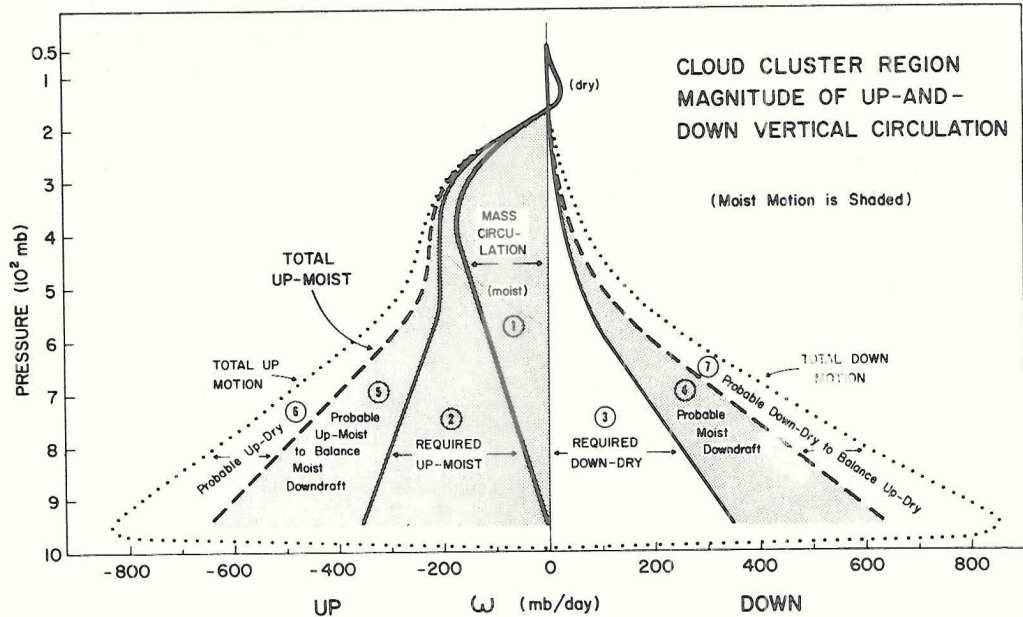


Fig. 34. Estimated complete vertical motion pattern of the cluster region. Numbered individual vertical motion components are discussed below.

moist and three dry. The moist or saturated motion has been shaded.

These seven vertical circulations are:

- 1) Mean upward motion as determined from the radiosonde cluster data (see Fig. 21). This has a maximum value of 180 mb/day at 350 mb. It has been assumed that the mean circulation goes up-moist.
- 2) Required local up-moist circulation with maximum value of about 350 mb/day at 950 mb.
- 3) Required local down-dry circulation with maximum value of about 350 mb/day at 950 mb. Circulations 2) and 3) must mutually balance each other.
- 4) Probable extra down-moist circulation as results with saturated downdrafts with rain. Maximum values assumed in lower troposphere of about 200 mb/day. This estimate is quite subjective.
- 5) Probable extra moist updraft to balance the moist downdraft. Motions 4) and 5) are mutually balancing.
- 6) Probable extra up-dry motion from meso or synoptic scale forced vertical motion as must be present to produce layered clouds.

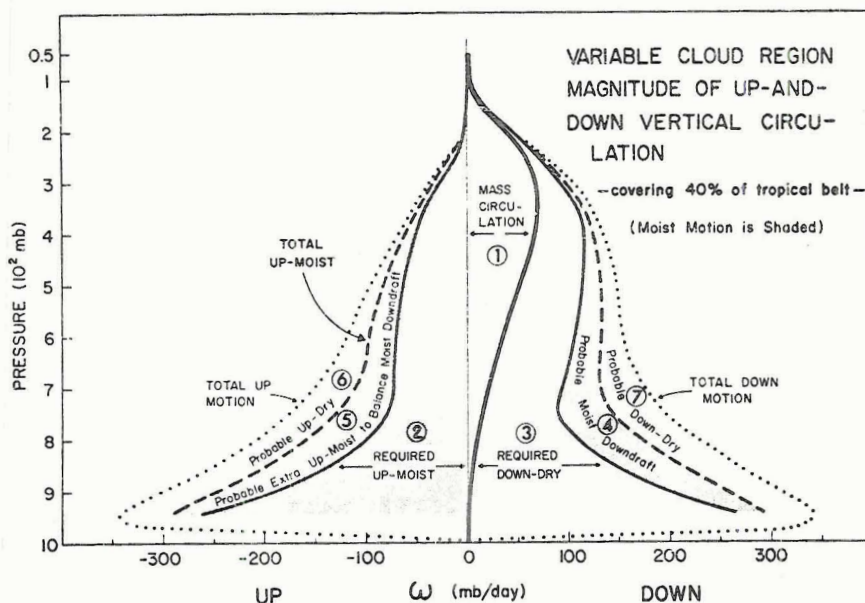


Fig. 35. Estimated complete vertical motion pattern of the variable cloud region. Numbered individual vertical motion components are as discussed for the cluster region.

- 7) Probable extra additional down-dry motion to balance the forced up-dry motion of 6). Motions 6) and 7) are mutually balancing.

If this estimate of the typical cluster vertical circulation is not too inaccurate, then we are forced to accept the reality of a very large recycling vertical circulation which, in the lower half of the troposphere, is from one to two orders of magnitude larger than the mean cluster upward motion. The implication of this very large local recycling circulation for vertical momentum and other dynamic influences may be substantial and requires careful consideration. The divergence pattern implied by the vertical motion of Fig. 34 exactly fits the mean divergence pattern of Fig. 20. Surface to 400 mb cluster convergence is due to the increase in downward motion being larger than the increase of upward motion.

Fig. 35 shows the author's estimate of the actual or probable vertical circulations occurring in the variable cloud region. Again, it is

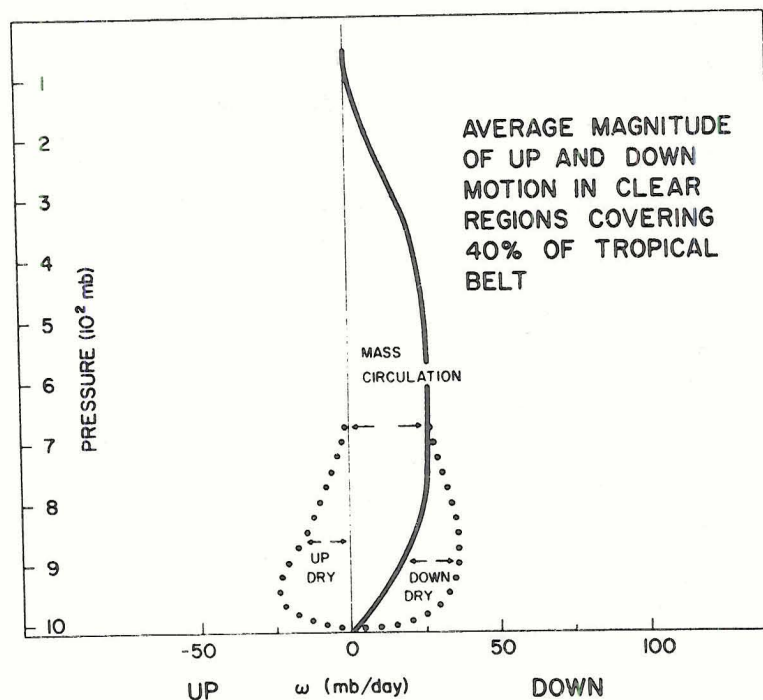


Fig. 36. Assumed total vertical motion in the clear regions.

to be noted how large the actual up-and-down local vertical circulations are in comparison with the mean vertical motion.

In the clear regions only a small extra or "probable" up-dry and down-dry circulation must be added to the mean circulation as shown in Fig. 36. This extra up- and-down dry circulation is thought to be due to boundary layer turbulent mixing.

Fig. 37 shows the author's estimate of the vertical profile of the average of the absolute magnitude of the mean, the required, and the probable vertical motion occurring for the entire oceanic tropical belt of summer. These local vertical circulations are very large even though we are averaging over the whole tropical region.

It was not expected that such a large required up-and-down compensating vertical circulation would be present at lower levels. Reed and

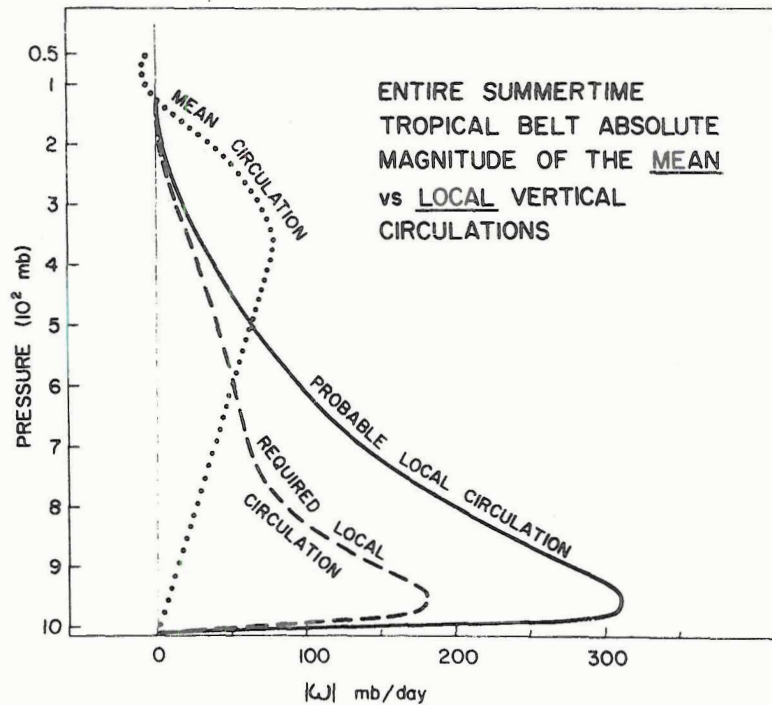


Fig. 37. Comparison of the magnitude of the mean and the local vertical circulations for the entire tropical belt of summer.

Recker (1971) have also deduced from broad-scale considerations that a large lower-tropospheric recycling circulation must be present, but their estimates are not as large. The implication of this large vertical circulation for the dynamics of the lower troposphere must be very great. The vertical momentum transfer by this extra circulation is probably very significant to inhibit establishment of vertical wind shears. It is observed that the vertical wind shear from cumulus cloud base to middle tropospheric levels in cumulus convective situations is typically very small. Table 3 shows the very high magnitudes of the "local" up and down circulation to the "mean" circulation at cloud base. An explanation of the lack of vertical vorticity balance and the need to hypothesize substantial sub-synoptic or cumulus vertical vorticity

transfer, as has been discussed by Williams (1970), Reed and Recker (1971), Gray (1972b) and Holton and Colton (1972), is likely to be associated with this strong vertical circulation requirement.

This magnitude of cluster vertical circulation fits the estimates of López (1972b) which were derived independently from a cumulus modeling approach which will be discussed in Chapter VIII.

Table 3

The top of the boundary layer "mean" vs. "local" required and probable up and down vertical circulation. All values are in mb/day.

	<u>Cluster Region</u>	<u>Variable Cloud Region</u>	<u>Clear Area</u>	<u>Whole Tropical Belt</u>
A. Absolute value of <u>mean</u> circulation	20	0	10	10
B. Absolute value of <u>required up or required down</u> "local" circula- tion	360	265	0	200
C. Absolute value of <u>probable up or probable down</u> "local" circulation	820	340	25	300
Ratio of A to B	1/18	0	-	1/20
Ratio of A to C	1/40	0	2/5	1/30

VII. PROBABLE TROPICAL REGION VAPOR AND ENERGY BUDGETS

The extra vertical circulation beyond that required to meet mass-vapor-energy budgets results in additional warming-cooling and condensation-evaporation rates. These must be added to the required values. They are believed to be close to the actual (or probable) rates of change really occurring. Figs. 38 and 39 show the author's estimates of the probable energy and vapor balances occurring within the cluster. In comparison with the radiation cooling and rainfall rates, these mutually balancing cluster energy and vapor exchange rates are indeed very large.

Even for the entire tropical belt these probable energy and vapor exchanges are very large in comparison with the radiation cooling and rainfall rates. They are shown in Figs. 40 and 41.

Figs. 42-43 portray tropospheric averages of the mean, required, and probable vertical circulation and the same values for the sinking warming--evaporation cooling rates for each of the three regions and for the entire tropical belt. Fig. 44 shows the large magnitude of condensation-evaporation to rainfall. For the whole tropical belt probable condensation-evaporation is about 6 times larger than rainfall; required condensation-evaporation about 3-1/2 times rainfall.

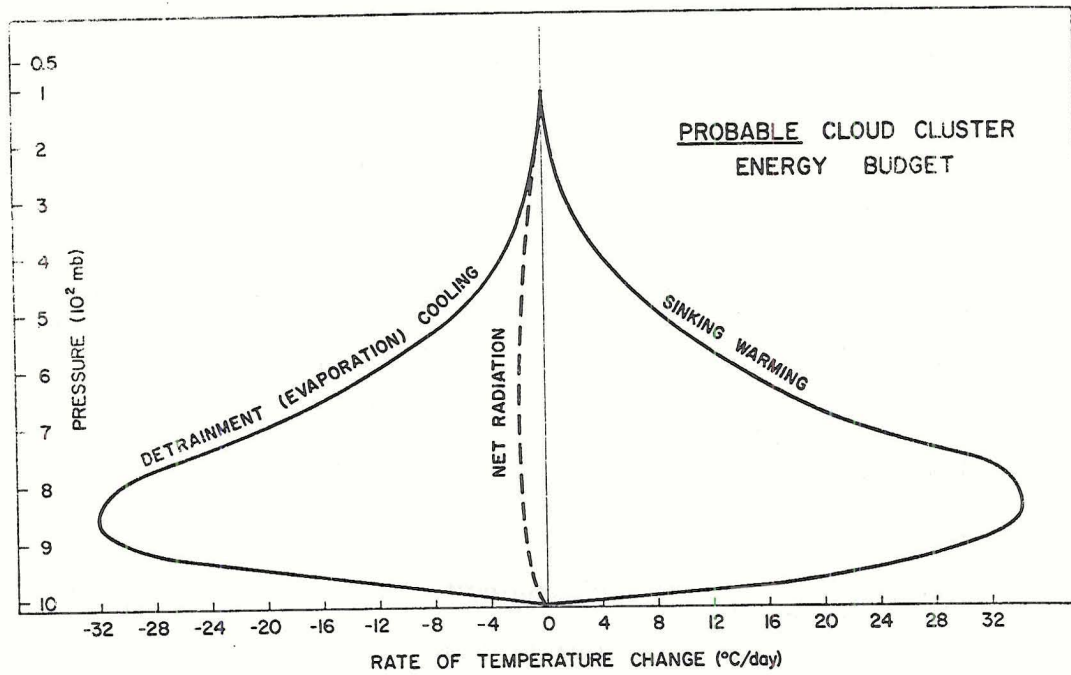


Fig. 38.

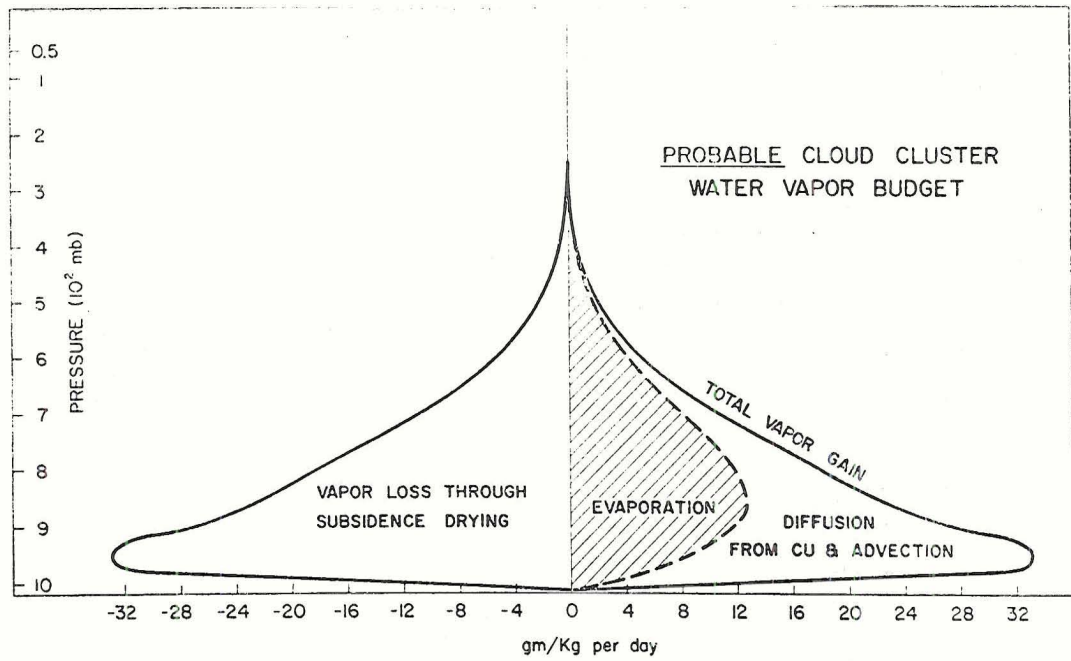


Fig. 39.

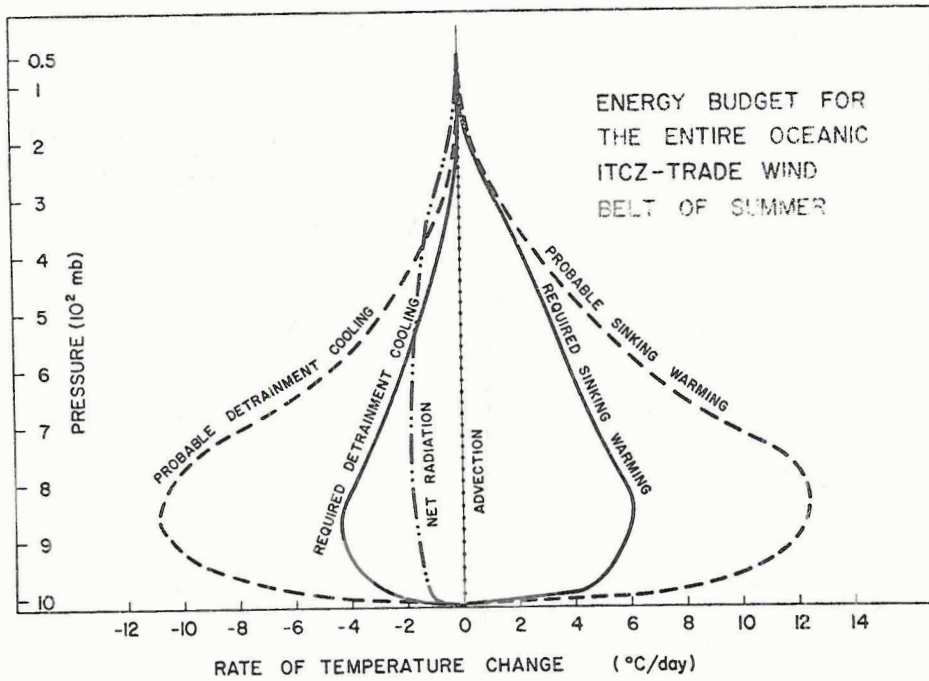


Fig. 40.

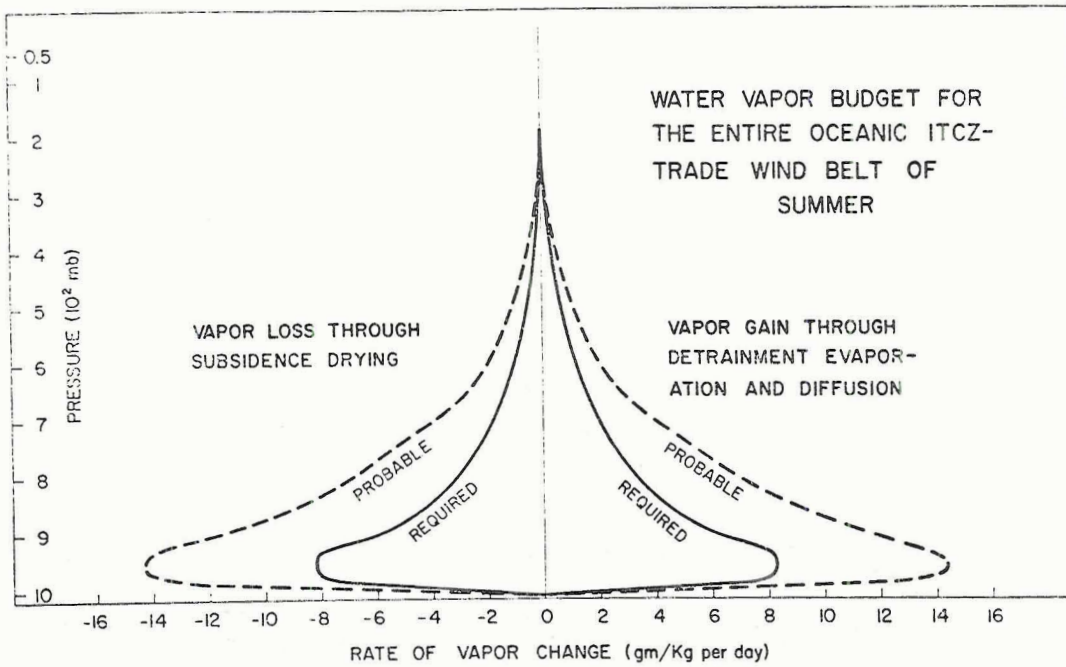


Fig. 41. Comparison of required and probable water vapor budgets for the entire tropical belt of summer.

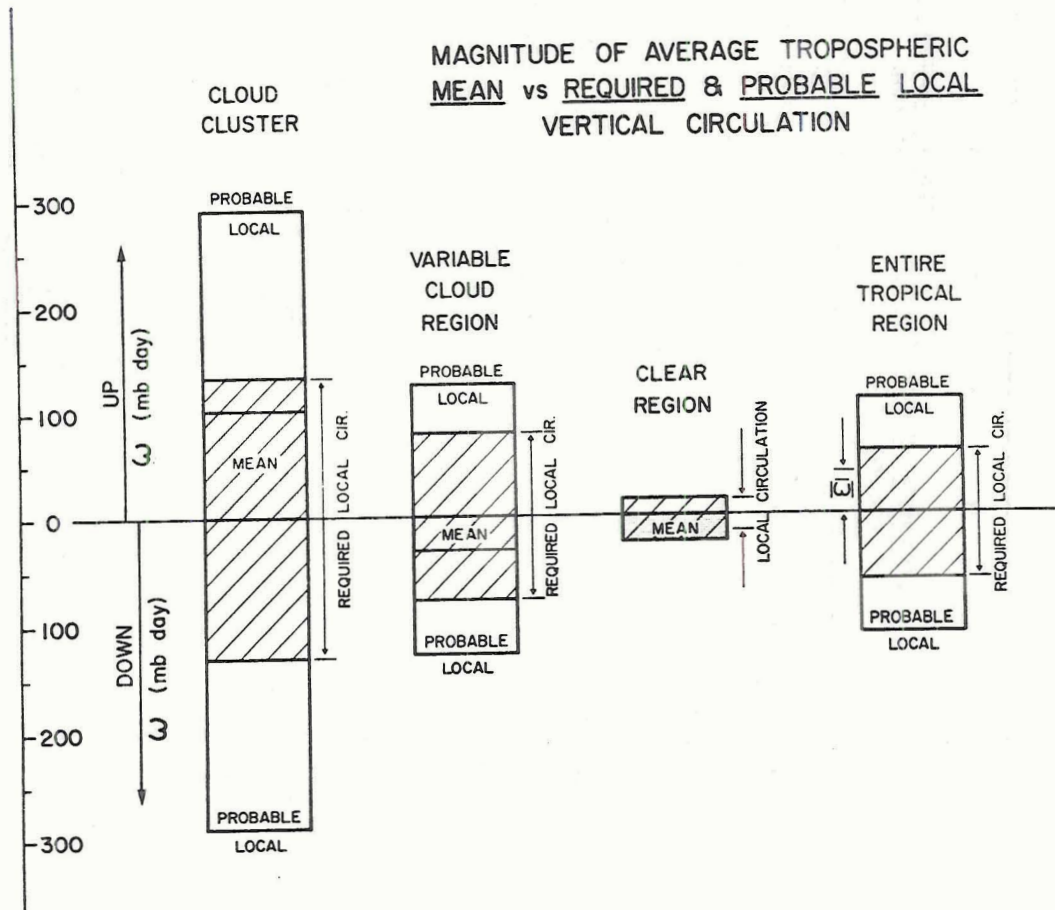


Fig. 42. Comparison of individual region mean vs. local circulations.

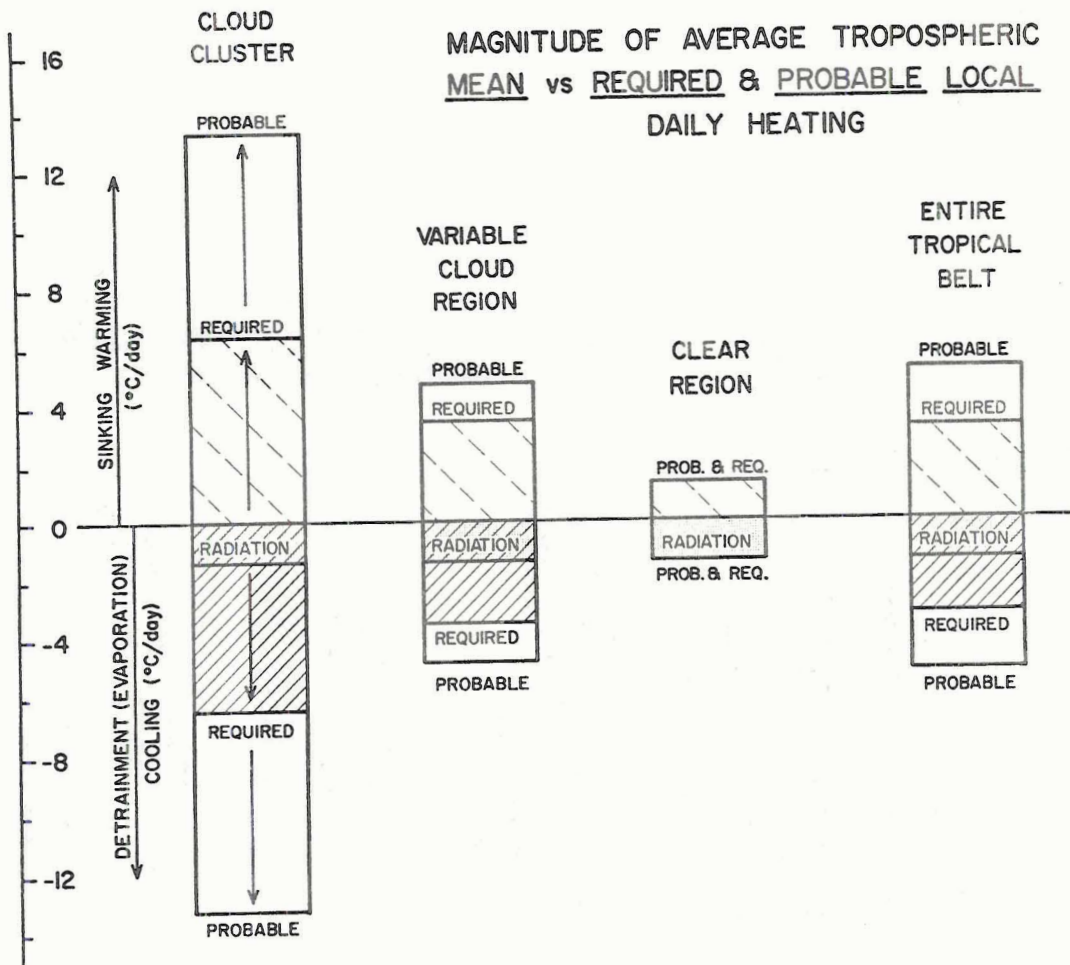


Fig. 43. Comparison of individual region sinking warming and evaporation cooling with the net radiation cooling.

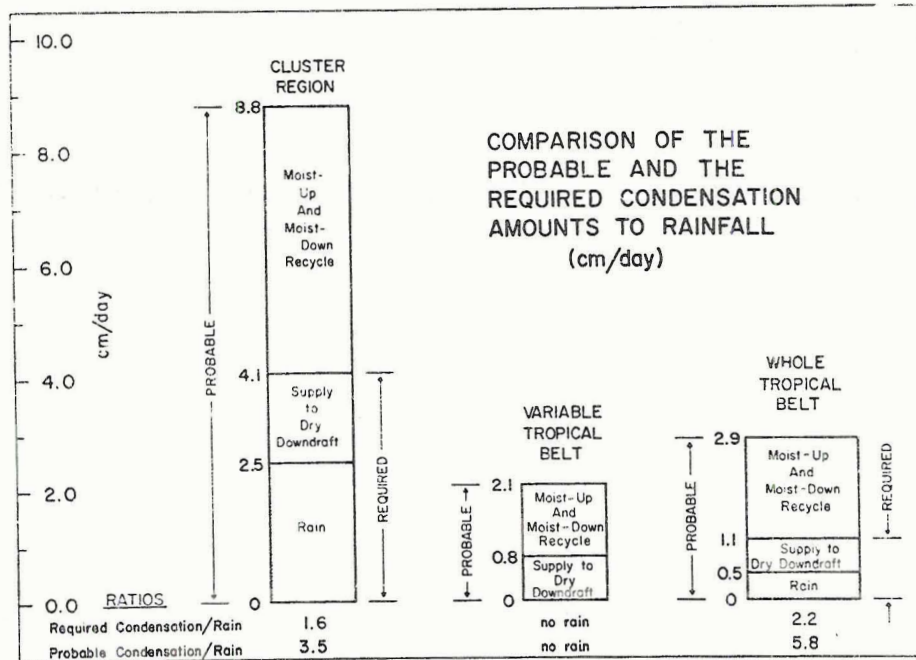


Fig. 44. Comparison of individual region condensation-evaporation vs. rainfall.

VIII. COMPARISON OF CLUSTER VERTICAL CIRCULATIONS
OBTAINED FROM THE BROAD-SCALE MODEL OF THIS
PAPER WITH THOSE OF CUMULUS SCALE
MODEL OF LÓPEZ (Paper II)

López (1972b-Paper II) has discussed the cluster vertical circulation as determined from a life cycle cumulus model in conjunction with radar and composite radiosonde cluster data. This cluster model, derived independent of the approach of this paper from cumulus and cluster scale consideration alone, will now be compared with the cluster model of this paper, derived from tropical belt and cluster-scale consideration without any cumulus-scale knowledge. Fig. 45 briefly outlines in flow diagram form how the two models were developed and how they were meshed for comparison.

Fig. 46-48 show the comparison of the two models with regard to their local vertical circulations, their sinking warming and evaporation cooling rates, and their water vapor loss-gains. One can clearly see how close each of these models were in specifying the required mass, energy, and water vapor budgets. This lended consistency and more credibility to the results of each approach. To ultimately verify cumulus-broaderscale interaction models, this inward meshing of the dynamics from opposite scales of consideration should always be a desired goal.

SMALL-SCALE MODEL (LÓPEZ)

LARGE-SCALE MODEL (GRAY)

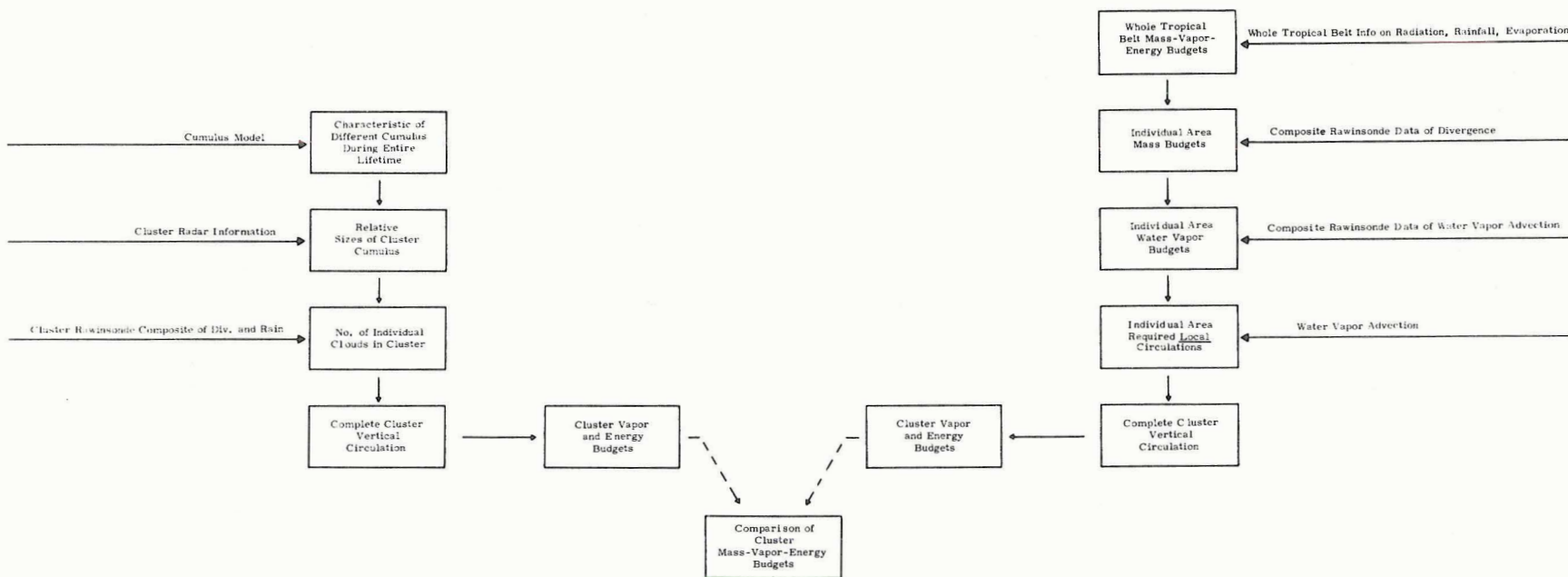


Fig. 45. Flow diagram of how the cloud cluster dynamics are independently determined and compared from the broadscale model of this manuscript (Paper III) and from the small scale model of López (1972b - Paper II).

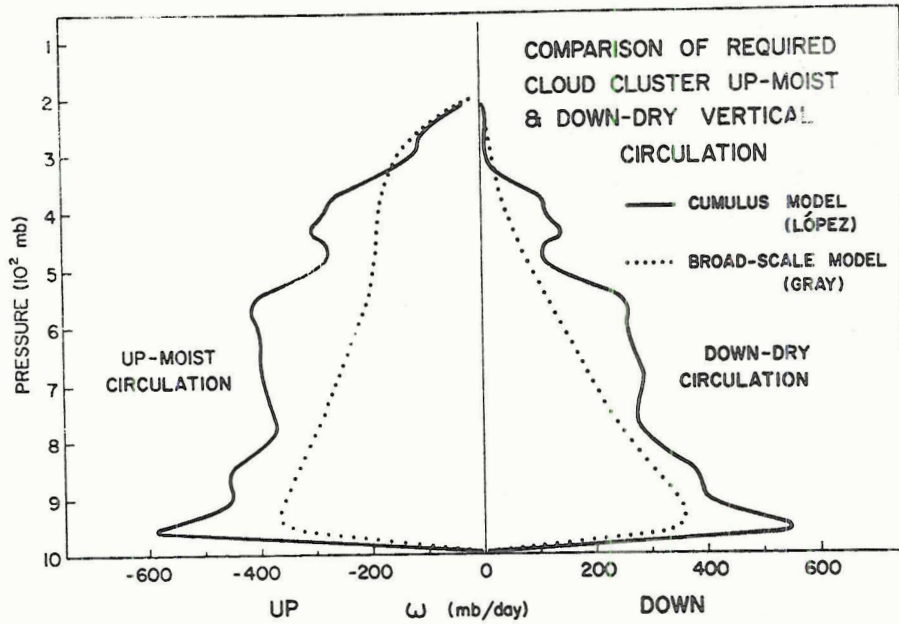


Fig. 46. Comparison of the cloud cluster vertical circulation as determined by the broad-scale model of this report and by the cumulus model of López (1972b).

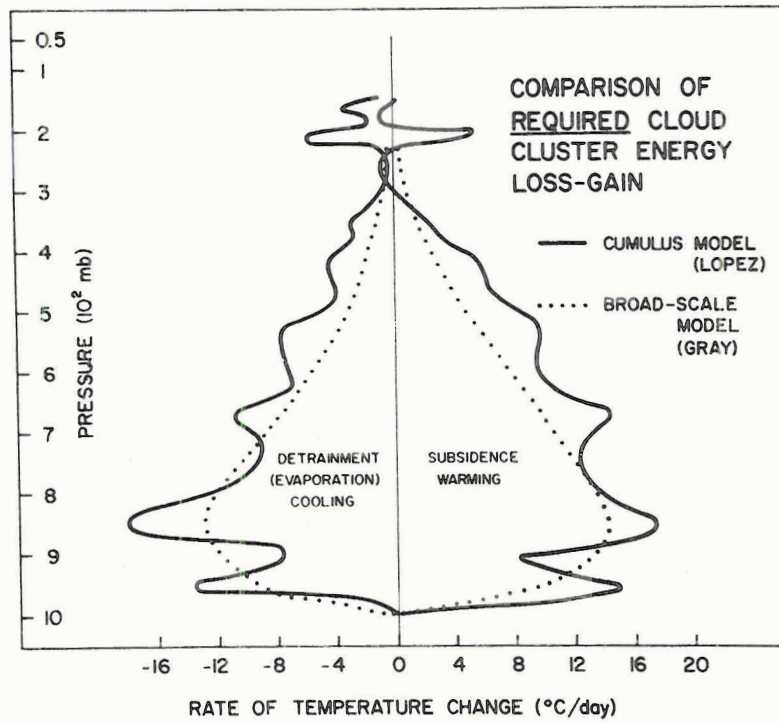


Fig. 47. Comparison of each model's subsidence warming and evaporation cooling.

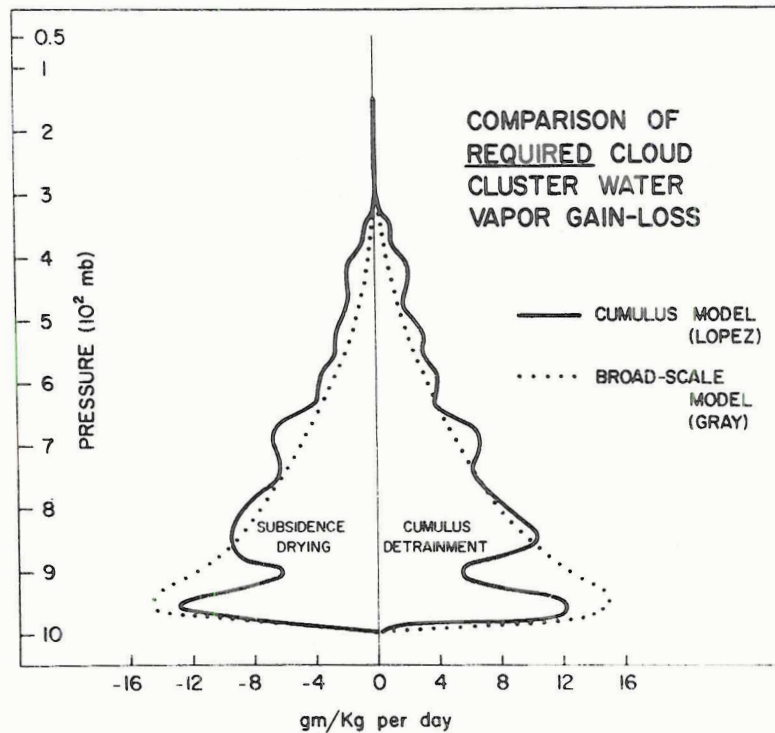


Fig. 48. Comparison of each model's water vapor budget.

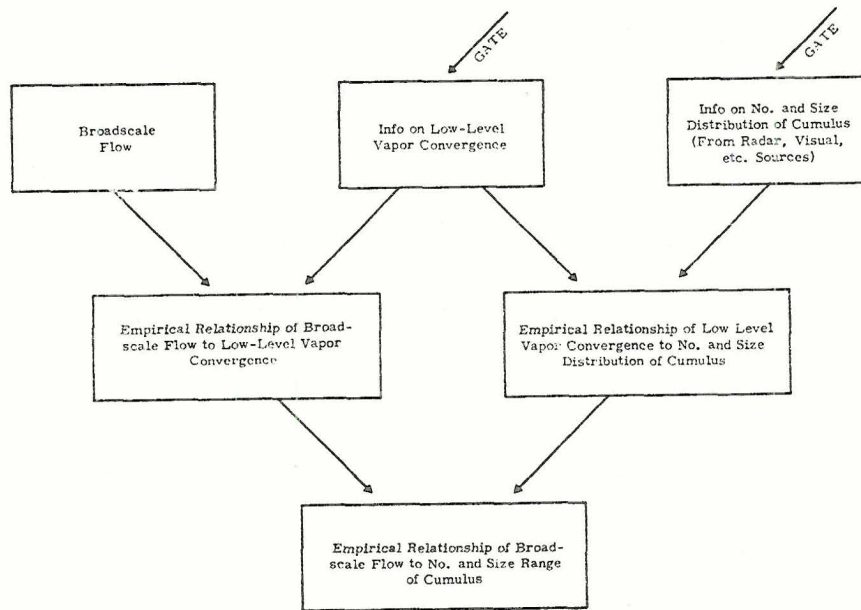
IX. PARAMETERIZATION OF MOIST PROCESSES

This paper has demonstrated the very large vertical circulation of the tropical atmosphere. It has shown that the summertime tropical atmosphere meets its mass-vapor-energy budgets in a rather complex way. The authors (Gray and López) feel that it is very difficult (or impossible) at the present time for any numerical model of tropical motion to adequately come to grips with the real problems of incorporating the cumulus convection in terms of the broader-scale flow. This will probably not be fully possible until we have more empirical information and general scientific consensus and understanding of

- 1) the individual cumulus dynamics with their characteristic mass, momentum, vapor, and sensible temperature rearrangements. This requires a good whole-life individual cumulus model.
- 2) the large magnitude of the local vertical circulation here described
- 3) the association of cumulus number and relative size distribution with various broad-scale features such as
 - a) low-level mass and moisture convergence
 - b) other broader-scale flow features such as the low-level relative vorticity and the tropospheric vertical wind shears, etc.

This knowledge will only come from an increase of our observational sampling of the tropical atmosphere and the cloud cluster. A judicious sampling and study of our already collected data (radiosonde and satellite) in the Western Pacific and in the West Indies will help to answer many of these questions. The coming GATE experiment and other tropical land experiments will hopefully help to fill many of the empirical gaps in our observation knowledge.

REQUIRED BACKGROUND RESEARCH
 RELATION OF BROADSCALE FLOW
 TO NUMBER AND SIZE OF CUMULUS



MODEL B

Fig. 49. Outline of proposed scheme for relating the broadscale flow to the number and size distributed of the cumulus.

The authors feel that the cumulus parameterization scheme which will finally prove workable will be one which handles the cumulus processes separately from the main working model.

We must first establish empirical relationships giving the association of the broadscale flow to the number and size of the cumulus (as in Fig. 49--Model B) and also empirical information on the influence of the cumulus on the surrounding circulation (as in Fig. 50--Model C). Only when this type of empirical evidence is obtained can we proceed confidently to an actual parameterization scheme as is speculatively proposed in Fig. 51. Here, the cumulus induced changes as determined by

REQUIRED BACKGROUND RESEARCH
INFLUENCE OF CUMULUS
ON SURROUNDING CIRCULATION

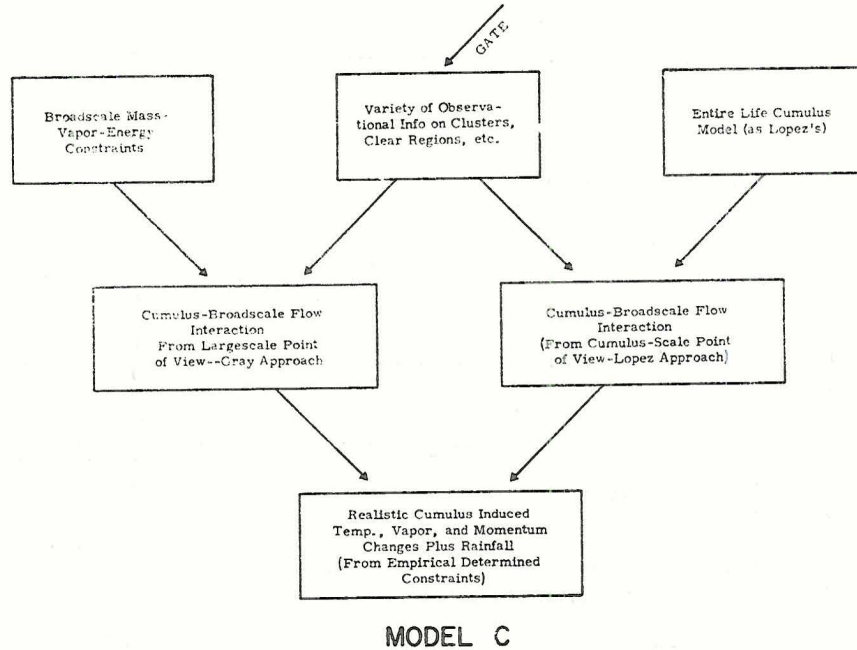
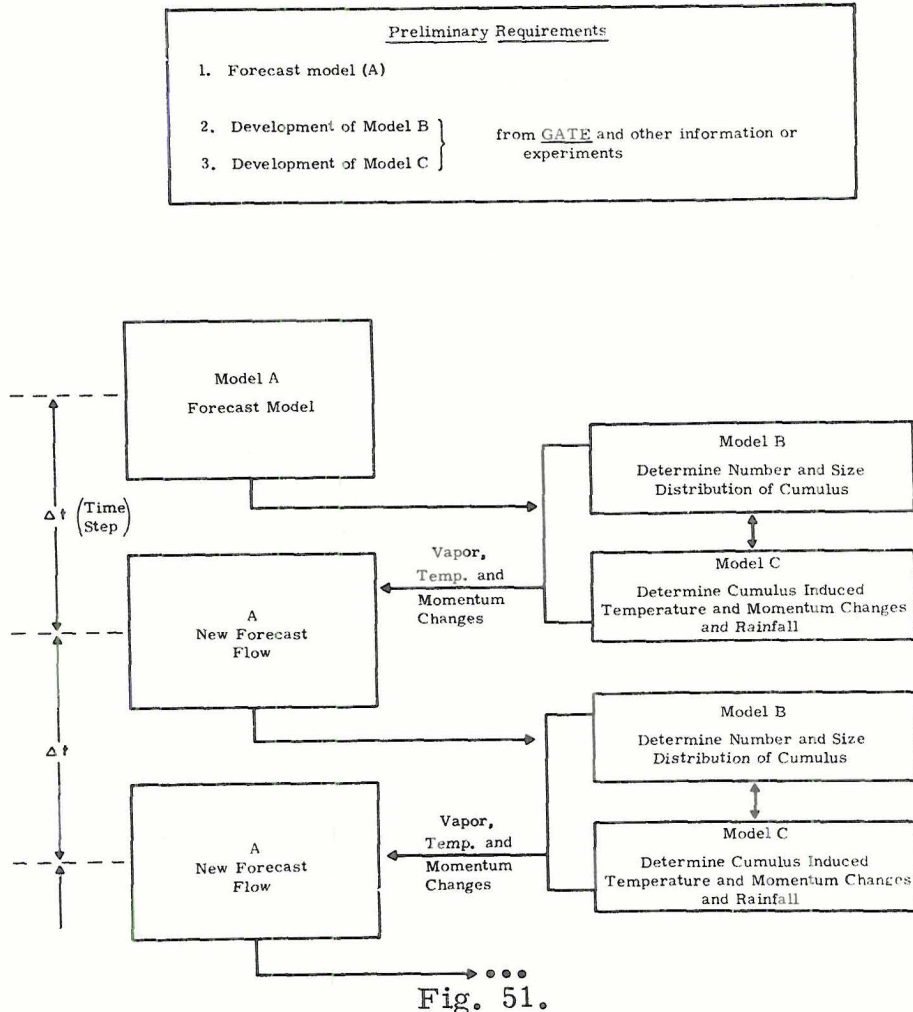


Fig. 50. Outline of proposed scheme for determining the influence of the cumulus on the surrounding circulation.

Models B and C are fed back to the basic working model (A) and new broadscale flow patterns specified at each time step.

In this figure the basic working model (A) uses already determined cumulus-broadscale relationships as given by Models B and C to specify its next timesteps. Empirical relationships of Models B and C are determined before Model A is run. Models B and C calibrate the cumulus with the broadscale flow. They must be based on empirical knowledge. They have yet to be realistically specified. Field programs and other research with observations should help to better specify the inputs of these auxiliary models.

PROPOSED CUMULUS PARAMETERIZATION SCHEME



Separate Treatment of Cumulus Cloud. In that the cumulus cloud is such a distinctive physical unit, it would appear that it should be independently treated probably in a fashion similar to that discussed by López (Paper II). The physics of the cumulus-broadscale interaction may not necessarily be overcome by applying the primitive equations to even smaller grids and time steps without additional insight into the character of the individual convective elements. At the same time cumulus parameterization schemes based on abbreviated or oversimplified cloud model schemes may prove to be inadequate at really coming to

grips with all of the real life cycle cumulus influences. The author feels that the minimum degree of cumulus model sophistication that will prove workable is probably that of whole-life one-dimensional model of López (1972a). In any rate, we will probably not be able to settle this question until we have a generally accepted sophisticated whole life cumulus model to which the simplified cumulus models can be compared.

X. DISCUSSION

Large Vertical Recycling. The large vertical recycling of air that has been discussed is a function of two primary tropospheric processes

- 1) the direct radiational cooling of the troposphere, and
- 2) the direct cooling nature of the cumulus clouds as they evaporate and die.

These two processes combine to produce substantial cooling of the atmosphere, especially in the lower troposphere. The net radiational cooling of the troposphere of about $1^{\circ}\text{C}/\text{day}$ is well known and accepted. The idea of the cumulus cloud as "a direct cooling agent — an indirect warming agent" has yet to be fully appreciated or accepted. To understand how the troposphere balances its radiation loss it is of fundamental importance to understand how condensation warms the atmosphere. Cumulus clouds, whether causing precipitation or not, do not directly act to warm the troposphere. In fact, cumulus clouds directly cool the environment in which they exist. By what mechanism then do the cumulus clouds act to balance the tropospheric radiation loss and at the same time directly cool?

As paradoxically as this may initially appear, this is indeed what goes on in the troposphere. The latent heat released from cumulus (both precipitating and nonprecipitating) goes primarily into potential energy gain and increasing the temperature of the rising parcel to that of the environmental temperature. The small extra (above environment) temperature increases of 1° to 2° of the rising parcel (which is required

for buoyancy) does not warm the environment unless it directly mixes out from the cloud at a higher temperature. The rising parcel typically continues rising until it loses its buoyancy and temperature excess. It then mixes to the environment at a temperature little different (or even cooler) than that of the environment. This does not warm the environment. Any diffusional or advective heat transports out from the rising (and warmer) cloud parcel are more than overcome by the evaporation of the residual cloud liquid water particles around the cumulus or when they die. Individual small cumulus last only 5-10 minutes; Cb's only about 25-30 minutes. The residual liquid particles which remain after the vertical motion in the cumulus has stopped cool the environment in and around the dying cloud at a rate of 2.4°C for every gm/kg evaporated. Being an open system, the cumulus converts all its condensation heat to potential energy and exports this to the surrounding environment. Even though rainfall may have occurred, there is typically no warming, but a local cooling of the environment. This is not to say that the total effect of the condensation to the "closed system" of the globe or hemisphere has not been one of warming. It has. The dry adiabatic sinking at some other location (to satisfy mass balance) has more than compensated for the local cooling if there has been rainfall. In this way the cumulus act in a delayed action sense. They produce a local sensible cooling, but a global averaged warming can result.

There is supporting data for this physical explanation:

- a) direct sensible temperature decreases around and after

cumulus convection has occurred, as reported by Kininmonth (1971) from data of the VEMHEX project of 1969.

- b) the lower tropospheric cool nature of the raining tropical cluster and easterly wave, as substantiated by Riehl (1945) and many others since. Why does this condensation not warm the environment?
- c) the lack of any tropospheric warming (or surface pressure falls) in an observational study of one thousand Pacific trade-wind cloud clusters by Williams (1970). The average observed and calculated rainfall for these clusters was 2-1/2 cm per day for a 4° latitude square area. This 1500 calories/cm² per day condensation energy release led to no tropospheric warming even though vertical wind shears and horizontal sensible temperature advective influences were small. Where did the heating go? Again, primarily to potential energy to be export to the surrounding environment.
- d) the direct cumulus cooling found by López (1972a) in his whole life cycle cloud model.
- e) the maximum warming of the hurricane centers. Here the highest temperatures are found in the center subsidence region. The maximum upward motion in the eye wall convection area has lower temperatures. A diffusion of sensible temperature into the eye-wall cloud is necessary to maintain its temperature (Shea, 1972).

We must thus view the cumulus precipitation warming process as one in which the cumulus initially cools the local environment but at the same time acts to warm the outer environment by compensating dry subsidence. The subsidence warming is larger than the local evaporation cooling and leads to a net large scale tropospheric sensible temperature warming. The warming occurs at the place where the sinking motion exists. Local warming can, at times, occur if the compensating sinking motion takes place near the rising motion as is the case with tropical storm genesis in regions of small vertical wind shear (Gray, 1968).

TEPHIGRAM PORTRAYAL
OF UP-MOIST, DOWN-DRY
VERTICAL CIRCULATION

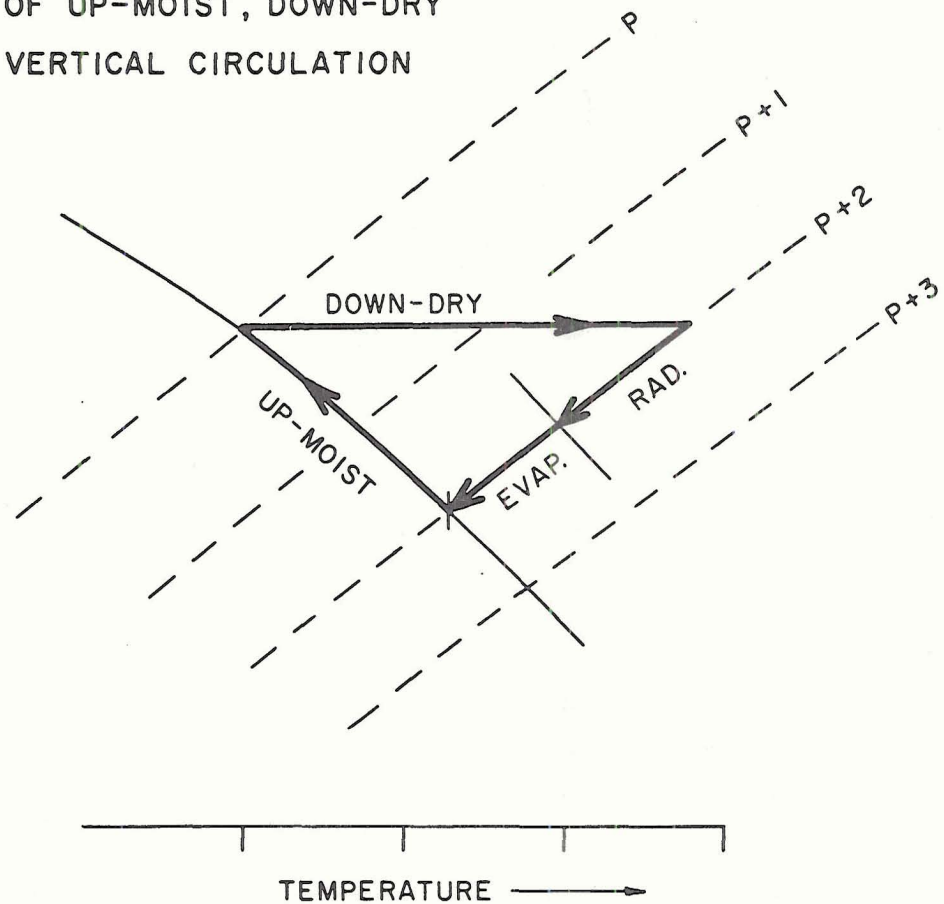


Fig. 52. Graphical portrayal of how an up-moist and down-dry vertical circulation can balance the radiation and evaporation energy losses.

The primary energy input to the troposphere can thus only come from a continuous up-moist and down-dry vertical circulation which acts to balance both the radiation and evaporation cooling as shown in Fig. 52.

This energy gain is paid for by a continuous water vapor loss. The clear area down-dry portion of this vertical circulation is continuously losing vapor which, for steady state, must be replaced by the cumulus. This is accomplished by vapor diffusion and by evaporation as shown in

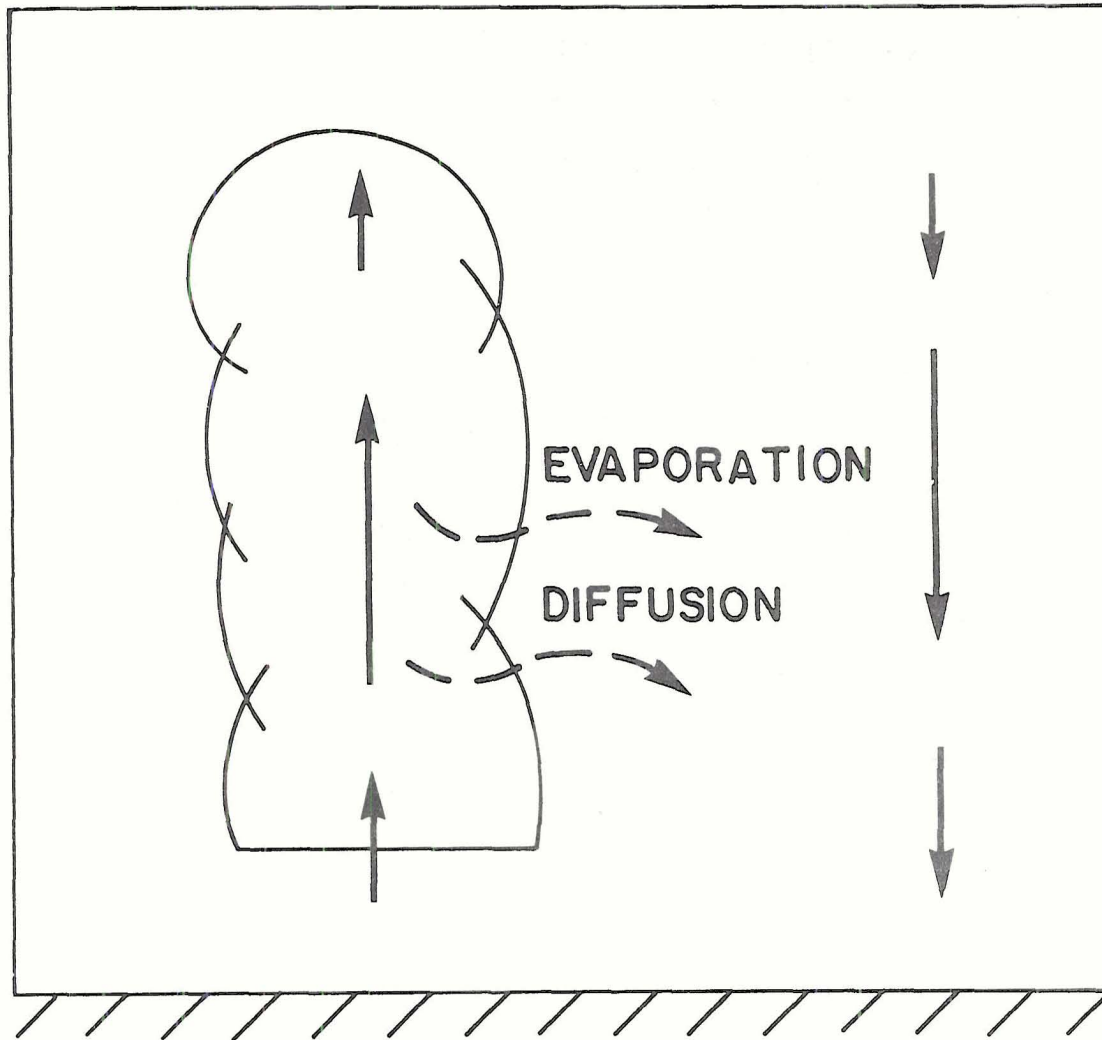


Fig. 53.

Fig. 53. This figure shows how the cumulus acts to increase the water vapor in the sinking air around it by both diffusion of vapor from the cloud and by liquid water evaporation on the edge of the cloud as the cloud dies.

There are now a number of meteorologists which are coming to think of the warming mechanism of the cumulus as resulting from compensating subsidence of the environment. The author has found general physical agreement on this idea in personal discussion and from the

papers R. López (op. cit.), Pearce and Riehl (1969), K. Ooyama (1971, 1972), M. Yanai (1971, 1972), and J. Charney (1968). In addition, some of these researchers, like López (op. cit.), Kinnemonth (1971), and Betts (1971, 1972, and personal communication), are now also accepting the idea of the cumulus cloud acting as a direct cooling agent. The earlier findings of Riehl (1945, 1965) and Elsberry (1966) on the lower tropospheric cooling of easterly waves might also be interpreted as generally supporting this point of view. Caution in literal interpretation of the "hot tower" hypothesis of Riehl and Malkus (1958, 1961) needs to be exercised. Their demonstration of the dominant role of vertical transports of mass occurring in selective cumulus or cumulonimbus towers is indeed correct, but these Cb towers are (from the immediate environmental warming point of view) "cool" and not "hot". They act to directly cool and not warm the environment. A "cooling tower" hypothesis does not, however, imply that the individual cumulus towers play any less fundamental role than that envisaged by Riehl and Malkus. The main problem of the cumulus acting as a direct heating rather than as a cooling source is that the required vertical circulation is reduced to unrealistic low values.

At a recent NCAR workshop on cumulus parameterization at Boulder, Colorado^{*}, a general concensus on the large required recycling of the cloud cluster atmosphere was arrived at by the author, López (1972a,

* July 10-14, 1972

1972b), Yanai (1972), Ooyama (1972), Rodenhaus (1972), and Zipser (1972).

Rate of Recycling in Generation of Individual Cumulus Elements.

The general stability of the cloud cluster boundary layer and the need for a lifting mechanism to initiate parcel condensation until free convection is obtained is generally accepted. This requires that substantial mechanical forcing be applied in order that buoyant elements be initiated. As discussed by López (1972a), it is not possible to generate cumulus over the oceans without mechanically forced cloud base vertical velocities of 1-5 m/sec. Underneath his cumulus (cu), towering cumulus (TWG) and cumulonimbus (Cb), he must have average local convergences during their forced ascent stages of about $3-6 \times 10^{-3} \text{ sec}^{-1}$. These values are one to two thousand times larger than the synoptic convergence. Table 4 lists the required mean forcing parameters used in his simulation of the three sizes of cumulus. Even if the active cumulus take up but one percent of the cluster area, these convergences are 10-20 times larger than that specified by synoptic convergence. The only way the extra convergence under the cluster cumulus can occur is by a large mass recycling mechanism which is 10-20 times greater than the synoptic mass convergence. Betts (1972) has composited wind data around growing cumulonimbus clouds in Venezuela and he finds convergence (for regions 2-5 times larger than López's Cb cloud base areas) in the sub-cloud layers of $\sim 2 \times 10^{-3} \text{ sec}^{-1}$, quite closely comparable with the required cumulonimbus boundary layer forcing of López's model. The recycling

dry and moist downdraft air which penetrates into the boundary layer from upper levels is thus the primary source of mass forcing for buoyant parcel initiation. Were the cluster cumulus to be forced only by the synoptic convergence of $3-5 \times 10^{-6} \text{ sec}^{-1}$, then the low level mass forcing requirements would permit only 1/1000 of the cluster area to be occupied by parcel ascent if all the mass sent into Cb's, or only 1/500 of the area if occupied by all towering cumulus or by all cumulus parcel ascent. López's (Paper II) radar data shows that the areas of the cluster occupied by active cumulus clouds are typically 10-20 times larger than these amounts. Given the typical cloud cluster synoptic convergences and stable lapse rate conditions, the fundamental requirement of large up- and-down mass recycling 10-20 times greater than the mean vertical mass flow at cloud base is clearly evident.

Table 4

Parameters used in Lopez's (1972a) simulation of cumulus

Cloud Type	Cloud Base Height	Mean Forced Convergence under Cloud during its initiation	Initial Radius	Duration of Forced up-draft through Cloud Base	Mean Value of Sinsoid-ually Forced Updraft
	(meters)	$-\nabla \cdot W$ (sec^{-1})	R_o (km)	T_o (minutes)	\bar{w}_o (m/sec)
Cb	520	$\sim 6 \times 10^{-3}$	2.0	20	3.3
TWG	520	$\sim 3 \times 10^{-3}$	1.0	15	1.7
Cu	520	$\sim 3 \times 10^{-3}$	0.5	15	1.7

Relationship of Cluster Mass Recycling to CISK Mechanism. It is obvious that synoptic-scale boundary layer induced frictional convergence from Ekman wind veering or the "so called Conditional Instability of the Second Kind (CISK)" mechanism as defined by Charney and Eliassen (1964) plays only a small direct role in the cluster upward mass transfers necessary to initiate the cumulus. This does not negate the fundamental need of the cluster for frictionally induced synoptic scale convergence, but it dictates that the primary direct function of the CISK process is to act as a mechanism for water vapor convergence. Unless the low levels of the cluster are continuously fed with water vapor, then the rain processes would act to decrease the cluster vapor and the resulting higher buoyant stability of the dryer environment would put unrealistically high requirements on the boundary layer mass forcing. Cumulus convection could not be sustained. This point has been emphasized by Rodenhaus (1971).

The very high correlation of boundary layer^{*} relative vorticity with cumulus convection along frontal zones, squall lines, on the cyclonic shearing side of the trade wind, in tropical storms, etc., illustrates what a fundamental role the low level frictional forcing plays in allowing the cumulus recycling mechanism to get going. The general lack of cumulus convection in anticyclones and other regions of negative vorticity where weak lower level friction divergence is occurring is primarily due to the sinking induced drying of the environment.

*The terms "boundary layer" and "sub-cloud layer" are used synonymously. This refers to the layer from the surface to 950 mb.

To understand the high correlation of cumulus convection with boundary layer convergence and the CISK mechanism, one must fully appreciate the powerful influence of relative humidity on cumulus buoyancy. Figs. 11 and 12 showed that the major difference between the cluster and clear regions is in the relative humidity above 950 mb. Table 5 compares the temperature difference between a lifted parcel and the environment for the cluster and clear regions. In this table the parcel has been lifted from a condensation level of 950 mb with assumed entrainment rates of zero, 10 and 20 percent per 100 mb of parcel ascent. This table clearly shows the very strong dependence of parcel ascent on environment relative humidity and entrainment. A 10% per 100 mb entrainment rate would lead to a 450 mb parcel minus environment temperature of -1.6°C in the cluster as compared with -6.0°C in the clear areas. These are very large differences.

The cluster divergence profile of Fig. 20 is a result of the combined low-level frictional forcing mechanism and the cumulus feed-back of the up-and-downdrafts. Cluster convergence above the boundary layer is primarily a consequence of the cumulus. Middle level convergence is necessary to feed the accelerating downdrafts. Fig. 34 shows that the 400 to 950 mb increase of the total downward motion is greater than the 950 to 400 mb increase of the total upward motion. This middle level convergence leads to additional water vapor convergence.

After boundary layer convergence has initiated and sustained an updraft impulse to the level of free convection, an accelerating upward

TABLE 5

CLOUD CLUSTER VS. CLEAR REGION BUOYANCY PARAMETER FOR MOIST
ASCENT FROM 950mb

Relative Humidity (percent)			Cumulus Parcel Temperature Minus Environment Temperature ($^{\circ}\text{C}$)					
			No Entrainment		For Environment Entrainment of 10% per 100mb		For Environment Entrainment of 20% per 100mb	
Pressure Level	Cluster	Clear Areas	Clusters	Clear Regions	Clusters	Clear Regions	Clusters	Clear Regions
950	80	66	0	0	0	0	0	0
850	77	55	+1.0	+0.7	+0.2	-0.8	-0.6	-2.6
750	70	40	+1.6	+1.3	0	-2.2	-2.8	-4.8
650	65	30	+2.0	+1.6	-0.2	-3.2	-3.7	-6.8
550	58	24	+2.7	+2.2	-0.8	-4.4	-5.2	-8.5
450	52	20	+3.0	+2.6	-1.6	-6.0	-7.0	-11.3

growth occurs which produces changes to the middle and upper tropospheric levels. If the updraft is sufficiently intense such that downdrafts and rain are produced, then further upsetting and influence to the middle and upper tropospheric levels occurs. The sharp increase of stability near the 200 mb level produces a rapid deceleration and mass divergence at this level. The accelerating downdrafts of the middle and lower troposphere produce cluster convergence at these levels. Even though middle and upper level broadscale responses to the individual cumuli occur, this does not negate the fundamental role of the boundary layer in initially dictating these responses.

Influence of Large-Scale Boundary Layer Convergence. The physics of the individual cumulus (as discussed by López), shows that the cloud cluster's mass convergence does not produce enough mass forcing underneath the individual cumulus such that it can directly release very much of the vapor convergence to rain. The cluster's convergence is too weak. Vapor accumulation is prevented and a steady state is obtained only by the establishment of an additional vigorous vertical mass recycling into the boundary layer. This extra up-moist and down-dry recycling would carry vapor upward and act to reduce the boundary layer vapor. The intensity of the recycling would increase until a balance was obtained between the overall cluster vapor convergence-evaporation and the cluster rainfall. At this point the downward mass flux into the boundary layer would be strong enough to produce enough mass forcing under enough ascending parcels such that cluster rainfall of 2.5 cm/day can occur.

Degree of Recycling. This degree of recycling may be defined as the ratio of the required absolute upward vertical motion at the top of the boundary layer, $|w_{up}|$, to the mean vertical motion, $-\bar{w}$, at this level, or $|w_{up}| / -\bar{w}$. The ratio is dependent upon the magnitude of the cluster water vapor accumulation from evaporation and convergence to the rainfall which the boundary layer mass convergence would produce from parcel forcing without recycling. Using López's cumulus model and the cluster observed mass convergence of $3 \times 10^{-6} \text{ sec}^{-1}$, the ratio of vapor accumulation to rainfall induced from the broadscale

boundary layer forcing by itself was found to be about 20 or 30 to 1. Boundary layer convergence of $3 \times 10^{-6} \text{ sec}^{-1}$ produce only enough mass forcing to the ascending parcel for a rainfall of about 0.1 cm/day. For cluster rainfall of 2.5 cm/day, an additional mass source about 25 times greater than that of the mean boundary layer convergence is required. The downward mass penetration from upper levels associated with the recycling mechanism is this additional mass source.

The CISK mechanism must thus be viewed not as a direct cumulus producing process, for in this it is much too weak, but instead as a required "trigger" for recycling. As far as cumulus convection is concerned, the most important aspect of the CISK mechanism is not the magnitude of the direct boundary layer mass convergence but rather the associated water vapor convergence.

Possible Importance of Recycling for Vertical Momentum Transfer.

In that the cluster sinking warming and the evaporation cooling largely balance each other and in that the up- and-down recycling mass largely balance, one might argue that it is not important to deal with the recycling mechanism directly but only with its net influence. From the cluster mass and energy budgets this may be a reasonable conclusion; for the water vapor and probably for the momentum budgets it is not. The correlation of the recycling up and down motion with specific humidity has been shown to be very large. It seems likely that there would also be a significant correlation of the recycling motion with horizontal momentum. If this proves to be the case, then the recycling process has

feed-back momentum influences which would also have to be parameterized along with the energy ones.

Definition of Planetary Boundary Layer. In this paper the planetary boundary layer is viewed as that layer where surface mechanical-driven gust-scale eddies (~50-500 m size) exist and decrease in density and intensity with height. Over the oceans this layer is typically one-half to one km thick (Gray, 1972c) and is primarily associated with the sub-cloud layer. To define the boundary layer with respect to a mixed layer which is dependent on the depth of the cumulus convection, as some researchers propose, is the obscure the important difference between gust-scale mechanically driven processes and cumulus thermally driven processes. The large vertical mass recycling portrayed in this paper show that a definition with respect to the top of the cumulus always puts the boundary layer near the tropopause in cluster situations and near 950 mb in clear situations. The top of this mixed layer is too variable. For simplicity the author proposes that the term "boundary layer" be used to apply only to the usual Ekman layer where surface generated mechanical gust-scale eddies are dominant. As long as surface winds are present, the mechanically driven gust-scale exchanges of this lowest km layer are always present regardless of the existence or degree of cumulus activity above.

ACKNOWLEDGEMENTS

This research has been jointly sponsored by the NOAA National Environmental Satellite Center and the National Science Foundation. The author has received much benefit from lengthy discussions on this subject matter with Dr. Raúl E. López. He also appreciates assistance in manuscript preparation from Mrs. Barbara Brumit and Mr. Larry Kovacic. Mr. Edward Buzzel successfully performed the many cluster numerical programming schemes from an original program of Mr. Knox Williams. Dr. Russel Elsberry performed a critical review of the manuscript.

BIBLIOGRAPHY

- Betts, A. U., 1971: Nonprecipitating Cumulus Convection and its Parameterization. Research Report of Dept. of Atm. Sci., Colo. St. U., (to be published in QJRMS), 42 pp.
- _____, 1972: A Composite Mesoscale Cumulonimbus Budget. Atm. Sci. Paper No. 186, Dept. of Atm. Sci., Colo. St. U., 48 pp.
- Budyko, M. I., 1956: Heat Balance of the Earth's Surface (translated from Russian in 1958 by the U.S. Weather Bureau), 255 pp.
- Chang, C. P., 1970: Westward Propagating Cloud Patterns in the Tropical Pacific as Seen From Time-Composite Satellite Photographs. J. Atm. Sci., 27, 133-138.
- Charney, J. G., 1969: The Intertropical Convergence Zone and the Hadley Circulation of the Atmosphere Proceedings of the WMO/IVGG Symposium on Numerical Weather Prediction. Tokyo, Nov., 1968, III, 73-79.
- _____ and A. Eliassen, 1964: On the Growth of the Hurricane Depression, J. of Atm. Sci., 21, 68-75.
- Elsberry, R., 1966: On the Mechanics and Thermodynamics of a Low-level Wave in the Easterlies. Dept. of Atm. Sci., Colo. St. U., 31 pp.
- Frank, N. L., 1970: Atlantic Tropical Systems of 1969. Mon. Wea. Rev., 98, 307-314.
- _____, 1971: Atlantic Tropical Systems of 1970. Mon. Wea. Rev., 99, 281-285.
- Gray, W. M., 1968: Global view of the Origin of Tropical Disturbances and Storms. Mon. Wea. Rev., 97, 669-700.
- _____, 1971: The Magnitude and the Fundamental Role of the Up-moist and Down-dry Vertical Circulation of the Troposphere. Presented at the 7th Technical Conference Hurricanes and Tropical Meteorology, Barbados.
- _____, 1972a: The Magnitude and Character of the Radiation Induced Vertical Circulation of the Troposphere. Proceedings of the Conference on Atmospheric Radiation, Aug., 7-9, Ft. Collins, Colo., p. 255-259.

BIBLIOGRAPHY (cont'd)

- _____, 1972b: The Structure and Dynamics of the Tropical Cloud Cluster. Colo. St. U., Atm. Sci. Paper (in preparation).
- _____, 1972c: A Diagnostic Study of the Planetary Boundary Layer Over the Oceans. Colo. St. U., Atm. Sci. Paper No. 179, 95 pp.
- Hayden, C.M., 1970: An Objective Analysis of Cloud Cluster Dimensions and Spacing in the Tropical North Pacific. Mon. Wea. Rev. 98, 534-540.
- Holton, J. and D.E. Colton, 1972: A Diagnostic Study of the Vorticity Balance at 200 mb in the Tropics During the Northern Summer. Contribution No. 258, Dept. of Atm. Sci., U. of Wash., (to appear in J. of Atm. Sci.).
- Kininmonth, W.R.: Thermal Modification of the Troposphere due to Convective Interaction. Atm. Sci. Paper No. 167, Dept. of Atm. Sci., Colo. St. U. 36 pp.
- López, R.E., 1968: Investigation of the Importance of Cumulus Convection and Ventilation in Early Tropical Storm Development. Atm. Sci. Paper No. 124, Dept. of Atm. Sci., Colo. St. U., 86 pp
- _____, 1972a: A Parametric Model of Cumulus Convection. Atm. Sci. Paper No. 188, Dept. of Atm. Sci., Colo. St. U., 100 pp.
- _____, 1972b: Cumulus and Mesoscale Interaction. Atm. Sci. Paper No. 189, Dept. of Atm. Sci., Colo. St. U., 90 pp.
- Malkus, J.S. and H. Riehl, 1964: Cloud Structure and Distributions Over the Tropical Pacific Ocean. University California Press, 229 pp.
- Martin, D.W. and V.E. Suomi, 1972: A Satellite Study of Cloud Clusters Over the Tropical North Atlantic. BAMS, 53, 135-156.
- Newton, C., 1963: Dynamics of Severe Convective Storms. AMS Monograph Vol. 5, No. 27, 33-58.
- Oort, A.H., and E.M. Rasmusson, 1971: Atmospheric Circulation Statistics. NOAA Professional Paper 5, U.S. Dept. of Commerce Publication, 323 pp.

BIBLIOGRAPHY (cont'd)

- Ooyama, K., 1971: A Theory on Parameterization of Cumulus Convection. J. of Meteor. Soc. of Japan, 49, 744-756.
- _____, 1972: Convective Transport by Implicit Buoyant Elements. Talk given at GATE workshop on cumulus convection, Boulder, Colo., July 10-14, 1972.
- Pearce, R., and H. Riehl, 1969: Parameterization of Convective Heat and Momentum Transfers Suggested by Analysis of Caribbean Data. Proceedings of WMO/IVGG Symposium on Numerical Weather Prediction, Tokyo, I, 75-84.
- Reed, R.J. and E.E. Recker, 1971: Structure and Properties of Synoptic-Scale Wave Disturbances in the Equatorial Western Pacific. J. of Atm. Sci., 28, 1117-1133.
- Riehl, H., 1945: Waves in the Easterlies and the Polar Front in the Tropics. Dept. of Meteor., U. of Chicago, Misc. Report No. 17.
- _____, 1965: Varying Structure of Waves in the Easterlies. Dynamics of Large-Scale Atmospheric Processes. Proceedings of the International Symposium, Moscow, June 23-30, 1965, 411-416.
- _____ and J.S. Malkus, 1958: On the Heat Balance in the Equatorial Trough Zone. Geophysica, 6, 503-538.
- _____, 1961: Some Aspects of Hurricane Daisy, 1958. Tellus, 13, 181-213.
- Rodenhaus, D., 1971: A Note Concerning the Effect of Gravitational Stability Upon the CISK Model of Tropical Disturbances. J. Atm. Sci., 28, 126-129.
- _____, 1972: Parameterization With a Cellular Model. Talk given at GATE workshop on cumulus convection. Boulder, Colo., July 10-14, 1972.
- Shea, D.J., 1972: The Structure and Dynamics of the Hurricane's Inner Core Region. Colo. St. U., Atm. Sci. Paper No. 182, 134 pp.
- Sellers, W.D., 1965: Physical Climatology. The U. of Chicago Press. 272 pp.

BIBLIOGRAPHY (cont'd)

- Wallace, J. M., 1970: Time-Longitude Sections of Tropical Cloudiness (Dec. 1966-Nov. 1967). ESSA Technical Report, NESC 56 (available from G. P. O., Washington D. C.), 37 pp.
- Williams, K. T., 1970: A Statistical Analysis of Satellite-Observed Trade Wind Cloud Clusters in the Western North Pacific. Atm. Sci. Paper No. 161, Dept. of Atm. Sci., Colo. St. U., Fort Collins, 80 pp.
- Yanai, M., 1971: A Review of Recent Studies of Tropical Meteorology Relevant to the Planning of GATE. Experimental Design Proposal by the Interim Scientific and Management Group (ISMG), Vol. 2, Annex 1.
- _____, et. al., 1972: Determination of Average Bulk Properties of Tropical Cloud Clusters From Large-Scale Heat and Moisture Budgets. Talk given at GATE workshop on cumulus convection, Boulder, Colo., July 10-14, 1972, (also available in manuscript form), 60 pp.
- Zipser, E. J., 1969: The Role of Organized Unsaturated Convective Downdraft in the Structure and Rapid Decay of an Equatorial Disturbance. J. of Appl. Meteor., 8, 799-814.
- _____, 1972: CITHK, CISK, Original CISK and Original Sin. Talk given at GATE workshop on cumulus convection. Boulder, Colo., July 10-14, 1972.